Automatic Generation Control and Voltage Stabilization in a Power System using Natural Computation based Control Approach



By

Tayyab Ali

Reg. No. 10-FET/PHDEE/S18

A dissertation submitted to I.I.U. in partial fulfillment of the requirements for the degree of

DOCTOR OF PHILOSOPHY

Department of Electrical and Computer Engineering Faculty of Engineering and Technology International Islamic University Islamabad



PhD OOS.45 TAA

Acrossion No 1/126253 Vily

Coole Generation - Computer science. Computer software. Devlopment

.

Copyright © 2023 by Tayyab Ali

All rights reserved. No part of the material protected by this copyright notice may be reproduced or utilized in any form or by any means, electronic or mechanical, including photocopying, recording or by any information storage and retrieval system, without the permission from the author.

DEDICATED

to

My Teachers,

Parents,

Wife,

Children,

Brothers and Sister

CERTIFICATE OF APPROVAL

Title of Thesis: Automatic Generation Control and Voltage Stabilization in a Power System

using Natural Computation based Control Approach

Name of Student: Mr. Tayyab Ali

Registration No.: 10-FET/PHDEE/S18

This thesis is accepted by the Department of Electrical and Computer Engineering (DECE), Faculty of Engineering and Technology (FET), International Islamic University (IIU) Islamabad, in partial fulfillment of the requirements for the Doctor of Philosophy (PhD) degree in Electrical Engineering.

Viva Voce Committee:

Supervisor

Dr. Suheel Abdullah Malik

Associate Professor, DECE, FET, IIU Islamabad

Internal Examiner

Prof. Dr. Aqdas Naveed Malik

Professor, DECE, FET, IIU Islamabad

External Examiner 1

Dr. Muhammad Zia

Professor.

Department of Engineering.

Quaid-i-Azam University, Islamabad

External Examiner 2

Dr. Muhammad Usman

Ex. Project Director,

Department of Engineering,

NESCOM AERO, Wah Cantt

Chairman DECE, FET, IIU Islamabad

Dr. Shahid Ikram

Assistant Professor, DECE, FET, IIU Islamabad

Dean FET, IIU Islamabad

Dr. Nadeem Ahmed Sheikh

Professor, DME, IIU Islamabad

- Duryfinu V

Mand

What I

ABSTRACT

Existing interconnected power systems (IPS) are being overloaded by the expansion of the industrial and residential sectors and the inclusion of renewable energy sources, resulting in significant fluctuations in load frequency, terminal voltage, and tie-line power deviation. Terminal voltage and load frequency control in an IPS is critical for maintaining the balance of active and reactive power under varying load conditions. This is achieved by load frequency control (LFC) and automatic voltage regulator (AVR). This work presents the exploration of natural computation based control approaches for combined control of terminal voltage and load frequency in multi-area multi-source IPSs. The multi-area IPSs include two, three and four areas. In the earlier part of this work, Archimedes optimization algorithm (AOA), learner performance based behavior optimization (LPBO), and modified particle swarm optimization (MPSO) based proportional integral-proportional derivative (PI-PD) control schemes were applied to two- and three-area single-source interconnected power systems under various step load perturbations (SLP) to control load frequency and terminal voltage simultaneously. The integral of time multiplied by the squared value of error (ITSE) was used as the error criterion for evaluating the performance of proposed control scheme. The output responses of LPBO-PI-PD, AOA-PI-PD, and MPSO-PI-PD were compared with an existing nonlinear threshold accepting algorithm (NLTA) based proportional integral derivative (PID) controller. Then, the dandelion optimizer (DO) based PI-PD controller was explored in two- and three-area multi-source IPSs with nonlinearities and different SLPs. The output responses of DO based PI-PD control scheme were compared with the hybrid approach of artificial electric field algorithm (HAEFA) based fuzzy PID, AOA-PI-PD, LPBO-PI-PD and MPSO-PI-PD control methods. Finally, a PID controller tuned with gradient based optimizer (GBO) was investigated in a four-area multi-source IPS. The output responses of GBO-PID control scheme were evaluated and compared with the responses of controllers such as integral-proportional derivative (I-PD), integral-proportional (I-P), and tilt integral derivative (TID) controllers tuned with GBO. Sensitivity analyses were also performed by varying the system parameters to verify the effectiveness of the proposed control schemes in different multi-area IPSs.

The comprehensive comparisons of the output responses between different control strategies and the results of the sensitivity analyses have clearly shown that the proposed natural computation based control approaches are highly effective and reliable to maintain terminal voltage, frequency, and tie-line power balance with fairly small deviations and fast settling time in a multi-area multi-source IPS.

LIST OF PUBLICATIONS

- [1]. Ali, T.; Malik, S.A.; Daraz, A.; Adeel, M.; Aslam, S.; Herodotou, H. Load Frequency Control and Automatic Voltage Regulation in Four-Area Interconnected Power Systems Using a Gradient-Based Optimizer. Energies 2023, 16, 2086. https://doi.org/10.3390/en16052086
- [2]. Ali, T.; Malik, S.A.; Daraz, A.; Aslam, S.; Alkhalifah, T. Dandelion Optimizer-Based Combined Automatic Voltage Regulation and Load Frequency Control in a Multi-Area, Multi-Source Interconnected Power System with Nonlinearities. Energies 2022, 15, 8499. https://doi.org/10.3390/en15228499
- [3]. Ali, T.; Malik, S.A.; Hameed, I.A.; Daraz, A.; Mujlid, H.; Azar, A.T. Load Frequency Control and Automatic Voltage Regulation in a Multi-Area Interconnected Power System Using Nature-Inspired Computation-Based Control Methodology. Sustainability 2022, 14, 12162. https://doi.org/10.3390/su141912162

ACKNOWLEDGEMENTS

In the name of Almighty Allah (SWT), who is the most gracious and the merciful. I would like to thank Almighty Allah for giving me the strength and patience to complete this research work. Peace and blessings of Almighty Allah be upon His last Prophet Muhammad (PBUH) and all his Sahaba (RA) who dedicated their lives for Dawah and spread of knowledge.

I am truly grateful to my supervisor Dr. Suheel Abdullah Malik whose inspiration, ideas and efforts make it possible for me to complete my higher studies. He has been a role model for me and many others in teaching, research and other aspects of life.

I am grateful to my father, mother, children, brothers and sister for their love and support throughout my life. I am also very thankful to my wife for her patience, encouragement and prayers during every single stage of my PhD degree.

Tayyab Ali

TABLE OF CONTENTS

CERTIFICATE OF APPROVAL	iv
ABSTRACT	v
LIST OF PUBLICATIONS	vi
ACKNOWLEDGEMENTS	v ii
TABLE OF CONTENTS	viii
LIST OF FIGURES	xi
LIST OF TABLES	xvi
LIST OF ABBREVIATIONS	. xviii
LIST OF SYMBOLS	xxi
CHAPTER 1	1
Introduction	1
1.1 Overview	1
1.2 Problem Statement	
1.3 Objectives of Research	
1.4 Organization of the Thesis	
CHAPTER 2	5
Literature Review	
2.1 Combined Study of AVR and LFC Systems	5
2.2 Study of Individual LFC Systems	
2.3 Study of Individual AVR Systems	17
CHAPTER 3	
Frequency and Voltage Stabilization in Multi-area Single-Source IPS	
3.1 Mathematical Modeling of Power System	
3.2 Proposed Control Methodology	
3.3 Nature-Inspired Computation Algorithms	23
3.3.1 Learner Performance based Behavior Optimization (LPBO)	
3.3.2 Archimedes Optimization Algorithm (AOA)	25
3.3.3 Modified Particle Swarm Optimization (MPSO)	25
3.4 Implementation and Results Discussion	
3.4.1 Frequency and Voltage Stabilization in a Two-area Single-Source IPS	
3.4.2 Frequency and Voltage Stabilization in a Three-area Single-Source IPS	
3.4.3 Sensitivity Analysis of a Three-area Single-Source IPS	46
CHAPTER 4	55

	and Voltage Stabilization in Multi-area Multi-source IPS with/withou
4.1 Ma	thematical Modeling of Power System5
4.2. No	onlinearities5
4.2.1	Generation Rate Constraint (GRC)
4.2.2	Governor Dead Band (GDB)5
4.2.3	Boiler Dynamics (BD)5
4.3 Pro	posed Methodology5
4.4 Da	ndelion Optimizer (DO)6
4.5 Im	plementation and Results Discussion
4.5.1 Nonli	Frequency and Voltage Stabilization in a Two-area Multi-source IPS without nearities
4.5.2 Nonli	Frequency and Voltage Stabilization in a Two-area Multi-source IPS witnesarities
	Frequency and Voltage Stabilization in a Three-area Multi-source IPS wit nearities
CHAPTE	R 59
Frequency	and Voltage Stabilization in a Four-area Multi-source IPS
5.1 Ma	thematical Modeling of Power System9
5.2. Pr	oposed Control Methodology9
5.2.1	PID Controller9
5.2.2	TID Controller9
5.2.3	I-PD Controller
5.2.4	I-P Controller
5.3 Gra	adient Based Optimizer (GBO)
5.3.1	GBO Initialization
5.3.2	Gradient Search Rule (GSR)
5.3.3	Local Escaping Operator (LEO)
5.4 Imp	plementation and Results Discussion
5.4.1	Frequency and Voltage Stabilization in a Four-area Multi-source IPS 10
5.4.2	Sensitivity Analysis of a Four-area Multi-source IPS
CHAPTE	R 6
Conclusion	ns and Future Work
6.1 Co	nclusions
6.1.1	Frequency and Voltage Stabilization in Multi-area Single-Source IPS

6.1.2 Frequency and Voltage Stabilization in Multi-area Multi-source IPS	with/withou
Nonlinearities	132
6.1.3 Frequency and Voltage Stabilization in a Four-area Multi-source IPS.	133
6.2 Future Work	134
REFERENCES	136
APPENDIX A	152
APPENDIX B	153
APPENDIX C	154

LIST OF FIGURES

Figure 1.1: Combined Model of LFC-AVR	2
Figure 3.1: Power System	0
Figure 3.2: Proposed control methodology with combined LFC-AVR system	2
Figure 3.3: Flow chart of LPBO algorithm	4
Figure 3.4: Flow chart of AOA	6
Figure 3.5: Flow chart of MPSO algorithm	7
Figure 3.6: Two-area single-source IPS model with LFC and AVR loops	9
Figure 3.7: Response of Δf1 with PI-PD control schemes in a two-area single-source IPS	1
Figure 3.8: Response of Δf_2 with PI-PD control schemes in a two-area single-source IPS 3	1
Figure 3.9: Response of V_{t1} with PI-PD control schemes in a two-area single-source IPS 3	2
Figure 3.10: Response of V_{12} with PI-PD control schemes in a two-area single-source IPS 3	3
Figure 3.11: Response of ΔP_{tie} with PI-PD control scheme in a two-area single-source IPS 3	4
Figure 3.12: Graphical comparisons of performance specifications of frequency deviation response	S
using PI-PD control schemes in a two-area single-source IPS	4
Figure 3.13: Graphical comparisons of performance specifications of terminal voltage responses using	g
PI-PD control schemes in a two-area single-source IPS	5
Figure 3.14: Three-area single-source IPS model with LFC and AVR loops	7
Figure 3.15: Response of Δf ₁ with PI-PD control schemes in a three-area single-source IPS3	9
Figure 3.16: Response of Δf ₂ with PI-PD control schemes in a three-area single-source IPS3	9
Figure 3.17: Response of Δf ₃ with PI-PD control schemes in a three-area single-source IPS 4	0
Figure 3.18: Response of V_{11} with PI-PD control schemes in a three-area single-source IPS	1
Figure 3.19: Response of V ₁₂ with PI-PD control schemes in a three-area single-source IPS	2
Figure 3.20: Response of V ₁₃ with PI-PD control schemes in a three-area single-source IPS	2
Figure 3.21: Graphical comparisons of performance specifications of frequency deviation response	S
using PI-PD control schemes in a three-area single-source IPS	3
Figure 3.22: Graphical comparisons of performance specifications of terminal voltage responses using	g
PI-PD control schemes in a three-area single-source IPS	1
Figure 3.23: Response of ΔP_{tiel} with PI-PD control schemes in a three-area single-source IPS4:	5
Figure 3.24: Response of ΔP _{te2} with PI-PD control schemes in a three-area single-source IPS4:	5
Figure 3.25: Response of ΔP_{te3} with PI-PD control schemes in a three-area single-source IPS 40	5
Figure 3.26: Response of Δf_1 with variations in T_1 using PI-PD control scheme in a three-area single	-
source IPS4	7
Figure 3.27: Response of Δf ₂ with variations in T ₁ using PI-PD control scheme in a three-area single	-
source IPS4	7

Figure 3.28: Response of Δf_3 with variations in T_t using PI-PD control scheme in a three-area single-
source IPS
Figure 3.29: Response of V_{t1} with variations in T_t using PI-PD control scheme in a three-area single-
source IPS48
Figure 3.30: Response of V_{12} with variations in T_t using PI-PD control scheme in a three-area single-
source IPS
Figure 3.31: Response of V_{13} with variations in T_t using PI-PD control scheme in a three-area single-
source IPS
Figure 3.32: Response of Δf_1 with variations in T_g using PI-PD control scheme in a three-area single-
source IPS
Figure 3.33: Response of Δf_2 with variations in T_g using PI-PD control scheme in a three-area single-
source IPS
Figure 3.34: Response of Δf_3 with variations in T_8 using PI-PD control scheme in a three-area single-
source IPS
Figure 3.35: Response of V_{t1} with variations in T_g using PI-PD control scheme in a three-area single-
source IPS
Figure 3.36: Response of V_{12} with variations in T_g using PI-PD control scheme in a three-area single-
source IPS
Figure 3.37: Response of V_{13} with variations in T_g using PI-PD control scheme in a three-area single-
source IPS
Figure 3.38: Graphical comparisons of performance specifications of frequency deviation and
terminal voltage responses (Settling Time) in a three-area single-source IPS with variations in T ₈ and
T _b
Figure 3.39: Graphical comparisons of performance specifications of frequency deviation responses
(Undershoot) in a three-area single-source IPS with variations in T _g and T _t
Figure 4.1: Power System
Figure 4.2: Transfer function model of boiler dynamics
Figure 4.3: Proposed control methodology
Figure 4.4: Flow chart of DO
Figure 4.5: Two-area multi-source IPS model without nonlinearities
Figure 4.6: Response of Δf1 with PI-PD control methodologies in a two-area multi-source IPS without
nonlinearities
Figure 4.7: Response of Δf ₂ with PI-PD control methodologies in a two-area multi-source IPS without
nonlinearities
Figure 4.8: Response of V_{t1} with PI-PD control methodologies in a two-area multi-source IPS without
nonlinearities

Figure 4.9: Response of V2 with PI-PD control methodologies in a two-area multi-source IPS without
nonlinearities
Figure 4.10: Response of ΔP_{te} with PI-PD control methodologies in a two-area multi-source IPS
without nonlinearities
Figure 4.11: Graphical comparisons of performance specifications of frequency deviation responses
using PI-PD control methodologies in a two-area multi-source IPS without nonlinearities71
Figure 4.12: Graphical comparisons of performance specifications of terminal voltage responses using
PI-PD control methodologies in a two-area multi-source IPS without nonlinearities
Figure 4.13: Graphical comparison of performance specifications of tie-line power deviation response
(ΔP_{tot}) using PI-PD control methodologies in a two-area multi-source IPS without nonlinearities 72
Figure 4.14: Two-area multi-source IPS model with nonlinearities
Figure 4.15: Response of Δf_1 with PI-PD control methodologies in a two-area multi-source IPS with
nonlinearities
Figure 4.16: Response of Δf_2 with PI-PD control methodologies in a two-area multi-source IPS with
nonlinearities
Figure 4.17: Response of V_{t1} with PI-PD control methodologies in a two-area multi-source IPS with
nonlinearities
Figure 4.18: Response of V_{12} with PI-PD control methodologies in a two-area multi-source IPS with
nonlinearities
Figure 4.19: Response of ΔP_{te} with PI-PD control methodologies in a two-area multi-source IPS with
nonlinearities
Figure 4.20: Graphical comparisons of performance specifications of frequency deviation responses
using PI-PD control methodologies in a two-area multi-source IPS with nonlinearities
Figure 4.21: Graphical comparisons of performance specifications of terminal voltage responses using
PI-PD control methodologies in a two-area multi-source IPS with nonlinearities
Figure 4.22: Graphical comparison of performance specifications of tie-line power deviation response
(ΔP_{ne}) using PI-PD control methodologies in a two-area multi-source IPS with nonlinearities 80
Figure 4.23: Three-area multi-source IPS model with nonlinearities
Figure 4.24: Response of Δf_i with PI-PD control methodologies in a three-area multi-source IPS with
nonlinearities
Figure 4.25: Response of Δf ₂ with PI-PD control methodologies in a three-area multi-source IPS with
nonlinearities
Figure 4.26: Response of Δf_3 with PI-PD control methodologies in a three-area multi-source IPS with
nonlinearities
Figure 4.27: Response of Vt1 with PI-PD control methodologies in a three-area multi-source IPS with
nonlinearities

Figure 4.28: Response of V_{12} with PI-PD control methodologies in a three-area multi-source IPS with
nonlinearities
Figure 4.29: Response of V ₁₃ with PI-PD control methodologies in a three-area multi-source IPS with
nonlinearities
Figure 4.30: Response of ΔP_{tel} with PI-PD control methodologies in a three-area multi-source IPS
with nonlinearities
Figure 4.31: Response of $\Delta P_{\text{he}2}$ with PI-PD control methodologies in a three-area multi-source IPS
with nonlinearities
Figure 4.32: Response of ΔP_{be3} with PI-PD control methodologies in a three-area multi-source IPS
with nonlinearities
Figure 4.33: Graphical comparisons of performance specifications of frequency deviation responses
using PI-PD control methodologies in a three-area multi-source IPS with nonlinearities92
Figure 4.34: Graphical comparisons of performance specifications of terminal voltage responses using
PI-PD control methodologies in a three-area multi-source IPS with nonlinearities
Figure 4.35: Graphical comparisons of performance specifications of tie-line power deviation
responses using PI-PD control methodologies in a three-area multi-source IPS with nonlinearities 94
Figure 5.1: Power System
Figure 5.2: Proposed control methodology
Figure 5.3: Flow chart of GBO
Figure 5.4: Response of Δf ₁ with GBO based control strategies in a four-area multi-source IPS 106
Figure 5.5: Response of Δf ₂ with GBO based control strategies in a four-area multi-source IPS 107
Figure 5.6: Response of Δf ₃ with GBO based control strategies in a four-area multi-source IPS 107
Figure 5.7: Response of Δf_4 with GBO based control strategies in a four-area multi-source IPS 108
Figure 5.8: Response of V_{11} with GBO based control strategies in a four-area multi-source IPS 109
Figure 5.9: Response of V_{12} with GBO based control strategies in a four-area multi-source IPS 110
Figure 5.10: Response of V_{13} with GBO based control strategies in a four-area multi-source IPS 110
Figure 5.11: Response of V_{14} with GBO based control strategies in a four-area multi-source IPS 111
Figure 5.12: Response of ΔP_{tiel} with GBO based control strategies in a four-area multi-source IPS 112
Figure 5.13: Response of ΔP_{tie2} with GBO based control strategies in a four-area multi-source IPS 113
Figure 5.14: Response of ΔP_{he3} with GBO based control strategies in a four-area multi-source IPS 113
Figure 5. 15: Response of ΔP_{te4} with GBO based control strategies in a four-area multi-source IPS 114
Figure 5.16: Graphical comparisons of performance specifications of frequency deviation responses
using GBO based control strategies in a four-area multi-source IPS
Figure 5.17: Graphical comparisons of performance specifications of terminal voltage responses using
GBO based control strategies in a four-area multi-source IPS

Figure 5.18: Graphical comparisons of performance specifications of tie-line power deviation
responses using GBO based control strategies in a four-area multi-source IPS
Figure 5.19: Response of Δf_1 with $\pm 25\%$ variations in system parameters using GBO based control
strategy in a four-area multi-source IPS
Figure 5.20: Response of Δf_2 with $\pm 25\%$ variations in system parameters using GBO based control
strategy in a four-area multi-source IPS
Figure 5.21: Response of Δ/3 with ±25% variations in system parameters using GBO based control
strategy in a four-area multi-source IPS
Figure 5.22: Response of Δf_4 with $\pm 25\%$ variations in system parameters using GBO based control
strategy in a four-area multi-source IPS
Figure 5.23: Graphical comparisons of performance specifications of frequency deviation responses
with ±25% variations in system parameters using GBO-PID control strategy in a four-area multi-
source IPS
Figure 5.24: Response of V_{t1} with $\pm 25\%$ variations in system parameters using GBO based control
strategy in a four-area multi-source IPS
Figure 5.25: Response of V_{12} with $\pm 25\%$ variations in system parameters using GBO based control
strategy in a four-area multi-source IPS
Figure 5.26: Response of V_{13} with $\pm 25\%$ variations in system parameters using GBO based control
strategy in a four-area multi-source IPS
Figure 5.27: Response of V_{14} with $\pm 25\%$ variations in system parameters using GBO based control
strategy in a four-area multi-source IPS
Figure 5.28: Graphical comparisons of performance specifications of terminal voltage responses with
±25% variations in system parameters using GBO-PID control strategy in a four-area multi-source
IPS
Figure 5.29: Response of ΔP_{tie1} with ±25% variations in system parameters using GBO based control
strategy in a four-area multi-source IPS
Figure 5.30: Response of ΔP_{tie2} with ±25% variations in system parameters using GBO based control
strategy in a four-area multi-source IPS
Figure 5.31: Response of ΔP_{tie3} with ±25% variations in system parameters using GBO based control
strategy in a four-area multi-source IPS
Figure 5.32: Response of ΔP_{tre4} with ±25% variations in system parameters using GBO based control
strategy in a four-area multi-source IPS
Figure 5.33: Graphical comparisons of performance specifications of tie-line power deviation
responses with ±25% variations in system parameters using GBO-PID control strategy in a four-area
multi-source IPS

LIST OF TABLES

Table 3.1: Parameters setting of MPSO, LPBO, and AOA
Table 3.2: Optimal values of controller parameters for a two-area single-source IPS
Table 3.3: Performance specifications of frequency deviation responses in a two-area single-source
IPS
Table 3.4: Performance specifications of terminal voltage responses in a two-area single-source IPS 33
Table 3.5: Optimal values of controller parameters for a three-area single-source IPS
Table 3.6: Performance specifications of frequency deviation responses in a three-area single-source
IPS40
Table 3.7: Performance specifications of terminal voltage responses in a three-area single-source IPS
Table 3.8: Settling time responses using PI-PD control scheme with variations in system parameters 53
Table 3.9: Overshoot and undershoot responses using PI-PD control scheme with variations in system
parameters53
Table 4.1: Parameters setting of AOA, LPBO, MPSO, and DO
Table 4.2: Optimal values of controller parameters for a two-area multi-source IPS without
nonlinearities
Table 4.3: Performance specifications of frequency deviation responses in a two-area multi-source
IPS without nonlinearities
Table 4.4: Performance specifications of terminal voltage responses in a two-area multi-source IPS
without nonlinearities
Table 4.5: Performance specifications of tie-line power deviation responses in a two-area multi-source
IPS without nonlinearities
Table 4.6: Optimal values of controller parameters for a two-area multi-source IPS with nonlinearities
Table 4.7: Performance specifications of frequency deviation responses in a two-area multi-source
IPS with nonlinearities
Table 4.8: Performance specifications of terminal voltage responses in a two-area multi-source IPS
with nonlinearities
Table 4.9: Performance specifications of tie-line power deviation responses in a two-area multi-source
IPS with nonlinearities
Table 4.10: Optimal values of controller parameters for a three-area multi-source IPS with
nonlinearities
Table 4.11: Performance specifications of frequency deviation responses in a three-area multi-source
IPS with nonlinearities

Table 4.12: Performance specifications of terminal voltage responses in a three-area multi-source IPS
with nonlinearities
Table 4.13: Performance specifications of tie-line power deviation responses in a three-area multi-
source IPS with nonlinearities
Table 5.1: Optimal values of controller parameters for a four-area multi-source IPS 105
Table 5.2: Performance specifications of frequency deviation responses in a four-area multi-source
IPS
Table 5.3: Performance specifications of terminal voltage responses in a four-area multi-source IPS
Table 5.4: Performance specifications of tie-line power deviation responses in a four-area multi-
source IPS
Table 5.5: Performance specifications of frequency deviation responses with ±25% variations in
system parameters using GBO-PID control strategy in a four-area multi-source IPS
Table 5.6: Performance specifications of terminal voltage responses with ±25% variations in system
parameters using GBO-PID control strategy in a four-area multi-source IPS
Table 5.7: Performance specifications of tie-line power deviation responses with ±25% variations in
system parameters using GBO-PID control strategy in a four-area multi-source IPS

LIST OF ABBREVIATIONS

AOA Archimedes Optimization Algorithm Nonlinear Threshold Accepting Algorithm **NLTA** Automatic Voltage Regulator AVR PI-PD Proportional Integral-Proportional Derivative **MPSO Modified Particle Swarm Optimization** Interconnected Power System IPS **LPBO** Learner Performance based Behavior Optimization **LFC Load Frequency Control** DO **Dandelion Optimizer** GRC Generation Rate Constraint I-P Integra-Proportional SLP Step Load Perturbation Proportional Integral Derivative PID

Hybridized Approach of the Artificial Electric Field Algorithm

GDB Governor Dead Band

BD Boiler Dynamics

Abbreviation

HAEFA

Definition

GBO Gradient Based Optimizer

I-PD Integral -Proportional Derivative

TID Tilt Integral Derivative

IPS Interconnected Power System

IPFC Interline Power Flow Controller

UPFC Unified Power Flow Controller

SMES Superconducting Magnetic Energy Storage

RFB Redox Flow Battery

FESS Flywheel Energy Storage System

CES Capacitive Energy Storage System

UC Ultra Capacitor

HVDC High Voltage DC

ADRC Active Disturbance Rejection Control

SMC Sliding Mode Control

ANN Artificial Neural Network

FLC Fuzzy Logic Controller

PSS Power System Stabilizer

MPC Model Predictive Controller

Z-N Ziegler-Nichols

GA Genetic Algorithm

FA Firefly Optimization

FDO Fitness Dependent Optimizer

BFO Bacterial Foraging Optimization

HHO Harris Hawks Optimization

DE Differential Evolution

MFO Moth Flame Optimization

GWO Grey Wolf Optimizer

LSA Lightning Search Algorithm

GOA Grasshopper Optimization Algorithm

SCA Sine Cosine Algorithm

MOL Many Optimizing Liaisons Algorithm

ABC Artificial Bee Colony

AFA Artificial Flora Algorithm

WOA Whale Optimization Algorithm

LUS Local Unimodal Sampling

ITSE Integral of Time multiplied by the Square of Error

s-s Steady-State

LIST OF SYMBOLS

Symbol	Definition
\mathbf{R}_{i}	Speed regulation of hydro power plant in ith area
\mathbf{B}_{i}	Area bias factor in ith area
$V_{t(i)}$	Terminal voltage in i th area
$\Delta V_{t(i)}$	Deviation in terminal voltage in ith area
Δfi	Frequency deviation in i th area
$\Delta P_{tic(i)}$	Tie-line power deviation in ith area
$V_{s(i)}$	Sensor voltage in ith area
$\Delta P_{D(l)}$	Load deviation in ith area
$K_{\mathbf{g}}$	Gain of hydro governor
$T_{\mathbf{g}}$	Time constant of hydro governor
K_t	Gain of hydro turbine
T_t	Time constant of hydro turbine
G_{l}	ith cross coupling coefficient for AVR and LFC loops
R_t , R_h , R_g , R_w	Speed regulation of thermal reheat, hydro, gas, and wind power plants
T_{gr}	Time constant of speed governor
Kre	Gain of reheat steam turbine
T_{re}	Time constant of reheat steam turbine
T_{tr}	Time constant of thermal turbine
T_h	Main servo time constant
T_{rs}	Speed governor rest time
T_{rh}	Transient droop time constant
$T_{\mathbf{w}}$	Water time constant
X	Speed governor lead time constant
Y	Speed governor lag time constant
a,b,c	Valve positional time constant

T_{CR} Combustion reaction time delay

T_f Fuel time constant

T_{CD} Compressor discharge volume time constant

 T_{w1} , T_{w2} Wind turbine time constants

 K_{w1} , K_{w2} Wind plant gain constants

K_{PV} Solar PV gain constant

T_{PV} Solar PV time constant

 T_p or T_{ps} Time constant of power system

K_p or K_{ps} Gain of power system

K_a Gain of amplifier

T_a Time constant of amplifier

T_e Time constant of exciter

Ke Gain of exciter

T_g Time constant of generator field

K_g Gain of generator field

T_s Time constant of voltage sensor

K_s Gain of voltage sensor

K_l ith cross coupling coefficient for AVR and LFC loops

Ps Synchronizing power coefficient

 T_y Tie-line synchronizing time constants (for $i \neq j$)

H Inertia constant

D Frequency sensitive load coefficient

K_{LFC} (s) Transfer function of the controller of LFC loop

K_{AVR} (s) Transfer function of the controller of AVR loop

CHAPTER 1

Introduction

This chapter presents a brief description of load frequency control and automatic voltage regulation in an interconnected power system. Moreover, problem statement, objectives of research and organization of the thesis are also provided in this chapter.

1.1 Overview

The power system is built by interconnecting several complex electrical networks that include power generation, transmission and distribution systems. Due to an increase in power demand, power grids operate as multi-area multi-source interconnected power systems (IPSs). These multi-area multi-source systems are connected through AC tie-line. Due to the increasing share of renewable energy and load demand, the complexity of IPS is increasing. This leads to power quality issues, e.g. slow settling times and increased transient components in voltage, frequency, and tie-line power deviation responses. In a power system, it is critical to keep the electrical power at the desired voltage and frequency so that the devices connected to the power system will operate smoothly. The advantage of IPS is that in the event of a failure of a particular generating unit, power can be provided from one area to other areas. In a power system, load is always dynamic and changes with time. The difference between generation and load demand leads to an imbalance between reactive and active power of the system. This imbalance leads to fluctuations in voltage, frequency, and tie-line power. Over- and under-voltages can damage electrical equipment, while under- and over-frequency incidents can cause historic power outages.

An efficient power system must be able to satisfy customer demand at all times while balancing load demand [1]. Active power affects the frequency of the system, while reactive power depends on the system voltage. Two control loops, such as an automatic voltage regulator (AVR) and load frequency control (LFC) are integrated into a power system to maintain power at rated voltage and frequency respectively. The AVR and LFC loops are coupled together to control the terminal voltage and load frequency simultaneously. The AVR control loop essentially reduces the voltage fluctuations to meet the reactive power demand using generator excitation, while the LFC control loop reduces the frequency fluctuations by changing the magnitude of the active power through its governor action as shown in Figure 1.1 [2]. Δf and V_t denote the load frequency and terminal voltage respectively.

To ensure the stability of the power system, the frequency and terminal voltage should be kept within the prescribed limits. When generation exceeds load demand, frequency increases above a certain value and vice versa. In this case, governing action is used to adjust supply to demand. The change in terminal voltage is controlled by adjusting the excitation current of the generator field before the reactive power loads the system. Voltage and frequency controllers have become more important with the growth of interconnected power systems to make power system operation more reliable. Moreover, the performance of voltage and frequency controller depends on their tuning. Therefore, both the controller design and the tuning method are very important for the optimal control of an IPS. To reduce frequency, terminal voltage, and tie-line power deviations in the interconnected power system, the development of an effective control design is always essential.

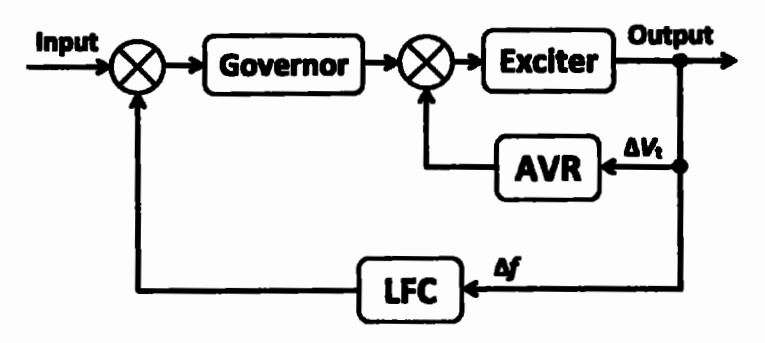


Figure 1.1: Combined Model of LFC-AVR

1.2 Problem Statement

The investigation of LFC and an AVR control loops allows a combined control of load frequency and terminal voltage in a multi-area multi-source IPS. Due to the dynamic load behavior and the proliferation of renewable energy sources in the existing IPS, it is a very difficult task for the control and power engineers to supply all loads with the desired voltage and frequency. An efficient and reliable control approach is always required to minimize voltage, frequency, and tie-line power deviations under such conditions. Numerous studies have been presented on individual and combined control of LFC and AVR control loops in IPSs. After an extensive literature search, it was found that combined AVR and LFC systems have been studied very rarely compared to individual AVR or LFC systems. This served as motivation for the authors to investigate multi-area multi-source IPSs to control terminal voltage and load frequency using LFC and AVR systems.

This study combines the analysis of LFC and AVR control loops in two-, three- and four-area IPSs, which include hydro, thermal reheat, gas, wind, and solar photovoltaic

systems. In addition, nonlinearities including boiler dynamics (BD), governor dead band (GDB), and generation rate constraint (GRC) were included in multi-area multi-source IPSs for more realistic studies. TID, I-P, PID, PI-PD, and I-PD controllers have been successfully explored for effective control of load frequency and terminal voltage in different IPSs. Numerous engineering optimization problems have been solved in recent years using nature-inspired computational algorithms. In addition, the parameters of controllers have also been tuned using these methods. In this research study, recently discovered nature-inspired computational algorithms, including the dandelion optimizer (DO), gradient based optimizer (GBO), learner performance based behavior algorithm (LPBO), Archimedes optimization algorithm (AOA), and modified particle swarm optimization (MPSO) were successfully used to tune the proposed controllers. The integral of time multiplied by the square of error (ITSE) was used as an error index to formulate the cost functions of proposed control methods. In addition, extensive comparisons were made between the proposed and other control strategies to verify the effectiveness of the suggested control approaches.

1.3 Objectives of Research

The main objectives of the research are given below.

- > To develop mathematical models for combined LFC and AVR loops in multi-area multisource IPSs including two-area, three-area, and four-area with diverse generation units including thermal reheat, hydro, gas, wind, and solar generation units.
- > To deduce mathematical models of multi-area multi-source IPS with various nonlinearities including GRC, GDB, and BD.
- > Design and implementation of controllers including PI-PD, I-PD, I-P, PID, and TID.
- > Optimization of controller parameters using nature-inspired computation algorithms including GBO, DO, LPBO, AOA, and MPSO.
- > Comprehensive comparative analysis between different control methods.

1.4 Organization of the Thesis

This thesis consists of six chapters. The chapter-wise description of the thesis is summarized as follows:

Chapter 1: This chapter gives a brief introduction to AVR and LFC loops in IPS. It also describes the motivation for this work, the problem statement, and the goals of this research.

Chapter 2: This chapter contains a detailed literature review of AVR and LFC loops in different IPS under different conditions.

Chapter 3: In this chapter, the design and implementation of PI-PD for the combined control of LFC and AVR control loops in a two- and three-area IPS are discussed. The gains of the proposed PI-PD controller were determined using LPBO, AOA, and MPSO algorithms. Initially, the proposed control methods were applied to a two-area IPS with hydro plant in each area. After successful results in a two-area IPS, the proposed methodology was applied to a three-area IPS. Finally, the reliability and effectiveness of the proposed method was investigated in a three-area IPS with variations of system parameters in a range of ±50%.

Chapter 4: It deals with the combined control of AVR and LFC loops in two- and three-area IPS with PI-PD controller considering various nonlinearities such as BD, GRC and GDB. The gains of the proposed PI-PD controller were obtained using DO, LPBO, AOA and MPSO algorithms. First, the proposed control methods were applied to two-area IPS with hydro, thermal reheat and gas generation units in each area. Then, the proposed control approaches were applied to two- and three-area IPS with nonlinearities such as BD, GDB and GRC to obtain more realistic and practical studies.

Chapter 5: This chapter is about the use of PID, I-PD, I-P and TID controllers to control LFC and AVR control loops in a four-area IPS. The gains of the controllers were determined using the GBO method. The proposed control method was applied to a four-area IPS, which has different generating units in each of the four areas, including hydro, thermal reheat, gas, wind, and solar photovoltaic power plants. A sensitivity analysis was performed by varying the parameters of the four-area IPS within a range of ±25% to demonstrate the robustness of the proposed GBO-PID control mechanism.

Chapter 6: This will include an evaluation of the major contributions of the work covered in the thesis. It also discusses the scope of future AVR and LFC work in multi-area IPSs.

CHAPTER 2

Literature Review

This chapter presents the summary of literature survey relevant to combined and individual study of LFC and AVR loop in different interconnected power systems.

In a power system, the demand of active and reactive power is never constant; it changes frequently with varying load conditions. The power supply must meet certain basic requirements for voltage and frequency constancy. To keep load frequency and terminal voltage constant and trouble-free, LFC and AVR control loops incorporated in IPS. The LFC loop modifies the frequency and amplitude of the active power, while the AVR loop mainly controls the terminal voltage and reactive power. The LFC loop eliminates frequency fluctuations through its regulator, while the AVR loop reduces voltage fluctuations by using generator excitation. In combined LFC and AVR operation, both the AVR and LFC loops are cross-coupled. Various control strategies for combined control of voltage and frequency using AVR and LFC loops have been presented in the past. A brief description of these control strategies is given in the next section.

2.1 Combined Study of AVR and LFC Systems

Aditi Gupta et al. proposed PI and I controllers with damper winding for the AVR and LFC loops respectively in a single-area IPS. According to simulation studies, the system response was improved in terms of settling time, undershoot and overshoot [2]. Satish Kumar and Lalit Chandra explored a harris hawks optimization (HHO) based two degrees of freedom (2DOF) based tilt integral derivative (TID) controller for simultaneous control of terminal voltage and load frequency in a three-area IPS with nonlinearities including GDB and GRC. In each area, electric vehicles, combined cycle power plant (CCPP), and single-stage thermal plants with reheat turbine were considered. The performances of TID and PIDF controller were compared with proposed controller in the presence random and sinusoidal load variations. The strength of the proposed controller was also evaluated using sensitivity analysis [3].

Chandrakala and Balamurugun investigated PID controllers based on Ziegler-Nichols (Z-N) and simulated annealing (SA) to control terminal voltage and load frequency in a two-area IPS. The proposed approach provided a response with a steady state error of zero and a lower settling time [4]. Gupta and Srivastava studied the hybrid controller of neural network (NN) and fast traversal filter (FTF) for load frequency and terminal voltage control in a

single-area IPS. The proposed control scheme required few data samples for the weight training process, which ultimately increased the speed response of the system [5].

Z-N based PID and fuzzy logic controllers (FLCs) were examined by Devashish Sharma et al. to stabilize terminal voltage and load frequency in a single-area IPS. The system's dynamic behavior has been enhanced in terms of settling time, overshoot and damping oscillations [6]. Rumi and Lalit employed lightning search algorithm (LSA) based PI with fractional derivative and filter (PID^uF) and PID with filter (PIDF) controller for two-area IPS. There were several nonlinearities in the power system including GRC and GDB. In addition, IPS also included interline power flow controller (IPFC) and superconducting magnetic energy storage (SMES) systems. The comparative analysis showed that the proposed control technique was superior to the classical controllers [7].

Deepak and Ajit investigated a moth flame optimization (MFO) based fractional-order PID (FOPID) controller for a two-area IPS. By comparing the dynamic performance of the optimized PID controller with other techniques, the superiority and effectiveness of the recommended MFO-FOPID control scheme was demonstrated [8]. K. Sahani et al. proposed a firefly optimization (FA) based PID controller for combined control of terminal voltage and load frequency in a two-area IPS. Each control area had thermal and hydroelectric power units. The effectiveness of the proposed control approach over existing meta-heuristic methods was made clear through a comparison [9].

Javed and Zahra examined a hybrid dynamic model for combined analysis of LFC and AVR systems in a single-area IPS with GDB and GRC nonlinearities. The LFC system consists of the liberalized Phillips-Heffron model while excitation loop has a power system stabilizer (PSS). Damped control and time domain simulations were used to assess the dynamic performance of suggested control approach. Simulation results have shown that the proposed method is highly reliable under various loading conditions [10].

Kalyan and Rao investigated the response of a two-area IPS for a combined study of AVR and LFC loops. A PID controller based on the differential evolution and artificial electric field (DE-AEFA) approach was used for optimal control of IPS. A parallel high voltage DC (HVDC) link to the existing AC was also built to further increase the efficiency of the system. A sensitivity analysis was also performed to demonstrate the adaptability of the suggested control strategy [11].

Kalyan and Rao suggested a DE-AEFA based PID controller for simultaneous stabilization of load frequency and terminal voltage in a two-area-IPS. To further improve the

dynamic behavior of IPS, redox flow batteries (RFBs) were installed in both areas and an IPFC was installed in the tie-line. The results of the simulations clearly demonstrate the effectiveness of RFBs and IPFC in reducing tie-line, terminal voltage and load frequency deviations [12]. Abhineet and Parida studied the behavior of thermal reheat and non-reheat systems in two-area IPS to control AVR and LFC loops. They investigated PI and PIDF controllers to control terminal voltage and load frequency respectively. The ideal parameters of PI and PIDF controllers were found using the sine cosine algorithm (SCA). The IPS included unified power flow controller (UPFC) and RFBs to further optimize system dynamics. A sensitivity study was carried out by modifying the system parameters to demonstrate the versatility of the PIDF and PI controllers [13].

Nabil Nahas et al. studied a PID controller based on a nonlinear threshold accepting algorithm (NLTA) for effective control of load frequency and terminal voltage in a two-area IPS. The proposed control strategy performed much better than previous heuristics and internal model based control methods in uncertain dynamic environments [14] Naga Sai Kalyan proposed a grey wolf optimizer (GWO) based proportional integral double derivative (PIDD) controller for terminal voltage and load frequency stabilization in a two-area IPS. The suggested PIDD controller's performance was compared to that of the PI, PID, and PIDN controllers. The dynamic performance of IPS was further improved by integrating SMES devices with UPFC in tie-line [15].

Pachunoori Anusha et al. investigated a FA based PID controller for stabilization of terminal voltage and load frequency control in a two-area IPS with TD, GRC, GDB nonlinearities. The response of FA-PID was compared with PI and I controllers. The PID controller outperformed the PI, PI, and I controllers in terms of frequency, terminal voltage, and tie-line power variations [16]. Stephen Oladipo et al. explored an accelerated PID controller (PIDA) to control load frequency and terminal voltage in a single-area IPS. PIDA was tuned with a hybridized pathfinder algorithm (PFA) and pollinated algorithm (FPA). The obtained results showed that the proposed control scheme outperformed several other controllers such as FPA-PID, MFO-PID, PSO-PID, GA-PID, and TLBO (Teaching and Learning Based Optimization) based PIDN controllers [17].

Satish and Lalit employed a tilt-integral-derivative with filter (TIDF) controller based on HHO for combined control of AVR and LFC loops in a three-area IPS with GDB and GRC nonlinearities. Each IPS area included a thermal plant with reheat turbine and combined cycle gas turbine (CCGT) plant. The comprehensive analysis clearly demonstrated that the

proposed TIDF controller outperforms both the PI and PID controllers. A hardware configuration in a three-area IPS was used to further investigate the performance of the proposed control technique [18]. Sheikh Safiullah et al. developed an active disturbance rejection control (ADRC) strategy based on a second-order error-driven control law for terminal voltage and load frequency stabilization in a three-area IPS. The IPS included solar, thermal, geothermal, and wind power units. An IEEE-39 bus system was used to validate the comparison between PID and ADRC. Due to its strong ability to suppress disturbances, an ADRC controller was found to be better than a PID controller in terms of controlling system dynamics [19].

Satish Kumar et al. investigated the performance of a two degree of freedom (2DOF) integral-tilt derivative with filter (I-TDF) controller based on HHO for combined control of load frequency and terminal voltage in a three-area IPS. It was found that the proposed control strategy performed better compared to TID and TIDF controllers. The suggested controller's efficacy was tested using random load disturbances. The resilience of the proposed controller was clearly demonstrated by studying the system behavior when system parameters were changed [20]. Biswanath Dekaraja proposed artificial flora algorithm (AFA) based cascaded fuzzy PD-tilt integral derivative (CFPD-TID) controller for the combined analysis of AVR and LFC loops in a three-area IPS. The effects of RFBs and HVDC links on the dynamics of a three-area IPS were also discussed. Compared to TID and CPD-TID controllers, the proposed controller CFPD-TID improved the system dynamics in terms of settling time, undershoot and overshoot [21].

Biswanath Dekaraja et al. designed a cascaded fractional order tilt derivative with filter (FOTDF) and fractional order proportional derivative with filter (FOPDN) controller for efficient control of AVR and LFC loops in a two-area IPS. The IPS included hydro and dishstirring solar thermal system in area-1 whereas solar thermal and thermal power generation units in area-2. The best parameters of the proposed controller were determined using AFA. The investigations clearly showed that the proposed control method performed better than TIDN and PIDN controllers [22].

Biswanath Dekaraja et al. proposed a cascaded proportional derivative with filter (PDN) and fractional order PID with filter (FOPIDN) for load frequency and terminal voltage stabilization in a three-area IPS. The best parameters of the proposed controller were determined using AFA. The impact of various energy storage technologies such as SMES devices, RFBs, capacitive energy storage systems (CES) and flywheel energy storage systems

(FESS) was also investigated with the inclusion of the HVDC link. The proposed CPDN-FOPIDN controller provided lower values for settling time, overshoot, and undershoot than the FOPIDN controller. The study results showed that RFBs provide better system performance compared to FESS, CES, and SMES devices [23]. Hady H. Fayek and Eugen Rusu explored accelerated PID (PIDA) controller based on doctor and patient optimization (DPO) for terminal voltage and load frequency control in two interconnected sustainable micro grids. Solar energy and biofuels were used to power the two micro grids. The micro grid had the capability of storing energy. The results showed that the proposed control strategy exhibited relatively better response compared to other control techniques [24].

Naga Sai Kalyan et al. employed the hybridized artificial electric field algorithm (HAEFA) to tune the fuzzy PID controller to stabilize load frequency and terminal voltage in a two-area IPS. In addition, various energy storage systems such as SMES, RFBs, and ultra capacitors (UCs) have been considered in IPS. The performance comparison between fuzzy PID and other controllers such as PI and PID showed that the proposed fuzzy PID with the inclusion of RFBs was superior in reducing terminal voltage and load frequency deviations [25]. Arabinda Ghosh et al. investigated a PID controller based on hybridized particle swarm optimization (PSO) and Ziegler-Nichols (Z-N) method for terminal voltage and load frequency stabilization in a two-area IPS. The performance of the proposed method was compared with fuzzy PID, fuzzy PI, and PI controllers. In addition, the uncertainty of the system parameters was introduced to evaluate the robustness of the proposed strategy. It was found that the proposed control approach quickly led to better results [26].

Chandrashekar and Jayapal studied PI, PID, and FLC in a deregulated two-area IPS, which included thermal, wind, and solar power units. Simulation results showed that FLC performed better than other controllers for both variable and constant distributed participation matrices (DPMs) in terms of overshoot and settling time [27]. Grover et al. designed a PI controller based hardware-in-loop (HIL) strategy for combined control of AVR and LFC loops in a single-area IPS under various load conditions. The PI based control method was developed for continuous operation. The proposed control method was successful in reducing the variations of frequency and terminal voltage [28].

Ghassan Abdullah et al. proposed a PID controller for terminal voltage and load frequency control in a single-area IPS. The PID controller was tuned with nature-inspired computational methods such as FA, Z-N, PSO and genetic algorithm (GA). Comparison of the results showed that FA-PID performed better in controlling frequency and terminal

voltage deviation [29]. Nour Yakine Kouba et al. successfully studied a PSO based PID control for AVR and LFC loops in a two-area IPS. The proposed method proved to be very successful when the results of PSO-PID were compared with those of bacterial foraging optimization (BFO), GA, and Z-N methods [30].

Rumi Rajbongshi et al. investigated the effectiveness of a PSS and proposed a LSA based fractional-order (PI^ADF) controller in a three-area IPS with nonlinearities such as GRC, TD and GDB. It was found that PI^ADF with PSS improved the system dynamics by reducing oscillations [31]. Reza Mohammadikia et al. investigated the model predictive control (MPC) technique to increase the efficiency of LFC and AVR control loops in a two-area IPS with different load disturbance in each area. The proposed control technique outperformed the PI and PID controllers in both steady-state and transient performance [32].

Rumi and Lalit developed a LSA based fractional integral derivative controller with filter (FOIDF) to control AVR and LFC loops in a three-area IPS. IPS had diesel, solar, thermal, wind, and thermal with reheat turbine power units. Various nonlinearities including GRC and GDB were also included in IPS. The response of IPS was improved by including various energy storage systems including SMES and CES in coordination with IPFC and flexible AC transmission systems (FACTS) devices. The comparison clearly showed the superiority of FOIDF over the other control methodologies. Moreover, it can be concluded that IPFC-SMES scheme worked more effectively than IPFC-CES [33].

Srikanth Goud et al. designed PID controller based on seagull optimization algorithm (SOA) to control AVR and LFC loops in a multi-area IPS. In addition, SMES and battery energy storage (BES) devices were successively incorporated into the system. The efficiency of the suggested controller was clearly demonstrated when compared to other controllers. The simulation results showed that the SMES based SOA-PID responded effectively compared to the BES based SOA-PID control strategy [34]. Vineet Kumar et al. presented a HHO based MPC to control load frequency and terminal voltage in a three-area IPS with nonlinearities. In addition, dynamic energy storage technologies such as virtual inertia and redox flow battery (VI-RFB) had been incorporated into the IPS. The robustness of the proposed HHO-MPC controller with VI-RFB was successfully illustrated by simulation results [35].

Ahmed Hossam-Eldin et al. proposed a fuzzy proportional integral derivative double derivative (FPIDD2) controller based gradient based optimization (GBO) algorithm for terminal voltage and load frequency control loops in a two-area IPS. The IPS had different power units such as thermal, gas, hydraulic, wind, solar with nonlinearities including GRC

and GDB. The dynamic responses of GBO-FPIDD2 were compared with the GBO tuned integral derivative-tilt controller (ID-T). The performance comparison clearly depicted that the FPIDD2 controller has a higher ability to reduce terminal voltage and load frequency deviations in both areas than the GBO-ID-T controller [36]. Sheikh Safiullah et al. explored a integral double derivative (IDD) controller based on novel state observer (SO) for simultaneous terminal voltage and load frequency stabilization in a three-area IPS with nonlinearities. The hybrid system included different generating units such as electric vehicle (EV), diesel, thermal, and solar thermal. The system parameters were changed in order to conduct a comprehensive sensitivity analysis to test the robustness of the suggested control mechanism [37].

Mausri Bhuyan et al. investigated a dynamic butterfly optimization algorithm (DBOA) based cascaded PI-TID controller for terminal voltage and load frequency stabilization in a single-area IPS. The hybrid system was modeled using solar chimney, hybrid electric vehicle, solar gas turbine, and biodiesel-fueled generator. To show the efficacy of the suggested technique, simulations were carried out with uncertainties to obtain dynamic responses [38]. Sheikh Safiullah et al. developed a magnetotactic bacterial optimization (MBO) and artificial neural network (ANN) based second order ADRC for combined terminal voltage and load frequency stabilization in a multi-area and standard IEEE-39 bus IPS. The IPS had wind and solar thermal units. Advanced electric vehicles (EVs) were also included in the system for energy storage purposes. The simulation results showed that the second-order controller ANN-ADRC performed relatively better than the controller MBO-ADRC [39].

Vincet Kumar et al. recommended a HHO based MPC for performance enhancement of AVR and LFC loops in a multi-area IPS. The effectiveness of suggested control strategy was confirmed by evaluating the transient response of the proposed MPC-HHO algorithm with different controllers such as IDDF, PID, fuzzy PID, and FOPID controllers [40]. Soundarrajan et al. designed a PSO based PID controller for an AVR and LFC system in a single-area IPS. The results depicted that the proposed technique has superior characteristics such as ease of implementation, robust convergence, and high computational efficiency compared to traditional PID, fuzzy, and GA based controllers. In addition, the performance of the proposed control strategy was improved in terms of lower oscillations, overshoot and settling time [41].

Ahmad M. Hamza et al. explored PID controller based on BFO and Z-N control methods for the analysis of LFC and AVR loops in a single-area IPS. The performance comparison revealed that the response of BFO-PID controller is better than the Z-N-PID controller in terms of settling time and overshoot [42]. Nour EL Yakine Kouba et al. proposed a PSO based PID controller for combined load frequency and terminal voltage control in a two-area IPS. The results were compared with Z-N, GA, and BFO. The proposed approach was found to be more effective than other [43]. Srivastava and Gupta suggested a hybridized gaussian mixture model (GMM) and generalized fuzzy model (GFM) based controller for terminal voltage and load frequency stabilization in a single-area IPS. The proposed controller used GMM to optimize the membership functions and GFM to compute the desired output in a single iteration. The results of the simulations and comparative analyses have shown that the suggested control approach is capable of successfully controlling the terminal voltage and load frequency [44].

Nour EL Yakine Kouba et al. investigated a bat algorithm (BA) based PID controller to improve the responses of LFC and AVR control loops in a three-area IPS. The efficacy of the suggested control strategy was demonstrated by comparing the results with those of artificial bee colony (ABC), Z-N, BFO, PSO, and GA based PID controllers. The response of IPS was analyzed by varying the SLP in each area to confirm the robustness of the proposed control strategy. The feasibility of the BA-PID controller to solve the LFC-AVR problem was demonstrated by the results of the sensitivity analysis [45]. Soundarrajan et al. studied PID controllers based on PSO and its variants such as multi-objective PSO and stochastic PSO for terminal voltage and load frequency stabilization in a single-area IPS. The proposed controllers provided improved performance in terms of settling time and overshoot indicating that the proposed controllers can effectively adapt to dynamic load conditions [46]. Mohsen Azizi et al. designed a μ-synthesis strategy based robust distributed controller for effective control of AVR and LFC loops in an islanded micro grid with multiple distributed generation units. The proposed control method included many local droop controllers and an independent decentralized robust controller. The efficiency of the proposed controller design was proven by simulation results [47].

2.2 Study of Individual LFC Systems

A number of control methods have already been published for individual frequency control using an LFC control loop. Some of these methods are presented in this section. Sheetla Prasad et al. investigated the combination of nonlinear sliding mode control (SMC)

and generalized extended state observer (GESO) for an LFC system in a two-area IPS to study the frequency deviation problem. The purpose of GESO was to estimate the state and disturbance and reject the system disturbance. Considering random load disturbances, the performance of the proposed observer based controller was confirmed and compared with ADRC. The performance of the proposed control scheme was also evaluated in the presence of GRC and GDB nonlinearities. From the simulation results, it was clear that the proposed control scheme is very robust in the presence of nonlinearities and disturbances [48].

M. D. Pabitra et al. explored a PID controller based on the many optimizing liaisons (MOL) algorithm for a two-area IPS with a thermal system without reheat and GDB nonlinearity. The superiority of MOL-PID was confirmed by comparing its performance in transient analysis with that of the CPSO-PI controller [49]. Jianping Guo presented an adaptive SMC technique for an LFC system in a three-area IPS. The effectiveness of the proposed technique was verified by numerical simulations and comparison of its response with the classical SMC method. The overshoot and chattering responses, etc., clearly indicated the superiority of the proposed adaptive SMC technique over the classical SMC [50]. The two degrees of freedom based PID controller (2DOF-FOPID) has been applied by Sabita Tripathy et al. for frequency control in a two-area IPS consisting of thermal dishsterling solar, conventional steam, and geothermal power plants. The optimal gains of the proposed controller were found using the grasshopper optimization algorithm (GOA). The performance comparison between the 2DOF-FOPID and the classical PID controller clearly exhibited the effectiveness of the proposed 2DOF-FOPID controller [51].

The fuzzy-aided PID controller was employed by P. C. Sahu et al. for load frequency control in a multi-area IPS with nonlinearities. To find the optimal gain coefficients of the fuzzy-aided PID controller, the modified SCA was used. The proposed methodology was applied to IPS with three and five areas respectively. Nonlinearities such as GDB, GRC, BD, and TD were included in the five-area controller IPS for more realistic study. The responses of the fuzzy-aided PID controller were compared with different controllers such as PID and PI, etc. The performance comparison shows that the fuzzy PID controller is superior compared to other controllers [52]. Sheetla Prasad et al. suggested an effective control law for optimal control of three-area IPS in the presence of GDB and GRC nonlinearities. The simulation results were compared with linear sliding mode controllers. It was clearly found that the proposed strategy provided a response with minimal overshoot/undershoot and

quicker settling time. Moreover, the damping characteristics of the system were effectively changed as a function of the load disturbances and uncertainties [53].

Ajithapriyadarsini et al. used an adaptive fuzzy logic based DE technique to implement a PID controller for frequency control in a two-area IPS. When the simulation results of the proposed controller were compared with those of the traditional PID controller and the DE -tuned PID controller, it was found that the proposed control scheme had a better response than the others [54]. Emre Celik studied the dragonfly search algorithm (DSA) based cascaded fractional order proportional integral- fractional order proportional derivative (FOPI-FOPD) controller for the frequency control in multi-area IPSs. The proposed control method has been successfully applied to two and three-area IPS with/without nonlinearities. The comparison between the proposed and the published work clearly depicted that the frequency and tie-line power responses have been improved in terms of overshoot, undershoot and settling times [55].

Jeyalakshmi et al. proposed a PI controller based on hybridized fuzzy logic and a PSO algorithm for an LFC loop in a two-area IPS. The responses of the proposed approach were compared with GA and FLCs. The simulation results clearly intimated that the proposed control system provided robust dynamic performance in the presence of various disturbances [56]. Esmail et al. investigated different control strategies for designing LFC in a deregulated IPS environment. The power system models and different control strategies for LFC design were studied. In addition, the challenges and benefits associated with the studied control strategies were discussed [57].

Yang Mi et al. explored a unique decentralized sliding mode method (SM) for LFC loop in two-area time-delayed IPS with considerable wind power penetration. The simulation results clearly exhibited the effectiveness of the proposed methodology in reducing frequency and tie-line power deviations [58]. Banaja Mohanty developed an output-feedback SMC based on hybrid flower pollination-pattern search method (hFPA-PS) to cope with frequency deviations in a two-area deregulated IPS. In the presence of GRC, GDB, and TD nonlinearities, the dynamic responses of the system were studied. The performance comparison between the proposed and other control strategies indicated that the proposed technique outperformed the traditional controllers [59]. Nimai Charan Patel et al. designed a SCA based double loop PD+PI controller in a two-area IPS to control the system frequency. Gas, hydro, and thermal power plants were included in the IPS. The behavior of the system

was evaluated with and without HVDC link. The PD+PI dual loop controller was shown to outperform the PID controllers [60].

Banaja Mohanty has investigated an output-feedback SMC for a two-area IPS. The associated parameters of the controller are adjusted using the TLBO method. The superiority of the proposed method is demonstrated by comparing its results with DE, PSO, and GA. Moreover, a sensitivity analysis has shown the superiority of the proposed technique [61]. Yonghui Sun et al. employed an H-infinity sliding mode controller for an LFC loop in a two-area time delayed IPS. The objective of the sliding mode control law was to ensure that the sliding surface can be reached in a finite time. The superiority of the proposed approach was verified after satisfactory simulation results were obtained [62]. Chittaranjan Pradhan and Terje Gjengedal have designed a cascade PI-PD controller based on the adaptive Jaya optimization algorithm (AJOA) to control the system frequency in a two-area IPS. The results revealed that the AJOA-PI-PD controller successfully minimizes the frequency fluctuations compared to other controllers [63].

Preeti Dahiya et al. proposed a disrupted oppositional based gravitational search algorithm (DOGSA) tuned SMC for LFC loop in a deregulated two-area IPS. In the presence of different nonlinearities such as GRC, GDB, and TD, the dynamic response of the system was investigated and evaluated. The performance of the proposed control was compared with I, PI, ID, and PID controllers and it was found that the proposed DOGSA-SMC control scheme achieved significantly better results than the traditional controllers [64].

Yogendra Arya used the imperialistic competitive algorithm (ICA) to design an output scaling factor based fuzzy proportional integral (FPI) controller for two-area IPS. The superiority of the proposed controller was comprehensively demonstrated by comparing the results of the proposed and the PI/PID controllers tuned with the FA, GWO, PSO, GA, BFO, hybrid BFO-PSO, and hybrid hFA-PS algorithms [65]. Soumen Biswas et al. presented the GOA based three-degree-of-freedom PID (3DOF-PID) controller for the LFC loop in a two-area deregulated IPS. The SMES devices and UPFC have been incorporated. For more realistic studies, BD, GRC, and GDB were also included. The simulation results clearly demonstrated that the 3DOF-PID controller with GOA optimization is superior to classical PID controller [66].

Ahmed Fathy et al. explored a fuzzy PID controller based on the mine blast algorithm (MBA) for the frequency control in a three-area IPS with GRC and GDB nonlinearities. The results were compared with PSO, artificial bee colony, and ant lion optimizers based PID

controllers. The simulation results confirmed the superiority of the proposed control method, as it provided a better response in terms of statistical parameters than others [67]. The integral-proportional derivative (I-PD) was suggested by Amil Daraz et al. for the LFC loop in a two-area IPS. Using a fitness dependent optimizer (FDO) algorithm, the parameters of the proposed I-PD controller were determined. For further research, various nonlinearities such as TD, BD, GDB, and GRC were included in the IPS. The results of the proposed control scheme were compared with PSO, TLBO, and FA based controllers These results clearly show that the proposed control strategy is superior in terms of settling time, undershoot and overshoot [1].

Amil Daraz et al. developed an I-PD controller in a two-area IPS to control system frequency. I-PD controller was optimized using the FDO technique. To verify the effectiveness of the proposed controller, a thorough performance comparison between DE, TLBO and local unimodal sampling (LUS) based control methods is performed. The performance evaluation showed that the proposed FDO-I- PD controller performed better than the others [68]. Amil Daraz et al. designed an improved-fitness dependent optimizer (I-FDO) based fractional order integral-tilt derivative (FOI-TD) controller for a two-area IPS with nonlinearities including BD, GDB, TD, and GRC. The performance of the I-FDO method was compared with PSO, TLBO, and FDO techniques. In addition, the response of the proposed controller was compared to integral-tilt derivative (I-TD), PID, and fractional order tilt integral derivative (FOTID) controllers. The performance analysis exhibited that the proposed controller performs better in reducing frequency and tie-line deviations than other controllers [69].

Amil Daraz et al. studied an I-FDO based fractional order I-PD (FOI-PD) controller LFC problem in a restructured two-area IPS. Numerous nonlinearities, including BD, TD, GRC, and GDB, were incorporated into the IPS. The effectiveness of the proposed control strategy was evaluated by comparing its response with TLBO, FDO, and FA. RFBs were also installed in each area with thyristor controlled series compensators (TCSC) in the tie-line of the power system to improve the system performance. The results clearly manifested that the proposed strategy performs better in terms of lower undershoot, overshoot, and settling times [70].

Amil Daraz et al. investigated a hybridized SCA with FDO (hSC-FDO) based fractional order integral-tilt derivative with filter (FOI-TDN) controller for LFC loop in a two-area IPS with nonlinearities. A thyristor-controlled phase shifter was installed in the

interconnection line and capacitive energy storage devices were incorporated in each area to improve system performance. The performance of the proposed control strategy was validated by comparing it with FDO, FA, and PSO [71]. The authors have presented a lot of control strategies for frequency control in an IPS. They have successfully used nature-inspired computational algorithms to tune various controllers. These studies can be found in [72]–[113].

2.3 Study of Individual AVR Systems

A number of control techniques have already been published for individual voltage control using an AVR control loop. In this section, some of these techniques are presented. S. Panda et al. presented MOL algorithm based PID controllers for AVR loop. The proposed method's efficacy was demonstrated by comparing its results with those of control methods based on ABC, PSO, and DE. To verify the effectiveness of the proposed control method, a sensitivity analysis of the MOL-PID control technique was also performed by varying the system parameters [114].

Mustafa and Erdinc explored a SCA based fractional order PID controller with fractional filter (FOPIDFF) to control terminal voltage in a power system. From the results, it was clear that the SCA-FOPIDFF has significantly increased the performance of the AVR system [115]. Baran Hekimoglu and Serdar Ekinci proposed a GOA based PID controller for voltage regulation. The performance of the proposed control method was compared with ABC, DE, and Z-N based PID controllers. It was found that the proposed technique was quite efficient and improved the transient response of the AVR system [116]. Supol Kansit and Wudhichai Assawinchaichote suggested a PID controller based on hybridized PSO and the gravitational search algorithm (PSOGSA) for an AVR system. The design was evaluated using bode analysis and transient response analysis. The comparative analysis clearly manifested that the proposed PSOGSA-PID was superior to MOL, PSO, and Z-N based PID controllers [117].

Suid and Ahmad designed a sigmoid PID (SPID) controller based on the nonlinear SCA to control terminal voltage in a power system. According to the simulation results, the proposed control method improved the transient response of the AVR system in terms of steady state error and % overshoot [118]. Saleh Masoud et al. investigated a fractional order PID (FOPID) controller based on gradient based optimization (GBO) for voltage regulation in a power system. The results indicated that the proposed AVR design has higher stability and excellent dynamic behavior compared to previous designs [119]. Emre Celik and Rafet

Durgut investigated a PID controller based on the symbiotic organisms' algorithm for an AVR system. The performance of the proposed methodology was evaluated using root locus analysis and bode analysis etc. By comparing the results of the proposed methodology with published data, the effectiveness of the proposed technique was clearly demonstrated by the authors [120].

Baran Hekimoglu developed a SCA based PID controller for voltage regulation in a power system. Compared to PID control approaches based on bio-geography based optimization (BBO), ABC, DE, and Z-N methods, the proposed method was found to be effective and reliable in improving the transient response of AVR system [121]. Salman Habib et al. presented an improved whale optimization algorithm (WOA) based PID controller for voltage stabilization in a power system. The performance of the AVR system was evaluated using root-locus, bode plot, and pole-zero diagrams. By comparing the results with eight different control strategies, it was shown that the proposed IWOA-AVR design outperformed them in terms of stability and transient responses [122].

Touquer Ahmed et al. explored a fractional order PID (FOPID) controller for an AVR system based on the jaya optimization algorithm (JOA). The results of the proposed approach were compared with those of improved kidney inspired algorithm (IKA), salp swarm algorithm (SSA), pattern search (PS), bibliography based optimization (BBO), LUS, WOA, GOA, ABC, PSO, and DE algorithms to demonstrate the efficacy of the proposed control method. The robustness of the proposed control technique was confirmed by sensitivity analysis [123].

A PID with second-order derivative (PIDD²) controller based on enhanced aquila optimizer (enAO) was designed by Serdar Ekinci to regulate voltage in a power system. Modified opposition based learning (OBL) and the Nelder-Mead (NM) simplex search algorithms were used to develop enAO. By comparing the performance of the proposed technique with that of previously presented AVR systems, the excellent performance of the proposed approach was clearly demonstrated [124]. Researchers have presented numerous control methods for voltage regulation control. These control methods are well explained in [125]–[140].

CHAPTER 3

Frequency and Voltage Stabilization in Multi-area Single-Source IPS

This chapter deals with the design and implementation of the proportional integral-proportional derivative (PI-PD) controller for two- and three-area single-source interconnected power systems using nature inspired computation algorithms including learner performance based behavior optimization (LPBO), Archimedes optimization algorithm (AOA) and modified particle swarm optimization (MPSO).

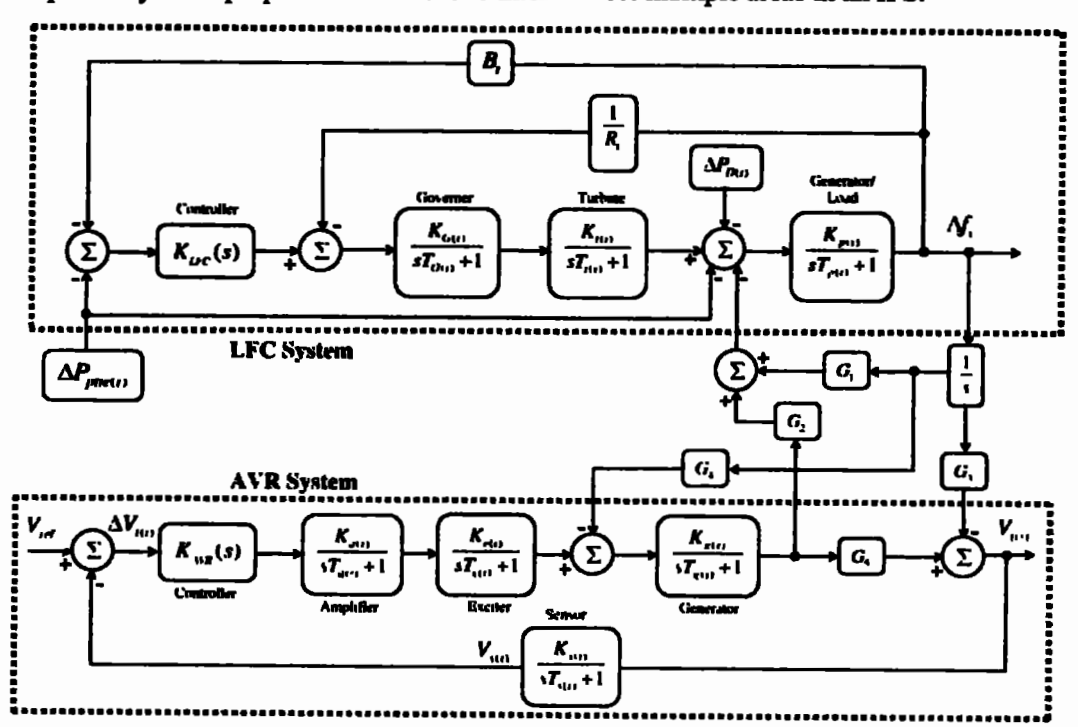
3.1 Mathematical Modeling of Power System

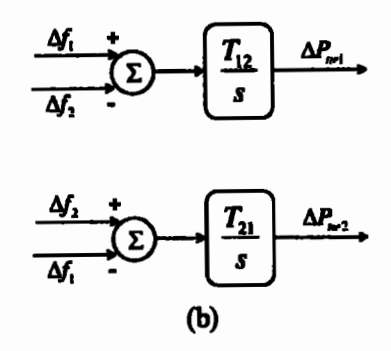
The multi-area single-source IPS under study is shown in Figure 3.1, where i^{th} and j^{th} represent area-1 and area-2 respectively [14]. The IPS consists of a hydro power plant. The LFC loop of i^{th} area consists of a controller $(K_{LFC}(s))$ and hydro power plant that comprises

turbine
$$\left(\frac{K_{r(i)}}{sT_{r(i)}+1}\right)$$
, governor $\left(\frac{K_{G(i)}}{sT_{G(i)}+1}\right)$, i^{th} area's bias factor (B_i) , speed regulation (R_i) ,

and generator/load
$$\left(\frac{K_{p(t)}}{sT_{p(t)}+1}\right)$$
. $\Delta P_{D(t)}$, $\Delta f_{(t)}$, $\Delta V_{t(t)}$, and $\Delta P_{te(t)}$ denote the load deviation,

frequency deviation, deviation in terminal voltage, and tie-line power deviation respectively. $V_{t(i)}$, $V_{ref(i)}$, and $V_{s(i)}$ refer to the terminal output, reference, and sensor voltage in i^{th} area respectively. The purpose of tie-line is to interconnect multiple areas in an IPS.





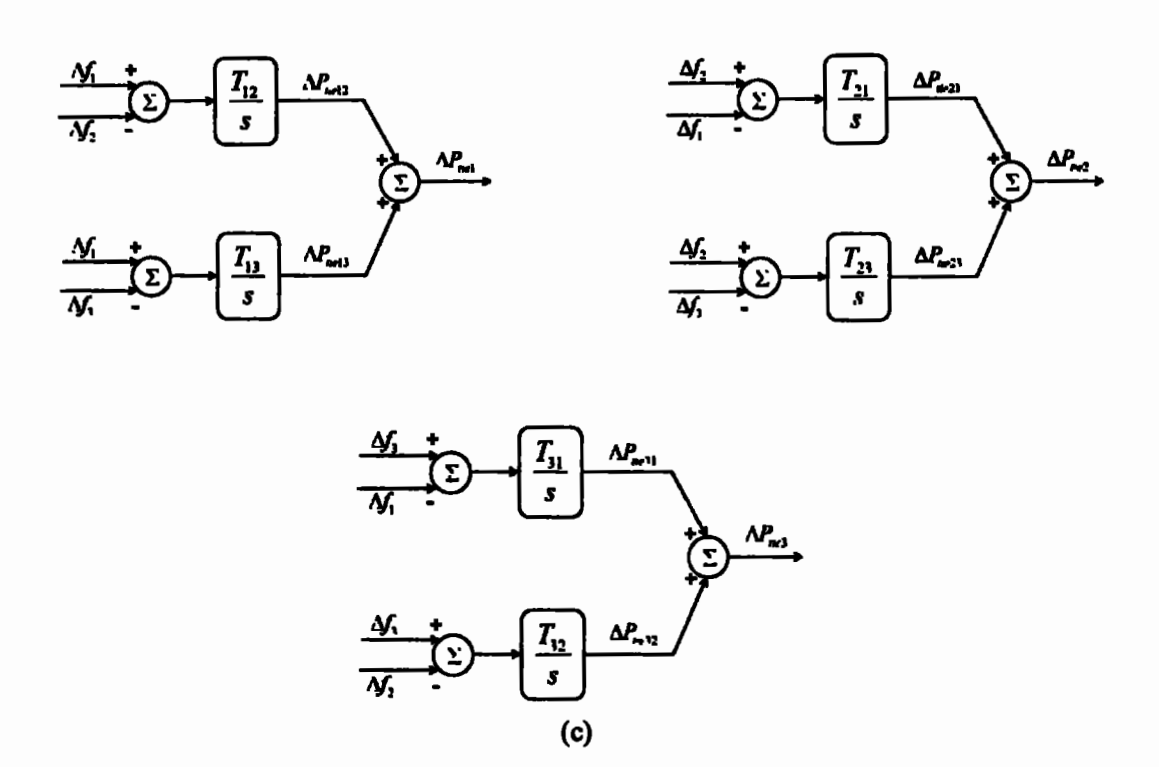


Figure 3.1: Power System

(a) Combined LFC-AVR model (b) Two-area tie-line (c) Three-area tie-lines.

The transfer function model of the hydro power plant $(G_H(s))$ is provided in Eq. (3.1). The definitions of all symbols/terms used in Eq. (3.1) and IPS are provided in List of Symbols section.

$$G_H(s) = \frac{K_{G(t)}K_{I(t)}}{(sT_{G(t)}+1)(sT_{I(t)}+1)}$$
(3.1)

The AVR loop of i^{th} area consists of a controller $(K_{AVR}(s))$, amplifier $\left(\frac{K_{a(t)}}{sT_{a(t)}+1}\right)$, generator

$$\left(\frac{K_{g(t)}}{sT_{g(t)}+1}\right)$$
, exciter $\left(\frac{K_{e(t)}}{sT_{e(t)}+1}\right)$, and sensor $\left(\frac{K_{g(t)}}{sT_{g(t)}+1}\right)$. G_1 , G_2 , G_3 , G_4 , and G_5 are the

coefficients for mutual coupling between AVR and LFC loops. The synchronization coefficient between i^{th} and j^{th} area is represented by T_{ij} . The sensor continuously senses the terminal voltage and provides the error voltage signal after comparing it with the reference voltage. The controller generates the signal for the amplifier from the error signal. The amplified signal is then given to the excitation unit to control the field excitation and the terminal voltage is regulated accordingly.

3.2 Proposed Control Methodology

The PID controller is often used in industrial applications because it is simpler to build and implement. PID controllers often work effectively, although modified PID control structures have been shown to be better at combined control of LFC and AVR control loops. PI-PD is also a modified form of the PID controller, designed to achieve the best transient and steady-state response while eliminating system errors [141]. The PI controller is located in feed forward path while PD controller is located in feedback path. The modified structure of PI-PD has proven that it can effectively improve the dynamic performance of systems. Recently, the PI-PD controller has been used effectively in a variety of applications [142]—[150]. The proposed control methodology to control load frequency and terminal voltage in multi-area IPS is given in Figure 3.2. Eq. (3.2) is used to obtain the control signal U(s) generated by PI-PD controller with IPS:

$$U(s) = (K_{\rho l} + \frac{K_{l}}{s})E(s) - (K_{\rho 2} + K_{d}s)Y(s)$$
(3.2)

$$E(s) = Y(s) - R(s) \tag{3.3}$$

where U(s). Y(s), R(s), and E(s) denote the control, output, reference, and error signals respectively. K_{p1} , K_{p2} , K_i , and K_d are the gain coefficients of PI-PD controller. The cost function (J) depends on the error signal E(s), which is essentially the difference between the output signal and the reference signal.

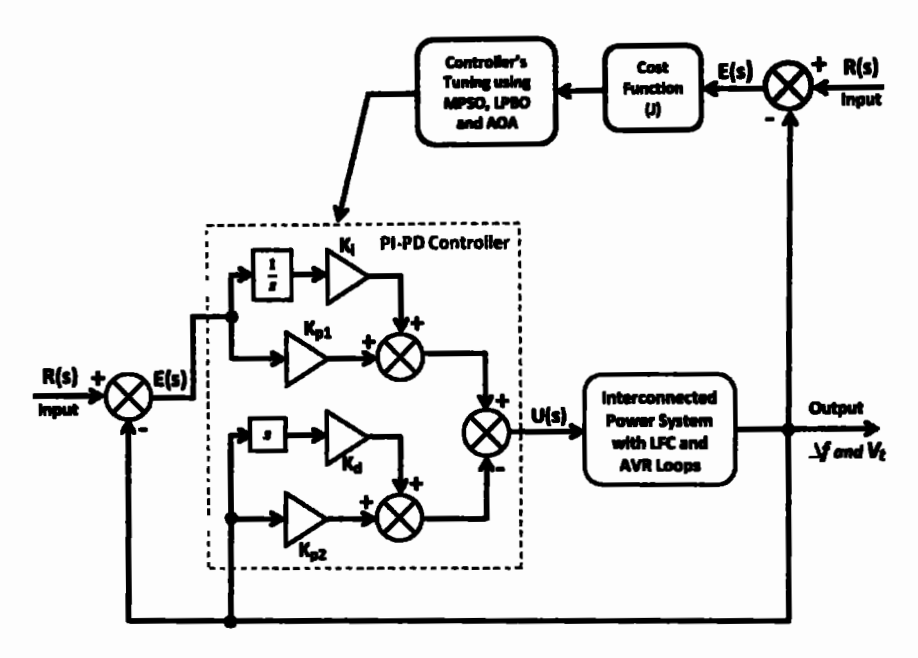


Figure 3.2: Proposed control methodology with combined LFC-AVR system

The cost function (J) can be computed using different types of error indices such as the integral of the squared value of the error signal (ISE), the integral of the time multiplied with the absolute value of the error signal (ITAE), the integral of the time multiplied with the squared value of the error signal (ITSE), and the integral of the absolute value of error (IAE) represented by the following equations [8][22]:

$$J_{\text{ISE, two-area}} = \int_{0}^{T} [\Delta f_{1}^{2} + \Delta f_{2}^{2} + \Delta V_{t1}^{2} + \Delta V_{t2}^{2} + \Delta P_{ne12}^{2}] dt$$
(3.4)

$$J_{\text{ITAE, two-area}} = \int_{0}^{T} t[|\Delta f_{1}| + |\Delta f_{2}| + |\Delta V_{11}| + |\Delta V_{12}| + |\Delta P_{pise12}|] dt$$
(3.5)

$$J_{\text{ITSE, two-area}} = \int_{0}^{T} t [\Delta f_{1}^{2} + \Delta f_{2}^{2} + \Delta V_{t1}^{2} + \Delta V_{t2}^{2} + \Delta P_{he12}^{2}] dt$$
(3.6)

$$J_{IAE, two-area} = \int_{0}^{T} [|\Delta f_{1}| + |\Delta f_{2}| + |\Delta V_{i1}| + |\Delta V_{i2}| + |\Delta P_{ptie12}|] dt$$
(3.7)

For three-area IPS, we can write:

$$J_{\text{ISE, three-area}} = \int_{0}^{T} \left[\Delta f_{1}^{2} + \Delta f_{2}^{2} + \Delta f_{3}^{2} + \Delta V_{t1}^{2} + \Delta V_{t2}^{2} + \Delta V_{t3}^{2} + \Delta P_{tte1}^{2} + \Delta P_{tte2}^{2} + \Delta P_{tte2}^{2} \right] dt$$
(3.8)

$$J_{\text{IAE,three-area}} = \int_{0}^{T} [|\Delta f_{1}| + |\Delta f_{2}| + |\Delta f_{3}| + |\Delta V_{t1}| + |\Delta V_{t2}| + |\Delta V_{t3}| + |\Delta P_{pire1}| + |\Delta P_{pire2}| + |\Delta P_{pire3}|] dt$$
(3.9)

$$J_{\text{ITSE ,three-area}} = \int_{0}^{T} t [\Delta f_{1}^{2} + \Delta f_{2}^{2} + \Delta f_{3}^{2} + \Delta V_{t1}^{2} + \Delta V_{t2}^{2} + \Delta V_{t3}^{2} + \Delta P_{tw1}^{2} + \Delta P_{tw2}^{2} + \Delta P_{tw2}^{2}] dt$$
(3.10)

$$J_{\text{ITAE, three-area}} = \int_{0}^{f} t[|\Delta f_{1}| + |\Delta f_{2}| + |\Delta f_{3}| + |\Delta V_{i1}| + |\Delta V_{i2}| + |\Delta V_{i3}| + |\Delta V_{pite1}| + |\Delta P_{pite2}| + |\Delta P_{pite3}|] dt$$
(3.11)

where,

$$\Delta V_{t1} = V_{ref} - V_{t1}$$

$$\Delta V_{t2} = V_{ref} - V_{t2}$$

$$\Delta V_{t3} = V_{ref} - V_{t3}$$
(3.12)

$$\Delta P_{pite1} = \Delta P_{pite12} + \Delta P_{pite13}$$

$$\Delta P_{pite2} = \Delta P_{pite21} + \Delta P_{pite23}$$

$$\Delta P_{pite3} = \Delta P_{pite31} + \Delta P_{pite32}$$
(3.13)

In this study, nature-inspired computation-based algorithms such as LPBO, AOA, and MPSO have been explored to optimize the cost function (J) using the ITSE error index to obtain optimal gain coefficients of controllers.

3.3 Nature-Inspired Computation Algorithms

Due to their ability to solve complex valued problems in engineering, nature-inspired computation algorithms have gained brilliant attention in IPS. Researchers have recently introduced some new nature-inspired computational algorithms such as artificial rabbits optimization [151], dandelion optimizer [152], sea-horse optimizer [153], Archimedes optimization algorithm (AOA) [154], transient search algorithm [155], and learner performance based behavior optimization (LPBO) [156] etc. Keeping in view their remarkable contribution in different engineering applications, an effort was made in this work to effectively control load frequency and terminal voltage using nature-inspired computation techniques.

3.3.1 Learner Performance based Behavior Optimization (LPBO)

Rashid and Rahman presented a novel nature-inspired learner performance based behavior optimization (LPBO) technique in 2020. The basic concept behind this algorithm is based on the fact that how students are admitted to different departments of a university is based on their high school performance. After admission, students must be able to improve their intellectual level to improve their skills. In this way, both exploitation and exploration phases are preserved. In this algorithm, a random population is generated with various ranges of grade point average (GPA). The applications of some of these learners will be rejected or accepted based on their fitness. After that, the population is divided in to subpopulation. Fitness is calculated and is then sorted into separate groups. The new population's structure is changed using crossover and mutation operators. A specified number of learners is acquired by different departments based on the minimum GPA criteria. This rejection and acceptance process is continued until all departments have their vacancies filled. Population fitness is improved in each iteration based on group learning, intellectual level, and teaching level

[156]. Figure 3.3 presents the flow chart of the LPBO algorithm. Note that the LPBO population represents the PI-PD controller's parameters in this case.

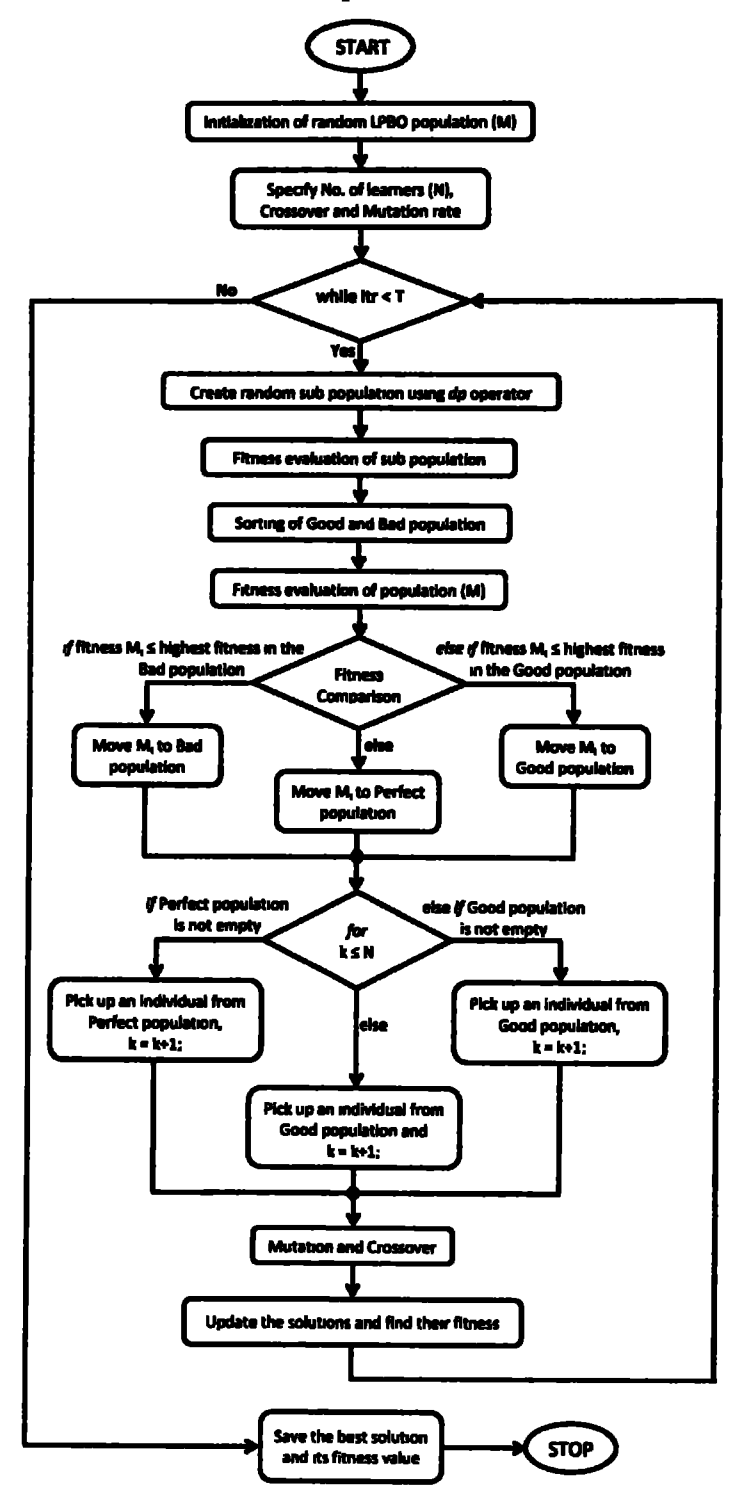


Figure 3.3: Flow chart of LPBO algorithm

3.3.2 Archimedes Optimization Algorithm (AOA)

The Archimedes optimization algorithm (AOA) is a new state-of-the-art algorithm based on the Archimedes principle that can deal with both convex and non-convex problems. It was invented in 2021 by Fatma and Houssein [154]. It defines the relationship between a buoyant force and an object submerged in water. The object will sink if the displaced fluid weight is less than the weight of the object. Similarly, if the displaced fluid and object weight are equal, the object floats on the fluid. An object has volume, acceleration, and density that results in the buoyancy force, as a result fluid's net force is always zero. AOA is a very effective nature-inspired algorithm in a way that it analyzes a problem with a global optimum solution.AOA fences in both exploitation and exploration phases since it is a global optimization algorithm. A comprehensive area must be examined to identify the global optimum solution of a given problem. Firstly, the fluid's random position is initialized and then AOA evaluates the initial population fitness to discover the best possible solution until the selection criteria are met. The density and volume of each object changes at each AOA iteration. The new density, volume, and acceleration are obtained using the object's fitness. The AOA population represents the PI-PD controller's parameters. The AOA have been successfully used in different applications [157]-[161]. Figure 3.4 presents a flow chart diagram of AOA.

3.3.3 Modified Particle Swarm Optimization (MPSO)

Following the swarm intelligence, Eberhart and Kennedy proposed the PSO algorithm in 1995 [162]. In PSO, the movement of particles (candidate solutions) over a defined search space depends upon their velocity and position. The movement of particles is incited by the best possible positions known as local bests. These local bests lead particles toward the best possible position [163]. In MPSO, the global learning coefficient is updated using a combination of existing local and global learning coefficients. The modification in the PSO algorithm is being made to improve the convergence characteristics of the controller. Figure 3.5 depicts the flow chart of the MPSO algorithm. Remember that in this research work, the particles represent the PI-PD controller's parameters.

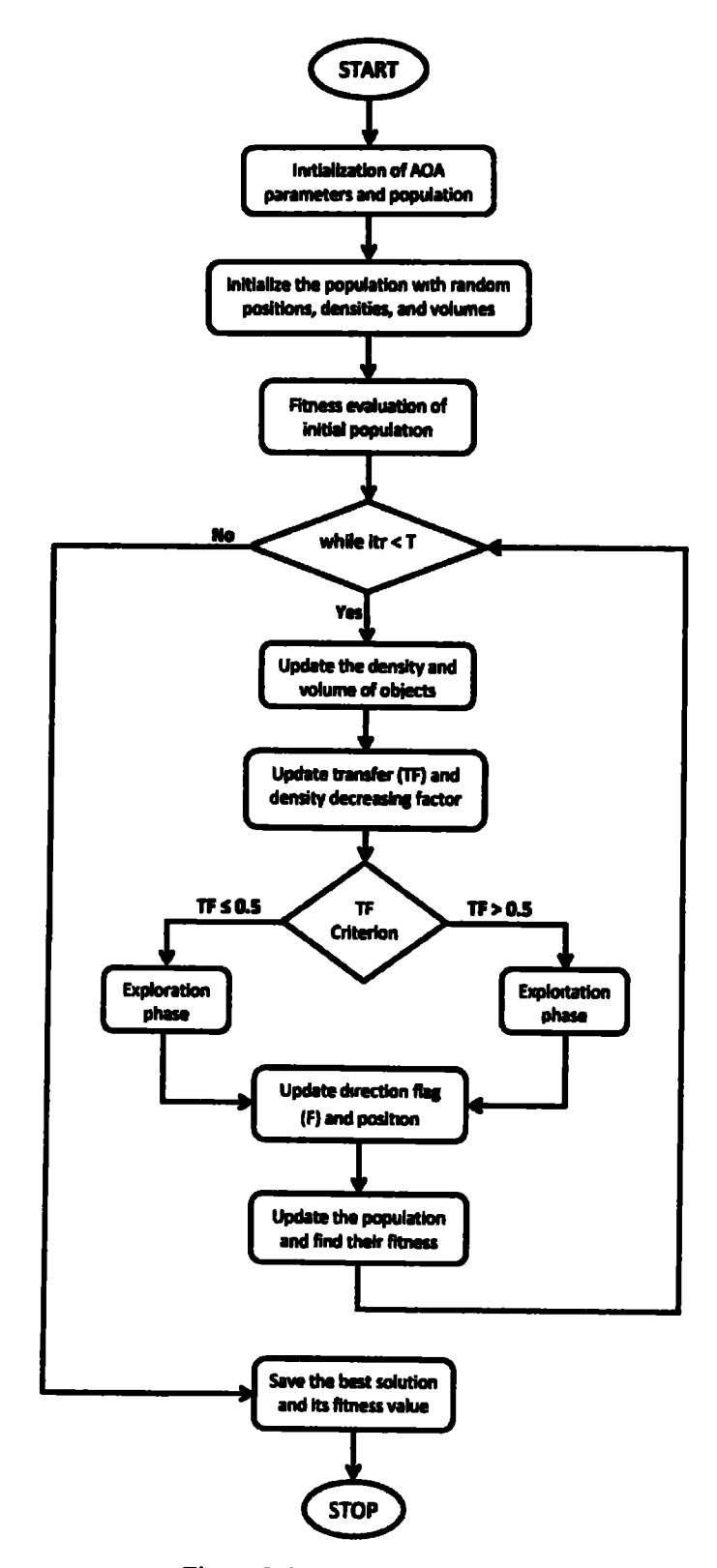


Figure 3.4: Flow chart of AOA

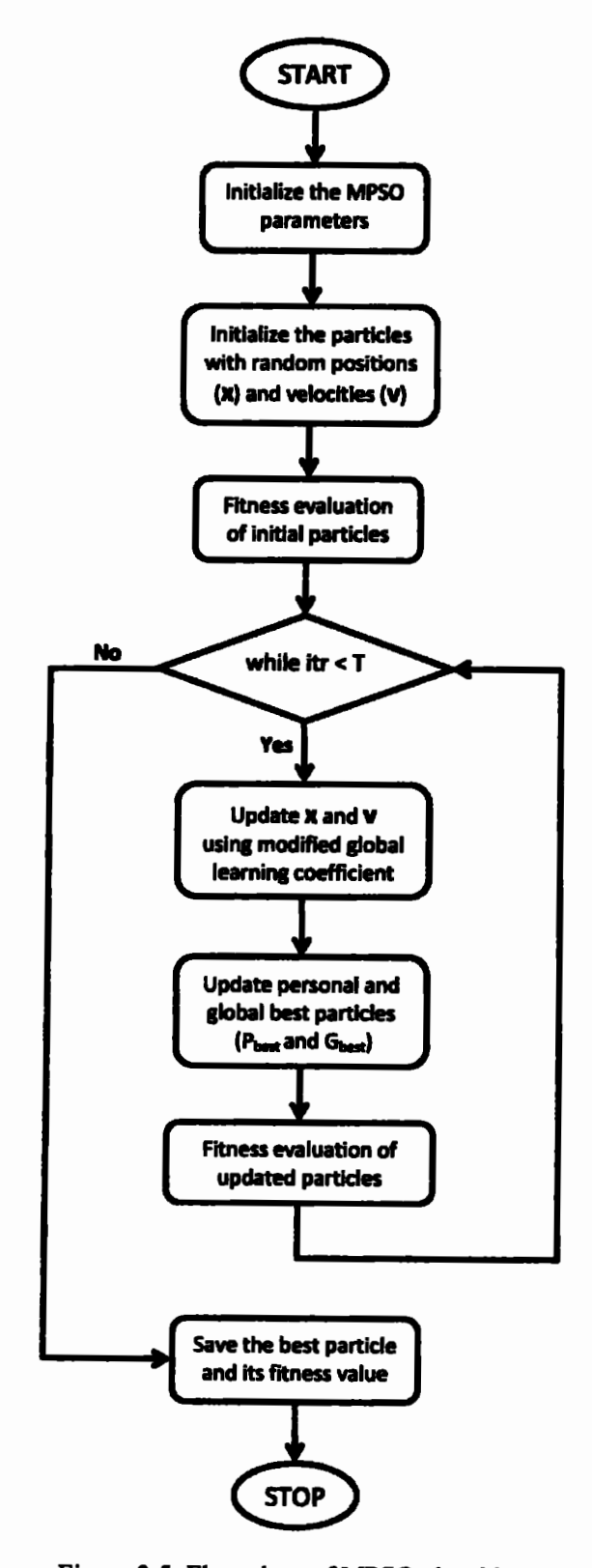


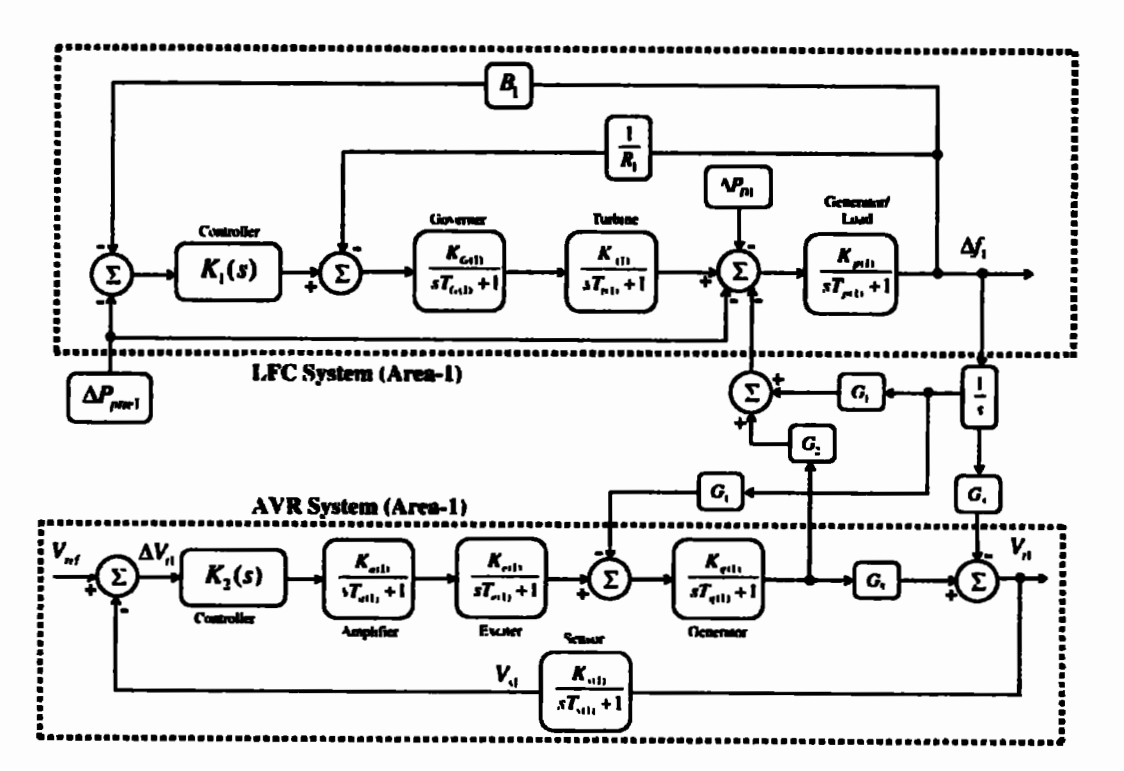
Figure 3.5: Flow chart of MPSO algorithm

3.4 Implementation and Results Discussion

Multiple simulations were carried out in MATLAB/Simulink to express the validation of the proposed control methodology. Firstly, a two-area single-source IPS was investigated using LPBO, AOA, and MPSO based PI-PD control schemes for combined control of LFC and AVR loops. After successful results in a two-area IPS, the proposed method was applied to a three-area single source IPS. Following the successful results in a three-area IPS, a sensitivity analysis was also performed by varying the system parameters to confirm the effectiveness of the proposed control schemes.

3.4.1 Frequency and Voltage Stabilization in a Two-area Single-Source IPS

The two-area IPS model under investigation with a collective LFC-AVR system is shown in Figure 3.6. The system parameters of the two-area IPS are specified in Appendix A. The system parameters of area-1 and area-2 were chosen from [14] for a direct comparison of the proposed methodology with the NLTA-PID controller. The parameters of optimization algorithms such as MPSO, LPBO, and AOA used in simulations are given in Table 3.1. The optimal parameters of MPSO-PI-PD, LPBO-PI-PD, and AOA-PI-PD control schemes are given in Table 3.2. For the sake of the assessment of the proposed control schemes, the evaluation of the time responses with 2% SLP in each area was carried out and comparisons were made with the results of NLTA-PID [14]. Further, a comparison between the proposed control schemes such as MPSO-PI-PD, LPBO-PI-PD, and AOA-PI-PD is also presented in detail in this section.



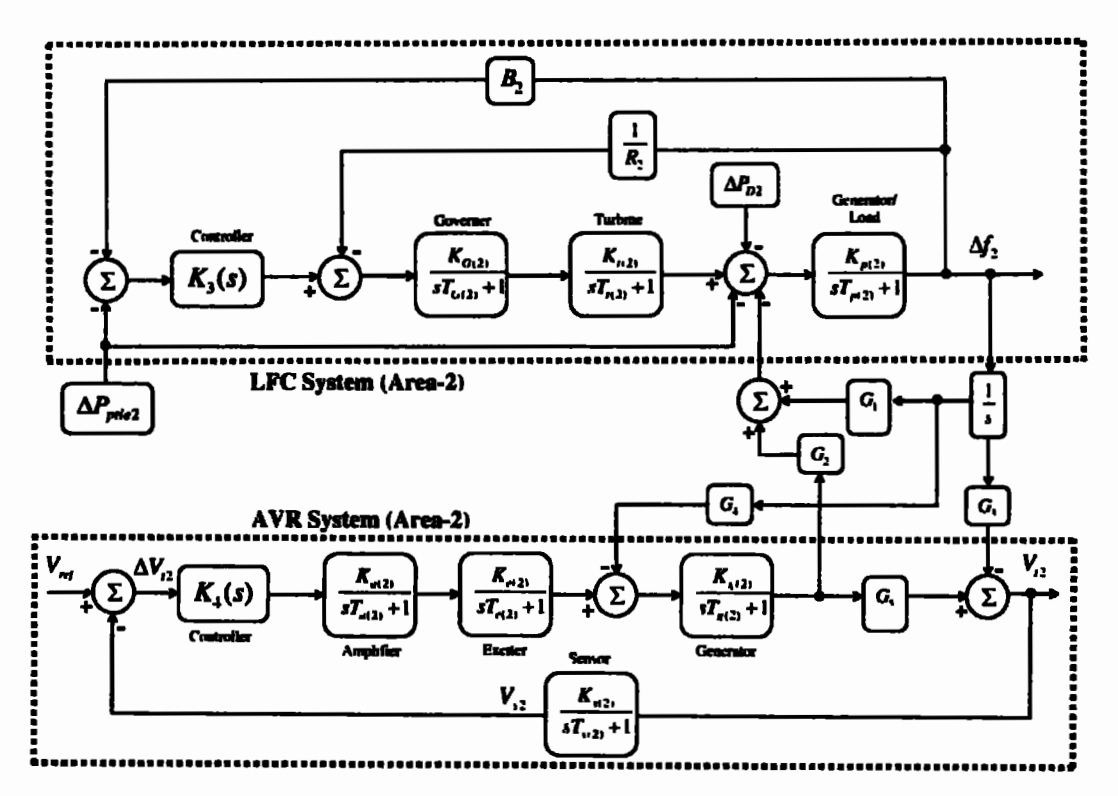


Figure 3.6: Two-area single-source IPS model with LFC and AVR loops

Table 3.1: Parameters setting of MPSO, LPBO, and AOA

MPSO	MPSO		AOA			
Parameter	Value	Parameter	Value	Parameter	Value	
Population size	20	Population size	20	Population size	20	
Iterations	10	Iterations	10	Iterations	10	
Inertia Weight Damping Ratio	1	Crossover Percentage	0.7	C ₁ (constant)	2	
Personal Learning Coefficient	2.74	Mutation Percentage	0.3	C ₂ (constant)	6	
Global Learning Coefficient	2.88	Mutation Rate	0.03	C ₃ (constant)	2	
Max. Velocity Limit	0.2	Number of Mutants	6	C4 (constant)	0.5	
Min. Velocity Limit	-0.2	Number of Offspring	14	Range of Normalization (u,l)	0.9, 0.1	

Table 3.2: Optimal values of controller parameters for a two-area single-source IPS

	Controller	NLTA-PID [14]	Controller Parameters	Proposed Control Schemes			
Area	Parameters			MPSO-PI-PD	LPBO-PI-PD	AOA-PI-PD	
	K _{pl}	1.995	K _{pl}	1.061	1.064	1.61	
	Kıı	1.943	Kı	0.630	1.396	1.512	
	Kdl	1.079	K _{p2}	1.162	1.071	1.88	
	K _{p2}	1.994	Kdl	1.621	1.795	1.263	
Area-1	K ₁₂	1.295	K _{p3}	1.063	1.850	1.01	
	K _{d2}	1.107	K ₁₂	1.419	0.772	1.68	
	-	-	K _{p4}	0.812	0.140	0.68	
	-	-	K _{d2}	0.283	0.483	0.37	
	K _{p3}	1.956	K _{p5}	0.564	0.965	0.90	
	K _{t3}	1.919	K ₁₃	0.792	0.667	0.67	
İ	K _{d3}	0.655	K _{p6}	0.775	0.670	1.44	
Area-2	K _{p4}	1.283	K _{d3}	1.106	0.616	1.60	
Alca-2	K ₁₄	0.586	K _p 7	1.903	1.522	1.50	
	K _{d4}	0.819	K,4	1.376	1.325	1.85	
	-	-	K _{p8}	0.799	0.507	0.74	
	-	-	K _{d4}	0.822	0.526	0.52	
	ITSE	2.84	ITSE	0.250	0.164	0.1892	

Figure 3.7 and 3.8 show the frequency deviation curves of area-1 and area-2 using NLTA-PID [14], MPSO-PI-PD, LPBO-PI-PD, and AOA-PI-PD control schemes in a two-area IPS respectively. It can be seen that the proposed control schemes provided a very satisfactory frequency deviation response. For area-1 LFC, the settling time of NLTA-PID [14] was lower than the proposed schemes but at the cost of a high undershoot. NLTA-PID provided an undershoot of -0.285, whereas the proposed MPSO-PI-PD, LPBO-PI-PD, and AOA-PI-PD provided-0.130, -0.135, and -0.115 respectively. It can be noticed that the proposed MPSO-PI-PD, LPBO-PI-PD, and AOA-PI-PD provided 54%, 53%, and 60% respectively better undershoot responses as compared to the NLTA-PID controller in area-1 LFC. For area-2 LFC, NLTA-PID provided a quick settling, but it provided an undershoot of -0.275, whereas the proposed MPSO-PI-PD, LPBO-PI-PD, and AOA-PI-PD provided-0.135, -0.170, and -0.120 respectively. The proposed MPSO-PI-PD, LPBO-PI-PD, and AOA-PI-PD provided 51%, 38%, and 56% respectively better undershoot responses as compared to the

NLTA-PID controller in area-2 LFC. The % overshoots and % steady-state (s-s) errors were almost zero with each proposed technique.

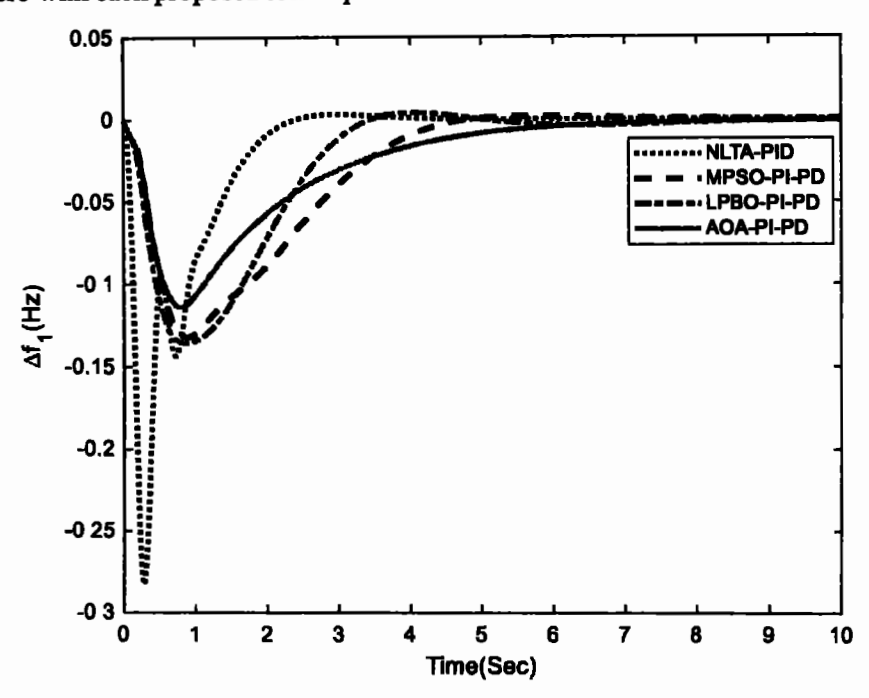


Figure 3.7: Response of Δf_1 with PI-PD control schemes in a two-area single-source IPS

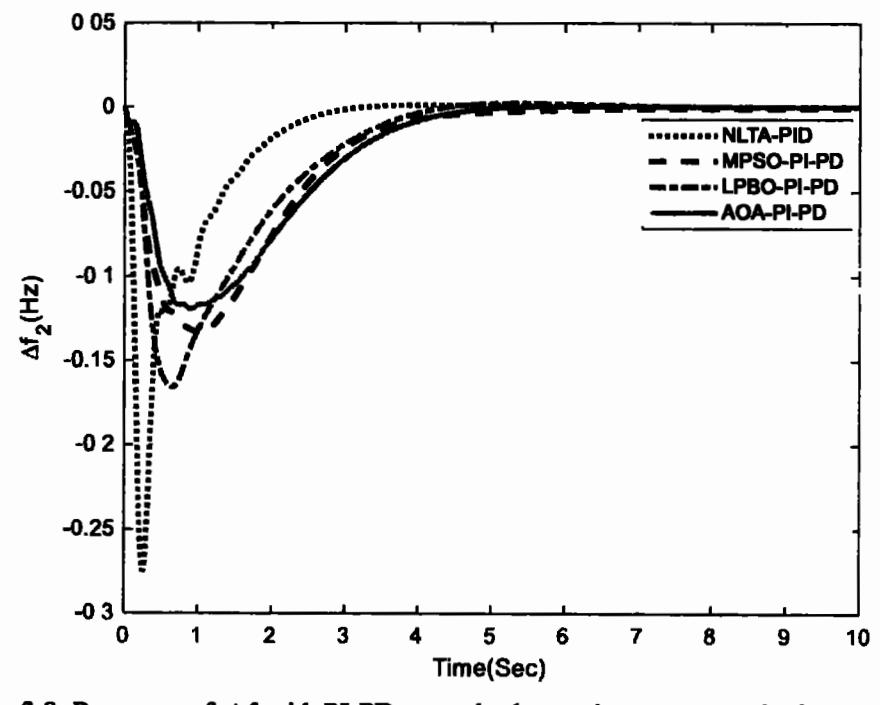


Figure 3.8: Response of Δf_2 with PI-PD control schemes in a two-area single-source IPS

Tables 3.3 presents the performance specifications of frequency deviation responses using NLTA-PID, MPSO-PI-PD, LPBO-PI-PD, and AOA-PI-PD control schemes in a two-area IPS respectively.

Table 3.3: Performance specifications of frequency deviation responses in a two-area single-source IPS

		Area-1			Area-2			
Control Scheme	Settling Time (s)	% Overshoot	Undershoot	% s-s Error	Settling Time (s)	% Overshoot	Undershoot	% s-s Error
NLTA-PID [14]	2.120	0.0005	-0.285	0	2.592	0	-0.275	0
MPSO-PI-PD	4.540	0	-0.13	0	4.92	0	-0.135	0
LPBO-PI-PD	6.95	0.005	-0.135	0	4.04	0	-0.17	0
AOA-PI-PD	6.675	0	-0.115	0	4.69	0	-0.12	0

Figure 3.9 and 3.10 show the terminal voltage of area-1 and area-2 AVR using the NLTA-PID, MPSO-PI-PD, LPBO-PI-PD, and AOA-PI-PD control schemes in a two-area IPS respectively. It is clear that the proposed control schemes provided a very satisfactory transient response in both area-1 and area-2 AVRs. It is identified that NLTA-PID provided 18% and 17% overshoot in area-1 and area-2 respectively, but the proposed technique provided a negligible % overshoot at the cost of the settling time with all tuning techniques. It can be observed that the proposed LPBO-PI-PD and AOA-PI-PD control schemes produced settling times approximately the same as those achieved by NLTA-PID.

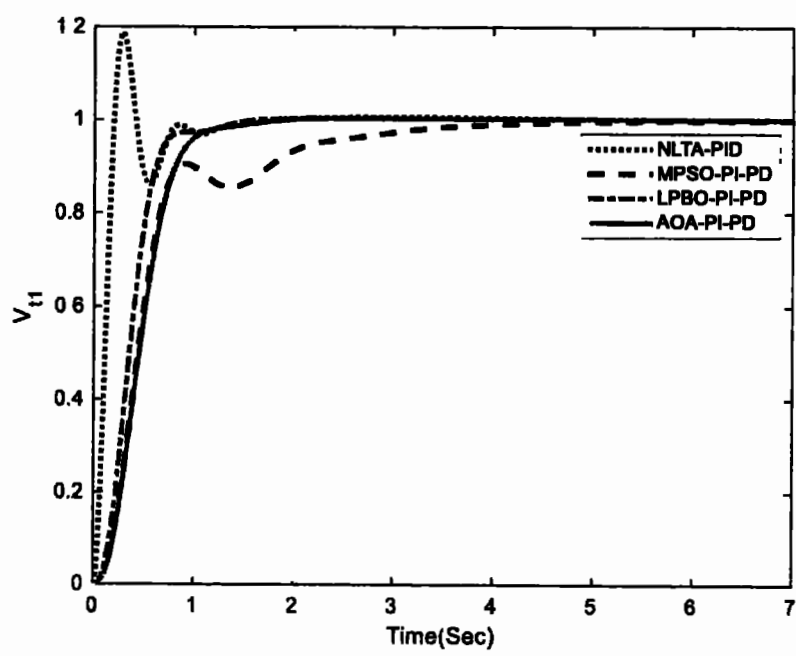


Figure 3.9: Response of V_{t1} with PI-PD control schemes in a two-area single-source IPS

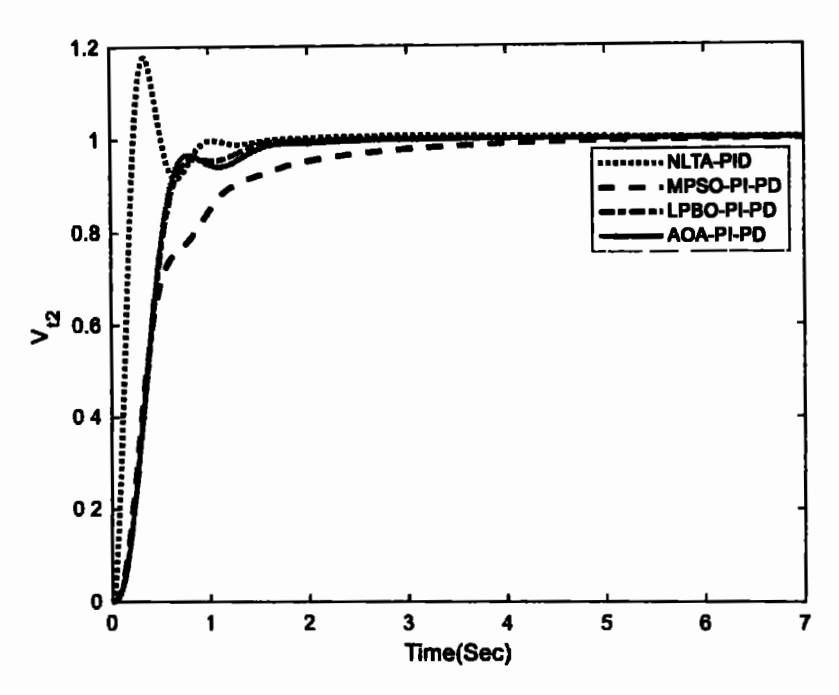


Figure 3.10: Response of V_2 with PI-PD control schemes in a two-area single-source IPS

Tables 3.4 presents the performance specifications of terminal voltage responses using NLTA-PID, MPSO-PI-PD, LPBO-PI-PD, and AOA-PI-PD control schemes in a two-area IPS respectively.

Table 3.4: Performance specifications of terminal voltage responses in a two-area single-source IPS

Control Scheme		Ar	ea-1		Ares-2			
	Rise Time (s)	Settling Time (s)	% Overshoot	% s-s Error	Rise Time (s)	Settling Time (s)	70	% s-s Error
NLTA-PID [14]	0.129	1.24	18.80	0	0.154	0.89	17.75	0
MPSO-PI-PD	0.653	3.30	0	0	1.077	3.17	0.0003	0
LPBO-PI-PD	0.454	1.22	0.28	0	0.464	1.38	0	0
AOA-PI-PD	0.610	1.23	0.27	0	0.435	1.49	0	0

Figure 3.11 shows the tie-line power deviation responses using NLTA-PID, MPSO-PI-PD, LPBO-PI-PD, and AOA-PI-PD control schemes in a two-area IPS respectively. It can be observed from the results that LPBO-PI-PD and AOA-PI-PD provided tie-line power deviation responses with no undershoot; however, this was at the cost of a slightly small overshoot. The performance responses provided by MPSO-PI-PD, LPBO-PI-PD, and AOA-PI-PD control schemes are satisfactory.

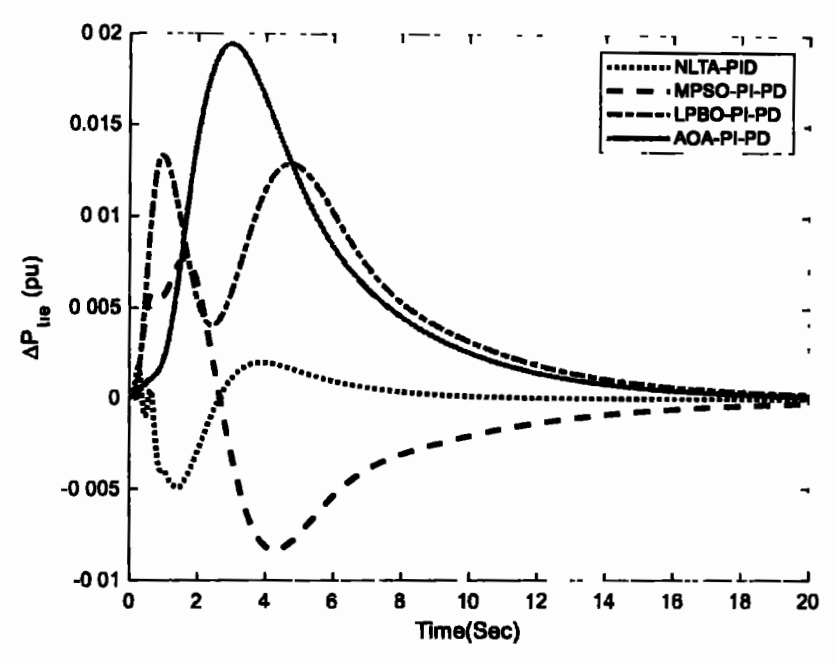


Figure 3.11: Response of ΔP_{tie} with PI-PD control scheme in a two-area single-source IPS

Figure 3.12 and 3.13 show the graphical comparisons of the performance specifications frequency deviation and terminal voltage responses using NLTA-PID, MPSO-PI-PD, LPBO-PI-PD, and AOA-PI-PD control schemes in a two-area IPS respectively.

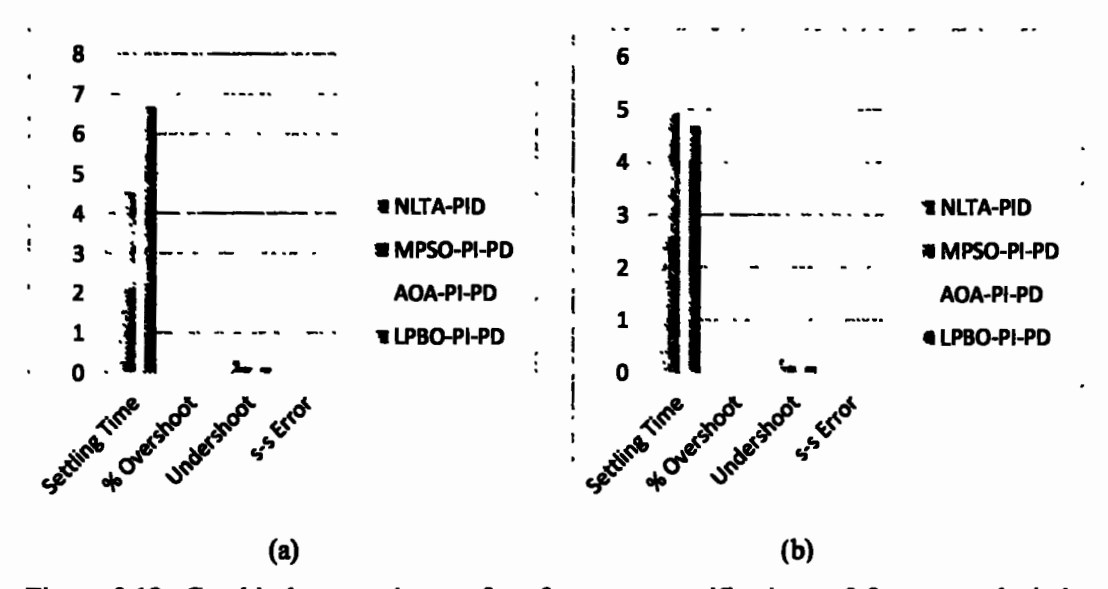


Figure 3.12: Graphical comparisons of performance specifications of frequency deviation responses using PI-PD control schemes in a two-area single-source IPS
(a) Δf_1 (b) Δf_2

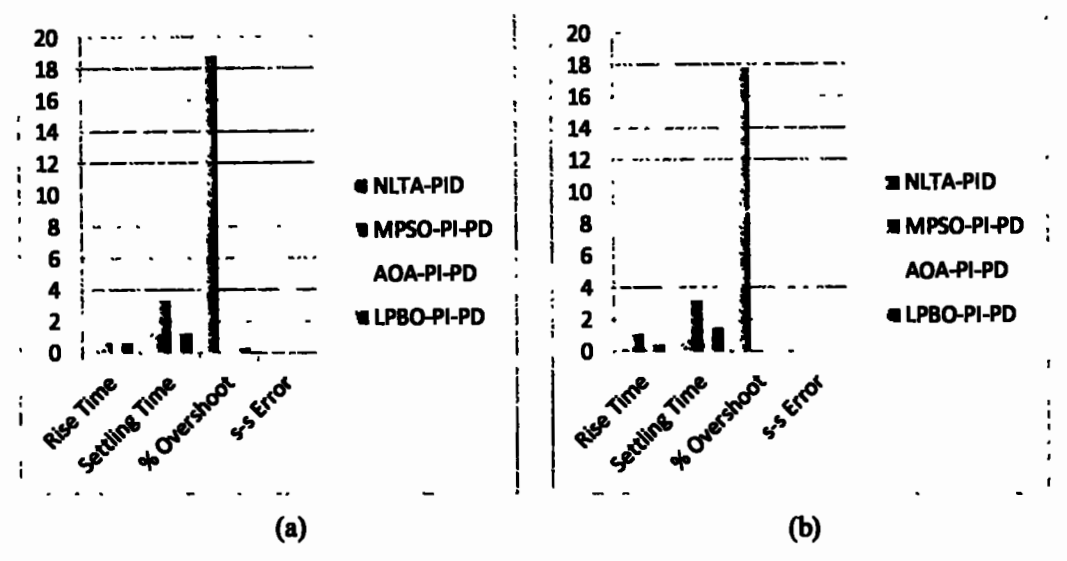
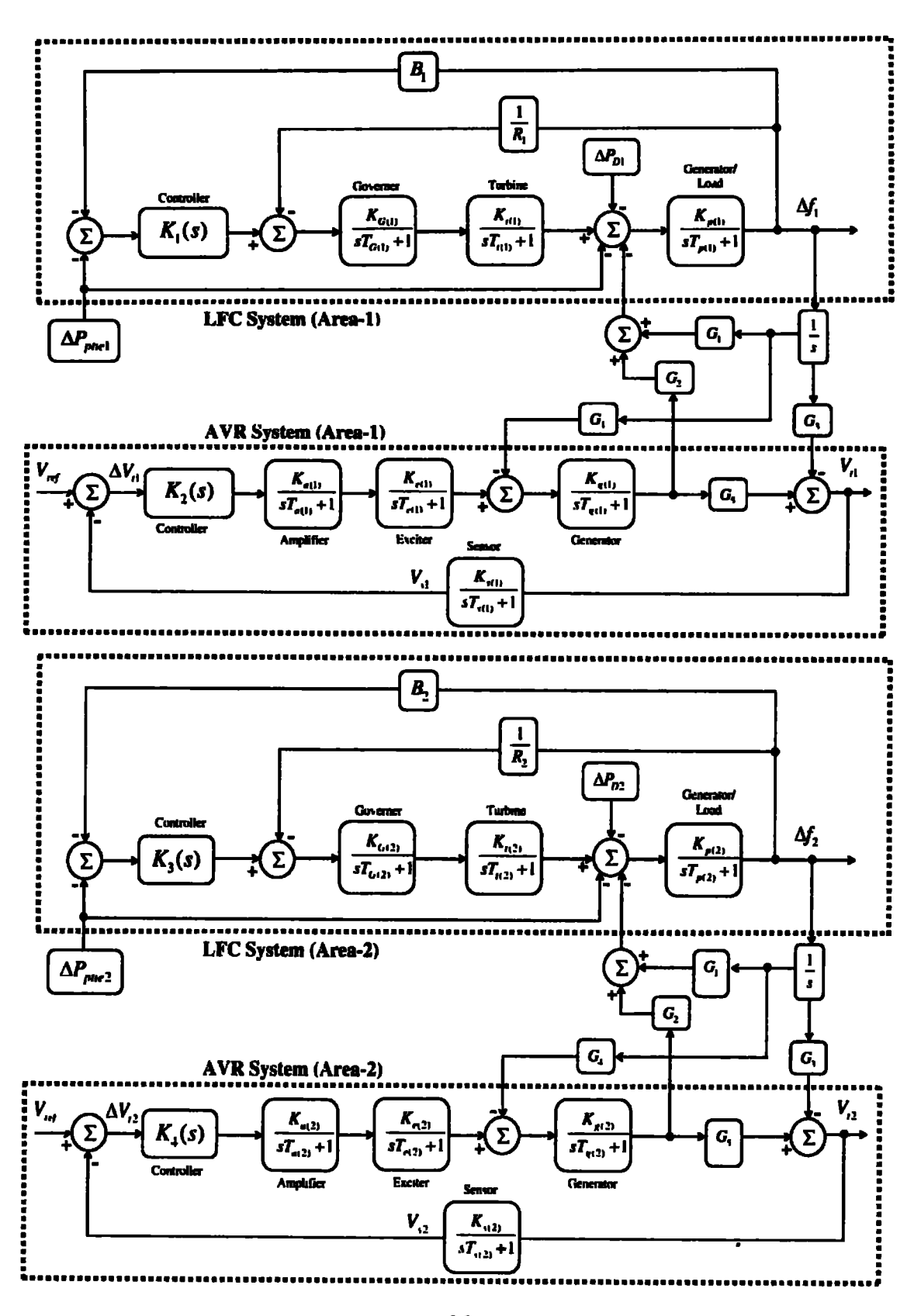


Figure 3.13: Graphical comparisons of performance specifications of terminal voltage responses using PI-PD control schemes in a two-area single-source IPS (a) V_{t1} (b) V_{t2}

It is very clear that the proposed PI-PD control schemes provided relatively better responses in terms of the undershoots in LFC loop and % overshoot in AVR loop as compared to NLTA-PID controller. Therefore, it is concluded that the proposed MPSO-PI-PD, LPBO-PI-PD, and AOA-PI-PD were effective for maintaining the load frequency and terminal voltage within the prescribed values with a satisfactory performance in a two-area IPS.

3.4.2 Frequency and Voltage Stabilization in a Three-area Single-Source IPS

In this section, the proposed methodology is applied to a three-area IPS model with 2% SLP for combined control LFC and AVR loops. The model under study is presented in Figure 3.14, while the model parameters are provided in Appendix A.



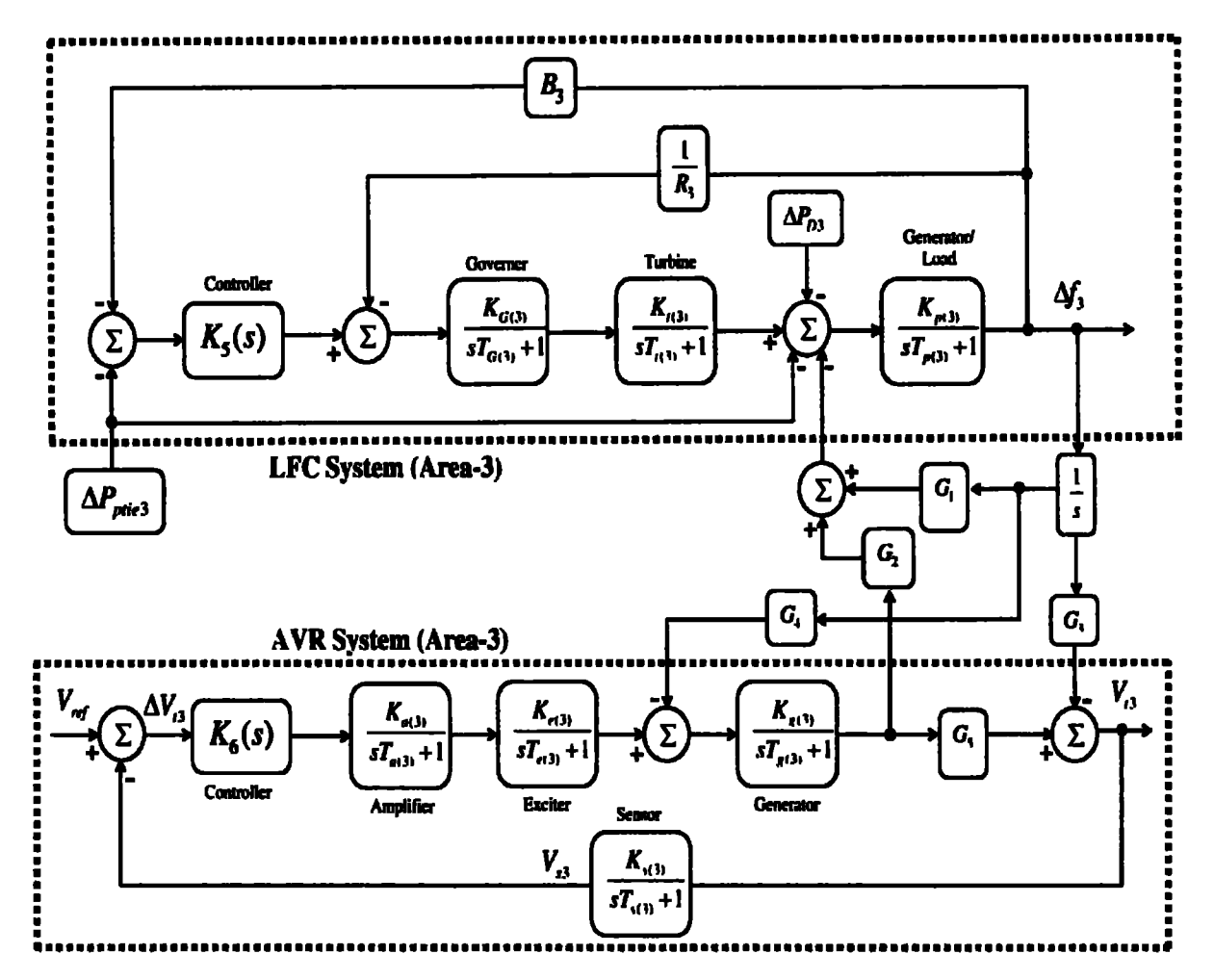


Figure 3.14: Three-area single-source IPS model with LFC and AVR loops

The optimal values of MPSO-PI-PD, LPBO-PI-PD, and AOA-PI-PD for a three-area IPS with combined LFC and AVR are given in Table 3.5. Figure 3.15, 3.16, and 3.17 show the frequency deviation responses using MPSO-PI-PD, LPBO-PI-PD, and AOA-PI-PD control schemes in a three-area IPS respectively while Tables 3.6 presents the performance specifications of frequency deviation responses using MPSO-PI-PD, LPBO-PI-PD, and AOA-PI-PD control schemes respectively. For area-1 LFC, LPBO-PI-PD provided 14% and 31% quick settling times as compared to the MPSO-PI-PD and AOA-PI-PD control schemes respectively. The % overshoot and % steady-state (s-s) error were zero in each case. Further, MPSO-PI-PD and AOA-PI-PD control schemes respectively. For area-2 LFC, LPBO-PI-PD yielded 3.3% and 11% quick settling times, as compared to the MPSO-PI-PD and AOA-PI-PD control schemes respectively. The % overshoot and % steady-state (s-s) error were zero in each case. Further, AOA-PI-PD exhibited 4.16% and 5.74% better undershoot responses as

compared to the MPSO-PI-PD and LPBO-PI-PD control schemes respectively. For area-3 LFC, MPSO-PI-PD provided 25% and 16% quick settling times as compared to the LPBO-PI-PD and AOA-PI-PD control schemes respectively. The % overshoot and % steady-state (s-s) error were again zero in each case. Further, AOA-PI-PD exhibited 22% and 34% better undershoot responses as compared to the MPSO-PI-PD and LPBO-PI-PD control schemes respectively.

Table 3.5: Optimal values of controller parameters for a three-area single-source IPS

Area	Controller	Pr	roposed Control Schemes					
Area	Parameters	MPSO-PI-PD	LPBO-PI-PD	AOA-PI-PD				
	K _{pl}	1.0995	0.66	1.51				
	Kıl	1.1028	0.59	1.29				
	K _{p2}	1.2737	0.96	-0.38				
Area-1	K _{dl}	0.831	0.53	0.55				
Alca-1	K _{p3}	1.5371	1.56	0.88				
İ	K ₁₂	1.965	1.62	1.91				
	K _{p4}	1.2543	0.85	1.13				
	K ₄₂	0.5936	0.56	0.5				
	K _{p5}	1.1106	0.77	0.86				
Area-2	K _t	0.9076	0.61	0.71				
	K _{p6}	0.8639	1.48	1.55				
	K _{d3}	1.3118	1.03	0.86				
	K _p 7	1.7917	1.68	1.91				
	K ₁₄	1.8286	1.57	1.97				
	K _{p8}	0.9068	0.83	1.074				
İ	K _{d4}	0.6882	0.73	1.071				
	K _{p9}	0.7914	0.78	1.9				
	K ₁₅	1.0795	1.12	1.26				
	K _{pl0}	1.2741	0.66	1.64				
Area-3	Kds	0.8581	1.56	0.42				
VICT-2	K _{pli}	1.2282	1.29	1.63				
	K ₁₆	1.4326	1.3	1.69				
	K _{pl2}	0.9527	0.77	1.43				
	K _{d6}	0.5874	0.45	1.33				
	ITSE	0.35	0.34	0.49				

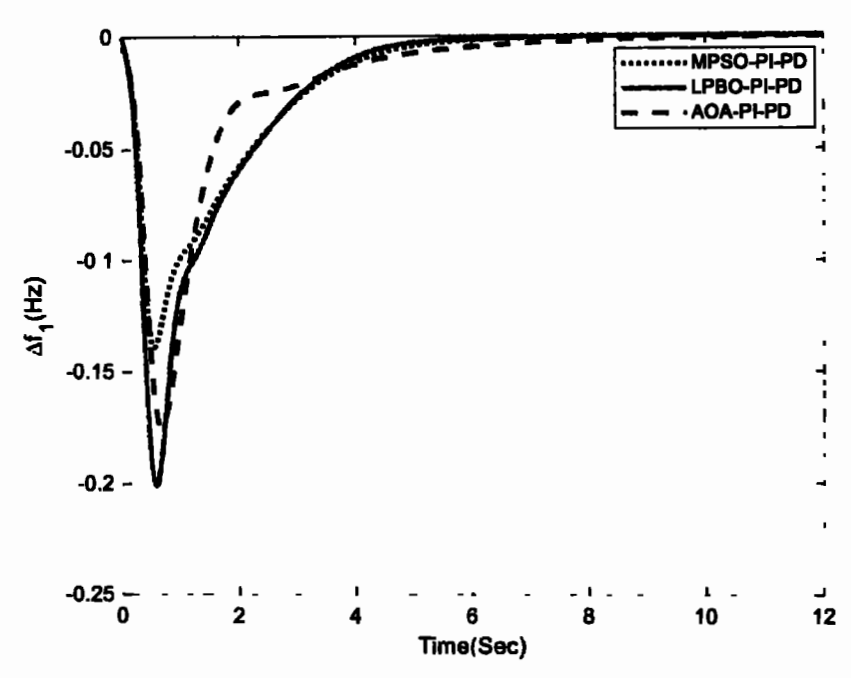


Figure 3.15: Response of Δf_1 with PI-PD control schemes in a three-area single-source IPS

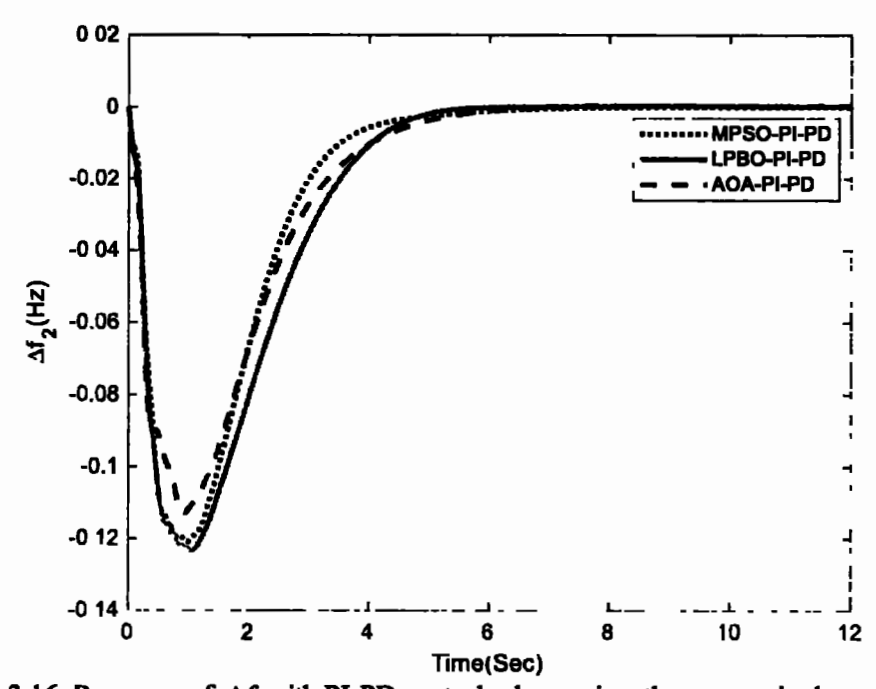


Figure 3.16: Response of Δf_2 with PI-PD control schemes in a three-area single-source IPS

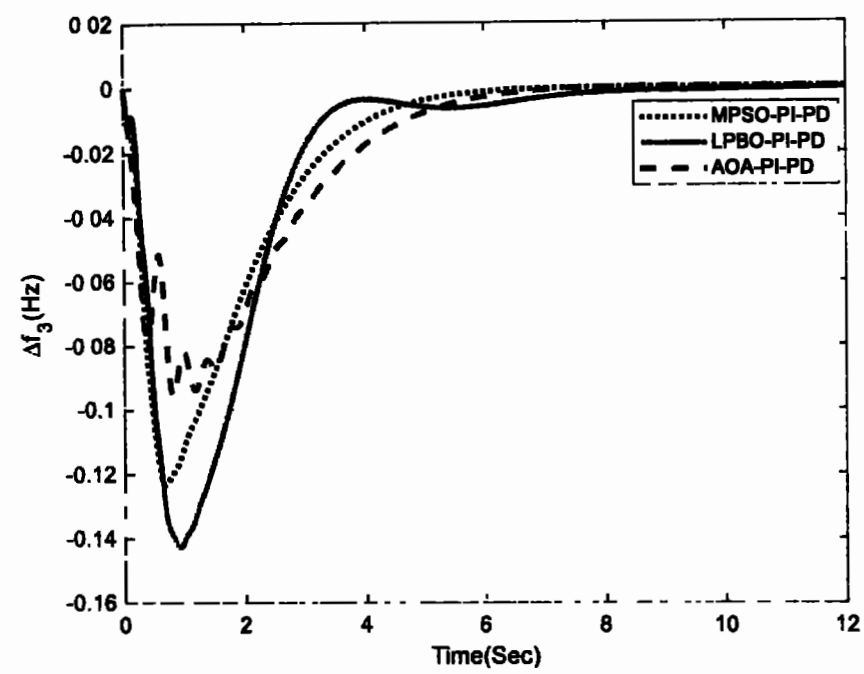


Figure 3.17: Response of Δf₃ with PI-PD control schemes in a three-area single-source IPS

Table 3.6: Performance specifications of frequency deviation responses in a three-area single-source IPS

Area	Control Scheme	Settling Time (s)	% Overshoot	Undershoot	% s-s Error
	MPSO-PI-PD	5.43	0	-0.14	0
Area-1	LPBO-PI-PD	4.65	0	-0.20	0
	AOA-PI-PD	6.73	0	-0.175	0
	MPSO-PI-PD	5.04	0	-0.120	0
Area-2	LPBO-PI-PD	4.87	0	-0.122	0
	AOA-PI-PD	5.46	0	-0.115	0
	PSO-PI-PD	5.40	0	-0.122	0
Area-3	LPBO-PI-PD	7.16	0	-0.143	0
	AOA-PI-PD	6.40	0	-0.095	0

Figure 3.18, 3.19, and 3.20 show the terminal voltage responses of area-1, area-2, and area-3 using MPSO-PI-PD, LPBO-PI-PD, and AOA-PI-PD control schemes in a three-area IPS respectively while Table 3.7 presents the performance specifications of terminal voltage

responses using the MPSO-PI-PD, LPBO-PI-PD, and AOA-PI-PD control schemes respectively. For area-1 AVR, AOA-PI-PD provided 26% and 2% quick rise times as compared to the MPSO-PI-PD and LPBO-PI-PD control schemes respectively. Moreover, AOA-PI-PD yielded 38% and 29% fast settling times as compared to the MPSO-PI-PD and LPBO-PI-PD control schemes respectively. Further, it was observed that the % overshoot and % steady-state (s-s) error were almost zero with each tuning technique in area-1 AVR. For area-2 AVR, MPSO-PI-PD offered 3% and 13% quick rise times as compared to the LPBO-PI-PD and AOA-PI-PD control schemes respectively, Moreover, AOA-PI-PD provided 21% and 19% fast settling times as compared to the MPSO-PI-PD and LPBO-PI-PD control schemes respectively. Further, it can be seen that the % overshoot and % steady-state (s-s) error were almost zero with each tuning technique in area-2 AVR. For area-3 AVR, LPBO-PI-PD produced 64% and 73% quick rise times as compared to the MPSO-PI-PD and AOA-PI-PD control schemes respectively. Moreover, AOA-PI-PD provided 0.3% and 5.45% fast settling times as compared to the MPSO-PI-PD and LPBO-PI-PD control schemes respectively. Further, it can be seen that the % overshoot and % steady-state (s-s) error were negligible with each tuning technique in area-3 AVR.

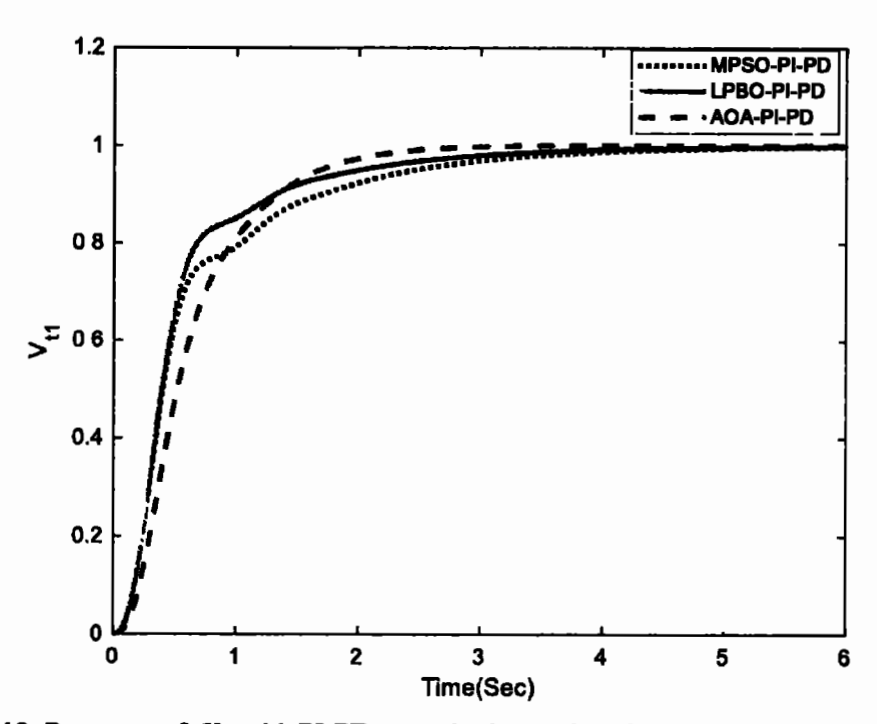


Figure 3.18: Response of V_{t1} with PI-PD control schemes in a three-area single-source IPS

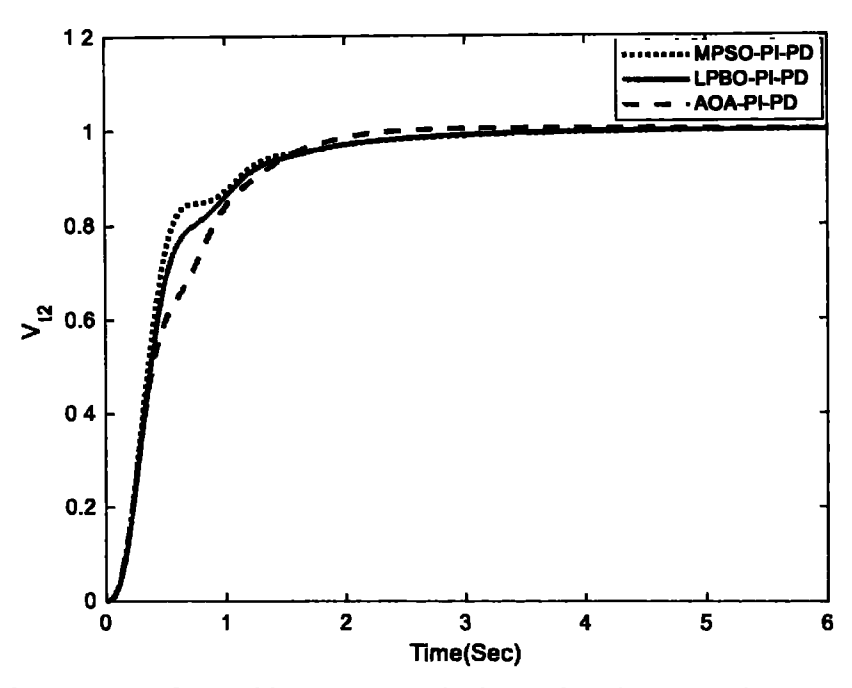


Figure 3.19: Response of V_{12} with PI-PD control schemes in a three-area single-source IPS

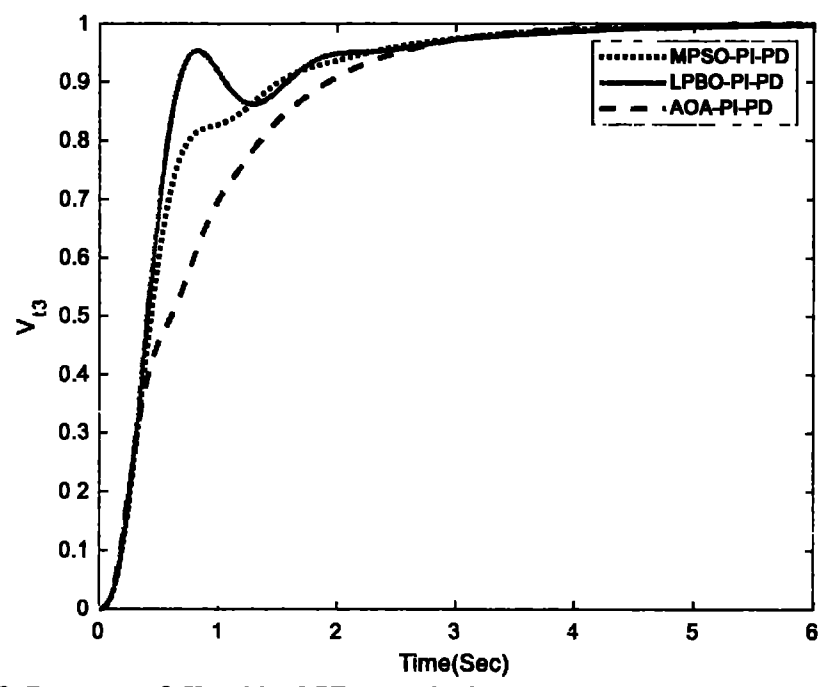


Figure 3.20: Response of V_{t3} with PI-PD control schemes in a three-area single-source IPS

Table 3.7: Performance specifications of terminal voltage responses in a three-area single-source IPS

A	Control	Rise Time	Settling Time	%	% s-s
Area	Scheme	(8)	(5)	Overshoot	Error
	MPSO-PI-PD	1.53	3.48	0	0
Area-1	LPBO-PI-PD	1.15	3.01	0	0
[AOA-PI-PD	1.13	2.15	0.08	0
	MPSO-PI-PD	0.95	2.44	0	0
Area-2	LPBO-PI-PD	0.98	2.37	0	0
Ī	AOA-PI-PD	1.09	1.92	0.37	0
	MPSO-PI-PD	1.32	3.30	0	0
Area-3	LPBO-PI-PD	0.48	3.48	0.001	0
	AOA-PI-PD	1.75	3.29	0	0

Figure 3.21 and 3.22 show the graphical comparisons of the performance specifications of frequency deviation and terminal voltage responses using MPSO-PI-PD, LPBO-PI-PD, and AOA-PI-PD control schemes in a three-area single--source IPS.

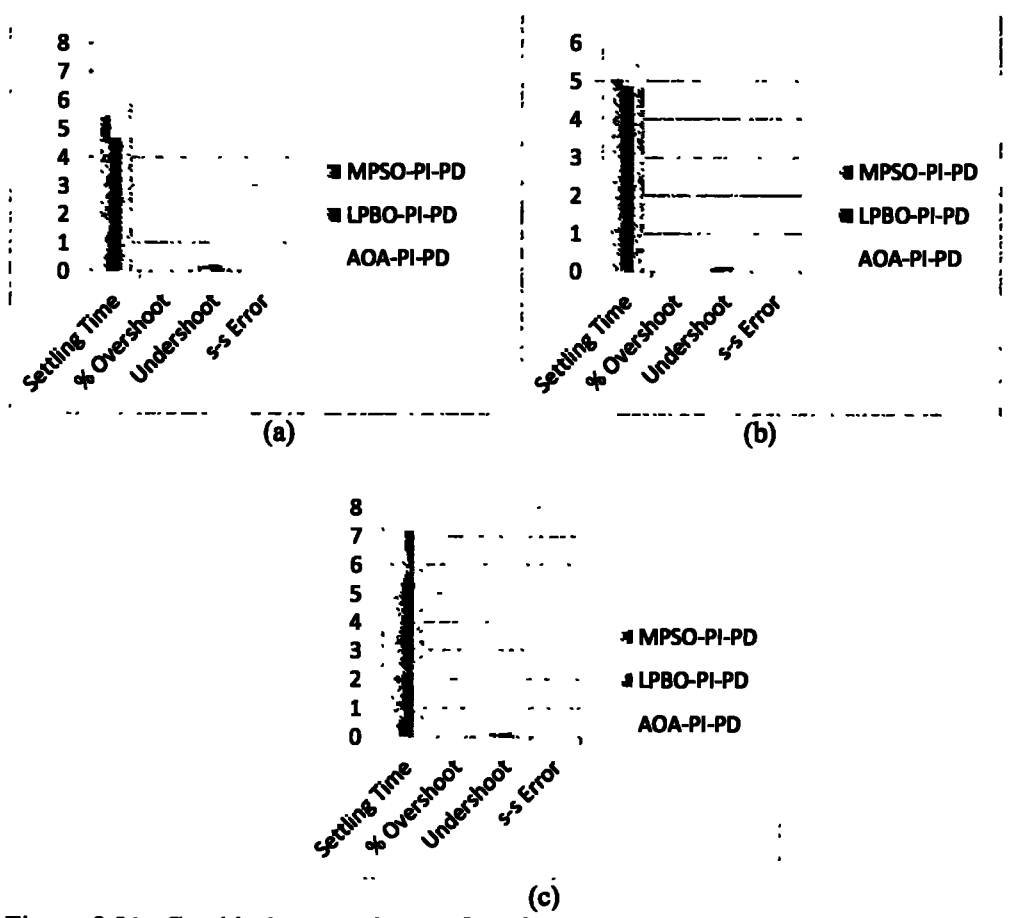


Figure 3.21: Graphical comparisons of performance specifications of frequency deviation responses using PI-PD control schemes in a three-area single-source IPS
(a) Δf_1 (b) Δf_2 (c) Δf_3

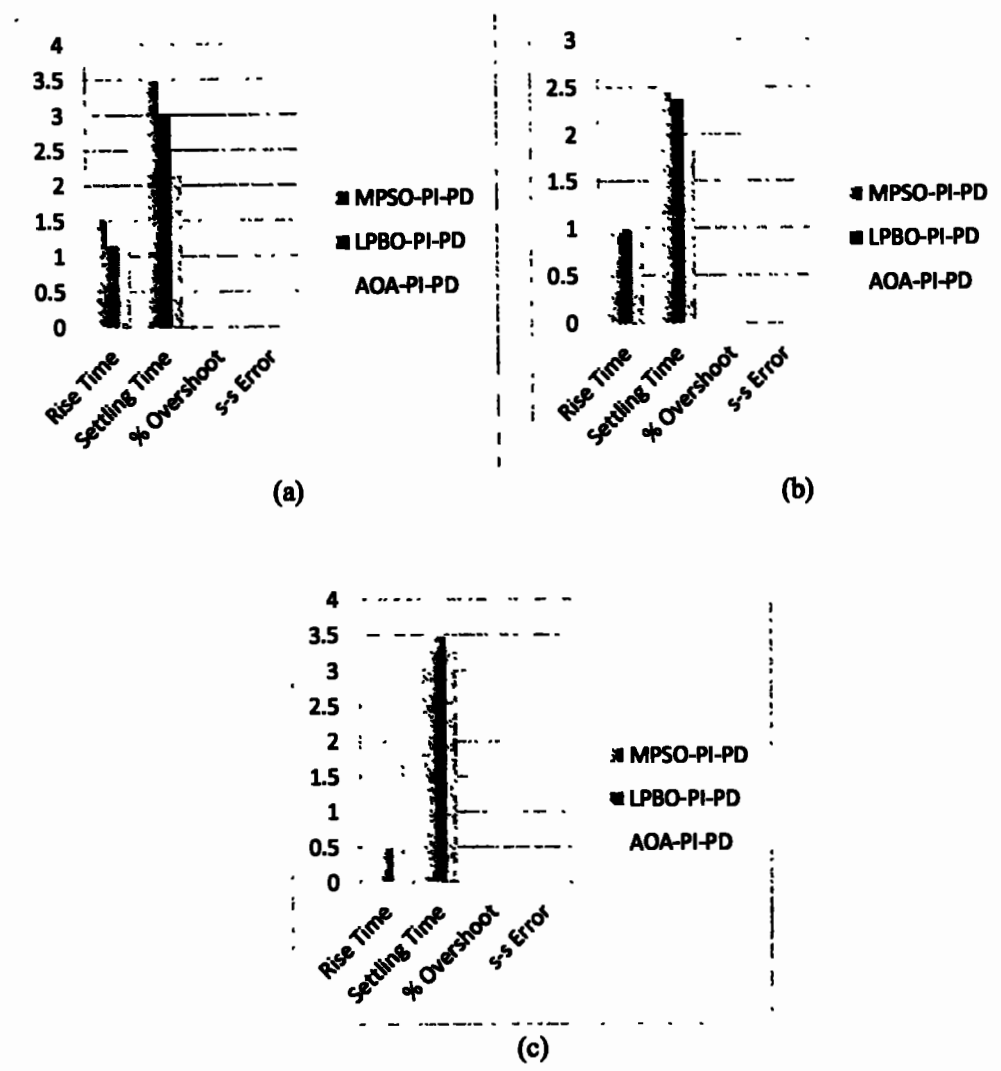


Figure 3.22: Graphical comparisons of performance specifications of terminal voltage responses using PI-PD control schemes in a three-area single-source IPS (a) V_{t1} (b) V_{t2} (c) V_{t3}

Figure 3.23, 3.24, and 3.25 show the tie-line power deviation responses in area-1, area-2, and area-3 using the MPSO-PI-PD, LPBO-PI-PD, and AOA-PI-PD control schemes in a three-area single-source IPS respectively. It can be inferred that PI-PD based control schemes including MPSO-PI-PD, LPBO-PI-PD, and AOA-PI-PD yielded satisfactory tie-line power deviation responses with negligible undershoots and % overshoot in the three-area IPS.

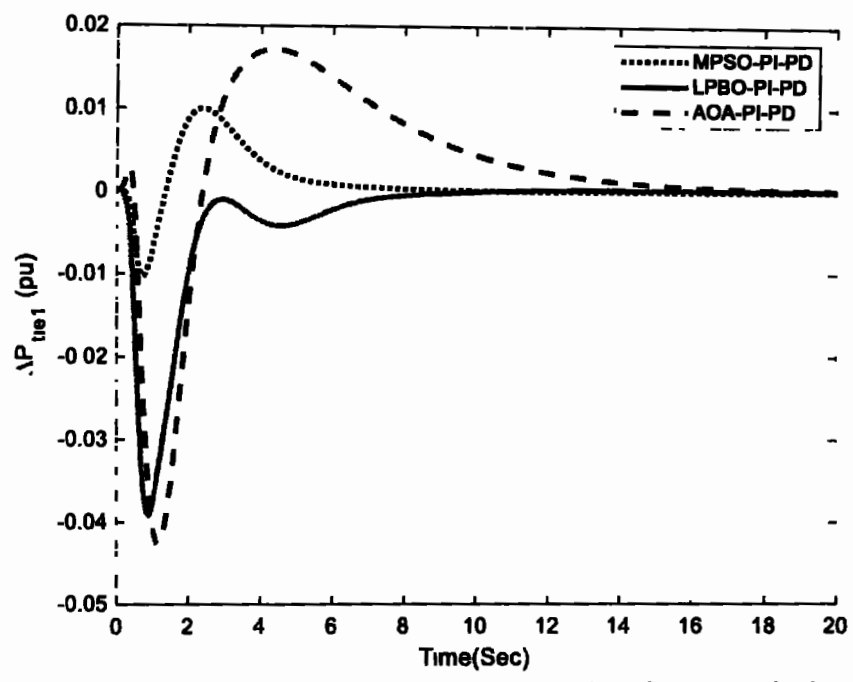


Figure 3.23: Response of ΔP_{nel} with PI-PD control schemes in a three-area single-source IPS

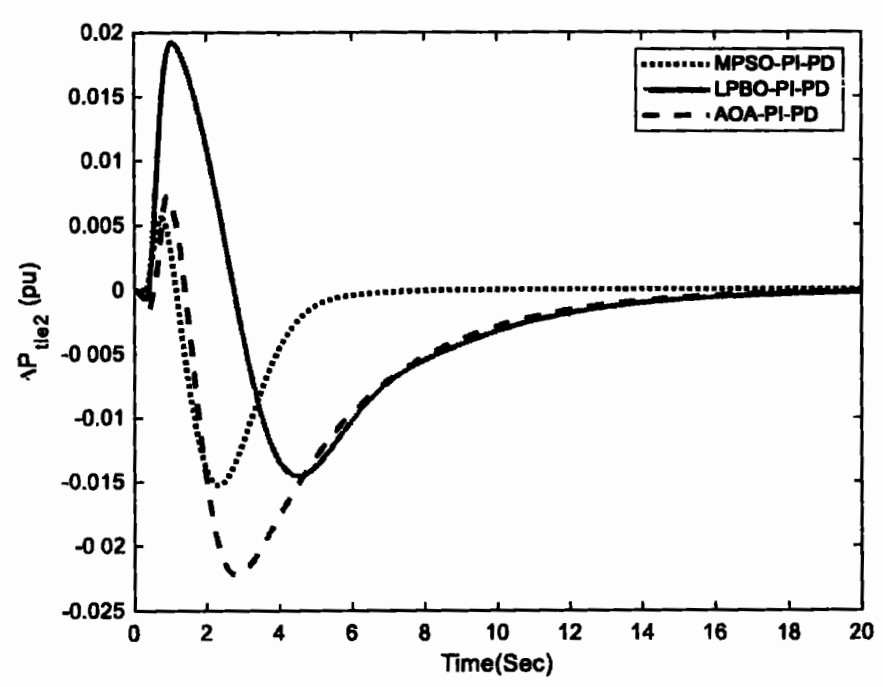


Figure 3.24: Response of ΔP_{ne2} with PI-PD control schemes in a three-area single-source IPS

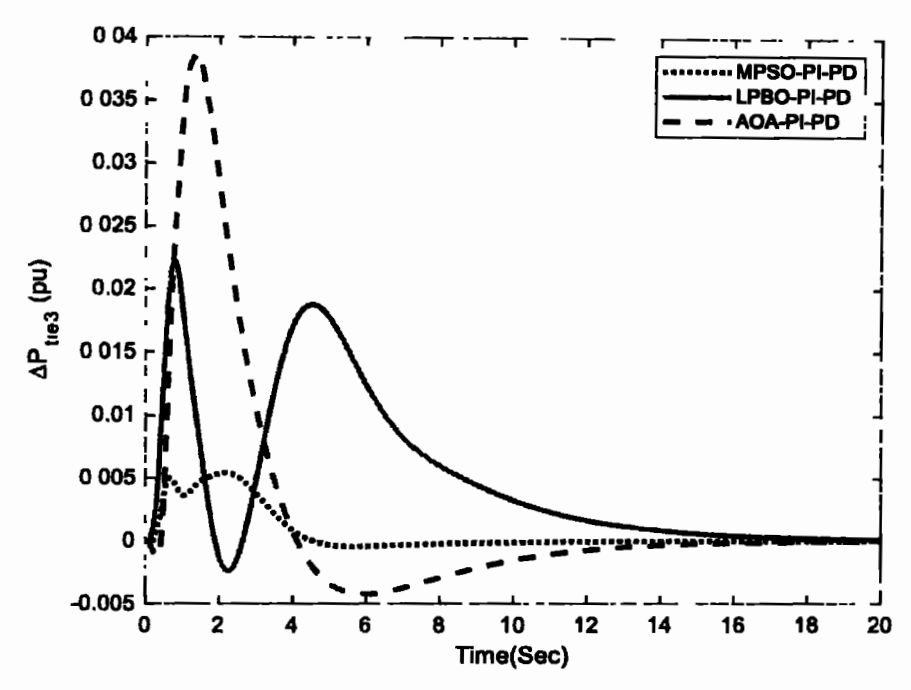


Figure 3.25: Response of ΔP_{tie3} with PI-PD control schemes in a three-area single-source IPS

3.4.3 Sensitivity Analysis of a Three-area Single-Source IPS

In this section, the robustness of the proposed nature-inspired computation based PI-PD control scheme was tested with large variations in the system parameters of the three-area IPS for combined control of load frequency and terminal voltage. Each area of IPS was again subjected to 2% SLP. The generator time constant (T_g) and turbine time constant (T_t) were varied to $\hat{A} \pm 50\%$ of their nominal values. The optimum parameters of the PI-PD control scheme were same as used in previous section. The frequency deviation responses using PI-PD control scheme with variations in T_t are depicted in Figures 3.26, 3.27, and 3.28 respectively whereas terminal voltage responses are provided in Figures 3.29, 3.30, and 3.31 respectively. Similarly, frequency deviation responses using PI-PD control scheme with variations in Tg are provided in Figures 3.32, 3.33, and 3.34 respectively whereas terminal voltage responses are presented in Figures 3.35, 3.36, and 3.37 respectively. Tables 3.8 and 3.9 present the performance specifications of frequency deviation and terminal voltage responses while Figure 3.38 and 3.39 show the graphical comparisons of the performance specifications in this scenario. From the obtained results, it is evident the % overshoot and % steady-state (s-s) error were almost zero in each case. The terminal voltage responses are almost indistinguishable to each other, despite the variation in system parameters. It is clearly observed that the system response under $\hat{A} \pm 50\%$ variations was very identical to response with nominal values. This indicates that the proposed LPBO-PI-PD control scheme is very

robust under variations in system parameters. These results clearly reveal that the re-tuning of the proposed controller is not necessary with large variations of atleast $\hat{A} \pm 50\%$.

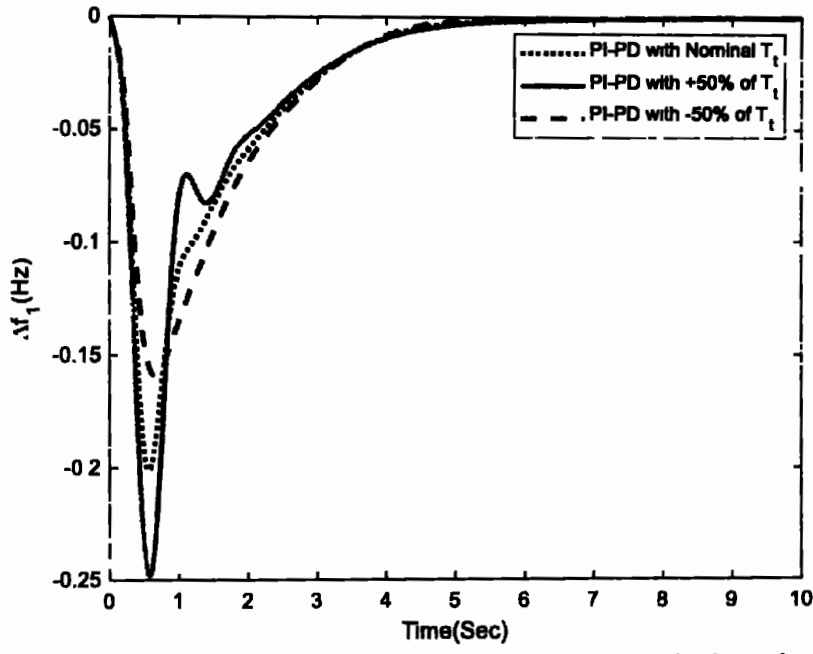


Figure 3.26: Response of Δf_1 with variations in T_1 using PI-PD control scheme in a three-area single-source IPS

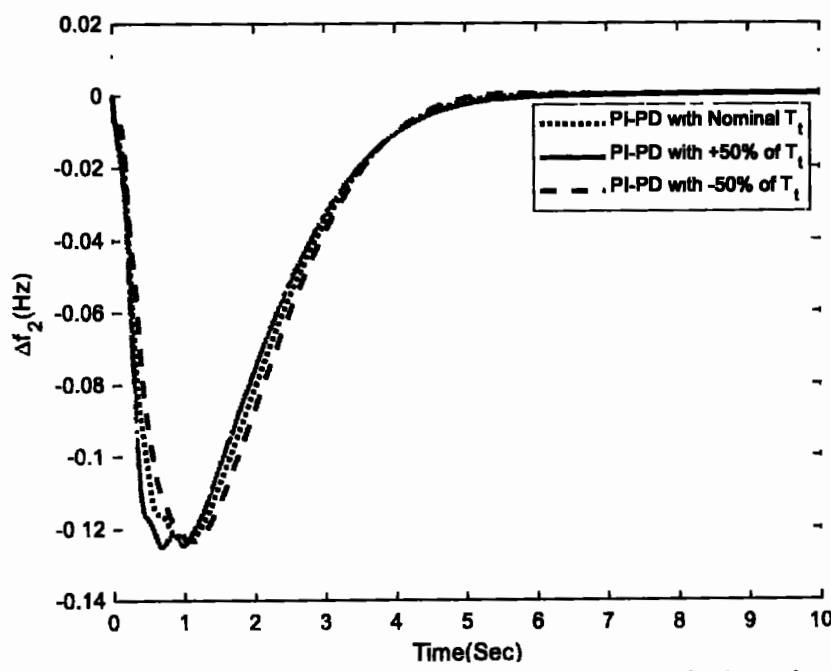


Figure 3.27: Response of Δf_2 with variations in T_t using PI-PD control scheme in a three-area single-source IPS

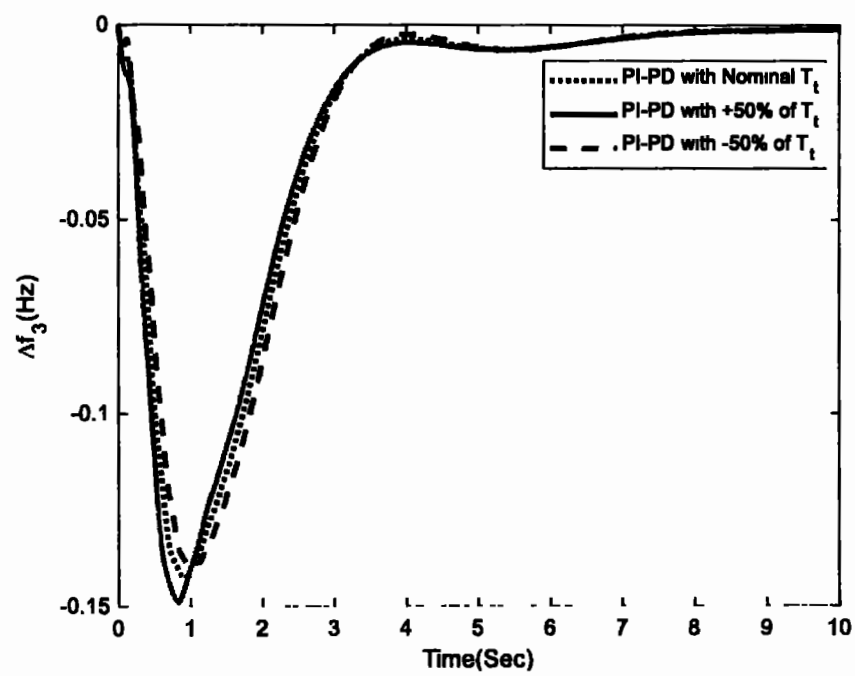


Figure 3.28: Response of Δf_3 with variations in T_t using PI-PD control scheme in a three-area single-source IPS

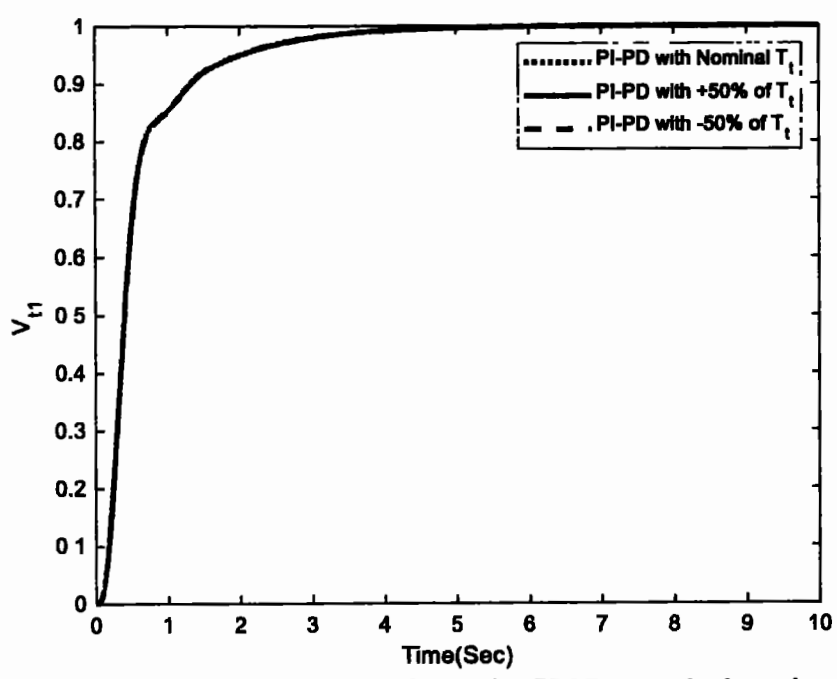


Figure 3.29: Response of V_{t1} with variations in T_t using PI-PD control scheme in a three-area single-source IPS

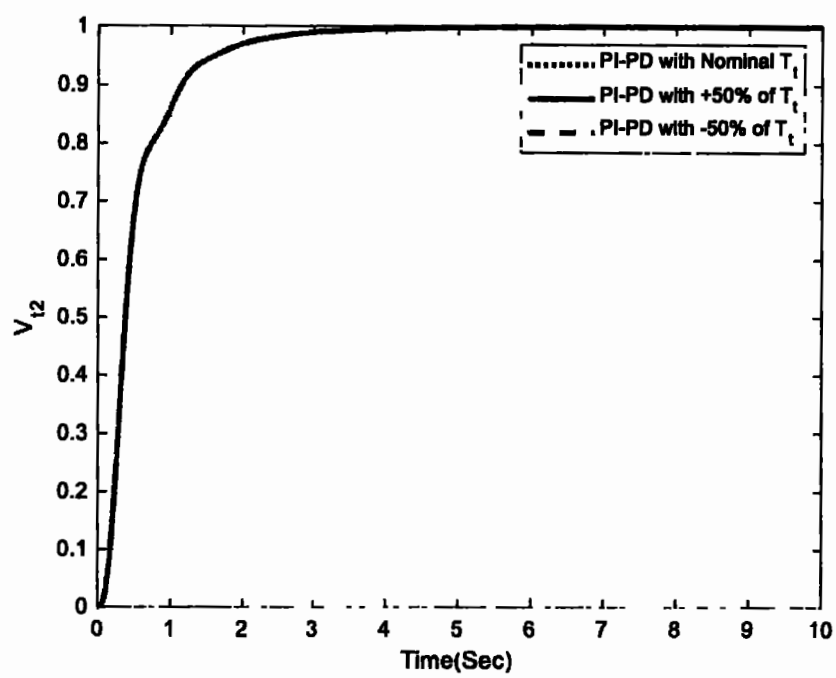


Figure 3.30: Response of V_2 with variations in T_t using PI-PD control scheme in a three-area single-source IPS

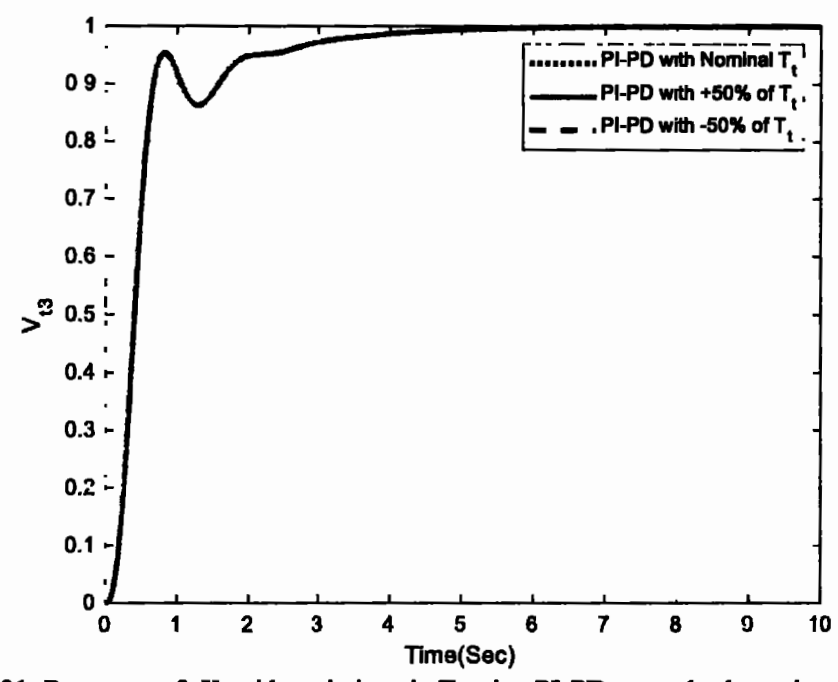


Figure 3.31: Response of V_{t3} with variations in T_t using PI-PD control scheme in a three-area single-source IPS

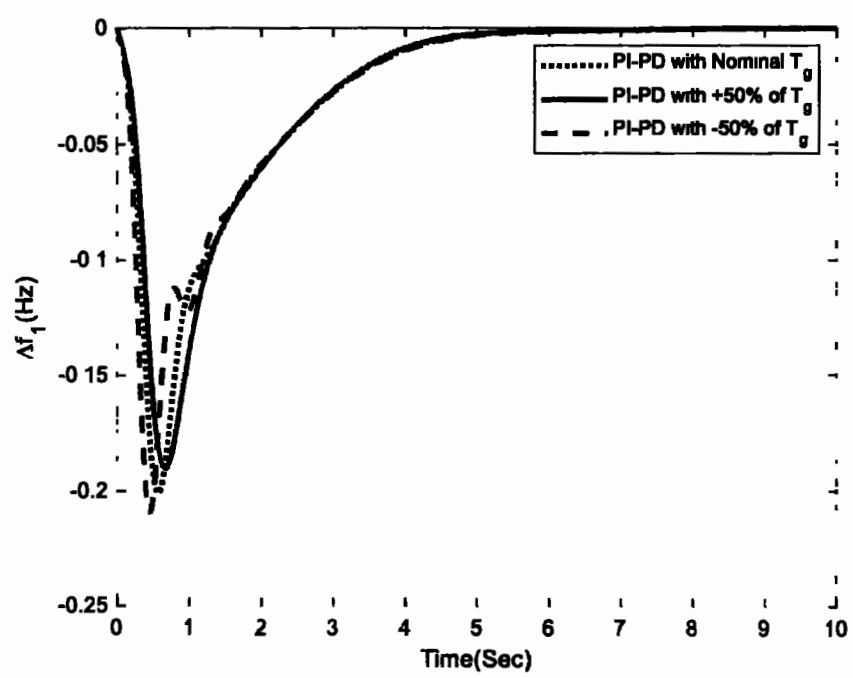


Figure 3.32: Response of Δf_1 with variations in T_g using PI-PD control scheme in a three-area single-source IPS

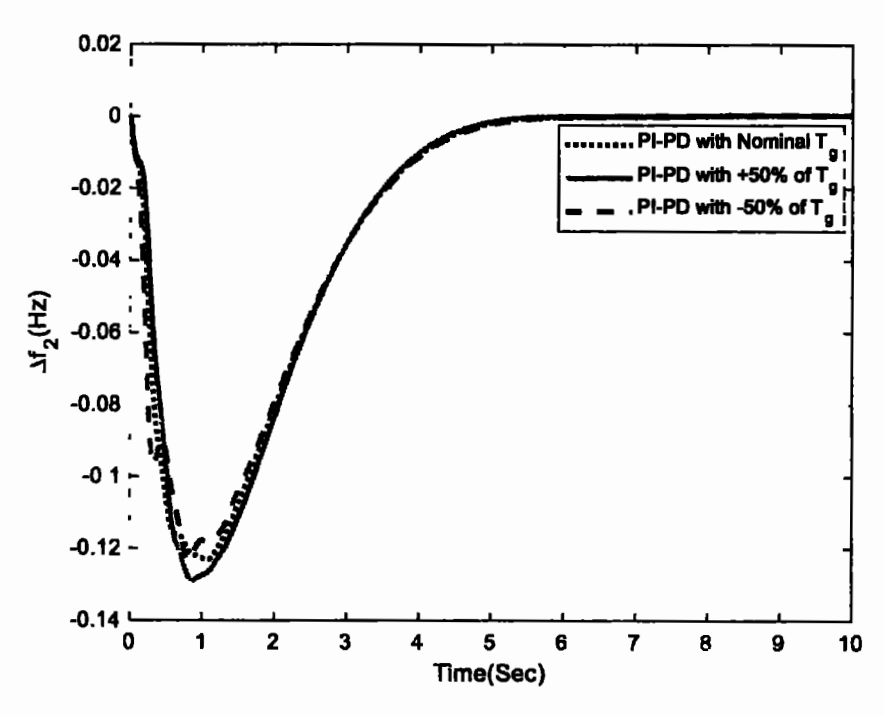


Figure 3.33: Response of Δf_2 with variations in T_g using PI-PD control scheme in a three-area single-source IPS

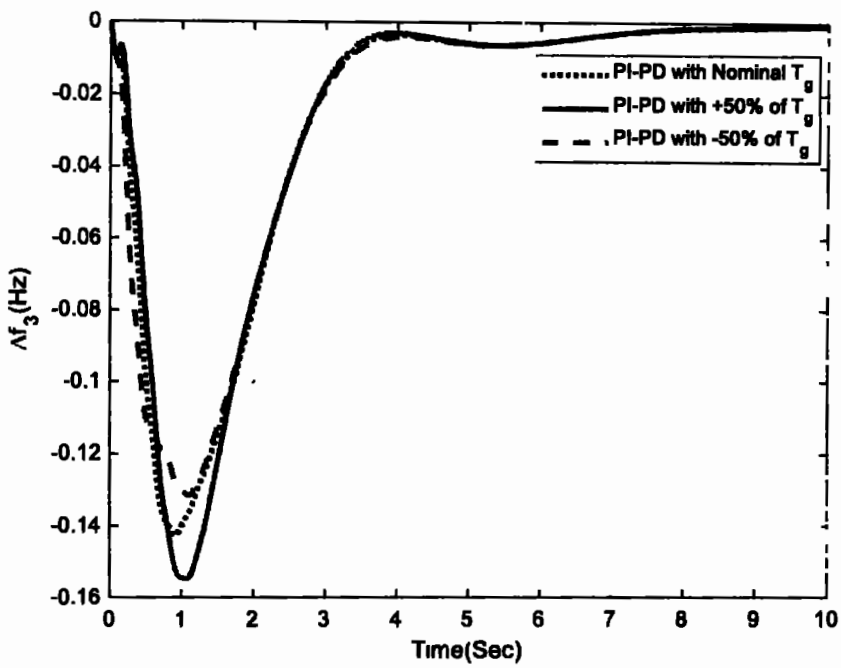


Figure 3.34: Response of Δf_3 with variations in T_g using PI-PD control scheme in a three-area single-source IPS

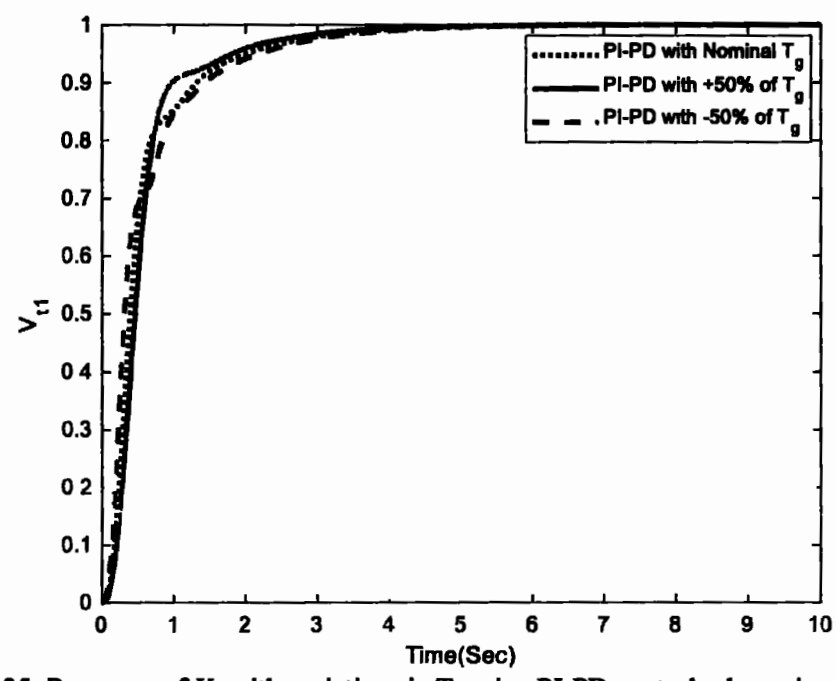


Figure 3.35: Response of V_{t1} with variations in T_g using PI-PD control scheme in a three-area single-source IPS

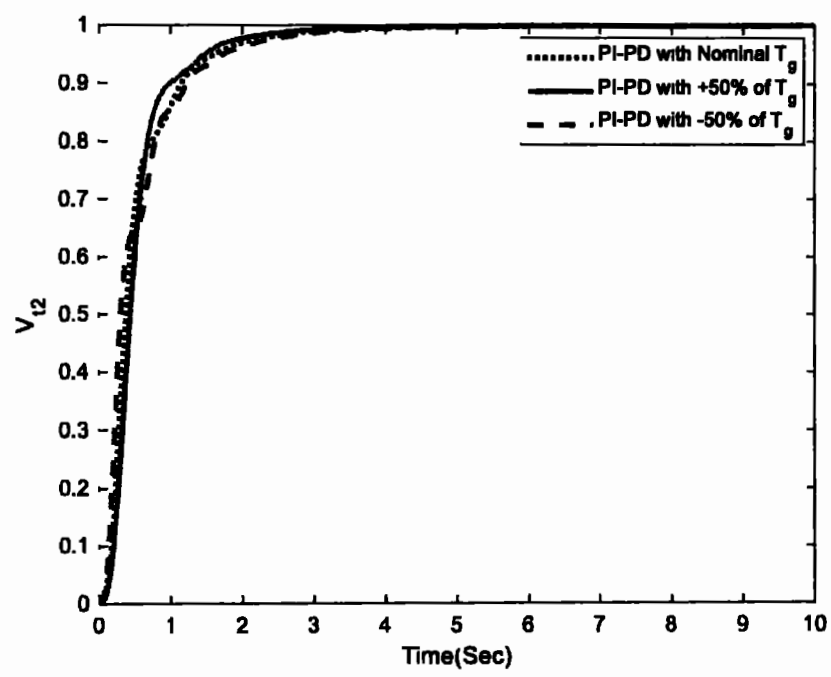


Figure 3.36: Response of V_{12} with variations in T_g using PI-PD control scheme in a three-area single-source IPS

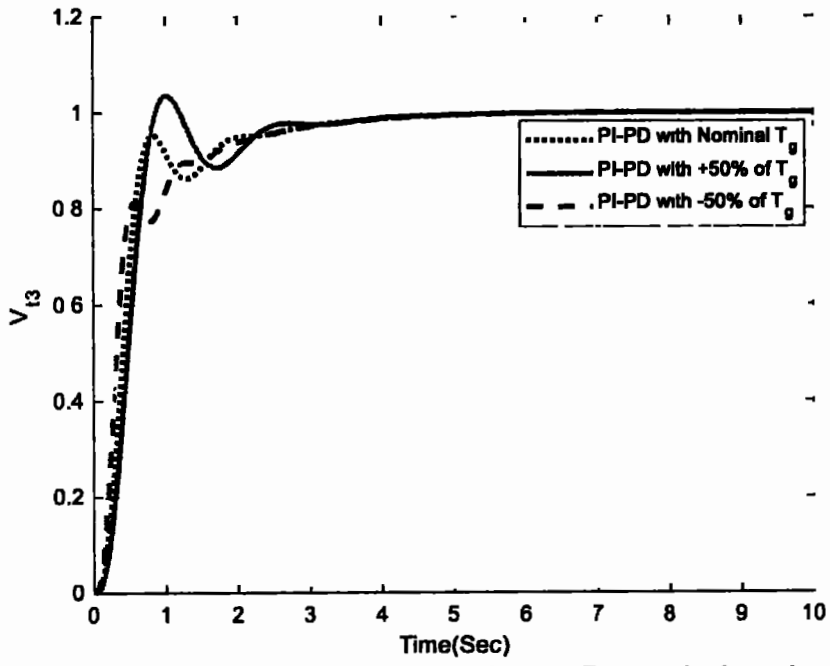


Figure 3.37: Response of V_{13} with variations in T_g using PI-PD control scheme in a three-area single-source IPS

Table 3.8: Settling time responses using PI-PD control scheme with variations in system parameters

Case	Settl	ing Time [L (s)	FC]	Settling Time [AVR] (s)			
	Δf_i	Δf_2	Δf3	V _{tl}	V ₁₂	V _B	
Nominal T _g , T _t	4.65	4.87	7.16	3.01	2.37	3.48	
+50% variation in T _{g1} , T _{g2} , T _{g3}	4.60	4.76	7.02	2.74	2.11	3.56	
-50% variation in T _{gl} , T _{g2} , T _{g3}	4.71	4.95	7.32	3.25	2.59	3.56	
+50% variation in T _{t1} , T _{t2} , T _{t3}	4.63	5.01	7.18	3.03	2.38	3.48	
-50% variation in T _{t1} , T _{t2} , T _{t3}	4.60	4.71	7.11	2.99	2.36	3.48	

Table 3.9: Overshoot and undershoot responses using PI-PD control scheme with variations in system parameters

Case	, , ,	% Overshoot (LFC)			Oversh (AVR)		%Undershoot (LFC)		
	Δf_l	Δf_2	Δf ₃	V _{tl}	V ₁₂	V _B	Δf_1	Δf_2	Δf3
Nominal Tg, Tt	0	0	0	0	0	0	-0.2	-0.12	-0.14
+50% variation in T _{g1} , T _{g2} , T _{g3}	0	0	0	0	0	3.4	-0.19	-0.13	-0.16
-50% variation in T _{g1} , T _{g2} , T _{g3}	0	0	0	0	0	0	-0.22	-0.13	-0.13
+50% variation in T ₁₁ , T ₁₂ , T ₁₃	0	0	0	0	0	0	-0.25	-0.13	-0.15
-50% variation in T _{t1} , T _{t2} , T _{t3}	0	0	0	0	0	0	-0.16	-0.13	-0.14

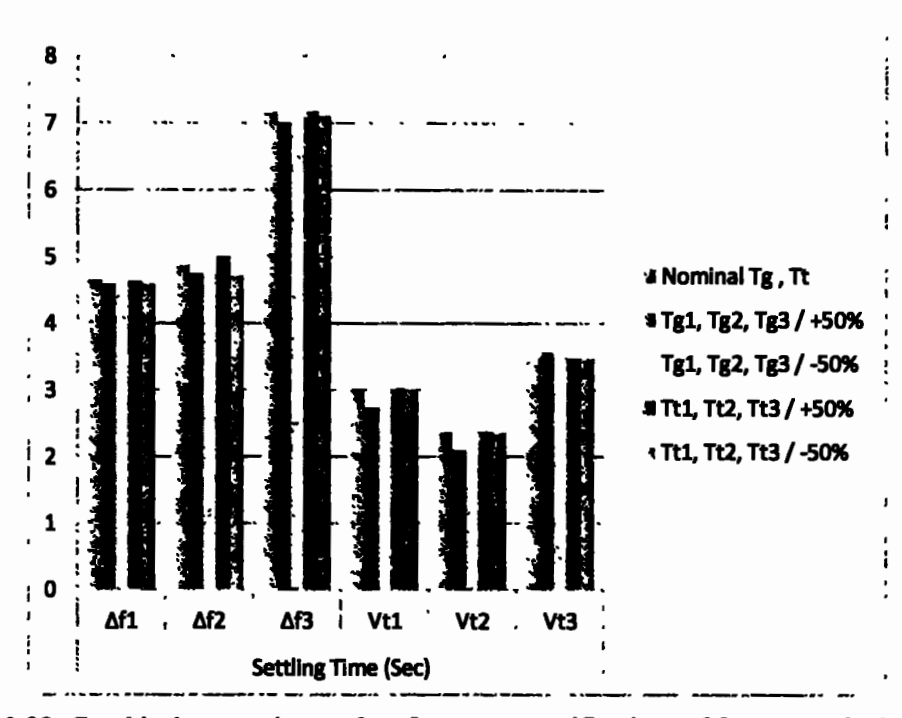


Figure 3.38: Graphical comparisons of performance specifications of frequency deviation and terminal voltage responses (Settling Time) in a three-area single-source IPS with variations in $T_{\rm g}$ and $T_{\rm t}$

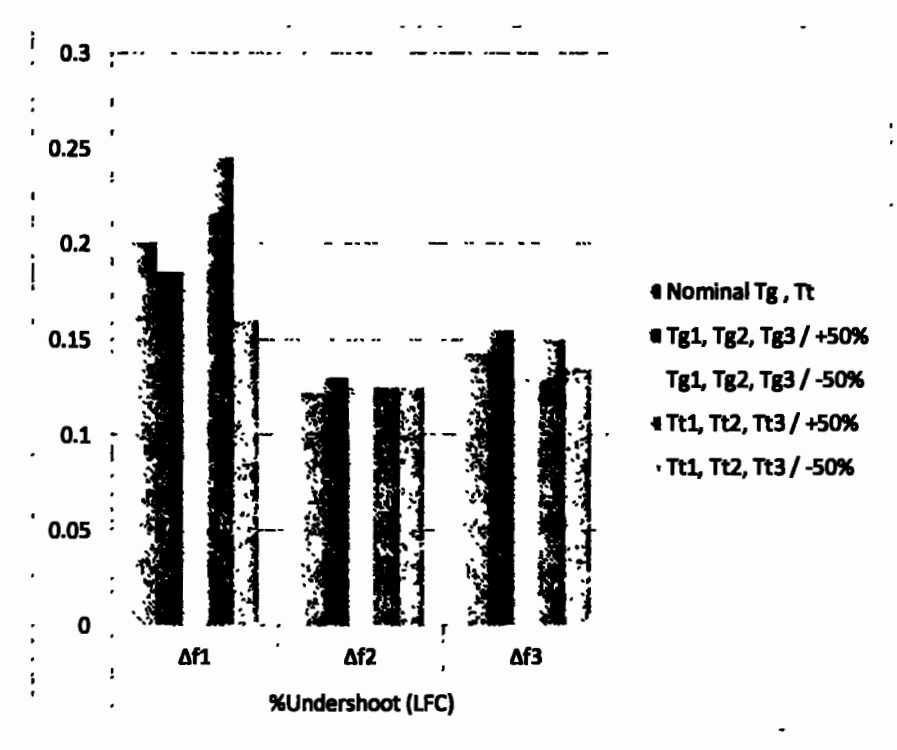


Figure 3.39: Graphical comparisons of performance specifications of frequency deviation responses (Undershoot) in a three-area single-source IPS with variations in $T_{\rm g}$ and $T_{\rm t}$

CHAPTER 4

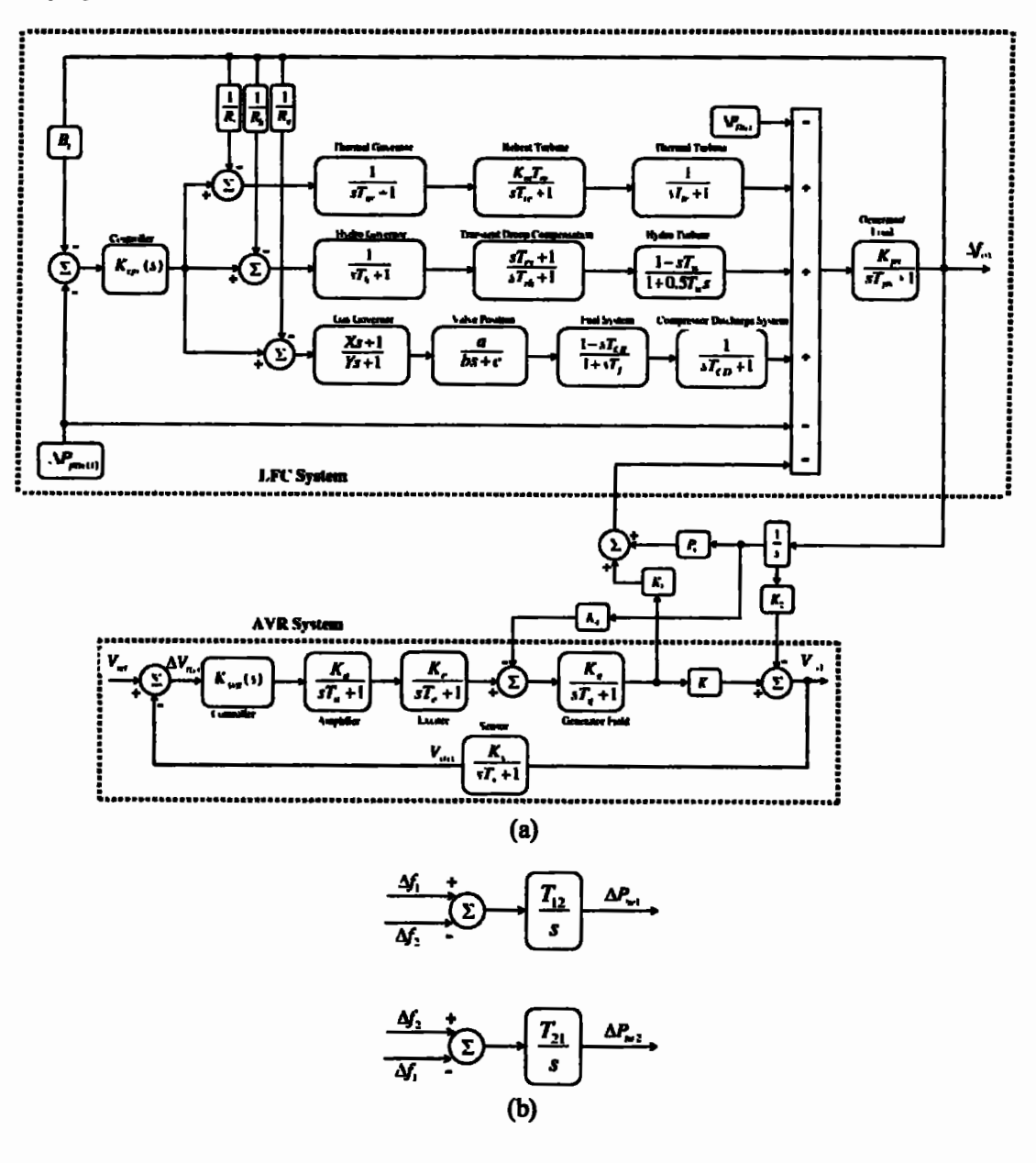
Frequency and Voltage Stabilization in Multi-area Multi-source IPS with/without Nonlinearities

This chapter deals with the design and implementation of the proportional integral-proportional derivative (PI-PD) controller for two- and three-area multi-source interconnected power systems with/without nonlinearities using nature inspired computation algorithms including dandelion optimizer (DO), learner performance based behavior optimization (LPBO), Archimedes optimization algorithm (AOA) and modified particle swarm optimization (MPSO).

4.1 Mathematical Modeling of Power System

The multi-area multi-source IPS under study is shown in Figure 4.1. The IPS consists of multiple areas with three different generation units including thermal reheat, hydro, and gas systems in each area [25]. The LFC loop of i^{th} area has a controller $(K_{LFC}(s))$, i^{th} area's bias factor (B_i) , thermal reheat speed regulation (R_i) , hydro speed regulation (R_i) , gas speed regulation (R_i) , and generator/load $\left(\frac{K_{PU}}{sT_{p(i)}+1}\right)$ with different blocks of power generation units. The thermal reheat unit consists of thermal governor $\left(\frac{1}{sT_p+1}\right)$, reheat turbine $\left(\frac{K_{R}T_{rr}}{sT_{rr}+1}\right)$, and thermal turbine $\left(\frac{1}{sT_{rr}+1}\right)$; hydro unit includes hydro governor $\left(\frac{1}{sT_{rr}+1}\right)$, and transient droop compensation $\left(\frac{sT_{rr}+1}{sT_{rr}+1}\right)$, hydro turbine $\left(\frac{1-sT_{rr}}{1+0.5T_{rr}s}\right)$; gas unit comprises gas governor $\left(\frac{Xs+1}{Ys+1}\right)$, valve position $\left(\frac{a}{bs+c}\right)$, fuel system $\left(\frac{1-sT_{cr}}{1+sT_f}\right)$, and compressor discharge system $\left(\frac{1}{sT_{co}+1}\right)$. $\Delta P_{D(i)}$, $\Delta f_{(i)}$, $\Delta V_{(i)}$, and $\Delta P_{ne(i)}$ denote the load deviation, frequency deviation, deviation in terminal voltage, and tie-line power deviation respectively. $V_{I(i)}$, $V_{ref(i)}$, and $V_{s(i)}$ refer to the terminal voltage, reference voltage, and sensor voltage in i^{th} area respectively. The AVR loop of i^{th} area consists of a

controller $(K_{AVR}(s))$, amplifier $\left(\frac{K_{s(t)}}{sT_{s(t)}+1}\right)$, generator $\left(\frac{K_{s(t)}}{sT_{s(t)}+1}\right)$, exciter $\left(\frac{K_{s(t)}}{sT_{s(t)}+1}\right)$, and sensor $\left(\frac{K_{s(t)}}{sT_{s(t)}+1}\right)$. K_1 , K_2 , K_3 , K_4 , and P_8 are the coefficients for mutual coupling between AVR and LFC loops. The synchronization coefficient between i^{th} and j^{th} area is represented by T_{ij} .



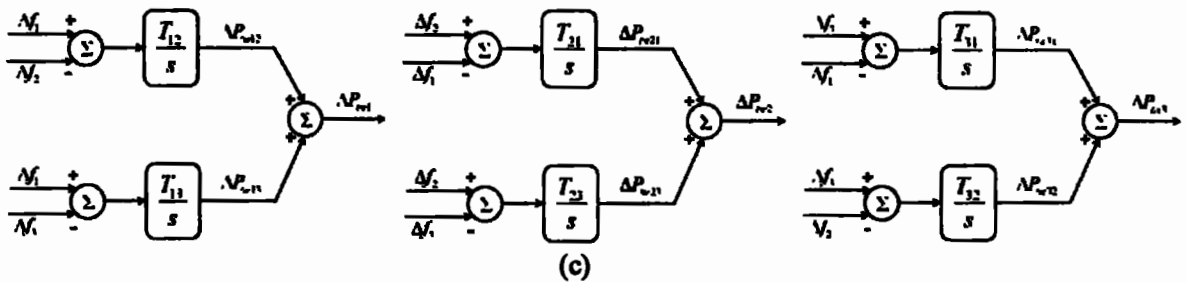


Figure 4.1: Power System

(a) Combined LFC-AVR model (b) Two-area tie-line (c) Three-area tie-lines

The transfer function models of the reheat thermal $(G_r(s))$, gas $(G_G(s))$, and hydro $(G_H(s))$ systems provided in Eq. (4.1), (4.2), and (4.3) respectively. The definitions of all symbols/terms used in Eq. (4.1-4.3) and IPS are provided in List of Symbols section.

$$G_{r}(s) = \frac{1 + T_{rr}K_{rr}s}{(1 + T_{rr}s)(1 + T_{rr}s)(1 + T_{rr}s)}$$
(4.1)

$$G_G(s) = \frac{a(1 - T_{CR}s)(1 + Xs)}{(1 + T_{CD}s)(1 + T_fs)(c + bs)(1 + Ys)}$$
(4.2)

$$G_H(s) = \frac{(1 + T_{rs}s)(1 - T_{w}s)}{(1 + T_{s}s)(1 + T_{s}s)(1 + 0.5T_{s}s)}$$
(4.3)

4.2. Nonlinearities

Several nonlinearities, including GRC, GDB, and BD, have been included in the multi-area multi-source IPS to increase the realism of the system. In this section, the details of each nonlinear component of the existing power system are explained.

4.2.1 Generation Rate Constraint (GRC)

The steam turbine is subject to thermodynamic and mechanical constraints, which are the main causes of GRC. The modeling of the power system must take this limitation into account, otherwise the system is likely to be subjected to severe turbulence leading to governor wear. The saturation type nonlinearity is used to characterize GRC, which fundamentally limits the steam turbine. The GRC of a thermal power plant is often lower than that of a hydroelectric plant. For a hydropower plant, the GRC is 360%/minute for lower generation and 270%/minute for higher generation. For a thermal power plant, the GRC is an upper limit of +3%/minute and a lower limit of -3%/minute [164].

4.2.2 Governor Dead Band (GDB)

The GDB is the measure of the total steady-state velocity variations that do not change the governor valve. The GDB is always defined as a percentage of the rated speed and

reflects the insensitivity of the speed control mechanism. GDB causes oscillations of the system and increases the perceived inaccuracy in steady state. To express the GDB and its transfer function model, backlash form of nonlinearity is used [165]. In this work, the value of GDB is assumed to be ±0.036%.

4.2.3 Boiler Dynamics (BD)

The model of the transfer function of the boiler dynamics is shown in Figure 4.2 [166]. The combustion control is included in the proposed model. The boiler system receives preheated input water and generates pressurized steam. When the boiler control system detects changes in pressure deviations and steam flow rate, the necessary controls are immediately applied [1][166]. This model can be used to study coal-fired plants with well-tuned combustion control as well as oil- or gas-fired plants with poor combustion control.

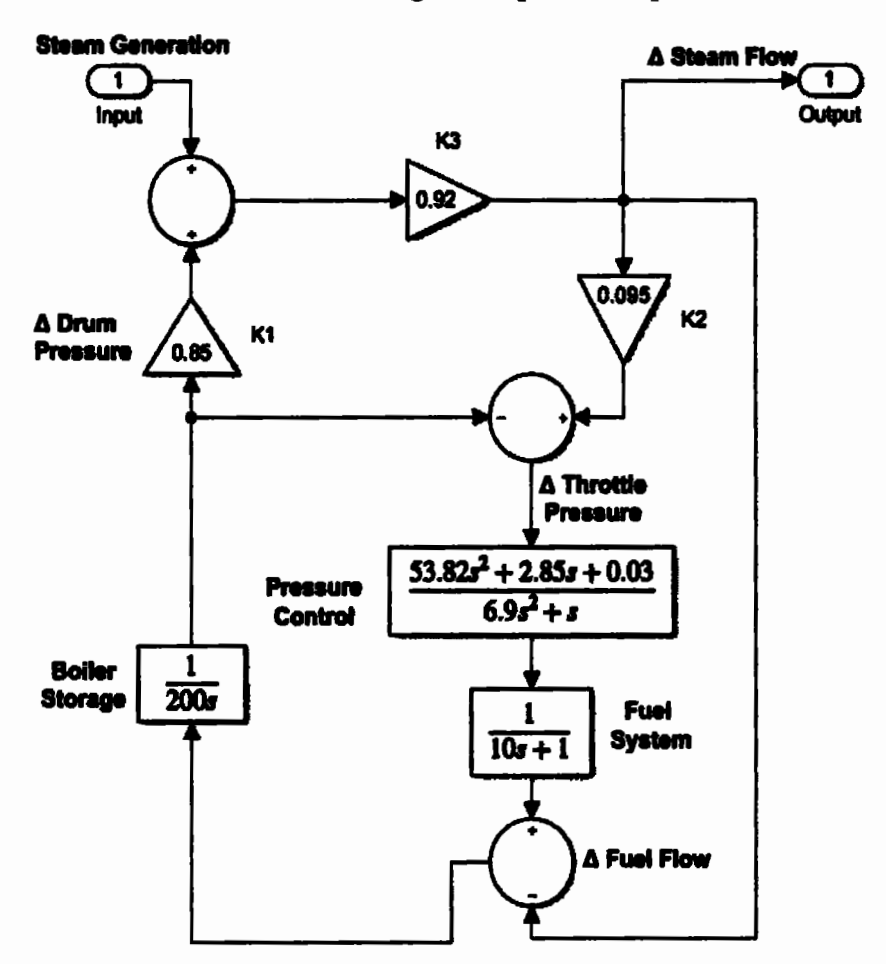


Figure 4.2: Transfer function model of boiler dynamics

4.3 Proposed Methodology

PI-PD controller has been investigated for simultaneous control of AVR and LFC loops in multi-area multi-source IPSs due to the excellent performance presented in the previous chapter. The proposed control methodology to control load frequency and terminal voltage in a four-area IPS is given in Figure 4.3. Eq. (4.4) is used to obtain the control signal U(s) generated by PI-PD controller with IPS:

$$U(s) = (K_{p1} + \frac{K_{l}}{s})E(s) - (K_{p2} + K_{d}s)Y(s)$$
(4.4)

$$E(s) = Y(s) - R(s) \tag{4.5}$$

where U(s), Y(s), R(s), and E(s) denote the control, output, reference, and error signals respectively. K_{p1} , K_{p2} , K_{i} , and K_{d} are the gain coefficients of PI-PD controller.

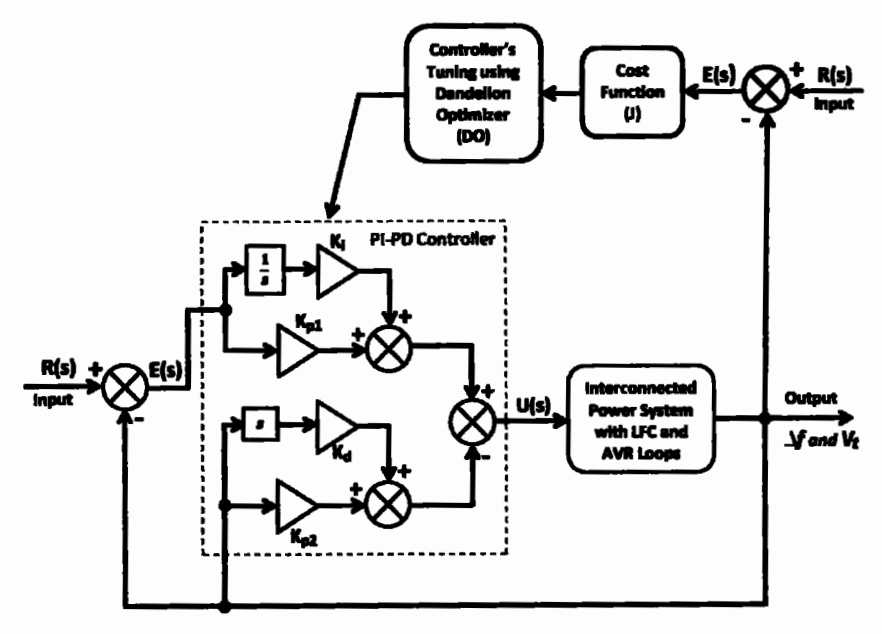


Figure 4.3: Proposed control methodology

The cost function (J) is optimized using nature-inspired computational strategies to determine the best controller parameters. In this work, DO algorithm has been explored for the optimization of the cost function (J). There are various error indices but ITSE has been used to formulate the cost function (J) as follows:

$$J_{\text{ITSE, two-area}} = \int_{0}^{T} t \left[\Delta f_{1}^{2} + \Delta f_{2}^{2} + \Delta V_{11}^{2} + \Delta V_{12}^{2} + \Delta P_{112}^{2} \right] dt$$
 (4.6)

$$J_{\text{ITSE, three-area}} = \int_{0}^{T} t \left[\Delta f_{1}^{2} + \Delta f_{2}^{2} + \Delta f_{3}^{2} + \Delta V_{i1}^{2} + \Delta V_{i2}^{2} + \Delta V_{i3}^{2} + \Delta V_{ie1}^{2} + \Delta P_{ie2}^{2} + \Delta P_{ie2}^{2} + \Delta P_{ie3}^{2} \right] dt$$
 (4.7)

where,

$$\Delta V_{i1} = V_{ref} - V_{i1}$$

$$\Delta V_{i2} = V_{ref} - V_{i2}$$

$$\Delta V_{i3} = V_{ref} - V_{i3}$$
(4.8)

$$\Delta P_{pixel} = \Delta P_{pixel2} + \Delta P_{pixel3}$$

$$\Delta P_{phe2} = \Delta P_{phe21} + \Delta P_{phe23} \tag{4.9}$$

$$\Delta P_{pise3} = \Delta P_{pise31} + \Delta P_{pise32}$$

4.4 Dandelion Optimizer (DO)

Shijie Zhao proposed the DO algorithm in 2022. The dandelion is a plant that uses the wind to spread its seeds [167]. During the rising phase, a vortex forms above the dandelion seed, and it rises as it is propelled aloft by wind and sunlight. In contrast, on a rainy day, there are no vortices over the seed. In this situation, only a local search is possible. When the seeds reach a certain height in the descending phase, they begin to sink steadily. In the landing phase, the dandelion seeds finally land by chance in a place where they develop new dandelions due to the influence of wind and weather. By passing on its seeds to the next generation, the dandelion continues to develop its population. The four main stages of the DO algorithm are listed below.

4.4.1 Initialization

It is considered that each dandelion seed in the DO algorithm indicates a potential solution. The population of DO can be expressed as:

$$population = \begin{bmatrix} x_1^1 & \dots & x_1^{D_{im}} \\ \dots & \dots & \dots \\ x_{pop}^1 & \dots & x_{pop}^{D_{im}} \end{bmatrix}$$
(4.10)

where, pop and Dim stand for the population size and the dimension of the variable respectively.

Between the specified problem's upper bound (UB) and lower bound (LB), each possible solution is produced at random and i^{th} individual X_i can be expressed as:

$$X_{i} = rand \times (UB - LB) + LB \tag{4.11}$$

where, i is an integer between 1 and pop whereas rand represents a random number between 0 and 1.

UB and LB can be written as:

$$LB = [lb_1, \dots, lb_{Dm}]$$

$$UB = [ub_1, \dots, ub_{Dm}]$$
(4.12)

According to DO, the initial elite is the individual with the highest fitness value, which is referred to as the best position for the dandelion seed to grow. The initial elite's mathematical formulation, using the minimal value as an illustration is:

$$f_{best} = \min(f(X_i))$$

$$X_{slite} = X(find(f_{best} == f(X_i)))$$
(4.13)

4.4.2 Rising stage

In order to float away from their parent plant, dandelion seeds must reach a specific height during the rising stage. Dandelion seeds rise to various heights depending on the air humidity and wind speed etc. The two weather conditions in this instance are as follows.

Case 1:

Wind speeds on a clear day can be thought of as having a lognormal distribution. $\ln Y \sim N(\mu, \sigma^2)$. The wind speed affects how high a dandelion seed will rise. If wind is stronger, dandelion flies higher and seeds scatter farther.

$$X_{t+1} = X_t + \alpha \times \nu_x \times \nu_y \times \ln Y \times (X_s - X_t)$$
(4.14)

where, X_s shows the randomly selected position at iteration t and X_t shows the dandelion seed's position at iteration t.

Eq. (21) shows the expression for the randomly generated position:

$$X_s = rand(1, Dim)^*(UB - LB) + LB \tag{4.15}$$

lnY shows a lognormal distribution subject to $\mu=0$ and $\sigma^2=1$.

$$\ln Y = \begin{cases} \frac{1}{y\sqrt{2\pi}} \exp[-\frac{1}{2\sigma^2} (\ln y)^2] \\ 0 \end{cases} \qquad y \ge 0$$

$$y < 0 \qquad (4.16)$$

where, y indicates the standard normal distribution (0, 1).

$$\alpha = rand() \times (\frac{1}{T^2}t^2 - \frac{2}{T}t + 1) \tag{4.17}$$

where, α represents a random perturbation between [0, 1].

 v_x and v_y demonstrate the dandelion's lift component coefficients.

$$r = \frac{1}{e^{\theta}}$$

$$v_{\tau} = r \cos \theta$$

$$v_{\nu} = r \sin \theta$$
(4.18)

where, θ varies randomly between $[-\pi, \pi]$.

Case 2:

Due to humidity and air resistance, dandelion seeds struggle to rise properly with the wind on wet day.

$$X_{t+1} = X_t \times k$$

$$k = 1 - rand() * q$$
(4.19)

A dandelion uses k to control its local search area. The domain (q) can be obtained using Eq. (34) as:

$$q = \frac{1}{T^2 - 2T + 1}t^2 - \frac{1}{T^2 - 2T + 1}t + 1 + \frac{1}{T^2 - 2T + 1}$$
(4.20)

The mathematical equation for the dandelion seed's ascending stage is finally:

$$X_{t+1} = \begin{cases} X_{t+1} = X_t + \alpha \times \nu_\tau \times \nu_\nu \times \ln Y \times (X_s - X_t) \\ X_{t+1} = X_t \times k \end{cases}$$
 randn< 1.5 else (4.21)

The random number generated by the function randn() follows the normal distribution.

4.4.3 Descending stage

In this stage, dandelion seeds rise to a particular height and then slowly sink (exploration phase). Brown motion is employed in DO to replicate the trajectory of a dandelion as it moves.

$$X_{t+1} = X_t - \alpha \times \beta_t \times (X_{mean_t} - \alpha \times \beta_t \times X_t)$$
 (4.22)

where, β_t indicates the Brownian motion.

$$X_{\text{mean_t}} = \frac{1}{pop} \sum_{i=1}^{pop} X_i \tag{4.23}$$

4.4.4 Landing stage

The DO algorithm concentrates on exploitation in this last stage. The dandelion seed makes its landing location at random based on the results of the prior two stages. The algorithm should converge to the optimal solution as the iterations increasingly advance.

The population's evolution finally leads to the following global optimal solution:

$$X_{t+1} = X_{elite} + levy(\lambda) \times \alpha \times (X_{elite} - X_t \times \delta)$$
(4.24)

where, X_{elite} denotes the seed's optimal position.

$$levy(\lambda) = s \times \frac{w \times \sigma}{\left|t\right|^{\frac{1}{\beta}}} \tag{4.25}$$

where, s is 0.01, β is a random number and its values may vary between 0 and 2. t and w are arbitrary numbers in the range [0, 1]. σ is expressed mathematically as follows:

$$\sigma = \left(\frac{\Gamma(1+\beta) \times \sin(\frac{\pi\beta}{2})}{\Gamma(\frac{1+\beta}{2}) \times \sin(\frac{\beta-1}{2})}\right)$$
(4.26)

The value of β is 1.5 whereas δ can be obtained as:

$$\delta = \frac{2t}{T} \tag{4.27}$$

The flow chart of DO algorithm is provided in Figure 4.4.

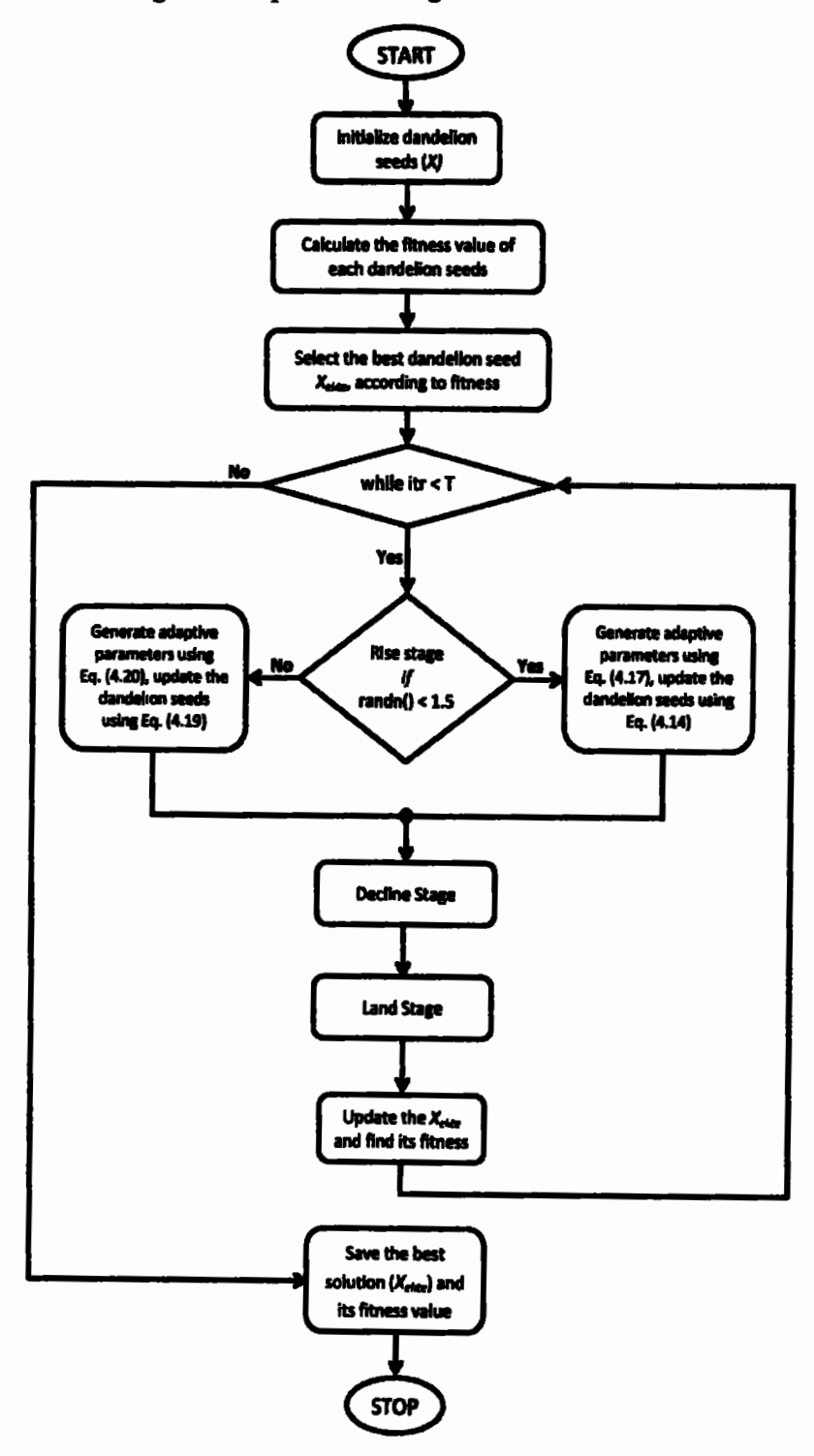


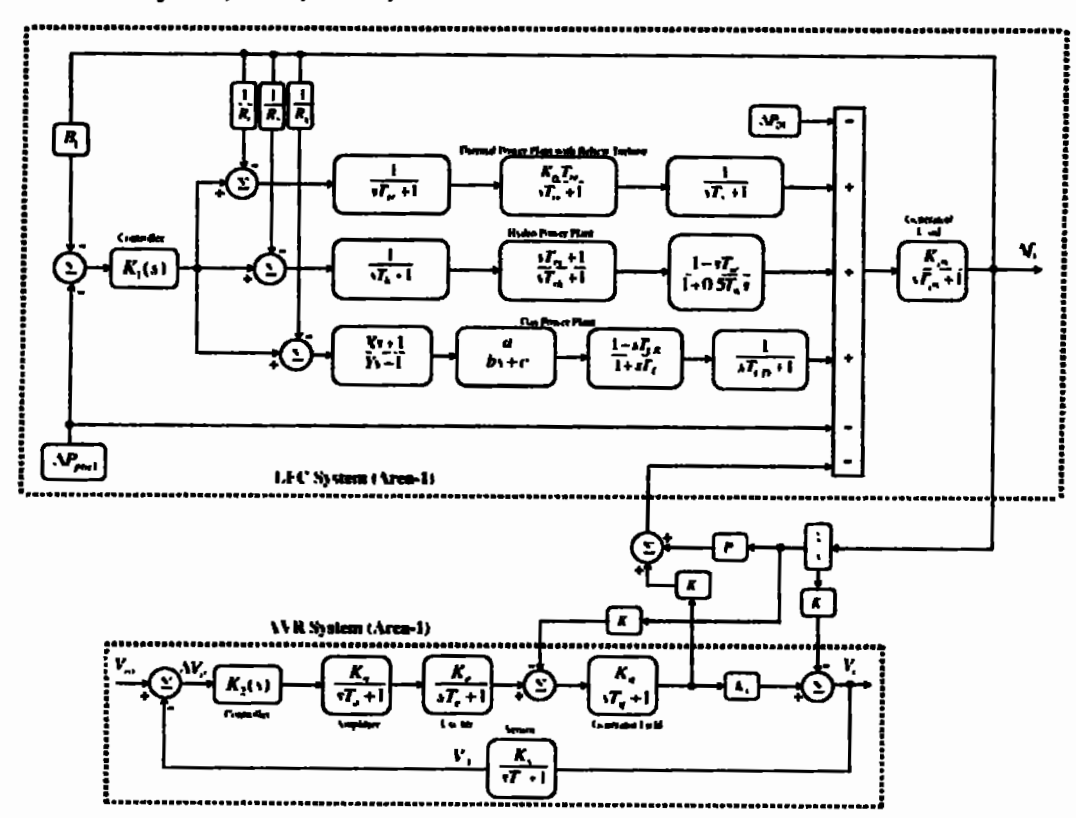
Figure 4.4: Flow chart of DO

4.5 Implementation and Results Discussion

To express the validation of the proposed control methods, numerous simulations were performed in MATLAB/Simulink to analyze the results. First, two-area multi-source IPS was examined using the PI-PD control methods based on the AOA, LPBO, MPSO,, and DO algorithms. In this IPS, both areas had three generating units including thermal reheat, gas, and hydro. The successful results led to the application of the proposed methodology to the same IPS with additional nonlinearities such as BD, GDB, and GRC. Finally, to confirm the exceptional performance of the proposed control method, three-area multi-source IPS with nonlinearities was also studied.

4.5.1 Frequency and Voltage Stabilization in a Two-area Multi-source IPS without Nonlinearities

Figure 4.5 shows the two-area multi-source IPS. The system parameters of the two-area IPS are given in Appendix B. The analysis of the dynamic response of the power system was performed with 10% SLP in area-1. The parameters of the optimization algorithms are given in Table 4.1. The optimal parameters of AOA, LPBO, MPSO, and DO based control methods are shown in Table 4.2. To evaluate the proposed DO based PI-PD control methods, the time response of each control method is evaluated and compared with the results of HAEFA fuzzy PID, AOA, LPBO, and MPSO based PI-PD controllers.



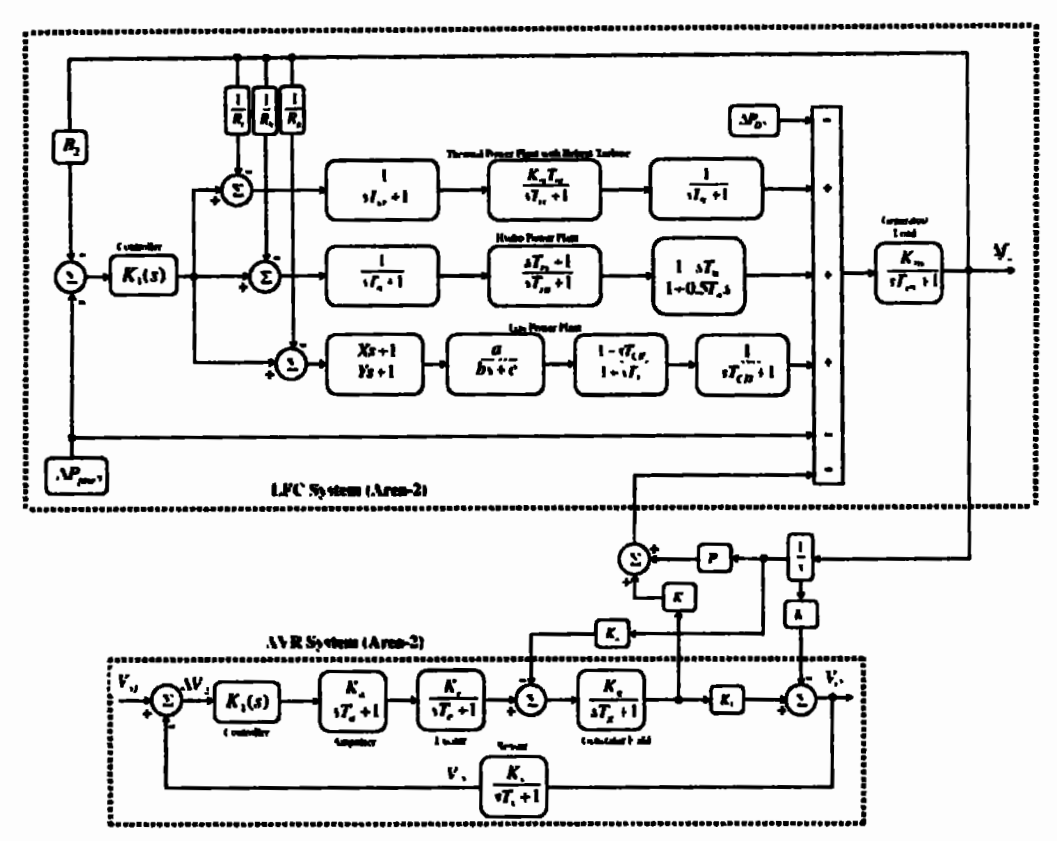


Figure 4.5: Two-area multi-source IPS model without nonlinearities

Table 4.1: Parameters setting of AOA, LPBO, MPSO, and DO

AOA		LPE	Ю	MPSC)	DC)
Parameter	Value	Parameter	Value	Parameter	Value	Parameter	Value
Iterations	4, 6,4	Iterations	4,6,4	Iterations	5,6,5	Iterations	5,6,5
Cı	2	Crossover Percentage	0.65	Inertia Weight Damping Ratio	1	Lower Bound	0
C ₂	6	Mutation Percentage	0.3	Personal Learning Coefficient	2.74	Upper Bound	2
C ₃	2	Mutation Rate	0.03	Global Learning Coefficient	2.88	Population size	20,10,20
C ₄	0.5	Number of Mutants	6	Max. Velocity Limit	0.2	-	•
Range of Normalization (u,l)	0.9, 0.1	Number of Offspring	14	Min. Velocity Limit	-0.2	-	-
Population size	25, 10,25	Population size	20,13,20	Population size	20,10,20	<u> </u>	

Table 4.2: Optimal values of controller parameters for a two-area multi-source IPS without nonlinearities

Area	Controller Parameters	AOA based PI-PD	LPBO based PI-PD	MPSO based PI-PD	DO based PI-PD
	K _{pl}	1.59	1.09	0.46	0.97
	K.1	0.93	1.10	0.78	1.97
	K _{p2}	0.89	1.44	1.14	0.67
Area-1	K _{d1}	1.57	1.27	1.47	1.39
AICH-1	K_{p3}	1.32	1.82	1.06	2
	K ₁₂	1.87	1.22	1.73	1.83
	K _{p4}	1.29	0.35	1.20	0.67
	K _{d2}	0.73	0.42	0.73	0.75
	K _{p5}	1.59	0.68	1.16	1.03
	K _{t3}	0.94	0.68	0.17	0.23
	K _{p6}	1.13	1.24	0.97	0.73
Агеа-2	K _{d3}	1.34	1.60	1.56	0.92
Arca-2	K _{p7}	1.82	1.78	1.38	2
	K,4	1.73	1.57	1.60	1.1
	K _{p8}	1.04	0.96	0.98	0.33
	K _{d4}	0.97	0.93	0.66	0.77
	ITSE	0.35	0.28	0.39	0.24

The frequency deviation responses of area-1 and area-2 are shown in Figure 4.6 and 4.7 while Tables 4.3 presents the performance specifications using DO, AOA, LPBO, and MPSO based PI-PD control methodologies.

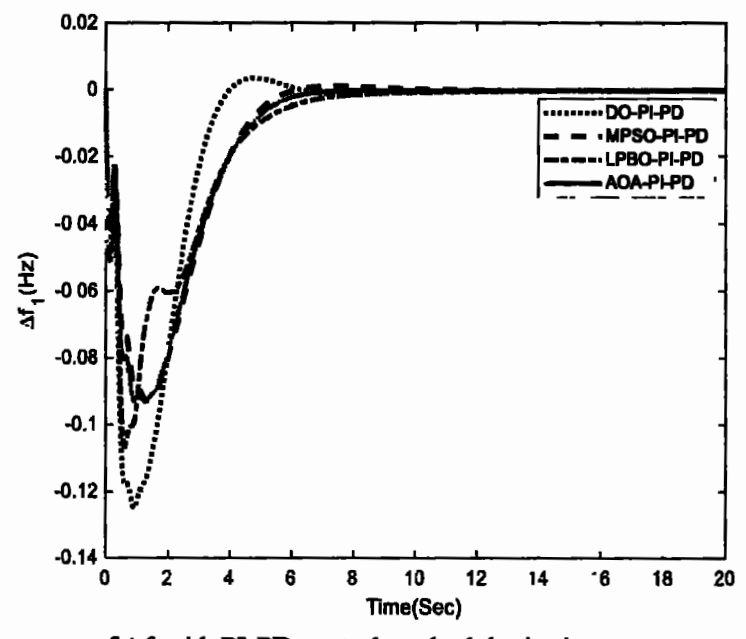


Figure 4.6: Response of Δf_i with PI-PD control methodologies in a two-area multi-source IPS without nonlinearities

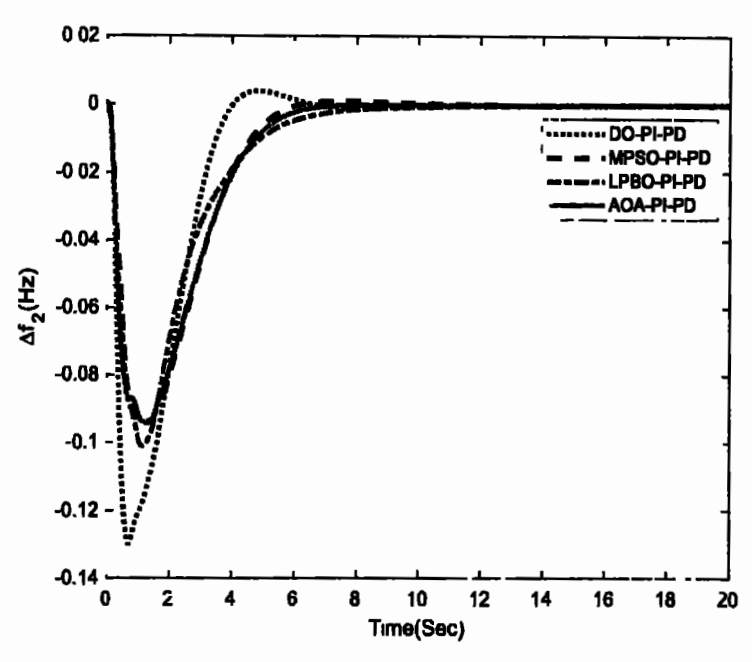


Figure 4.7: Response of Δf_2 with PI-PD control methodologies in a two-area multi-source IPS without nonlinearities

As can be seen, the frequency deviation responses from the suggested control methodologies are quite good. For area-1 LFC, DO based PI-PD provided settling time of 5.44s, which is lower than other control methodologies and relatively 53% better than HAEFA Fuzzy PID controller [25]. Particularly, AOA and LPBO based PI-PD yielded zero % overshoot. The MPSO based PI-PD gave a settling time of 5.60s for area-2 LFC, which is less than other control methodologies, that is 32% better than HAEFA Fuzzy PID controller. AOA and LPBO based PI-PD control methodologies provided zero % overshoot in both areas. The steady-state error is always zero when using the suggested methods.

Table 4.3: Performance specifications of frequency deviation responses in a two-area multisource IPS without nonlinearities

		Area-1				Area-2			
Control Methodology	Settling Time (s)	% Overshoot	Undershoot	% s-s Error	Settling Time (s)	% Overshoot	Undershoot	% s-s Error	
HAEFA Fuzzy PID [25]	11.61	0.0009	-0.01	0	8.28	0.0002	-0.0032	0	
AOA based PI-PD	6.12	0	-0.094	0	6.12	0	-0.094	0	
LPBO based PI-PD	7.14	0	-0.108	0	7.30	0	-0.102	0	
MPSO based PI-PD	5.55	0.001	-0.094	0	5.60	0.001	-0.095	0	
DO based PI-PD	5.44	0.004	-0.126	0	5.61	0.004	-0.130	0	

The terminal voltage responses of area-1 and area-2 are shown in Figure 4.8 and 4.9 while Tables 4.4 presents the performance specifications using DO, AOA, LPBO, and MPSO based PI-PD control methodologies. As can be observed, the terminal voltage responses produced by the suggested control methodologies were quite excellent. The proposed DO based PI-PD produced settling time of 1.32s and 1.40s in area-1 and area-2 AVR, which are lower than others. DO based PI-PD provided relatively 40% and 31% better AVR's settling time response compared to HAEFA Fuzzy PID controller in area-1 and area-2 AVR respectively. AOA based PI-PD provided 0.0020% overshoot in area-1 AVR whereas LPBO based PI-PD provided 0.016% overshoot in area-2 AVR. AOA based PI-PD produced 99.8% better overshoot response in area-2 AVR respectively compared to HAEFA Fuzzy PID controller. Furthermore, the steady-state error is zero in each case using the suggested methods.

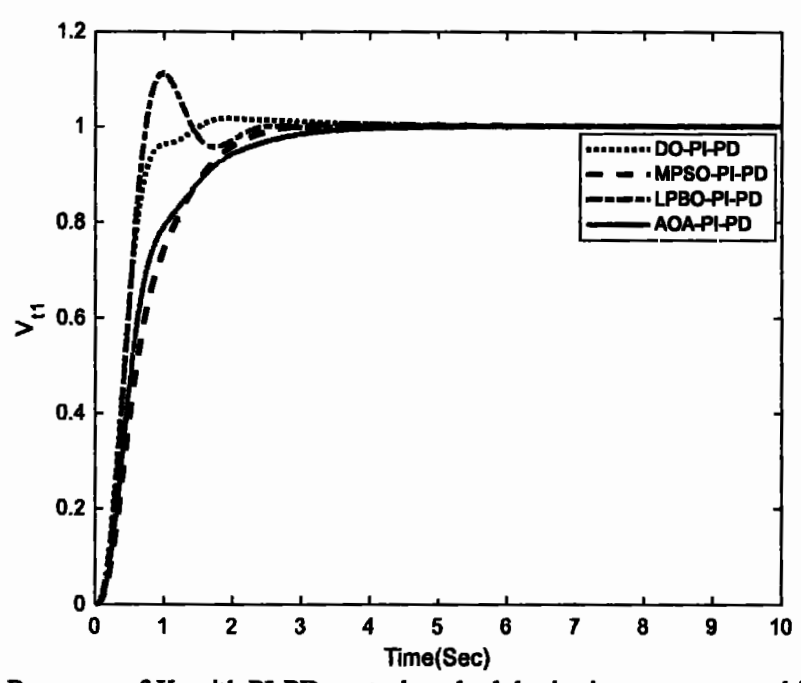


Figure 4.8: Response of V_{tl} with PI-PD control methodologies in a two-area multi-source IPS without nonlinearities

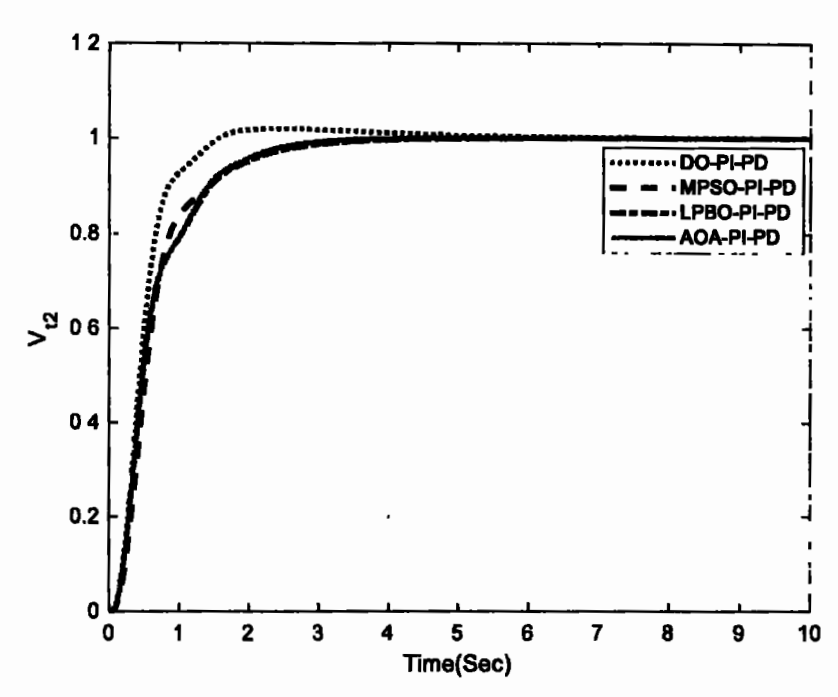


Figure 4.9: Response of V_2 with PI-PD control methodologies in a two-area multi-source IPS without nonlinearities

Table 4.4: Performance specifications of terminal voltage responses in a two-area multisource IPS without nonlinearities

		Area-1		Area-2			
Control Methodology	Settling Time (s)	% Overshoot	% s-s Error	Settling Time (s)	% Overshoot	% s-s Error	
HAEFA Fuzzy PID [25]	2.21	12	0	2.02	14	0	
AOA based PI-PD	2.85	0.0020	0	2.45	0.040	0	
LPBO based PI-PD	2.10	10.80	0	2.66	0.016	0	
MPSO based PI-PD	2.30	0.43	0	2.60	3.99e-04	0	
DO based PI-PD	1.32	1.63	0	1.40	1.94	0	

The tie-line power deviation responses are shown in Figure 4.10 while Tables 4.5 presents the performance specifications using DO, AOA, LPBO, and MPSO based PI-PD control methodologies. It can be observed that LPBO based PI-PD produced settling time of 3.87s that is better than other control methodologies, that is 75% relatively better than HAEFA Fuzzy PID controller. Moreover, each proposed control methodology provided negligible % overshoot and undershoot responses. With each control methodology, the steady-state error is zero, as can be observed.

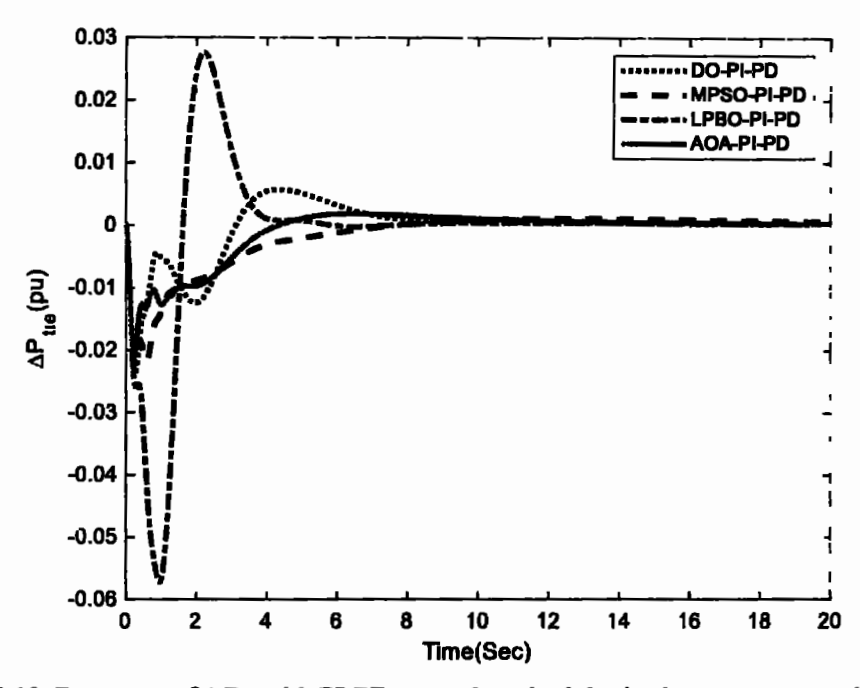


Figure 4.10: Response of ΔP_{tie} with PI-PD control methodologies in a two-area multi-source IPS without nonlinearities

Table 4.5: Performance specifications of tie-line power deviation responses in a two-area multi-source IPS without nonlinearities

Control Methodology	Settling Time (s)	% Overshoot	Undershoot	% s-s Error
HAEFA Fuzzy PID [25]	15.59	0.0005	-0.0035	0
AOA based PI-PD	12.80	0.0023	-0.021	0
LPBO based PI-PD	3.87	0.027	-0.057	0
MPSO based PI-PD	13.69	0.00125	-0.022	0
DO based PI-PD	8.84	0.006	-0.0235	0

Figure 4.11, 4.12, and 4.13 show the graphical comparisons of the performance specifications frequency deviation, terminal voltage, and tie-line power deviation responses using AOA, LPBO, MPSO, and DO based PI-PD control methodologies. In comparison to the HAEFA fuzzy PID controller, DO based PI-PD based control methodology offered relatively superior frequency deviation, terminal voltage, and tie-line power deviation responses.

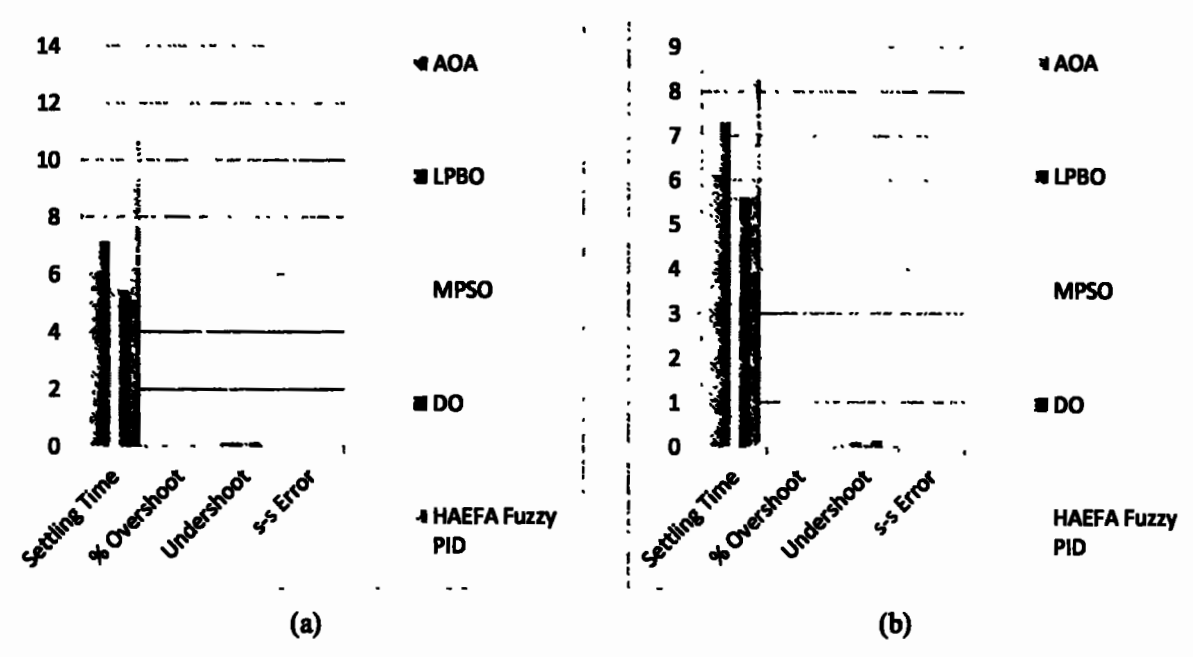


Figure 4.11: Graphical comparisons of performance specifications of frequency deviation responses using PI-PD control methodologies in a two-area multi-source IPS without nonlinearities

(a) Δf_1 (b) Δf_2

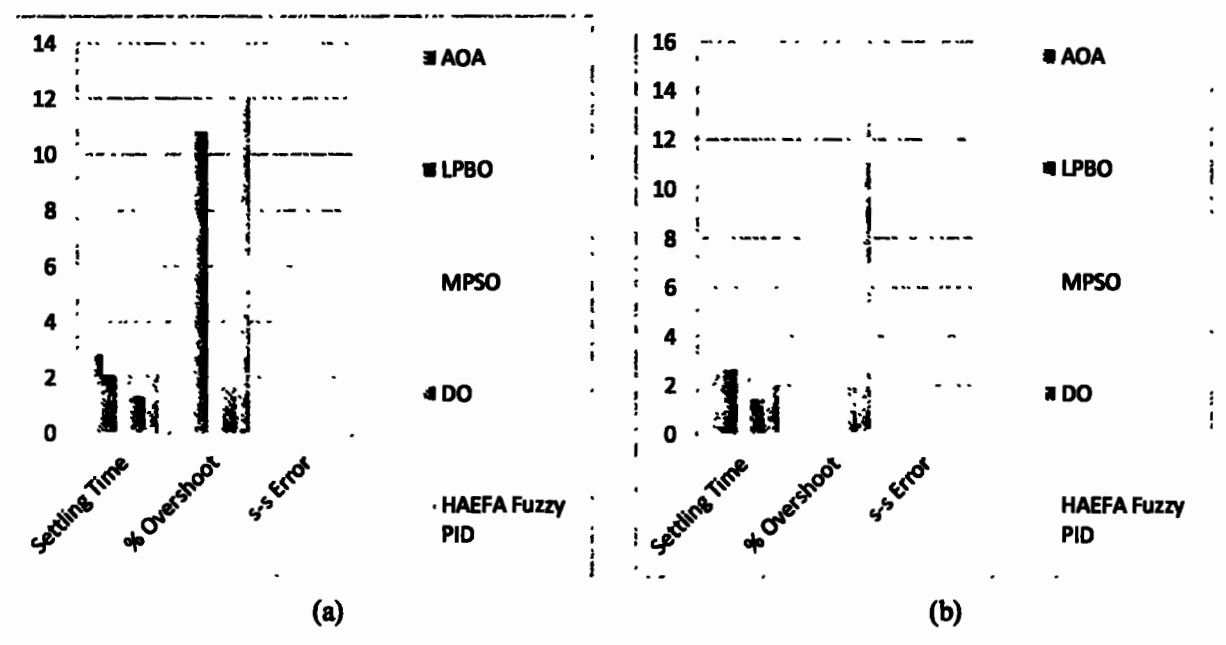


Figure 4.12: Graphical comparisons of performance specifications of terminal voltage responses using PI-PD control methodologies in a two-area multi-source IPS without nonlinearities

(a) V_{t1} (b) V_{t2}

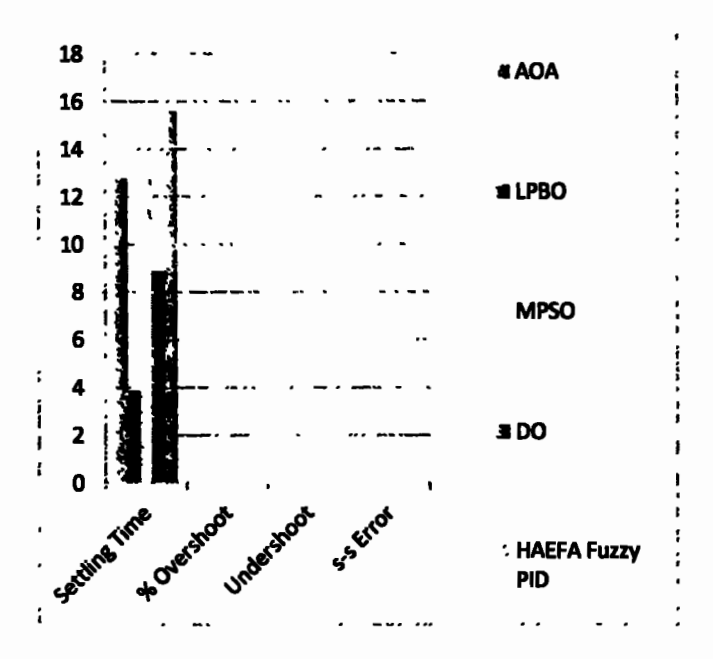


Figure 4.13: Graphical comparison of performance specifications of tie-line power deviation response (ΔP_{tie}) using PI-PD control methodologies in a two-area multi-source IPS without nonlinearities

4.5.2 Frequency and Voltage Stabilization in a Two-area Multi-source IPS with Nonlinearities

In this section, the proposed methods were applied to two-area multi-source IPS with BD, GRC, and GDB nonlinearities. In addition, the dynamic analysis of the power system was performed with 5% SLP in area-1 and area-2. The model under study is shown in Figure 4.14 and the parameters of the IPS model are listed in Appendix B.

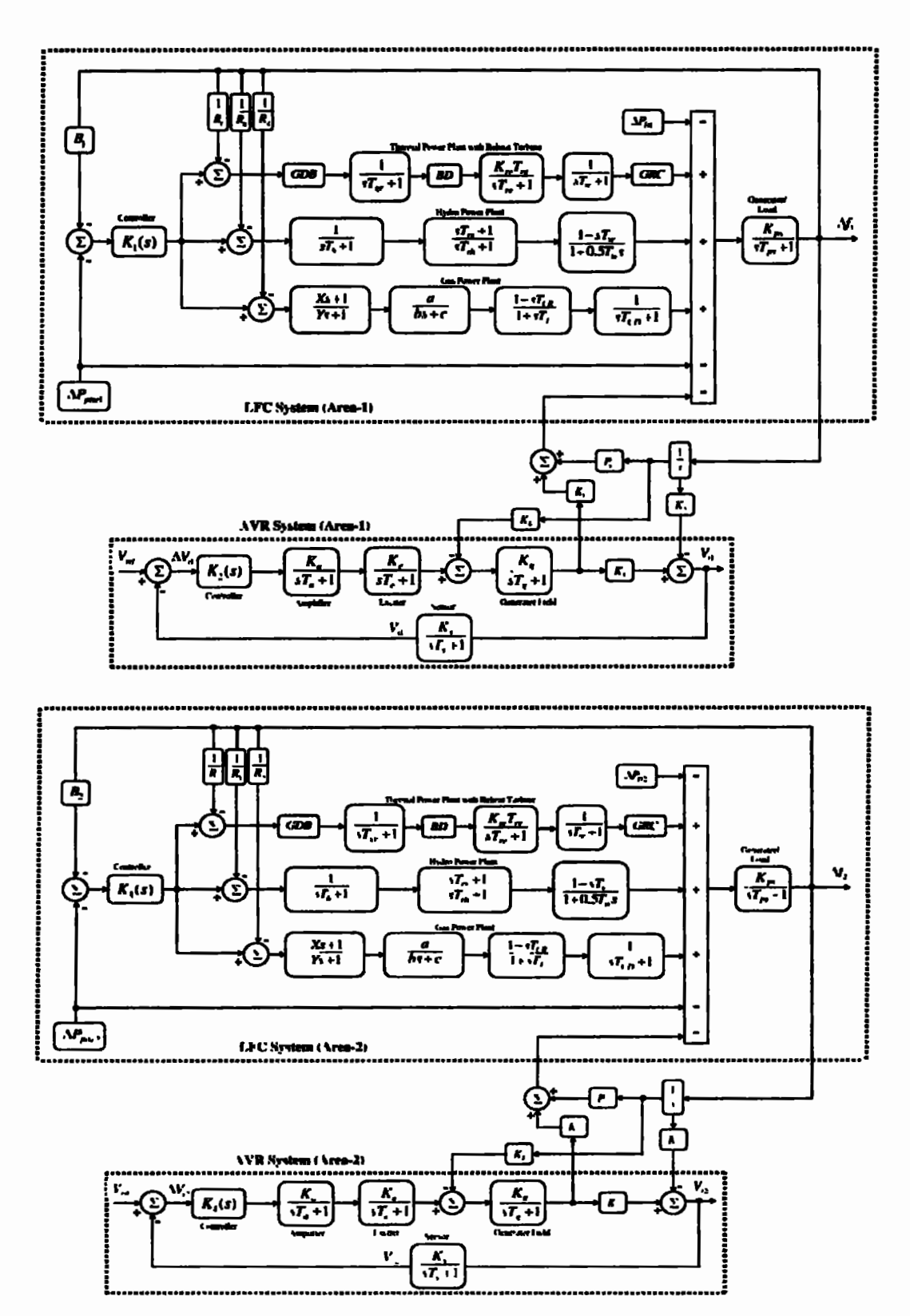


Figure 4.14: Two-area multi-source IPS model with nonlinearities

Table 4.6 provides the optimum values of AOA, LPBO, MPSO, and DO based PI-PD controllers for two-area realistic IPS with nonlinearities. The frequency deviation responses of area-1 and area-2 are shown in Figure 4.15 and 4.16 while Tables 4.7 presents the performance specifications using DO, AOA, LPBO, and MPSO based PI-PD control methodologies.

Table 4.6: Optimal values of controller parameters for a two-area multi-source IPS with nonlinearities

Area	Controller Parameters	AOA based PI-PD	LPBO based PI-PD	MPSO based PIPD	DO based PI-PD
	K _{p1}	0.24	0.0069	0.40	1.05
	Kıı	0.20	0.10	1.24	1.74
Area-1	K _{p2}	0.65	1.46	0	0.63
	K _{d1}	0.95	1.76	0.89	2
	K _{p3}	1.66	1.91	1.34	1.92
ĺ	K ₁₂	1.62	1.52	1.82	1.98
	K _{p4}	0.75	0.94	0.91	1.32
	K _{d2}	1.68	1.42	0.32	0.92
	K _{p5}	0.87	1.49	1.49	1.14
	K ₃	0.66	0.68	0.85	1.21
	K _{p6}	1.84	1.72	1.68	1.17
Агеа-2	Kd3	1.86	0.53	0.40	1.77
110.2	K _{p7}	1.31	1.17	1.94	1.37
	K,4	1.16	1.73	1.70	0.80
	K _{p8}	0.37	1.68	1.59	0.39
	K _{d4}	0.28	0.31	1.48	0.62
	ITSE	0.48	0.43	0.45	0.35

DO based PI-PD control method gave settling time of 7.21s for area-1 LFC, which is comparatively 0.7%, 13%, and 7% better than AOA, LPBO, and MPSO based PI-PD control methodologies respectively. AOA, LPBO, and MPSO based PI-PD control methodologies were all outperformed by 11%, 7%, and 2% respectively, in terms of settling time for area-2 LFC by the DO based PI-PD. As can be observed, DO based PI-PD offers a % overshoot and %undershoot response that is considerably better than others in both areas. Further, it can be seen that for each control methodology, the steady-state error is zero.

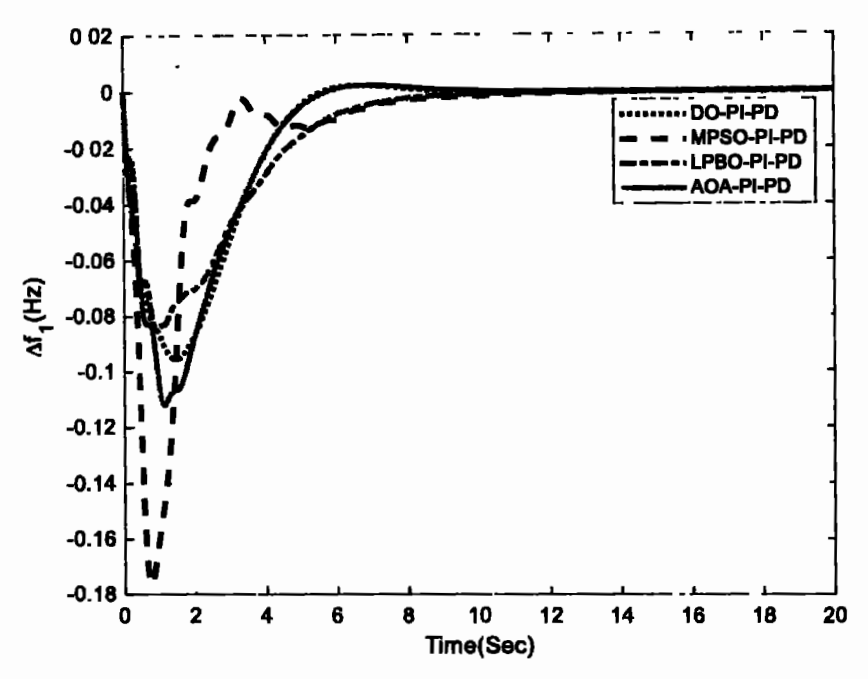


Figure 4.15: Response of Δf_1 with PI-PD control methodologies in a two-area multi-source IPS with nonlinearities

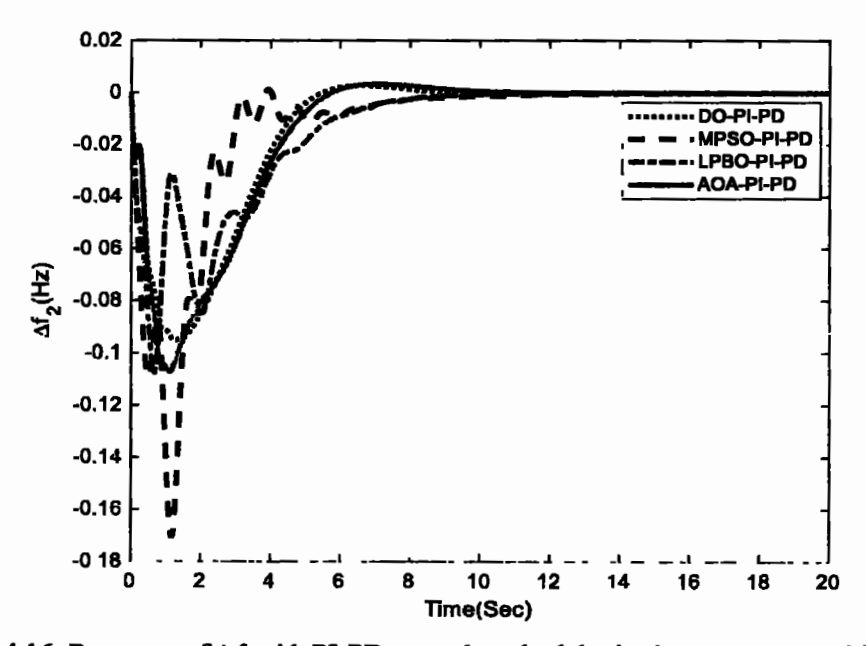


Figure 4.16: Response of Δf_2 with PI-PD control methodologies in a two-area multi-source IPS with nonlinearities

Table 4.7: Performance specifications of frequency deviation responses in a two-area multisource IPS with nonlinearities

		Are	:a-1		Area-2			
Control Methodology	Settling Time (s)	% Overshoot	Undershoot	% s-s Error	Settling Time (s)	% Overshoot	Undershoot	% s-s Error
AOA based PI-PD	7.26	0.0215	-0.121	0	8.47	0.0318	-0.107	0
LPBO based PI-PD	8.24	0	-0.0845	0	8.14	0	-0.1079	0
MPSO based PI-PD	7.72	0	-0.176	0	7.68	0.000975	-0.171	0
DO based PI-PD	7.21	0.00212	-0.0958	0	7.54	0.0026	-0.096	0

The terminal voltage responses of area- and area-2 are shown in Figure 4.17 and 4.18 while Tables 4.8 presents the performance specifications using DO, AOA, LPBO, and MPSO based PI-PD control methodologies.

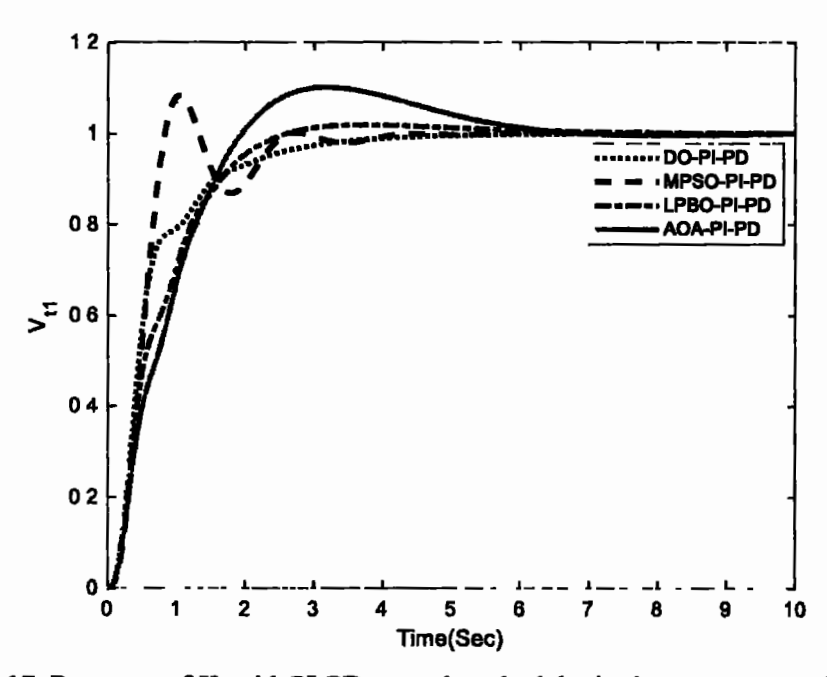


Figure 4.17: Response of V_{tl} with PI-PD control methodologies in a two-area multi-source IPS with nonlinearities

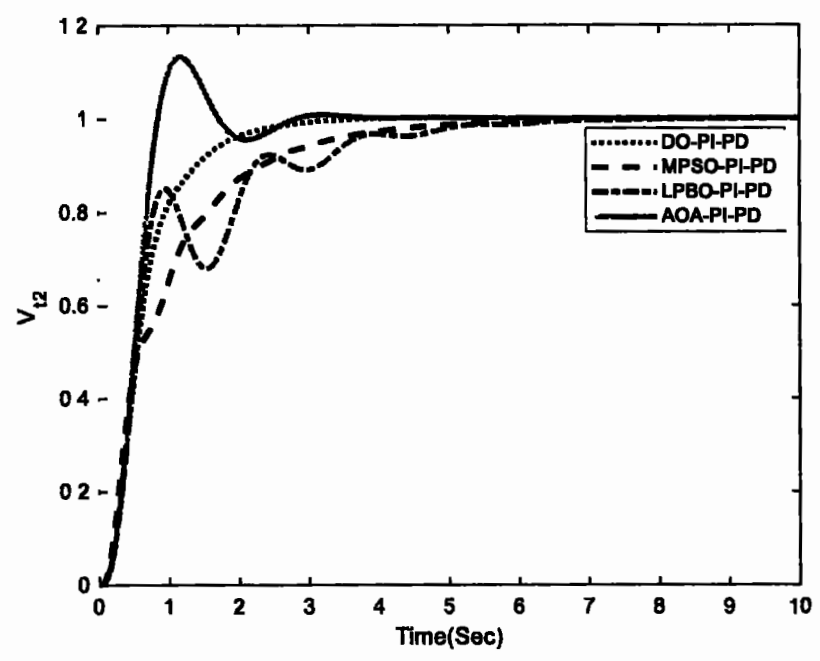


Figure 4.18: Response of V_2 with PI-PD control methodologies in a two-area multi-source IPS with nonlinearities

In area-1 AVR, DO based PI-PD provided a settling time of 3.30s that was 42%, 32%, and 5% superior than AOA, LPBO, and MPSO based PI-PD control methodologies respectively. As can be shown, the DO based PI-PD controller offers a relatively superior AVR 2's settling time response than the AOA, LPBO, and MPSO based PI-PD controllers by 1%, 51%, and 45% respectively. In both areas, almost zero % overshoot was produced by DO based PI-PD. The steady-state error is zero again with each control methodology in proposed IPS.

Table 4.8: Performance specifications of terminal voltage responses in a two-area multisource IPS with nonlinearities

		Area-1		Area-2			
Control Methodology	Settling Time (s)	% Overshoot	% s-s Error	Settling Time (8)	% Overshoot	% s-s Error	
AOA based PI-PD	5.67	10.03	0	2.51	12.90	0	
LPBO based PI-PD	4.83	3.09	0	5.07	0.0001	0	
MPSO based PI-PD	3.48	7.94	0	4.48	0.0025	0	
DO based PI-PD	3.30	0.0015	0	2.48	0.016	0	

The tie-line power deviation responses are shown in Figure 4.19 while Tables 4.9 presents the performance specifications using DO, AOA, LPBO, and MPSO based PI-PD control methodologies. It is clear that the AOA, LPBO, MPSO, and DO based PI-PD control methodologies delivered sufficient tie-line power deviation responses with minimal undershoots and overshoots. The DO based PI-PD delivered the lowest settling time (8.52s) in comparison to all other tuning schemes, which is respectively, 42%, 41%, and 9% better than LPBO, AOA, and MPSO based PI-PD control methodologies. DO based PI-PD produced 0.0056% overshoot, that is comparatively 66%, 89%, and 84% better than AOA, LPBO, and MPSO based PI-PD control methodologies respectively. It is clear that for all control strategies, the steady-state error is zero.

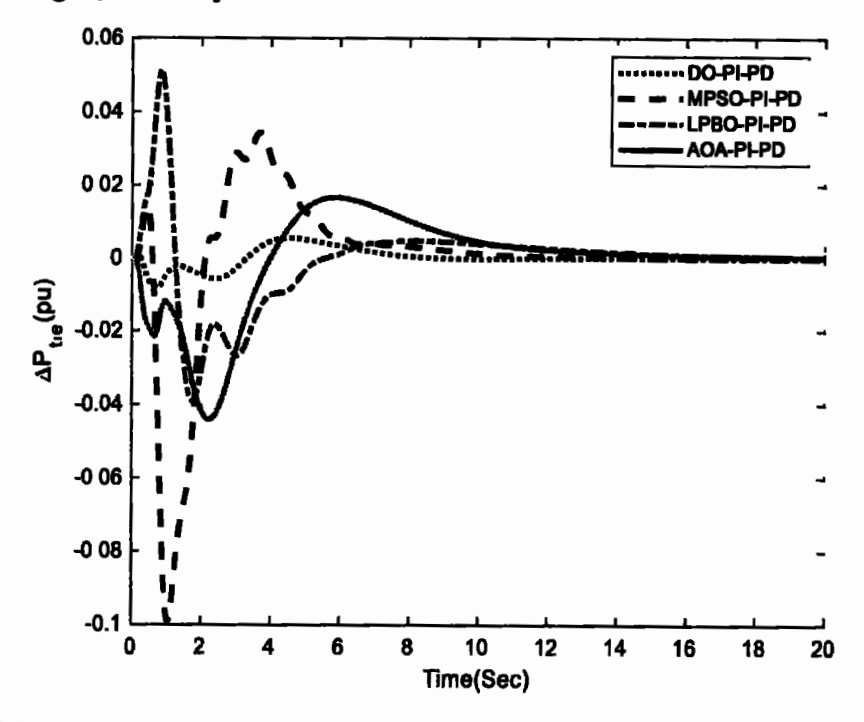


Figure 4.19: Response of ΔP_{tre} with PI-PD control methodologies in a two-area multi-source IPS with nonlinearities

Table 4.9: Performance specifications of tie-line power deviation responses in a two-area multi-source IPS with nonlinearities

Control Methodology	Settling Time (s)	% Overshoot	Undershoot	% s-s Error
AOA based PI-PD	14.49	0.0166	-0.0441	0
LPBO based PI-PD	14.58	0.051	-0.0392	0
MPSO based PI-PD	9.36	0.034	-0.0991	0
DO based PI-PD	8.52	0.0056	-0.00813	0

Figure 4.20, 4.21, and 4.22 show the graphical comparisons of the performance specifications of frequency deviation, terminal voltage, and tie-line power deviation responses using DO, AOA, LPBO, and MPSO based PI-PD control methodologies respectively. It is evident that in a two-area IPS with nonlinearities, PI-PD based control methodologies offer appropriate transient and steady state responses for frequency deviation, terminal voltage, and tie-line power deviation.

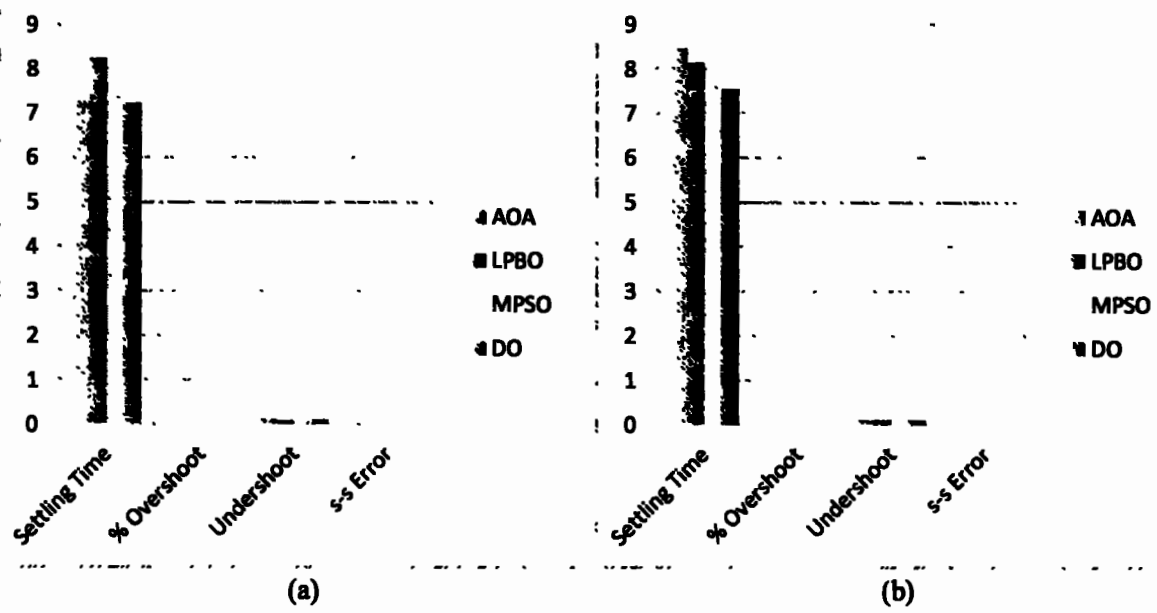


Figure 4.20: Graphical comparisons of performance specifications of frequency deviation responses using PI-PD control methodologies in a two-area multi-source IPS with nonlinearities

(a) Δf_1 (b) Δf_2

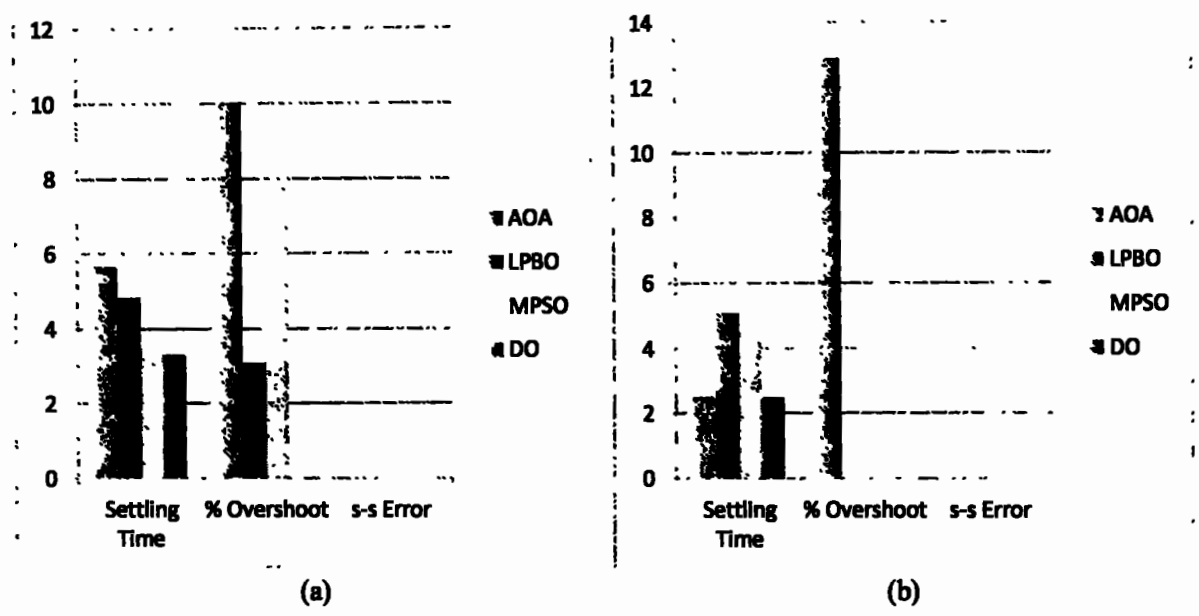


Figure 4.21: Graphical comparisons of performance specifications of terminal voltage responses using PI-PD control methodologies in a two-area multi-source IPS with nonlinearities

(a) V_{t1} (b) V_{t2}

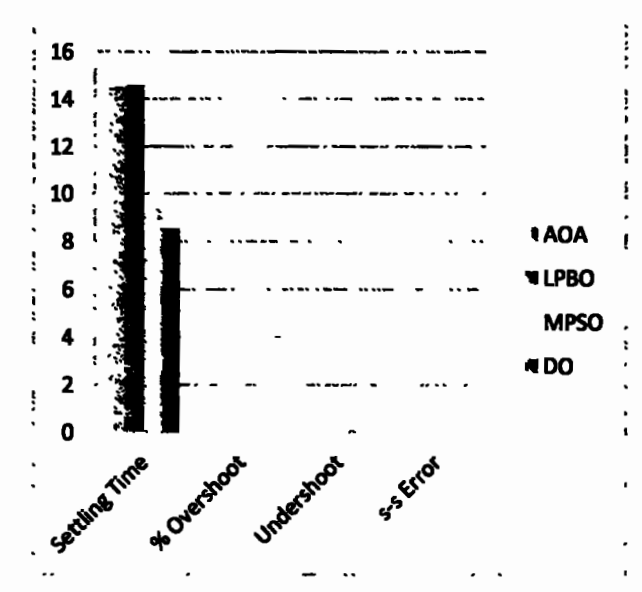
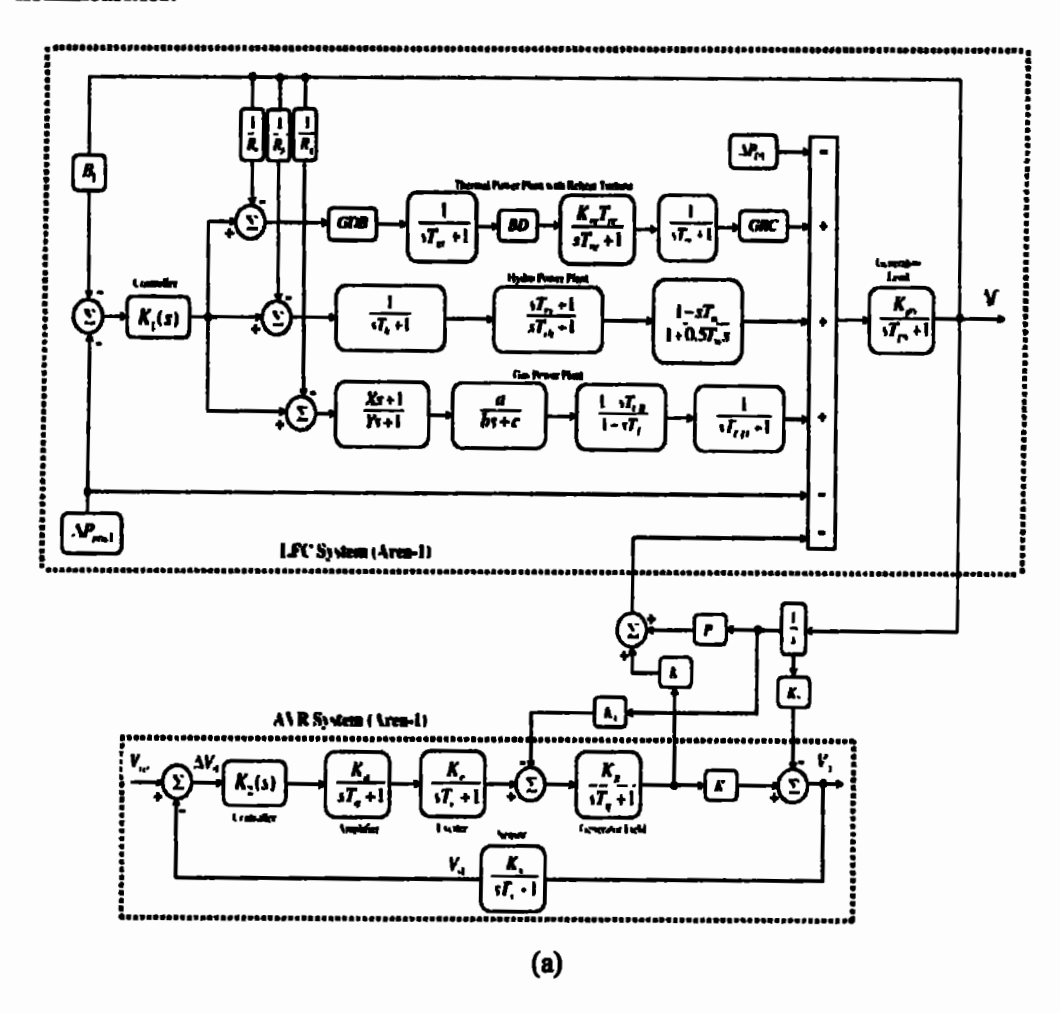


Figure 4.22: Graphical comparison of performance specifications of tie-line power deviation response (ΔP_{tle}) using PI-PD control methodologies in a two-area multi-source IPS with nonlinearities

4.5.3 Frequency and Voltage Stabilization in a Three-area Multi-source IPS with Nonlinearities

In this section, a three-area multi-source IPS with nonlinearities was selected for further investigation to demonstrate the effectiveness of the proposed DO based PI-PD control mechanism. Figure 4.23 shows the studied model and Appendix B contains the parameters of the IPS model. In addition, the dynamic analysis of the power system was performed with 2% SLP in area-1, area-2, and area-3. Table 4.10 shows the optimal parameters of DO, AOA, LPBO, and MPSO based PI-PD controllers for three-area IPS with nonlinearities.



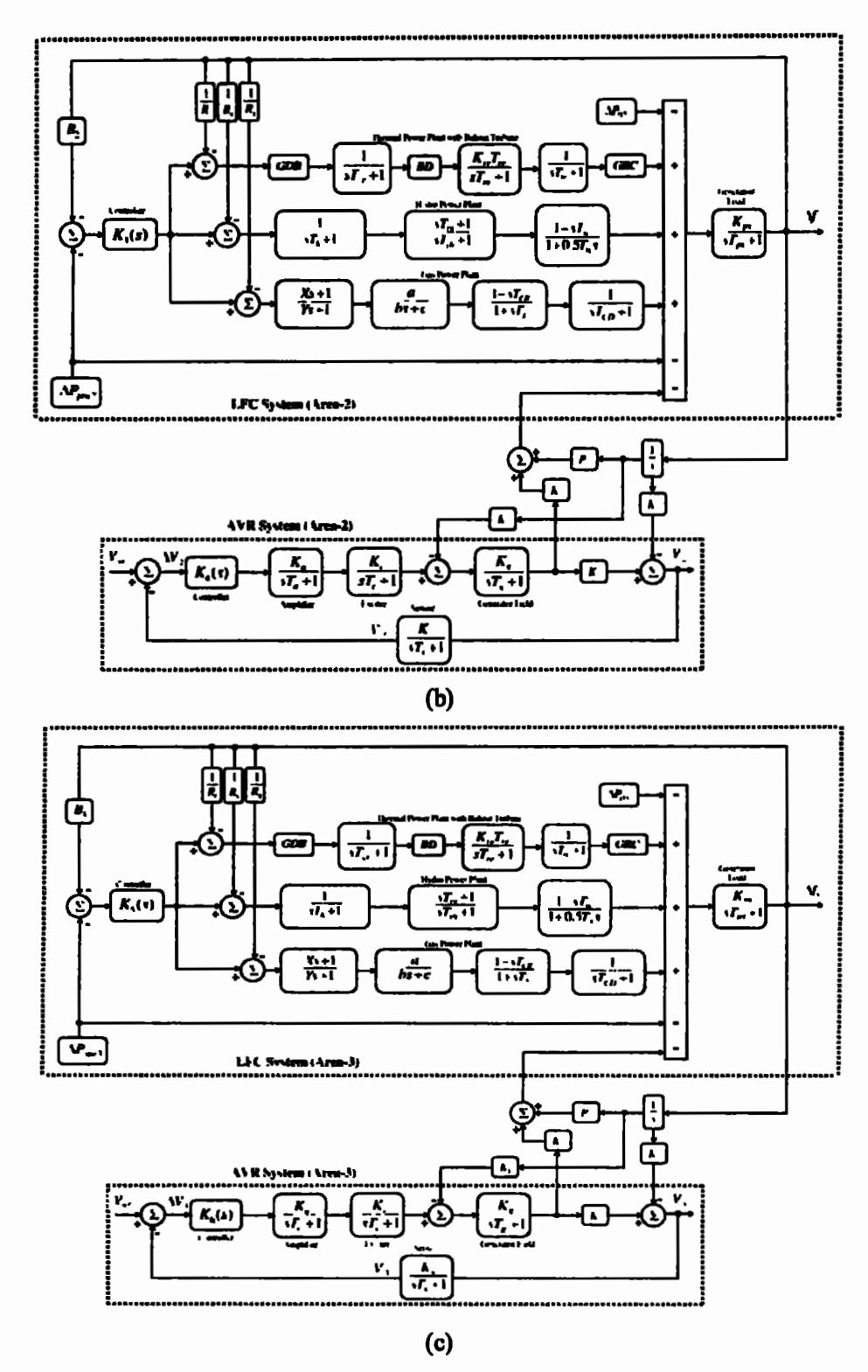


Figure 4.23: Three-area multi-source IPS model with nonlinearities

(a) Area-1 (b) Area-2 (c) Area-3

The frequency deviation responses of area-1, area-2, and area-3 are shown in Figure 4.24, 4.25, and 4.26 while Tables 4.11 presents the performance specifications using DO, AOA, LPBO, and MPSO based PI-PD control methodologies.

Table 4.10: Optimal values of controller parameters for a three-area multi-source IPS with nonlinearities

Area	Controller Parameters	AOA based PI-PD	LPBO based PI-PD	MPSO based PI-PD	DO based PI-PD
	K _{pl}	1.49	1.90	1.36	1.61
	Kıl	1.56	0.15	0.42	1.44
A 1	K _{p2}	1.44	0	0.62	0.32
Area-1	K _{d1}	1.93	0.74	0.43	1.52
	K _{p3}	1.83	1.68	1.16	0.99
	K ₁₂	1.63	0.95	1.00	1.60
	K _{p4}	1.57	0.32	0.92	1.10
	K _{d2}	1.61	0.26	0.27	0.40
	Kpš	1.78	0.66	1.15	1.66
	K _i 3	1.76	0.96	1.73	1.82
	K _{p6}	1.78	1.065	0.26	1.69
Area-2	K _{d3}	1.80	0.64	1.04	0.72
	K _{p7}	1.79	0.85	1.05	0.13
	K ₁₄	1.68	1.13	1.80	1.68
	K _{p8}	1.36	0.96	1.40	1.93
	K _{d4}	1.15	0.88	1.12	0.35
	K _{p9}	1.73	0.12	1.11	0.45
	K _{t5}	1.70	1.13	1.73	1.19
	K _{p10}	1.95	1.18	0.23	2
Area-3	K _{d5}	1.65	1.68	0.36	1.78
	Kpil	1.53	1.77	0.75	1.34
	K ₁₆	1.71	0.80	0.29	1.68
	K _{pl2}	1.71	0.37	0.09	1.13
	K _{d6}	1.56	1.42	0.21	1.05
	ITSE	0.90	0.81	0.90	0.89

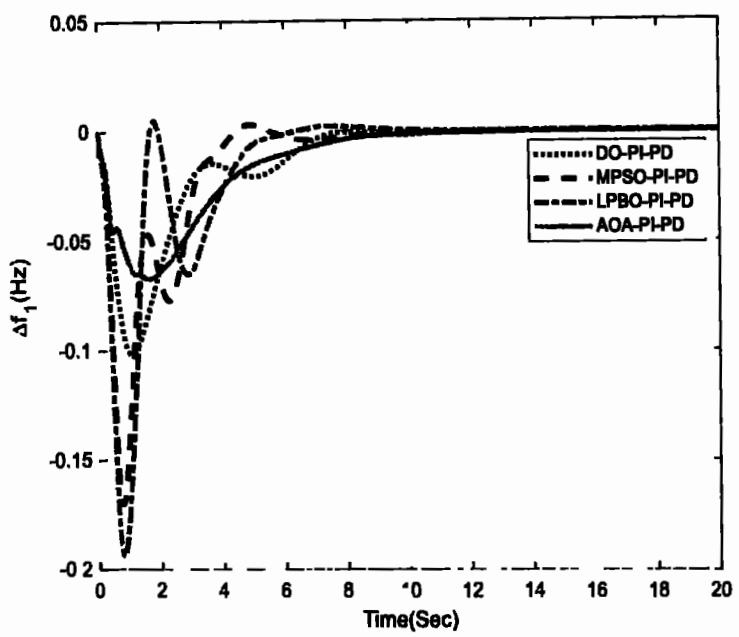


Figure 4.24: Response of Δf_1 with PI-PD control methodologies in a three-area multi-source IPS with nonlinearities

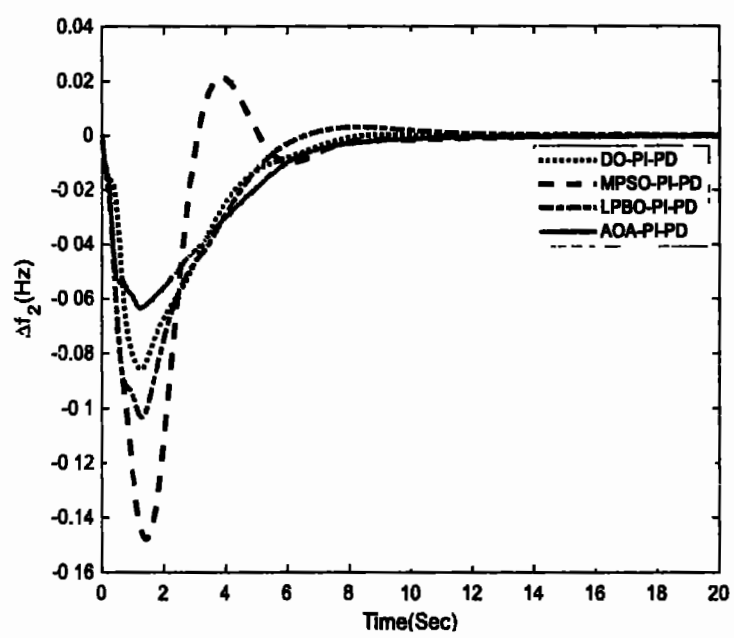


Figure 4.25: Response of Δf_2 with PI-PD control methodologies in a three-area multi-source IPS with nonlinearities

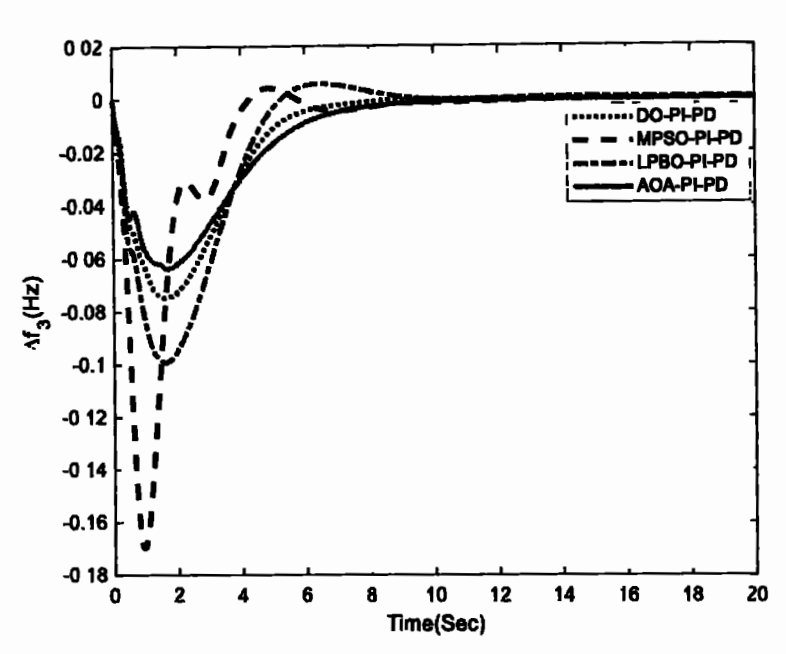


Figure 4.26: Response of Δf_3 with PI-PD control methodologies in a three-area multi-source IPS with nonlinearities

Table 4.11: Performance specifications of frequency deviation responses in a three-area multi-source IPS with nonlinearities

Area	Control Methodology	Settling Time (s)	% Overshoot	Undershoot	% s-s Error
Area-1	AOA based PI-PD	9.48	0	-0.067	0
	LPBO based PI-PD	5.21	0.0049	-0.19	0
	MPSO based PI-PD	7.74	0.0032	-0.17	0
	DO based PI-PD	7.21	0	-0.10	0
Area-2	AOA based PI-PD	9.62	0	0.0027	0
	LPBO based PI-PD	9.89	0.0030	-0.10	0
	MPSO based PI-PD	7.73	0.021	-0.15	0
	DO based PI-PD	7.59	0.00017	-0.086	0
Area-3	AOA based PI-PD	9.41	0	-0.0068	0
	LPBO based PI-PD	8.37	0.0057	-0.099	0
	MPSO based PI-PD	7.84	0.0041	-0.17	0
	DO based PI-PD	7.54	0	-0.075	0

For area-1 LFC, LPBO based PI-PD provided quickest settling time of 5.21s. For area-2 and area-3 LFC, all other proposed schemes have slower settling times than DO based PI-PD, which offers 7.59s and 7.54s respectively. This means DO based PI-PD controller provided relatively 21%, 23%, and 2% better settling time response compared to AOA, LPBO, and MPSO based PI-PD controllers in area-2. Similarly, DO based PI-PD controller produced relatively 20%, 10%, and 4% better settling time response compared to AOA, LPBO, and MPSO based PI-PD controllers in area-3. It is very clear that % overshoot and undershoot are almost negligible in all areas with proposed control methodologies. Overall, it can be seen that DO based PI-PD outperforms other schemes in terms of settling time, % overshoot, and undershoot responses. Moreover, with each control methodology applied to a given system, the steady-state error is zero.

The terminal voltage responses of area-1, area-2, and area-3 are shown in Figure 4.27, 4.28 and 4.29 while Tables 4.12 presents the performance specifications using DO, AOA, LPBO, and MPSO based PI-PD control methodologies.

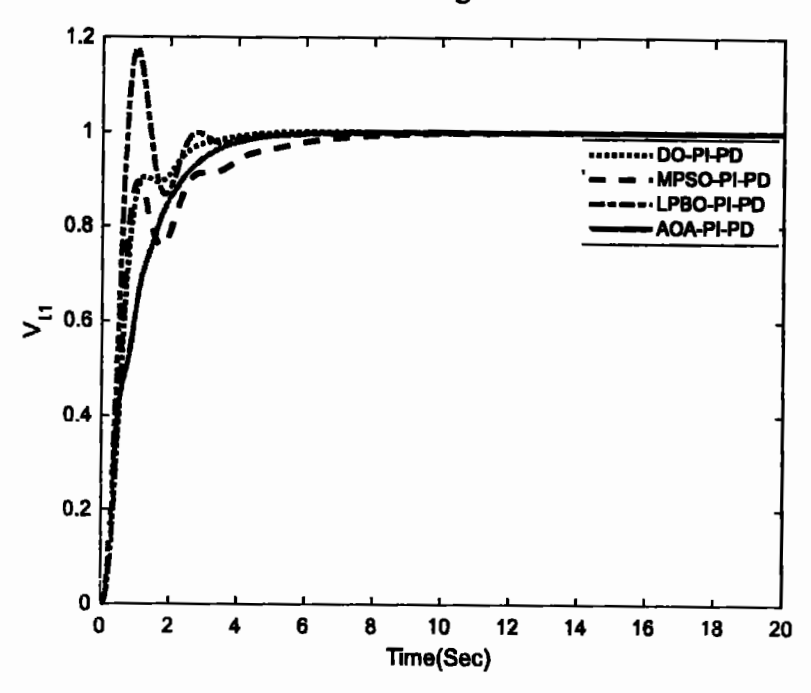


Figure 4.27: Response of V_{tl} with PI-PD control methodologies in a three-area multi-source IPS with nonlinearities

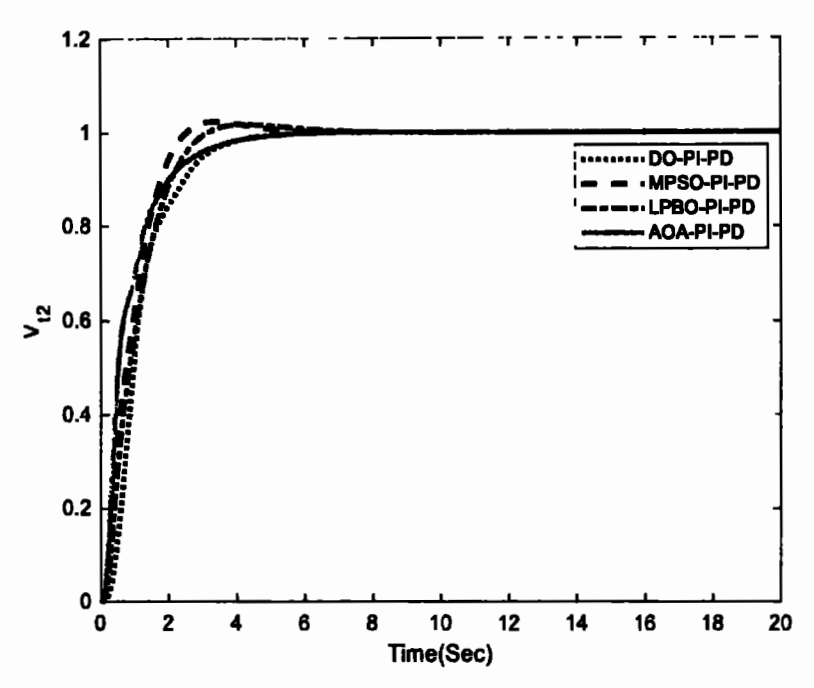


Figure 4.28: Response of V_2 with PI-PD control methodologies in a three-area multi-source IPS with nonlinearities

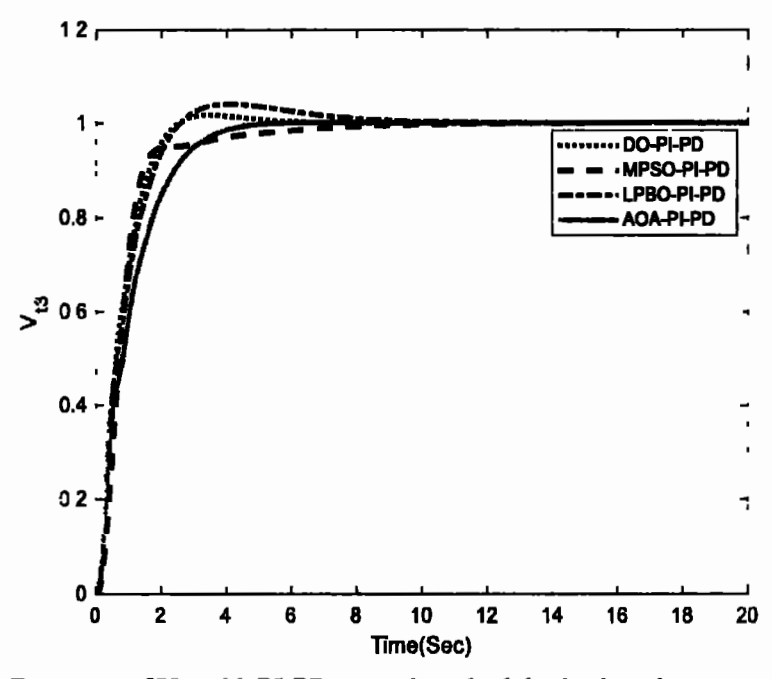


Figure 4.29: Response of V₁₃ with PI-PD control methodologies in a three-area multi-source IPS with nonlinearities

Table 4.12: Performance specifications of terminal voltage responses in a three-area multisource IPS with nonlinearities

Area	Control Methodology	Time		% s-s Error
	AOA based PI-PD	4.09	0.013	0
Area-1	LPBO based PI-PD	3.85	17.39	0
Alca-i	MPSO based PI-PD	6.10	0	0
	DO based PI-PD	3.27	0.034	0
	AOA based PI-PD	3.83	0.0056	0
Area-2	LPBO based PI-PD	2.80	1.67	0
Alca-2	MPSO based PI-PD	3.84	2.24	0
1	DO based PI-PD	2.02	9e-04	0
	AOA based PI-PD	3.78	0.098	0
Area-3	LPBO based PI-PD	7.04	6.09	0
/ILCa-5	MPSO based PI-PD	5.69	0	0
	DO based PI-PD	2.23	1.65	0

In areas 1, 2, and 3 respectively, DO based PI-PD achieved faster settling times of 3.27s, 2.02s, and 2.23s than other suggested techniques. This means DO based PI-PD controller provided relatively 20%, 15%, and 46% better settling time response compared to AOA, LPBO, and MPSO based PI-PD controllers in area-1 AVR respectively. Moreover, DO based PI-PD controller produced relatively 47.3%, 28%, and 47.4% better settling time response compared to AOA, LPBO, and MPSO based PI-PD controllers in area-2 AVR respectively. Finally, DO based PI-PD controller yielded relatively 41%, 61%, and 68% better settling time response compared to AOA, MPSO, and LPBO based PI-PD controllers in area-3 AVR respectively. As can be observed, overshoot and undershoot are once more quite little in all areas with each control methodologies. With each control methodology, the steady-state error is once more zero.

The tie-line power deviation responses in area-1, area-2, and area-3 are shown in Figure 4.30, 4.31, and 4.32 while Tables 4.13 presents the performance specifications using DO, AOA, LPBO, and MPSO based PI-PD control methodologies. DO based PI-PD provides quickest settling time of 10.79s and 10.35s in area-1 and area-3 respectively. In area-2, MPSO based PI-PD provided settling time of 11.13s, which is a little bit lower than the settling time of DO based PI-PD controller that is 11.31s. This means DO based PI-PD controller yielded relatively 13%, 11%, and 20% better settling time response compared to AOA, LPBO, and MPSO based PI-PD controllers in area-1. Further, DO based PI-PD controller produced relatively 2% and 7% better settling time response compared to AOA and LPBO based PI-PD controllers in area-2. Finally, DO based PI-PD controller provided relatively 12%, 24%, and 13% better settling time response compared to AOA, LPBO, and MPSO based PI-PD controllers in area-3. Overshoots are once again minimal with each control methodology in all areas.

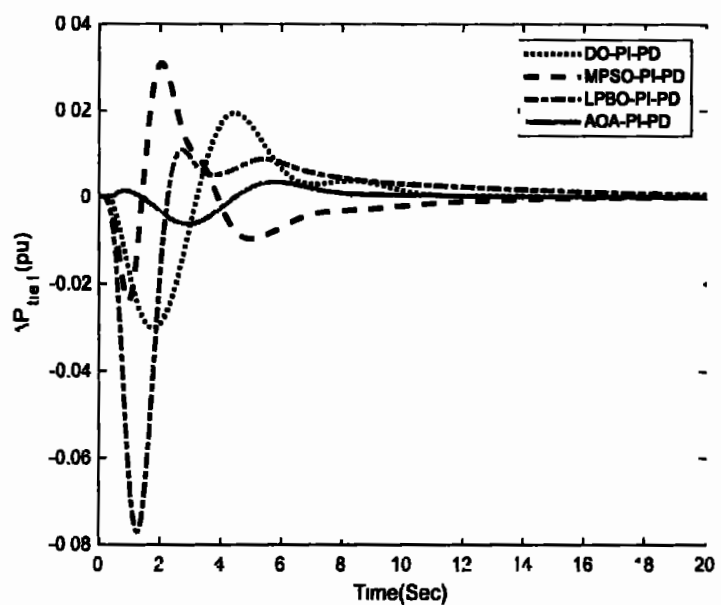


Figure 4.30: Response of ΔP_{tel} with PI-PD control methodologies in a three-area multi-source IPS with nonlinearities

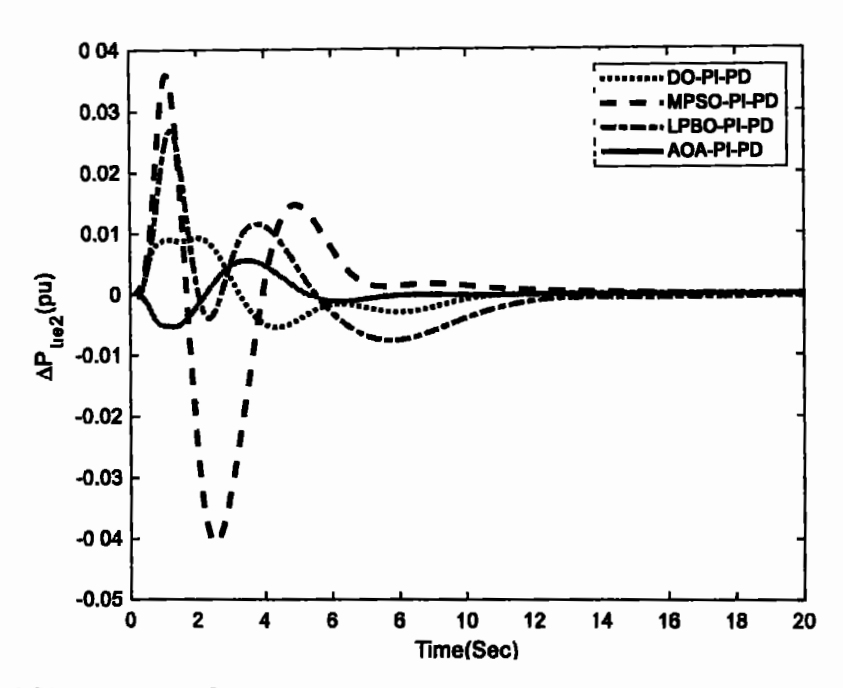


Figure 4.31: Response of ΔP_{te2} with PI-PD control methodologies in a three-area multi-source IPS with nonlinearities

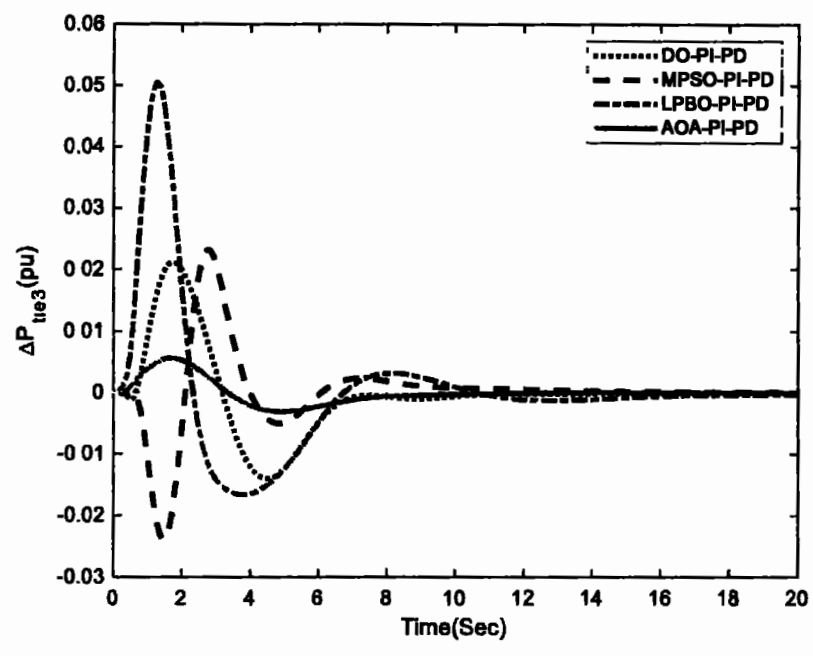


Figure 4.32: Response of ΔP_{te3} with PI-PD control methodologies in a three-area multi-source IPS with nonlinearities

Table 4.13: Performance specifications of tie-line power deviation responses in a three-area multi-source IPS with nonlinearities

Area	Control Methodology	Settling Time (s)	% Overshoot	Undershoot	% s-s Error
	AOA based PI-PD	12.42	0.0035	-0.006	0
Агеа-1	LPBO based PI-PD	12.19	0.011	-0.077	0
12421	MPSO based PI-PD	13.50	0.031	-0.024	0
	DO based PI-PD	10.79	0.019	-0.030	0
	AOA based PI-PD	11.51	0.0056	-0.0052	0
Area-2	LPBO based PI-PD	12.21	0.027	-0.0076	0
	MPSO based PI-PD	11.13	0.036	-0.041	0
	DO based PI-PD	11.31	0.0093	-0.0054	0
	AOA based PI-PD	11.71	0.0056	-0.0031	0
Агеа-3	LPBO based PI-PD	13.64	0.050	-0.017	0
Audi-3	MPSO based PI-PD	11.83	0.0232	-0.024	0
	DO based PI-PD	10.35	0.0211	-0.014	0

The performance metrics of DO, AOA, LPBO, and MPSO based PI-PD control methodologies are graphically compared in Figure 4.33, 4.34, and 4.35 respectively in a three-area multi-source with nonlinearities. It is clear that the DO based PI-PD controller outperforms conventional control strategies in terms of terminal voltage, frequency, and tieline power deviations.

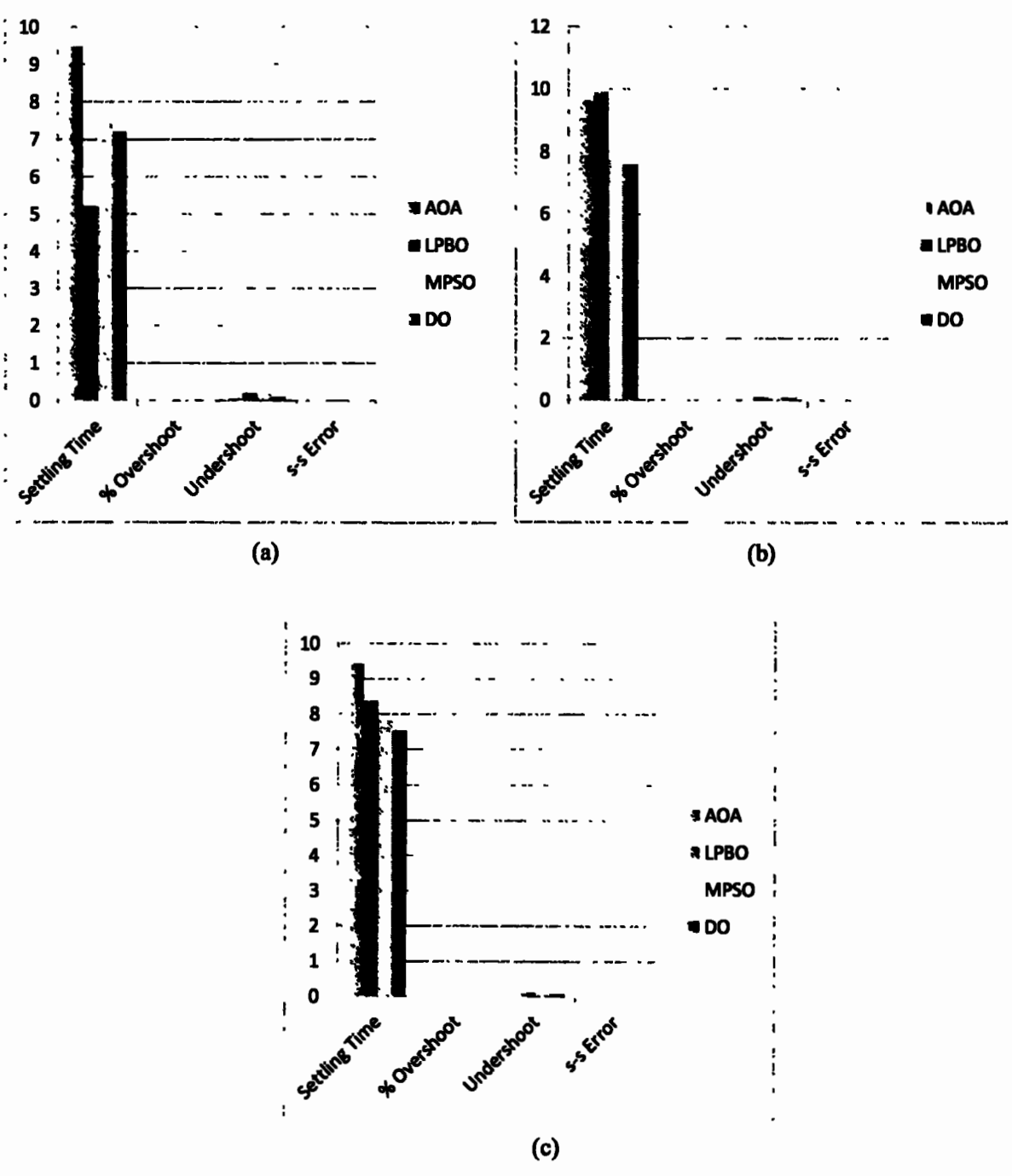


Figure 4.33: Graphical comparisons of performance specifications of frequency deviation responses using PI-PD control methodologies in a three-area multi-source IPS with nonlinearities

(a) Δf_1 (b) Δf_2 (c) Δf_3

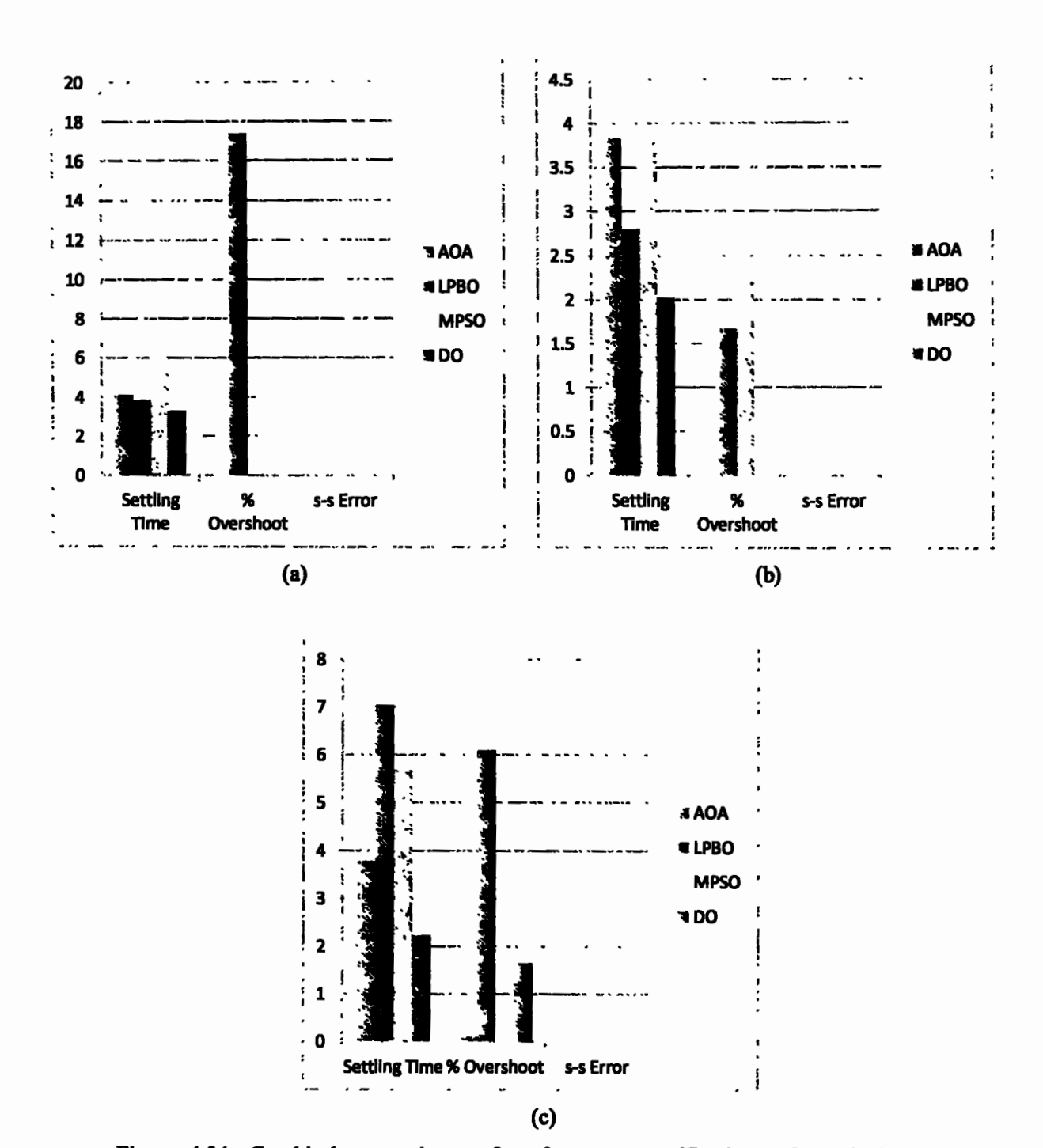


Figure 4.34: Graphical comparisons of performance specifications of terminal voltage responses using PI-PD control methodologies in a three-area multi-source IPS with nonlinearities

(a) V_{t1} (b) V_{t2} (c) V_{t3}

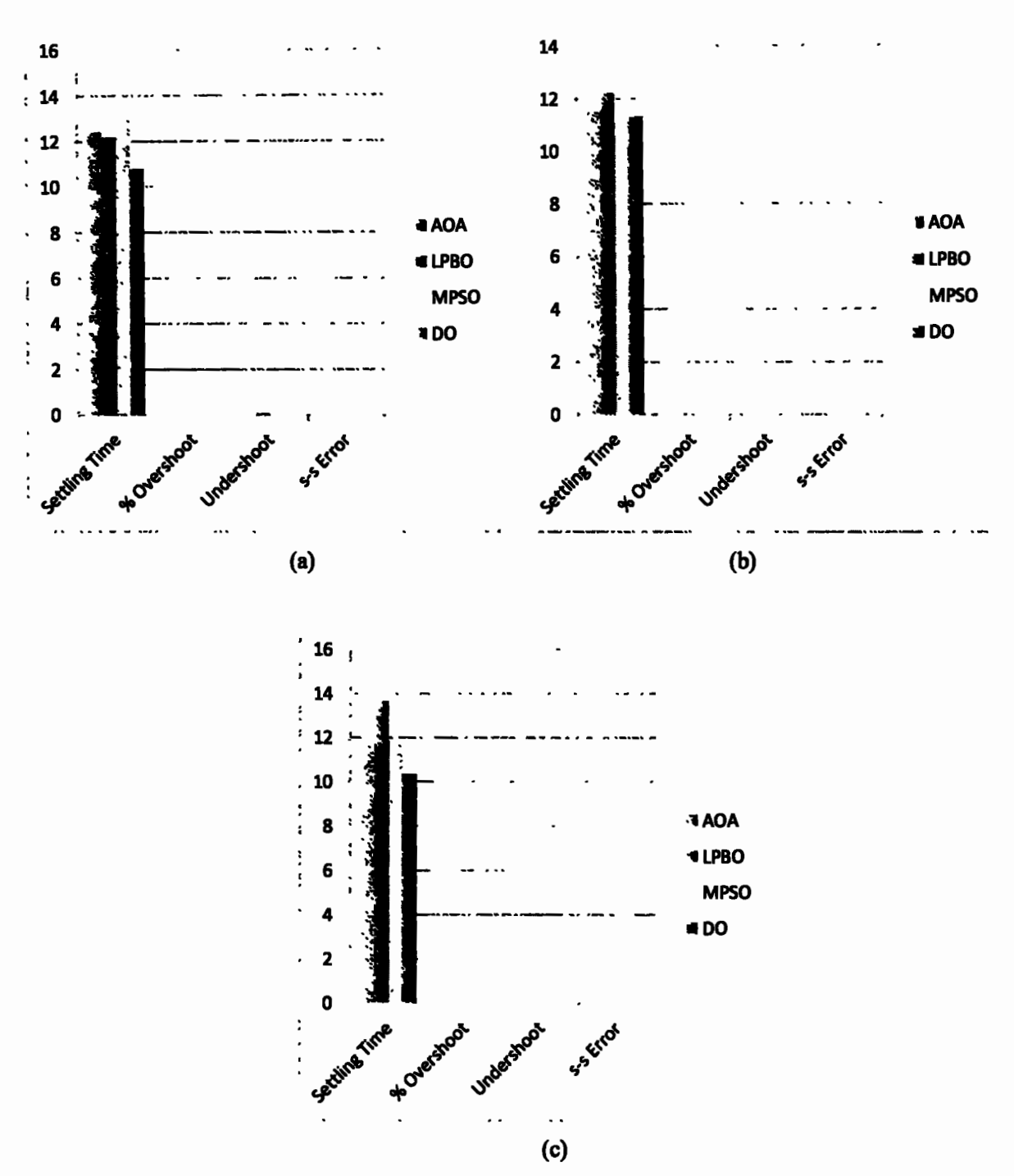


Figure 4.35: Graphical comparisons of performance specifications of tie-line power deviation responses using PI-PD control methodologies in a three-area multi-source IPS with nonlinearities

(a) ΔP_{tiel} (b) ΔP_{tie2} (c) ΔP_{tie3}

CHAPTER 5

Frequency and Voltage Stabilization in a Four-area Multi-source IPS

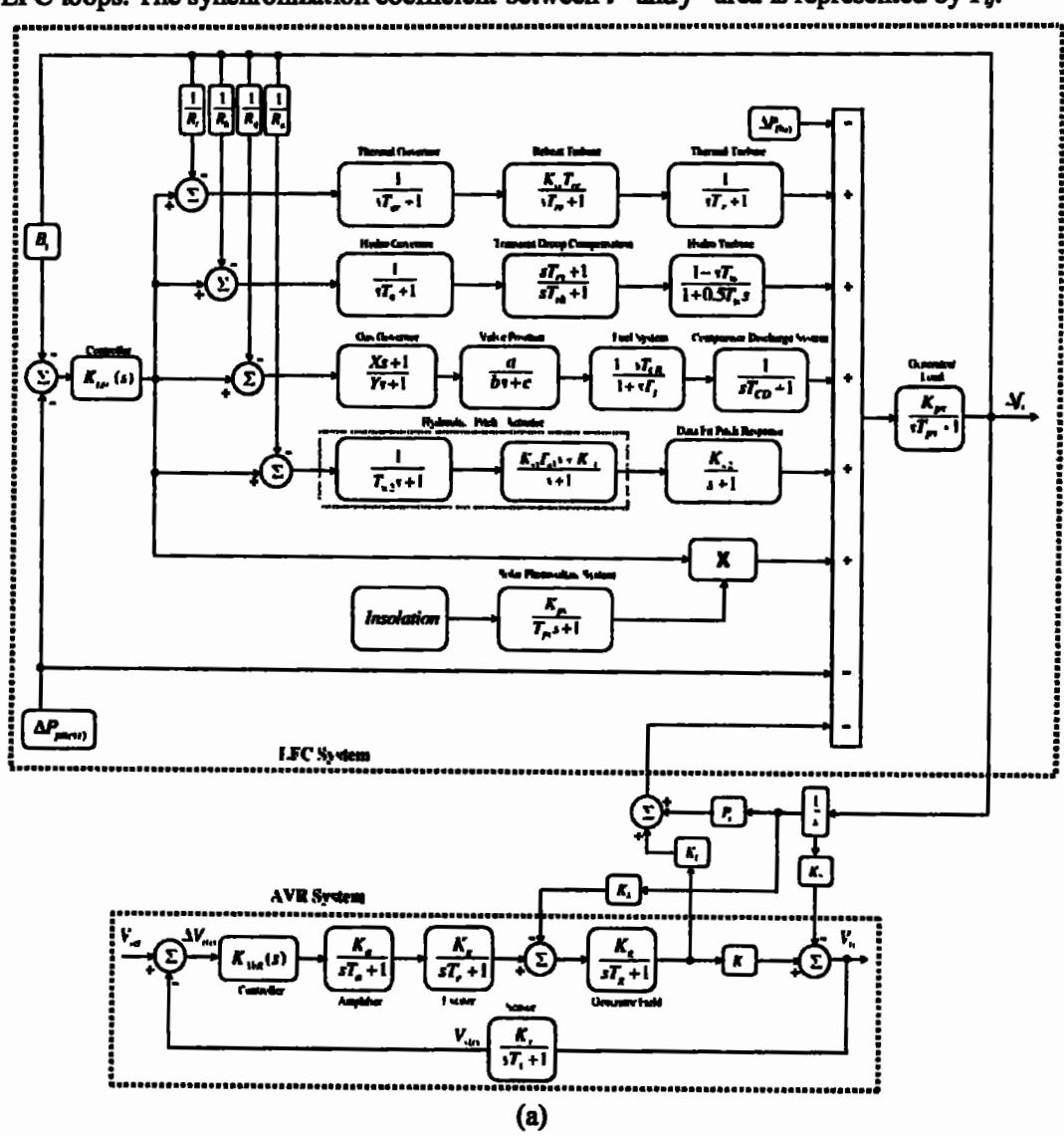
This chapter deals with the design and implementation of the proportional integral derivative (PID), tilt integral derivative (TID), integral-proportional (I-P) and integral-proportional derivative (I-PD) controllers for a four-area multi-source interconnected power system using gradient based optimizer (GBO).

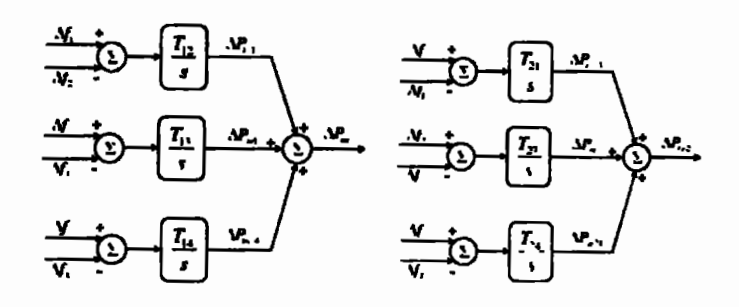
5.1 Mathematical Modeling of Power System

The four-area multi-source IPS under study is shown in Figure 5.1. IPS has three conventional generating units in each of the four areas, including thermal reheat, hydro. and gas with two renewable energy sources including solar photovoltaic and wind units [11][25]. The LFC loop of i^{th} area has a controller $(K_{LFC}(s))$, i^{th} area's bias factor (B_i) , thermal reheat speed regulation (R_i) , hydro speed regulation (R_i) , gas speed regulation (R_i) , and generator/load $\left(\frac{K_{p(t)}}{sT_{t+1}}\right)$ with different blocks of power generation units. The thermal reheat unit consists of thermal governor $\left(\frac{1}{sT+1}\right)$, reheat turbine $\left(\frac{K_nT_n}{sT+1}\right)$, and thermal turbine $\left(\frac{1}{sT+1}\right)$; hydro unit includes hydro governor $\left(\frac{1}{sT+1}\right)$, and transient droop compensation $\left(\frac{sT_{rs}+1}{sT_{rs}+1}\right)$, hydro turbine $\left(\frac{1-sT_{rs}}{1+0.5T_{rs}}\right)$; gas unit comprises gas governor $\left(\frac{Xs+1}{V_{s+1}}\right)$, valve position $\left(\frac{a}{hs+c}\right)$, fuel system $\left(\frac{1-sT_{CR}}{1+sT_c}\right)$, and compressor discharge system $\left(\frac{1}{sT+1}\right)$; wind unit consists of hydraulic pitch actuator $\left(\frac{K_{w1}(T_{w1}s+1)}{(T-s+1)(s+1)}\right)$ and data fit pitch response $\left(\frac{K_{w2}}{s+1}\right)$ blocks. $\Delta P_{D(s)}$, $\Delta f_{(s)}$, $\Delta V_{\ell(s)}$, and $\Delta P_{me(s)}$ denote the load deviation, frequency deviation, deviation in terminal voltage and tie-line power deviation respectively. $V_{t(i)}$, $V_{ref(i)}$, and $V_{s(i)}$ refer to the terminal voltage, reference voltage, and sensor voltage in ith area respectively. The AVR loop of ith area consists of a controller $(K_{AlR}(s))$, amplifier $\left(\frac{K_{a(t)}}{sT_{co}+1}\right)$, generator $\left(\frac{K_{g(t)}}{sT_{co}+1}\right)$, exciter $\left(\frac{K_{a(t)}}{sT_{co}+1}\right)$, and sensor

 $\left(\frac{K_{s(t)}}{sT_{s(t)}+1}\right)$. K_1 , K_2 , K_3 , K_4 , and P_5 are the coefficients for mutual coupling between AVR and

LFC loops. The synchronization coefficient between i^{th} and j^{th} area is represented by T_{ij} .





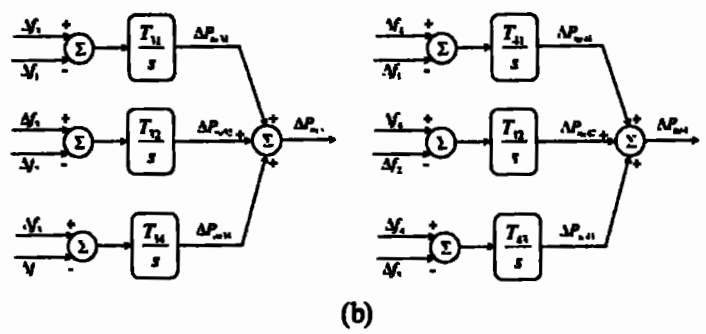


Figure 5.1: Power System

(a) Combined LFC-AVR model (b) Four-area tie-lines.

The transfer function models of the reheat thermal $(G_r(s))$, hydro $(G_H(s))$, gas $(G_G(s))$, wind $(G_W(s))$ and solar photovoltaic $(G_S(s))$ systems are provided in Eq. (5.1-5.5) respectively. The definitions of all symbols/terms used in Eq. (5.1-5.5) and IPS are provided in List of Symbols section.

$$G_{T}(s) = \frac{1 + T_{rc}K_{rc}s}{(1 + T_{rc}s)(1 + T_{rc}s)(1 + T_{rc}s)}$$
(5.1)

$$G_{H}(s) = \frac{(1 + T_{rs}s)(1 - T_{w}s)}{(1 + T_{ts}s)(1 + T_{rs}s)(1 + 0.5T_{w}s)}$$
(5.2)

$$G_G(s) = \frac{a(1+Xs)(1-T_{CR}s)}{(1+Ys)(c+bs)(1+T_{CS}s)(1+T_{CD}s)}$$
(5.3)

$$G_{W}(s) = \frac{K_{w1}K_{w2}(1 + T_{w1}s)}{(1 + T_{w1}s)(s^{2} + 2s + 1)}$$
(5.4)

$$G_s(s) = \frac{K_{pr}}{1 + T_{-}} \tag{5.5}$$

5.2. Proposed Control Methodology

Figure 5.2 demonstrates the proposed methodology with IPS. PID controller was explored for the load frequency and terminal voltage in a four-area IPS. Further, various other controllers including I-PD, TID, and I-P have also been explored to compare their results with GBO-PID. The description of proposed PID and other controllers is provided in this section.

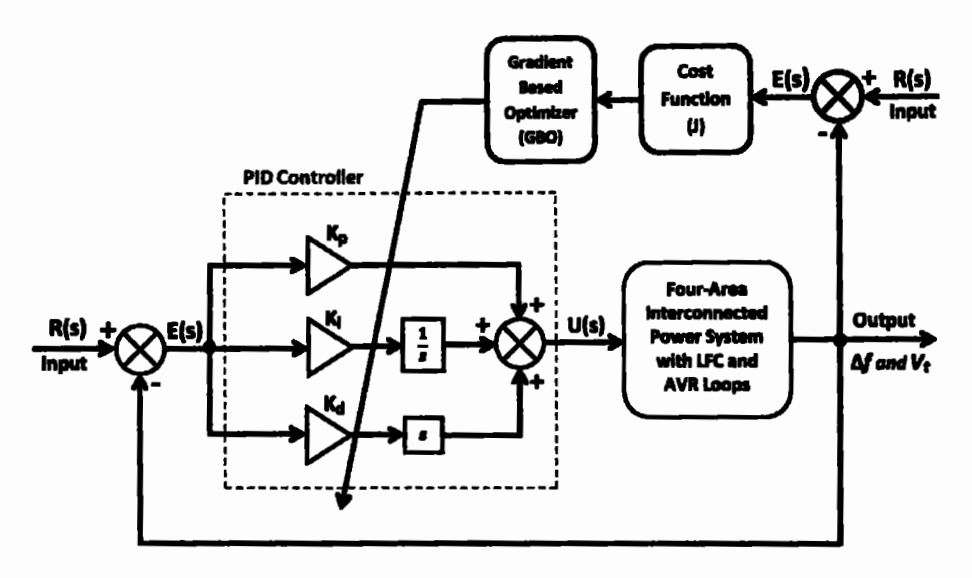


Figure 5.2: Proposed control methodology

5.2.1 PID Controller

The proportional integral derivative (PID) controller is utilized extensively in the industrial sector due to its inherited characteristics of simple design and excellent operational efficiency [168]–[175]. PID controllers are feedback control loop systems, which continuously calculate an error signal as the difference between the process variable and the set point to provide the control signal for the plant. PID controller has three gain coefficients including K_p , K_b and K_d . The control signal generated by PID controller $(U_{PID}(s))$ can be written as:

$$U_{PED}(s) = (K_p + \frac{K_r}{s} + K_d s)E(s)$$
 (5.6)

$$E(s) = Y(s) - R(s) \tag{5.7}$$

where, E(s), Y(s), and R(s) denote error, output, and reference signals respectively.

5.2.2 TID Controller

The tilt integral derivative (TID) controller's architecture is identical to PID but with a modification in proportional term of PID. The change is that PID's proportional gain term is replaced by $K_t(s)^{-1/n}$, where n represents a real number and K_t denotes the gain. TID combines integer and fractional order controllers. It quickly eliminates disturbances due to its superior dynamic features. TID has been used in different engineering application due to its excellent performance characteristics [176]–[180]. TID controller has three gain coefficients including K_t , K_t , and K_t . The control signal generated by TID controller $(U_{TID}(s))$ can be written as:

$$U_{no}(s) = (K_i s^{-\frac{1}{n}} + \frac{K_i}{s} + K_j s) E(s)$$
 (5.8)

5.2.3 I-PD Controller

The integral-proportional derivative (I-PD) controller has the capacity to enhance the transient response of the system. The proportional and derivative terms are placed in the feedback path of the I-PD controller, whereas the integrator controller is placed in the feed forward direction. I-PD controller has been explored for the frequency control applications in power systems [1][68]. I-PD controller has three gain coefficients including K_b , K_p , and K_d . The control signal generated by I-PD controller ($U_{I-PD}(s)$) can be written as:

$$U_{I-PD}(s) = \frac{K_{I}}{s} E(s) - (K_{P} + K_{A}s)Y(s)$$
 (5.9)

5.2.4 I-P Controller

In an integral-proportional (I-P) controller, only proportional term is placed in the feedback path whereas the integrator controller is placed in the feed forward direction. I-P controller has two gain coefficients including K_l and K_p . The control signal generated by I-P controller $(U_{l-P}(s))$ can be written as:

$$U_{t-p}(s) = \frac{K_{t}}{s} E(s) - K_{p} Y(s)$$
 (5.10)

I-P controller has been employed in different applications of control engineering [181], [182].

The optimal gains of controllers as highlighted in Eq. (5.6), (5.8), (5.9), and (5.10) are obtained using GBO. ITSE was used to formulate the cost function in a four-area IPS with GBO control methods. Therefore, the cost function (J) for a four-area IPS can be obtained as:

$$J_{\text{ITSE}} = \int_{0}^{T} t [\Delta f^{2} + \Delta V_{i}^{2} + + \Delta P_{te}^{2}] dt$$
 (5.11)

where,

$$\Delta f^{2} = \Delta f_{1}^{2} + \Delta f_{2}^{2} + \Delta f_{3}^{2} + \Delta f_{4}^{2}$$

$$\Delta V_{i}^{2} = \Delta V_{i1}^{2} + \Delta V_{i2}^{2} + \Delta V_{i3}^{2} + \Delta V_{i4}^{2}$$

$$\Delta P_{in}^{2} = \Delta P_{in1}^{2} + \Delta P_{in2}^{2} + \Delta P_{in3}^{2} + \Delta P_{in4}^{2}$$
(5.12)

$$\Delta V_{ij} = V_{ref} - V_{ij}$$

$$\Delta V_{i2} = V_{ref} - V_{i2}$$

$$\Delta V_{i3} = V_{ref} - V_{i3}$$
(5.13)

$$\Delta P_{pite1} = \Delta P_{pite12} + \Delta P_{pite13} + \Delta P_{pite14}$$

$$\Delta P_{pite2} = \Delta P_{pite21} + \Delta P_{pite23} + \Delta P_{pite24}$$

$$\Delta P_{pite3} = \Delta P_{pite31} + \Delta P_{pite32} + \Delta P_{pite34}$$

$$\Delta P_{pite4} = \Delta P_{pite41} + \Delta P_{pite42} + \Delta P_{pite43}$$
(5.14)

5.3 Gradient Based Optimizer (GBO)

In this study, the load frequency and terminal voltage in a four-area IPS were successfully controlled using a PID controller based on a gradient-based optimizer (GBO). GBO was discovered by Iman Ahmadianfar et al. in 2020 [183][184]. The GBO algorithm has recently found application in solving various engineering problems [185]–[187]. The GBO algorithm is inspired by Newton's gradient method; it uses a set of vectors to search the solution space of the problem. This search is performed using mutation methods such as local escape and the gradient search rule. An equilibrium point must be found where the gradient is zero for this algorithm to determine the best solution. In this approach, to determine the search directions, the derivatives of the objective function must be determined in conjunction with the constraints. The initial population is formed randomly, and the information from the previous iterations is used to determine a search direction. These cycles are repeated until a specific requirement is met. The steps in a GBO algorithm are as follows.

5.3.1 GBO Initialization

The GBO population is initialized as follows:

$$X_{n,d} = [X_{n,1}, X_{n,2},, X_{n,D}]$$
(5.15)

$$X_{n} = X_{nm} + rand(0,1) \times (X_{nm} - X_{nm})$$
 (5.16)

where, n = [1,2,...,N], d = [1,2,...,D], rand(0,1) generates random number between 0 and 1, X_{max} are the limits of decision variable.

5.3.2 Gradient Search Rule (GSR)

The gradient based technique, which forms the basis of GSR, finds the optimal solution by identifying the extreme point at which the gradient equals zero. The objectives of employing GSR include acceleration of convergence rate and exploration tendency enhancement. The numerical gradient approach and Taylor series can be used to express new position (x_{n+1}) as:

$$x_{n+1} = x_n - \frac{2\Delta x \times f(x_n)}{f(x_n + \Delta x) - f(x_n - \Delta x)}$$
 (5.17)

In the GBO algorithm, $x_n + \Delta x$ and $x_n - \Delta x$ represent the neighboring positions of x_n . The position $x_n + \Delta x$ has a worse fitness (x_{norst}) than x_n , while $x_n - \Delta x$ has better fitness (x_{best}) than x_n . The GSR can be written as:

$$GSR = randn \times \frac{2\Delta x \times x_{n}}{(x_{neal} - x_{best} + \varepsilon)}$$
 (5.18)

where Δx is the change in position after each iteration, ε is a small value between 0 and 0.1 and randn denotes a random number. In order to achieve a balance between the exploitation and exploration phases, the modified expression of GSR can be stated as:

$$GSR = randn \times \rho_1 \times \frac{2\Delta x \times x_n}{(x_{--} - x_{box} + \varepsilon)}$$
(5.19)

where ρ_i is a random number and it can be written as:

$$\rho_1 = (2 \times rand \times \alpha) - \alpha \tag{5.20}$$

$$\alpha = \left| \beta \times \sin \left(\frac{3\pi}{2} + \sin \left(\beta \times \frac{3\pi}{2} \right) \right) \right| \tag{5.21}$$

$$\beta = \beta_{\text{min}} + (\beta_{\text{max}} - \beta_{\text{min}}) \times \left(1 - \left(\frac{m}{M}\right)^3\right)^2$$
 (5.22)

where M represents total number of iterations, m shows current iteration, β_{max} and β_{min} have values of 1.2 and 0.2 respectively. The sine function representing the change from exploration to exploitation is represented by α . The difference Δx between the best candidate solution (x_{best}) and a position chosen at random (x_{cl}^{m}) can be written as:

$$\Delta x = rand(1:N) \times |step| \tag{5.23}$$

$$step = \frac{(x_{heat} - x_{i,1}^m) + \delta}{2} \tag{5.24}$$

$$\delta = 2 \times rand \times \left(\frac{\left| x_{r_1}^m + x_{r_2}^m + x_{r_3}^m + x_{r_4}^m - x_n^m \right|}{4} \right)$$
 (5.25)

where r1, r2, r3, and r4 are random number between l and N having different values. The updated position (x_{n+1}) can be expressed as:

$$x_{n+1} = x_n - GSR \tag{5.26}$$

For better utilization of the region close to x_n , the direction of movement (DM) has been introduced that can be written as:

$$DM = rand \times \rho_1 \times (x_{best} - x_n) \tag{5.27}$$

where ρ_2 is a random number, which can be obtained as:

$$\rho_2 = (2 \times rand \times \alpha) - \alpha \tag{5.28}$$

The modified position (X1") can be found using GSR and DM as:

$$X1_{\underline{}}^{\underline{A}} = x_{\underline{}}^{\underline{\underline{A}}} - GSR + DM \tag{5.29}$$

$$X1_{n}^{m} = x_{n}^{m} - randn \times \rho_{1} \times \frac{2\Delta x \times x_{n}^{m}}{(x_{norn} - x_{best} + \varepsilon)}$$

$$+ rand \times \rho_{2} \times (x_{best} - x_{n}^{m})$$

$$(5.30)$$

The new vector $(X2_*^n)$ can be created by replacing the position of the best vector (x_{best}) with x_*^n .

$$X2_{n}^{m} = x_{bast} - randn \times \rho_{1} \times \frac{2\Delta x \times x_{n}^{m}}{(yp_{n}^{m} - yq_{n}^{m} + \varepsilon)} + rand \times \rho_{2} \times (x_{c1}^{m} - x_{c2}^{m})$$

$$(5.31)$$

where.

$$yp_{n} = rand \times \left(\frac{[z_{n+1} + x_{n}]}{2} + rand \times \Delta x\right)$$
 (5.32)

$$yq_{n} = rand \times \left(\frac{\left[z_{n+1} + x_{n}\right]}{2} - rand \times \Delta x\right)$$
 (5.33)

 z_{n+1} represents a vector.

The new solution (x_n^{m+1}) can be defined at the next iteration as:

$$x_n^{m+1} = r_a \times (r_b \times X1_n^m + (1 - r_b) \times X2_n^m) + (1 - r_a) \times X3_n^m$$
(5.34)

where,

$$X3_{n}^{m} = X_{n}^{m} - \rho_{1} \times (X2_{n}^{m} - X1_{n}^{m})$$
 (5.35)

where r_a and r_b are random numbers between 0 and 1.

5.3.3 Local Escaping Operator (LEO)

To improve the GBO algorithm's capability to handle challenging problems, the LEO is included. The LEO solution (X_{LEO}^m) is can be obtained using following code:

if rand < pr

if rand < 0.5

$$X_{LEO}^{n} = X_{n}^{n+1} + f_{1} \times (u_{1} \times x_{best} - u_{2} \times x_{k}^{n}) + f_{2}$$
 (5.36)

$$\times \rho_1 \times (u_1 \times (X2'' - X1'') + u_2 \times (x_{r_1} - x_{r_2})) / 2$$

$$X_{\bullet}^{m+1} = X_{LEO}^{m}$$

else

$$X_{LEO}^{m} = x_{basi} + f_{1} \times (u_{1} \times x_{basi} - u_{2} \times x_{k}^{m}) + f_{2}$$

$$\times \rho_1 \times (u_1 \times (X2_1^m - X1_1^m) + u_2 \times (x_1^m - x_2^m)) / 2$$

$$X_{*}^{m+1} = X_{LEO}^{m} \tag{5.37}$$

end

end

where x_{ben} shows the best solution; x_{r1}^m, x_{r2}^m and x_k^m are randomly generated solutions; f_2 is a random number with a standard deviation of 1 and mean of 0 whereas f_1 is random number between -1 and 1; pr represents the probability; u_1 , u_2 , and u_3 can be obtained as:

$$u_1 = L_1 \times 2 \times rand + (1 - L_1) \tag{5.38}$$

$$u_1 = L_1 \times rand + (1 - L_1) \tag{5.39}$$

$$u_1 = L_1 \times 2 \times rand + (1 - L_1) \tag{5.40}$$

where L_I has a value of 1 if parameter u_I is less than 0.5, else it has a value of 0. x_k^m can be written as:

$$x_{k}^{m} = \begin{cases} x_{tand} & if u_{2} < 0.5 \\ x_{p}^{m} & otherwise \end{cases}$$
 (5.41)

where x_{rand} represents the new solution and x_p^m denotes random solution of the population $(p \in [1,2,...,N])$.

$$x_{mn} = X_{mn} + rand(0,1) \times (X_{mn} - X_{mn})$$
 (5.42)

$$x_{L}'' = L_{1} \times x_{L}'' + (1 - L_{1}) \times x_{LL}$$
 (5.43)

where L_2 has a value of 1 if parameter u_2 is less than 0.5, else it has a value of 0. By choosing values for the parameters u_1 , u_2 , and u_3 randomly, the population becomes more diverse and is able to avoid local optimal solutions. The flow chart of GBO is given in Figure 5.3.

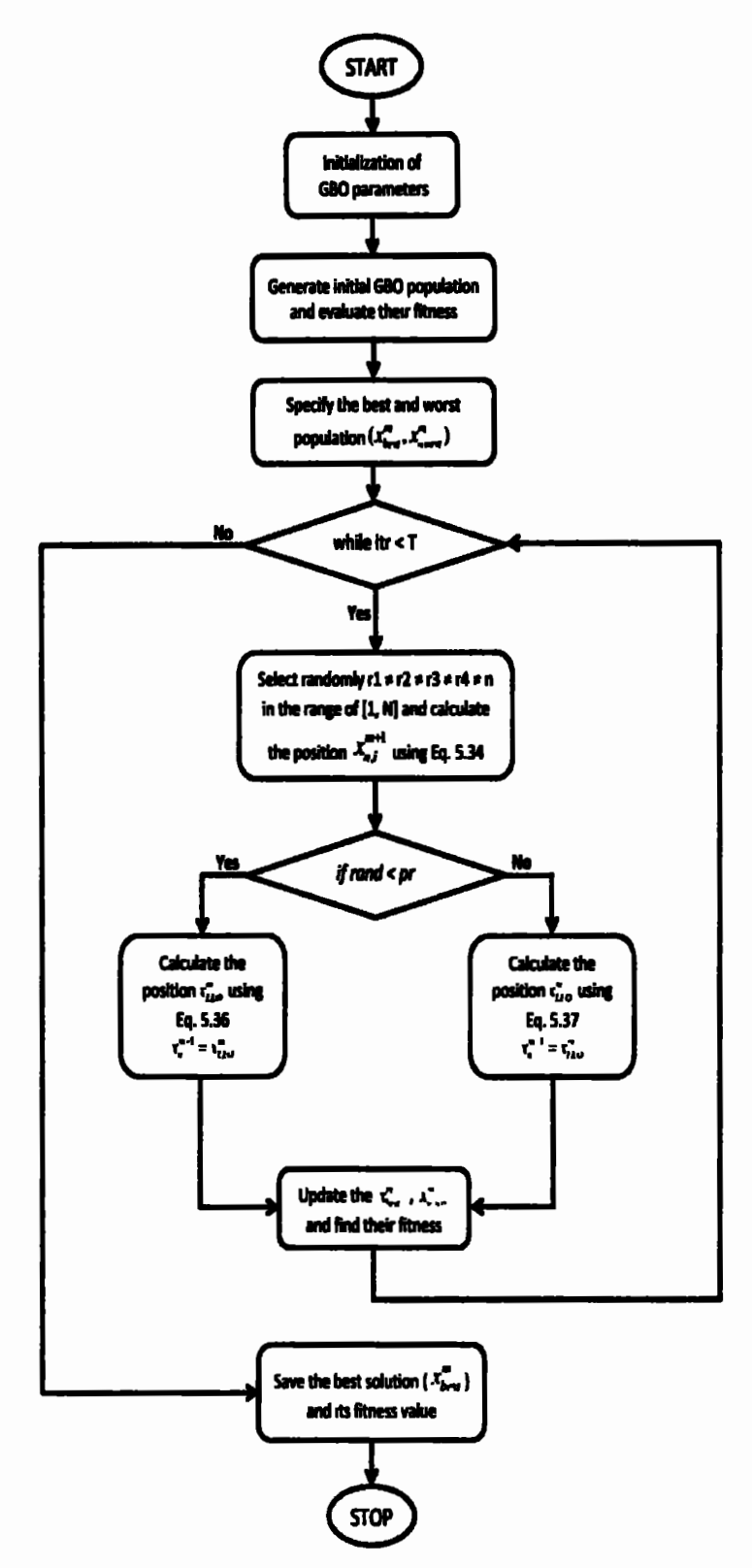


Figure 5.3: Flow chart of GBO

5.4 Implementation and Results Discussion

Extensive simulations were conducted in MATLAB/Simulink to validate the suggested control methodology. The rated power of the system is considered as 2000 MW. First, a four-area, five-source IPS with 5% SLP (0.05 p.u.) in each area was comprehensively examined using GBO-based control methodologies. Then, by changing the system settings in each of the four areas, a detailed sensitivity analysis was carried out. The population consists of thirty solutions whereas twenty iterations were considered in each simulation to obtain the optimal solution. The step input per unit was taken as reference terminal voltage.

5.4.1 Frequency and Voltage Stabilization in a Four-area Multi-source IPS

The four-area IPS model under investigation is provided in Figure 5.1. The system parameters of four-area IPS are specified in Appendix C. The optimal parameters of GBO-PID, GBO-I-PD, GBO-TID, and GBO-I-P control strategies are given in Table 5.1. This section presents implementation of proposed control strategy in a four-area multi-source IPS with 5% SLP and detailed comparisons of the GBO-PID with GBO-I-PD, GBO-TID, and GBO-I-P based control strategies.

Table 5.1: Optimal values of controller parameters for a four-area multi-source IPS

	GBO-I-P		GBO-TID		GBO-I-PD		GBO-PID	
Area	Parameter	Value	Parameter	Value	Parameter	Value	Parameter	Value
	Kpl	0.17	Ktl	0.76	K _i	0.0001	Kpi	1.43
	Kıı	2.42	K,1	1.29	Kpl	1.59	Kıi	1.27
A 1	-	-	Kdl	0.20	K _{d1}	1.97	K _{d1}	1.93
Area-1	K _{p2}	1.37	K _{t2}	0.97	K ₁₂	1.09	K _{p2}	1.08
ł	K,2	1.38	K ₁₂	0.29	K _{p2}	1.15	K ₁₂	1.11
İ	-	-	K _{d2}	1.18	K _{d2}	0.15	K _{d2}	0.67
	K _{p3}	1.43	K _{t3}	1.54	K ₁₃	0.74	K _{p3}	1.11
	K,3	0.82	K ₁₃	1.27	K _{p3}	0.25	K ₁₃	1
		-	Kd3	0.30	K _{d3}	0.54	K _{d3}	1.24
Area-2	K _{p4}	0.92	K ₁₄	0.44	K,4	0.35	K _{p4}	1.37
ļ	K,4	0.83	K ₁₄	0.18	K _{p4}	0.41	K,4	1.20
	•	-	K _{d4}	0.20	K _{d4}	0.14	K _{d4}	0.96
	K _{p5}	1.15	K _{t5}	1.82	K ₁₅	0.01	K _{p5}	1.74
	K,5	1.67	K,5	0.42	K _{p5}	0.65	K ₁₅	1.76
Area-3	-	-	K _{d5}	1.73	K _{d5}	1.28	K _{d5}	0.99
Alea-3	K _{p6}	1.11	K ₁₆	0.87	K,6	1.06	K _{p6}	1.33
	K,6	1.09	K,6	0.31	K _{p6}	0.85	K,6	1.27
	-		K _{t6}	0.24	K _{d6}	0.047	K _{d6}	1.13
	K _{p7}	0.12	K _{t7}	1.78	K ₁₇	0.99	K _{p7}	0.98
	K ₁₇	2.78	K ₁₇	0.28	K _{p7}	2	K ₁₇	1.94
Area-4	-	•	K _{d7}	0.62	K _{d7}	0.14	K _{d7}	1.39
A1 Ca-4	K _{p8}	1.10	K _{t8}	1.30	K,8	1.15	K _{p8}	1.24
	K,8	1.13	K,8	0.069	K _{p8}	1.28	K.8	0.61
	-		K _{d8}	1.50	K _{d8}	0.58	K _{d8}	1.26
	ITSE	2.18	ITSE	2.62	ITSE	3.43	ITSE	0.71

Figure 5.4, 5.5, 5.6, and 5.7 display the frequency deviation responses, while Table 5.2 presents the performance specifications of the four-area IPS utilizing the GBO-PID, GBO-I-PD, GBO-TID, and GBO-I-P control strategies. It can be seen that the proposed GBO-PID control method provided a very satisfactory settling time response in each area's LFC. GBO-PID provided settling times of 5.37s, 5.38s, 5.38s, and 5.98s in area-1, area-2, area-3, and area-4 LFC respectively which are better than GBO-I-PD, GBO-TID, and GBO-I-P control strategies at the cost of % overshoot and undershoot in each area. GBO-I-PD yielded better undershoot response (-0.049) with zero % overshoot compared to other control strategies in area-1 LFC. In comparison to other control strategies in area-2 LFC, GBO-I-PD provided better % overshoot (0.009%) and undershoot (-0.068) responses. In area-3 LFC, GBO-I-PD produced a better undershoot response (-0.08) with zero % overshoot (0.0039%) and undershoot response (-0.046) compared to other control strategies in area-4 LFC. The % steady-state (s-s) error is zero with all control strategies in each area.

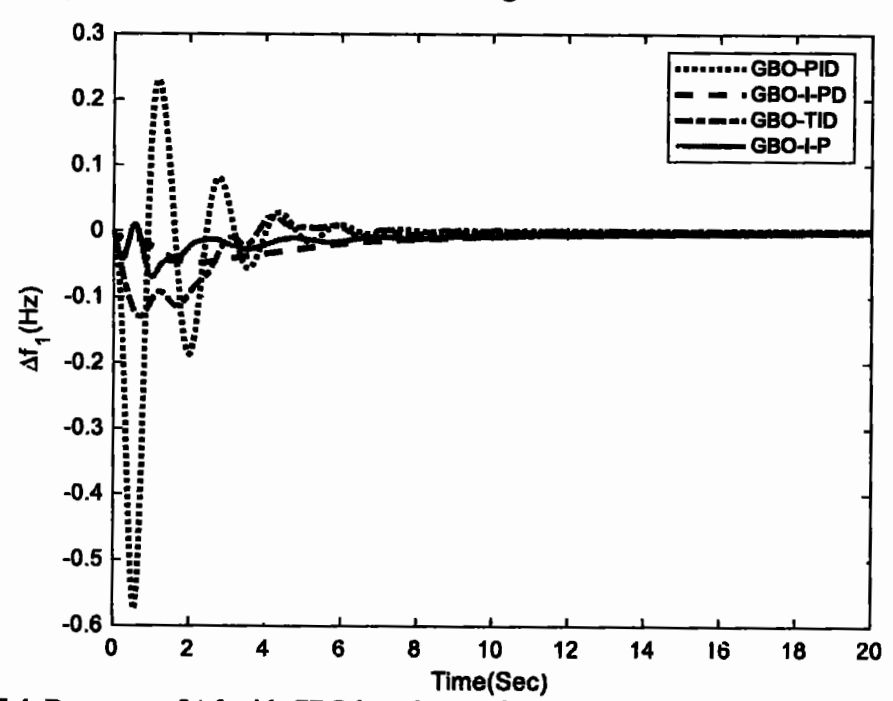


Figure 5.4: Response of Δf_1 with GBO based control strategies in a four-area multi-source IPS

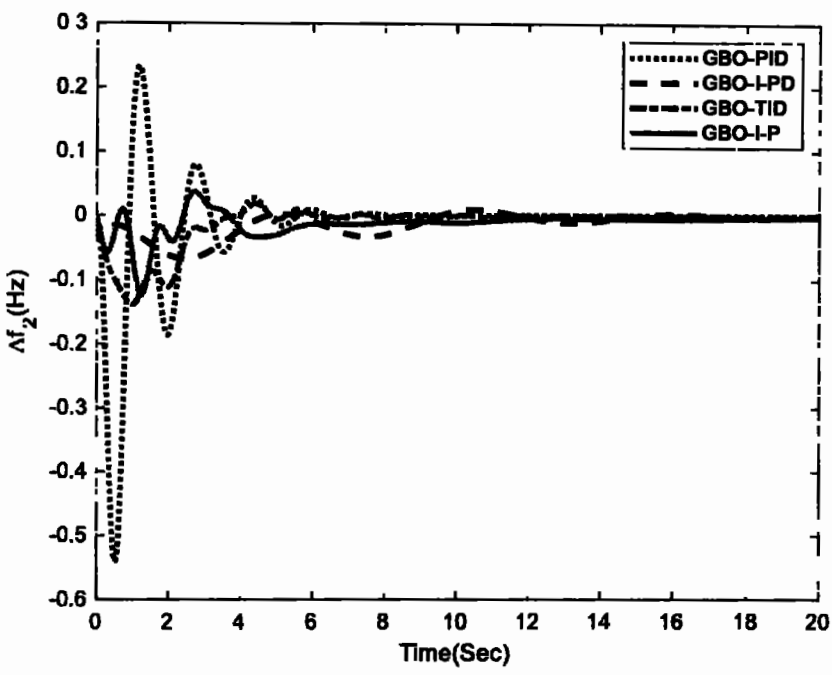


Figure 5.5: Response of Δf_2 with GBO based control strategies in a four-area multi-source IPS

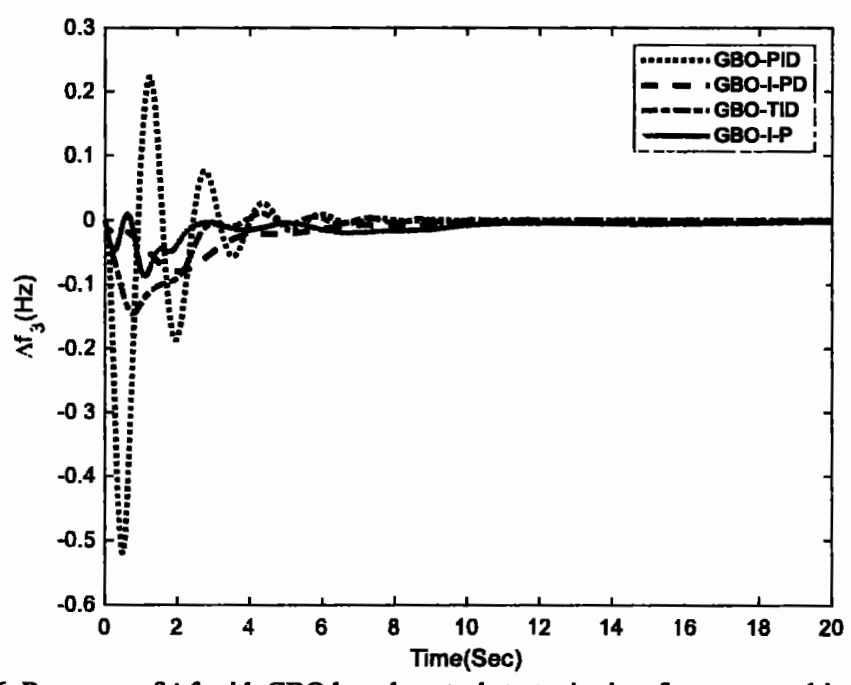


Figure 5.6: Response of Δf_3 with GBO based control strategies in a four-area multi-source IPS

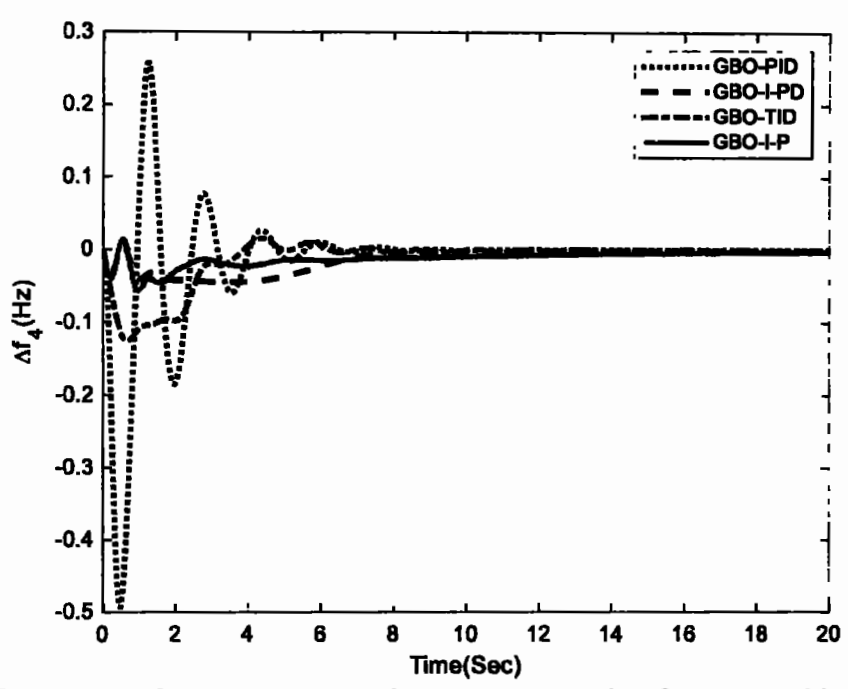


Figure 5.7: Response of Δf_4 with GBO based control strategies in a four-area multi-source IPS

Table 5.2: Performance specifications of frequency deviation responses in a four-area multisource IPS

			<u></u>	CE IF S					
		Are	a-1	Area-2					
Control Strategy	Settling Time (s)	% Overshoot	Undershoot	% s-s Error	Settling Time (s)	% Overshoot	Undershoot	% s-s Error	
GBO-PID	5.37	0.23	-0.58	0	5.38	0.23	-0.54	0	
GBO-I-PD	16.3	0	-0.049	0	19.54	0.009	-0.068	0	
GBO-TID	9.66	0.022	-0.13	0	9.51	0.018	-0.14	0	
GBO-I-P	16.10	0.0086	-0.07	0	16.49	0.036	-0.12	0	
		Are	ea-3		Area-4				
Control Strategy	Settling Time (s)	% Overshoot	Undershoot	% s-s Error	Settling Time (s)	% Overshoot	Undershoot	% s-s Error	
GBO-PID	5.38	0.22	-0.52	0	5.98	0.26	-0.49	0	
GBO-I-PD	11.0	0	-0.08	0	17.08	0.0039	-0.046	0	
GBO-TID	9.62	0.011	-0.15	0	9.68	0.015	-0.13	0	
GBO-I-P	17.66	0.009	-0.087	0	16.95	0.013	-0.057	0	

Figure 5.8, 5.9, 5.10, and 5.11 display the terminal voltage responses, while Table 5.3 presents the performance specifications of the four-area IPS utilizing the GBO-PID, GBO-I-PD, GBO-TID, and GBO-I-P control strategies respectively. For area-1 AVR, GBO-PID provided settling time of 3.96s that is quicker than GBO-TID and GBO-I-P control strategies. Moreover, GBO-PID yielded settling times of 4.09s, 4.36s, and 2.92s in area-2, area-3, and area-4 AVR, which are better than GBO-I-PD, GBO-TID, and GBO-I-P control strategies. GBO-I-PD produced settling time of 3.72s with 0.48% overshoot response, which are better than all other control strategies in area-1 AVR. GBO-PID yielded overshoot of 5.45% in area-2 AVR, which is better than GBO-I-PD, GBO-TID, and GBO-I-P control strategies. GBO-PID produced overshoot of 9%, which is better than GBO-I-PD and GBO-TID control strategies in area-3 AVR. GBO-I-P outperformed all other techniques in area-3 AVR by 5.52% in terms of overshoot response. GBO-PID provided 10.13% overshoot, which is better than GBO-TID control strategy in area-4 AVR. GBO-I-P yielded 4.36% overshoot that is better compared to all other techniques. The % steady-state (s-s) error is zero with all control strategies including GBO-PID in each area except GBO-TID which gave steady-state (s-s) error of 1.8% in area-2 AVR. It can be seen that the suggested GBO-PID control strategy produced AVR responses which are extremely satisfactory in terms of settling time and % overshoot.

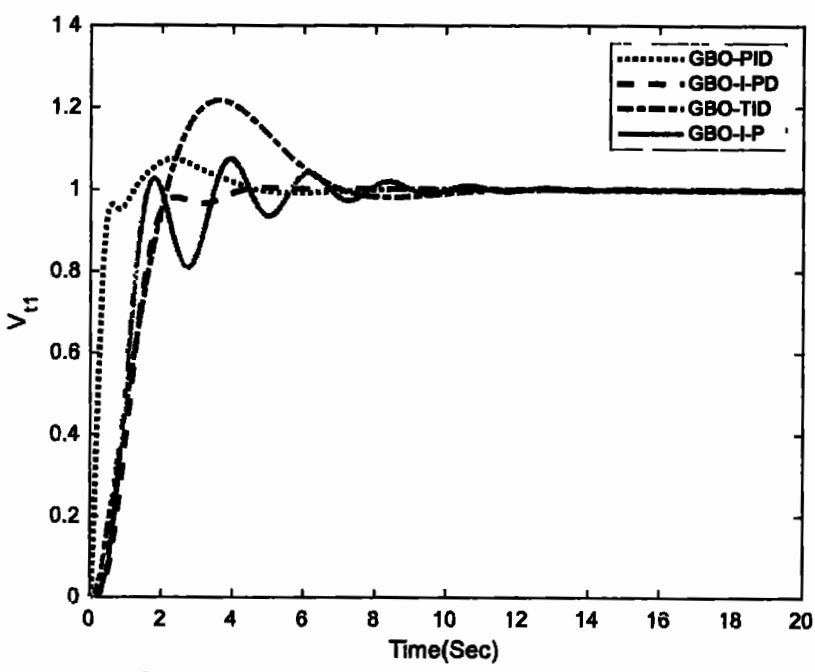


Figure 5.8: Response of V_{t1} with GBO based control strategies in a four-area multi-source IPS

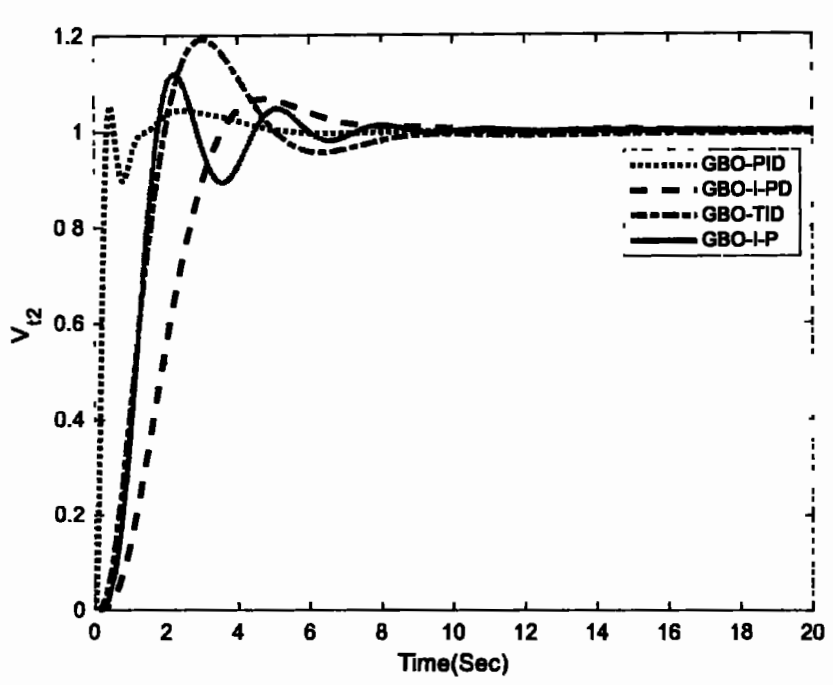


Figure 5.9: Response of V_2 with GBO based control strategies in a four-area multi-source IPS

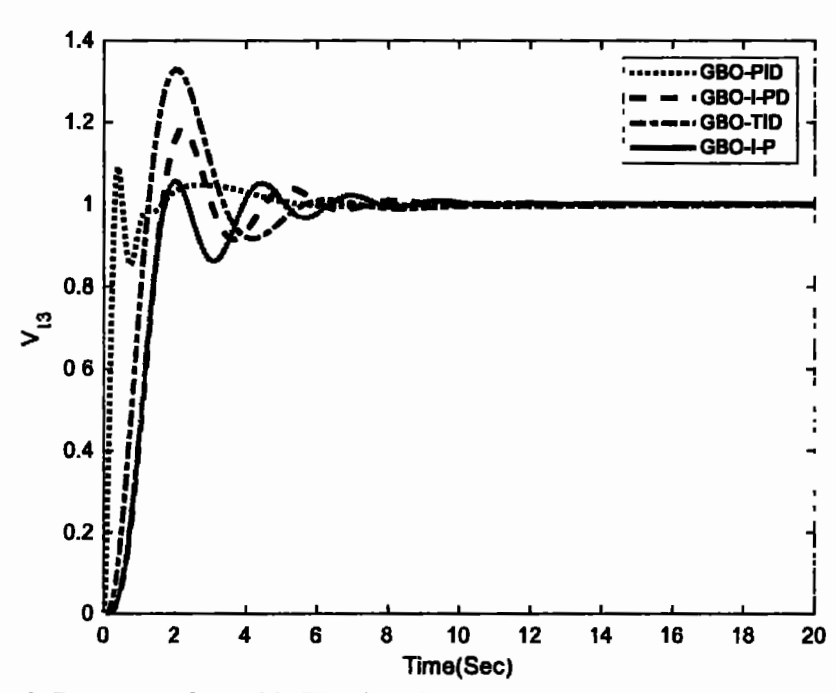


Figure 5.10: Response of V_{13} with GBO based control strategies in a four-area multi-source IPS

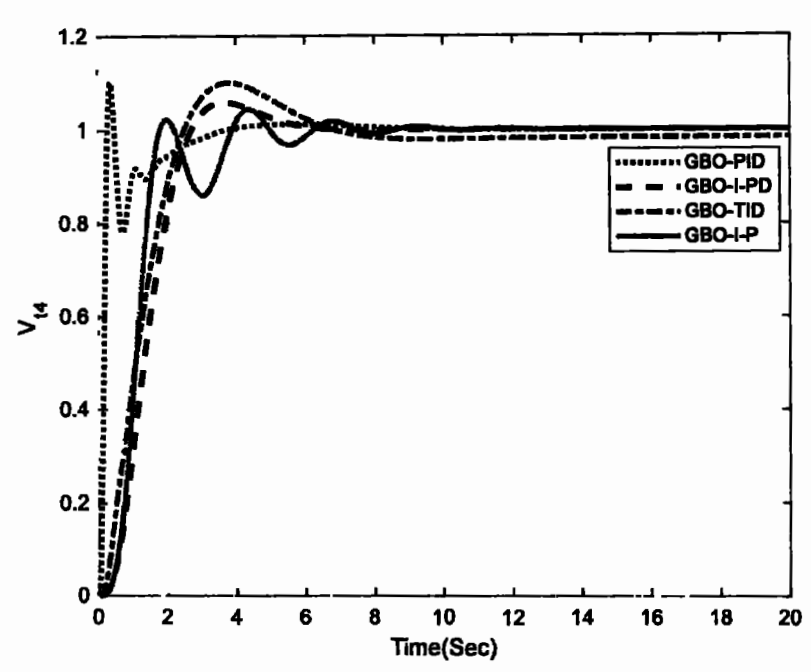


Figure 5.11: Response of $V_{\rm M}$ with GBO based control strategies in a four-area multi-source IPS

Table 5.3: Performance specifications of terminal voltage responses in a four-area multisource IPS

		Area-1		Area-2			
Control Strategy	Settling Time (s)	% Overshoot	% s-s Error	Settling Time (s)	% Overshoot	% s-s Error	
GBO-PID	3.96	7.52	0	4.09	5.45	0	
GBO-I-PD	3.72	0.48	0	6.75	6.66	0	
GBO-TID	6.60	21.91	0	7.68	19.71	1.8	
GBO-I-P	7.52	7.43	0	5.68	11.9	0	
		Area-3		Area-4			
Control Strategy	Settling Time (s)	% Overshoot	% s-s Error	Settling Time (s)	% Overshoot	% s-s Error	
GBO-PID	4.36	9.0	0	2.92	10.13	0	
GBO-I-PD	5.72	18.04	0	5.27	5.90	0	
GBO-TID	5.24	33.18	0	6.72	11.90	0	
GBO-I-P	7.01	5.52	0	5.92	4.36	0	

The tie-line power deviation responses curves are shown in Figure 5.12, 5.13, 5.14, and 5.15 while the performance specifications of the four-area IPS are presented in Table 5.4 respectively. It can be seen that the suggested GBO-PID control strategy produced tie-line power deviation responses that were incredibly satisfactory in terms of settling time in each area. GBO-PID provided settling times of 9.36s, 9.69s, and 8.45s in area-1, area-2, and area-3 respectively, which are better than GBO-I-PD, GBO-TID, and GBO-I-P control strategies. GBO-TID produced 9.63s settling time in area-4 which is better than all other control methodologies. GBO-TID yielded better overshoot (0.012%) response whereas GBO-I-PD produced better undershoot response (-0.0035) compared to other control methodologies in terms of area-1 tie-line power deviation. GBO-PID yielded 0.0025% overshoot with -0.0093 undershoot, which is better than GBO-I-PD and GBO-I-P control strategies in terms of area-2 tie-line power deviation. Moreover, GBO-TID yielded better undershoot response (-0.0053) compared to other control strategies in terms of area-2 tie-line power deviation. GBO-I-PD produced better overshoot response (0.0038) whereas GBO-PID yielded better undershoot response (-0.012) compared to other control strategies in terms of area-3 tie-line power deviation. GBO-TID yielded better overshoot response (0.0098) whereas GBO-I-P yielded better undershoot response (-0.007) compared to other control strategies in terms of area-4 tie-line power deviation. The % steady-state (s-s) error is zero with each control strategies except GBO-I-PD which produced negligible % steady-state (s-s) in area-1 and area-3.

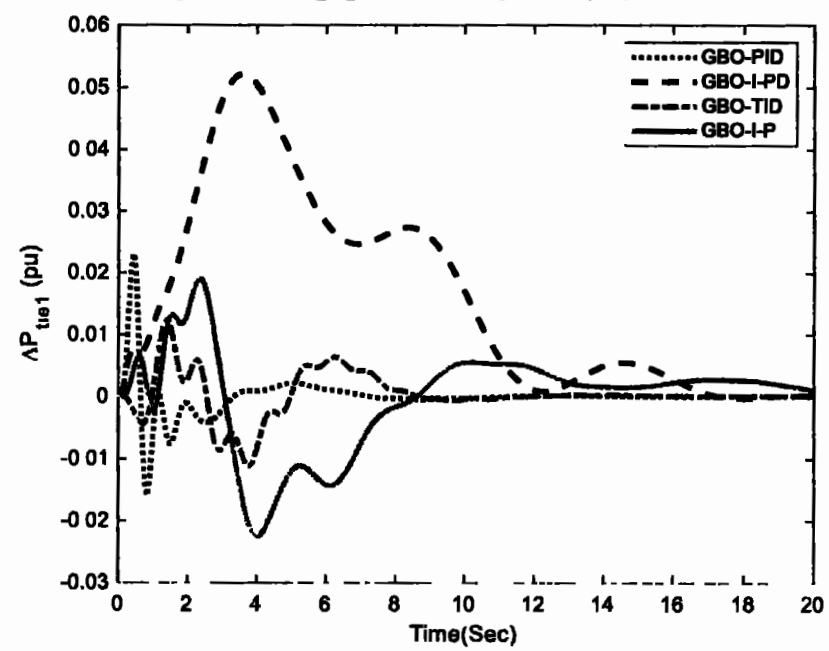


Figure 5.12: Response of ΔP_{tiel} with GBO based control strategies in a four-area multi-source IPS

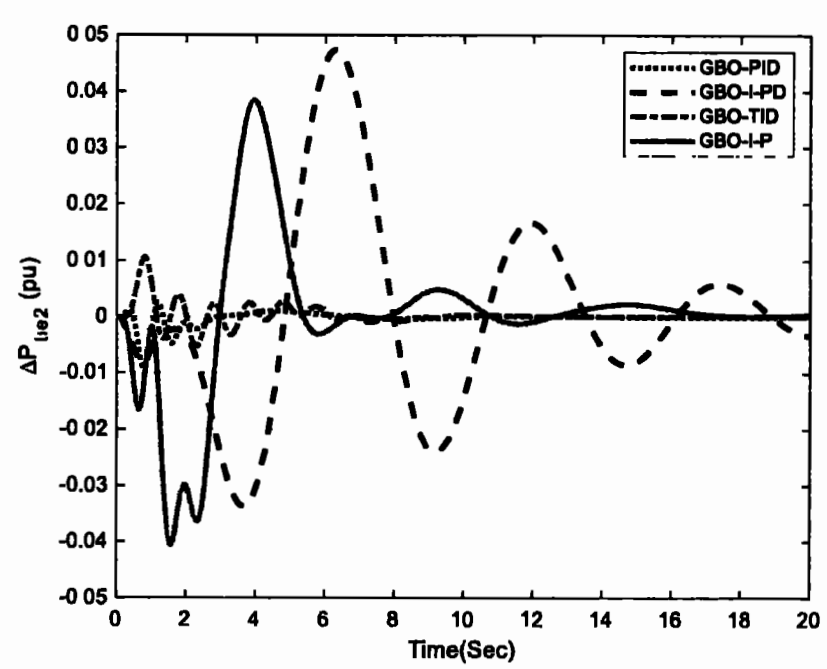


Figure 5.13: Response of ΔP_{tie2} with GBO based control strategies in a four-area multi-source IPS

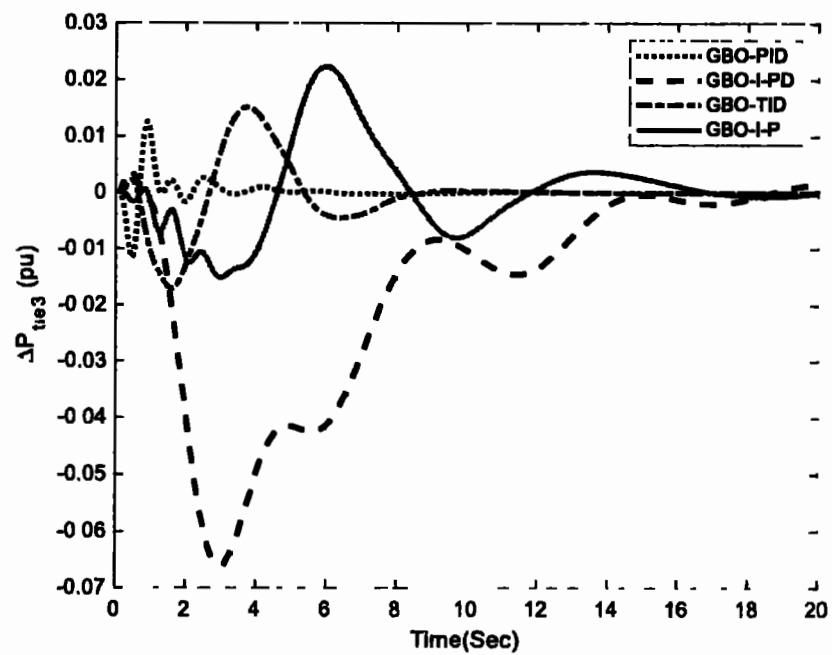


Figure 5.14: Response of ΔP_{tie3} with GBO based control strategies in a four-area multi-source IPS

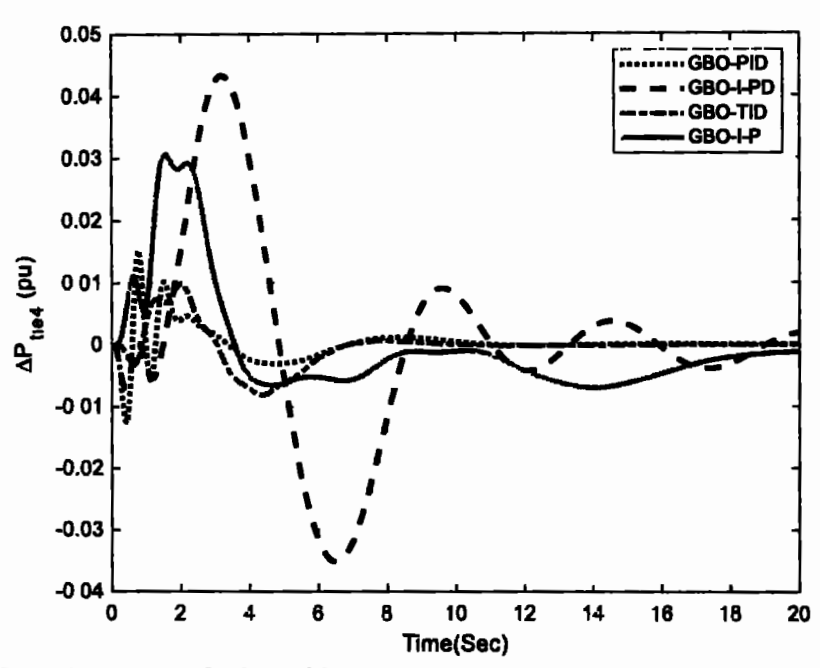


Figure 5. 15: Response of ΔP_{tie4} with GBO based control strategies in a four-area multisource IPS

Table 5.4: Performance specifications of tie-line power deviation responses in a four-area multi-source IPS

		munti-s	ource 11				
	Are	a-1	Area-2				
Settling Time (s)	% Overshoot	Undershoot	% s-s Error	Settling Time (s)	% Overshoot	Undershoot	% s-s Error
9.36	0.023	-0.016	0	9.69	0.0025	-0.0093	0
16.65	0.052	-0.0035	0.004	19.48	0.047	-0.034	0
11.18	0.012	-0.0112	0	11.02	0.011	-0.0053	0
19.50	0.019	-0.023	0	16.12	0.039	-0.040	0
	Are	a-3		Area-4			
Settling Time (s)	% Overshoot	Undershoot	% s-s Error	Settling Time (s)	% Overshoot	Undershoot	% \$-8 Error
8.45	0.013	-0.012	0	10.23	0.015	-0.013	0
18.71	0.0038	-0.066	0.004	19.47	0.043	-0.035	0
9.7	0.015	-0.017	0	9.63	0.0098	-0.0081	0
19.17	0.000	0.016	_	10.03	0.031	-0.007	0
	Time (s) 9.36 16.65 11.18 19.50 Settling Time (s) 8.45 18.71 9.7	Settling % Overshoot	Name	Name	Settling % Undershoot % s-s Error (s) 9.36 0.023 -0.016 0 9.69 16.65 0.052 -0.0035 0.004 19.48 11.18 0.012 -0.0112 0 11.02 19.50 0.019 -0.023 0 16.12 Area-3 Settling % Undershoot (s) Time (s) 0.013 -0.012 0 10.23 18.71 0.0038 -0.066 0.004 19.47 9.7 0.015 -0.017 0 9.63	Name	Name

Figure 5.16, 5.17, and 5.18 show the graphical comparisons of the performance specifications of frequency deviation, terminal voltage, and tie-line power deviation responses using GBO-PID, GBO-I-PD, GBO-TID, and GBO-I-P control strategies in a four-area IPS.

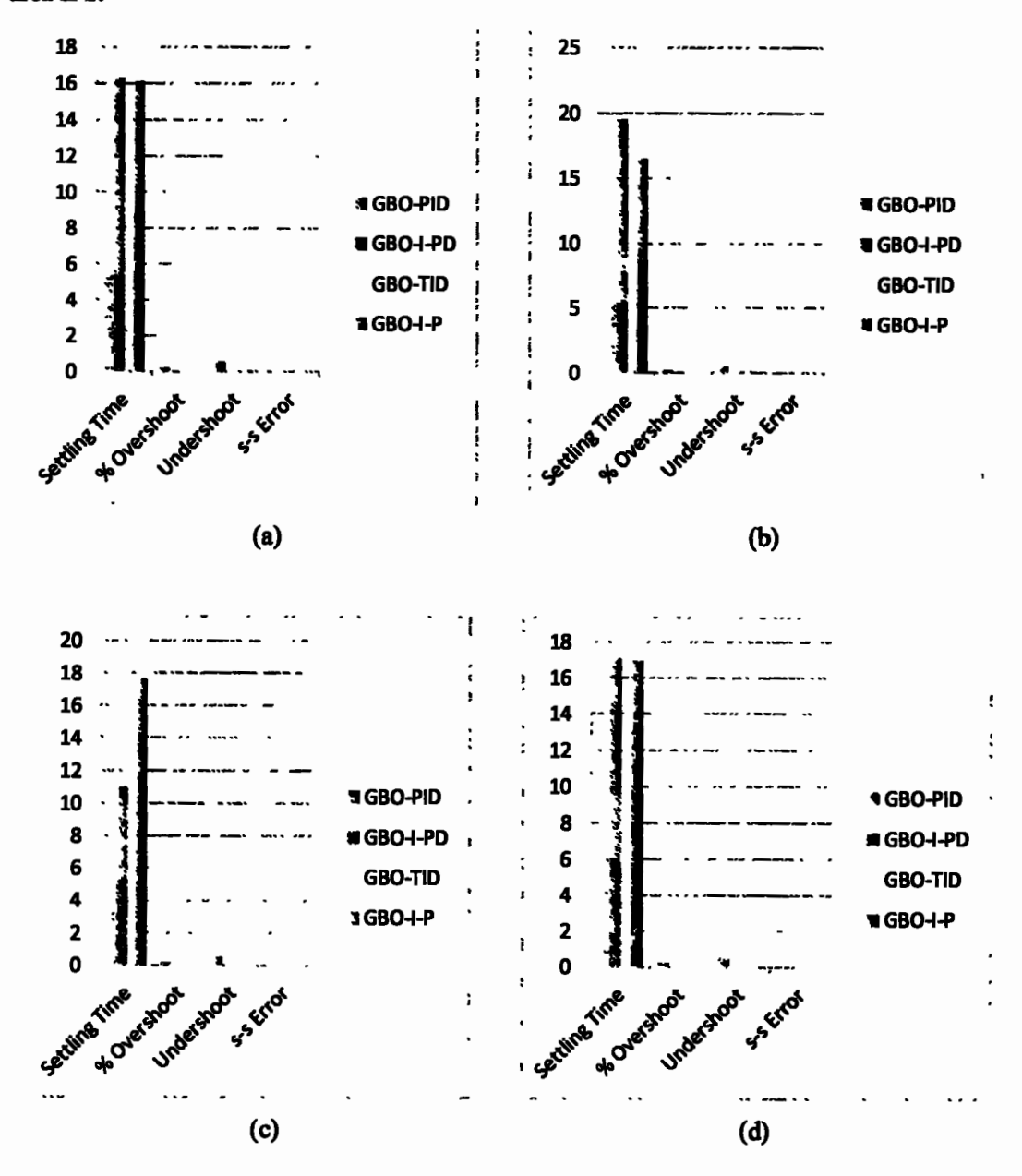


Figure 5.16: Graphical comparisons of performance specifications of frequency deviation responses using GBO based control strategies in a four-area multi-source IPS (a) Δf_1 (b) Δf_2 (c) Δf_3 (d) Δf_4

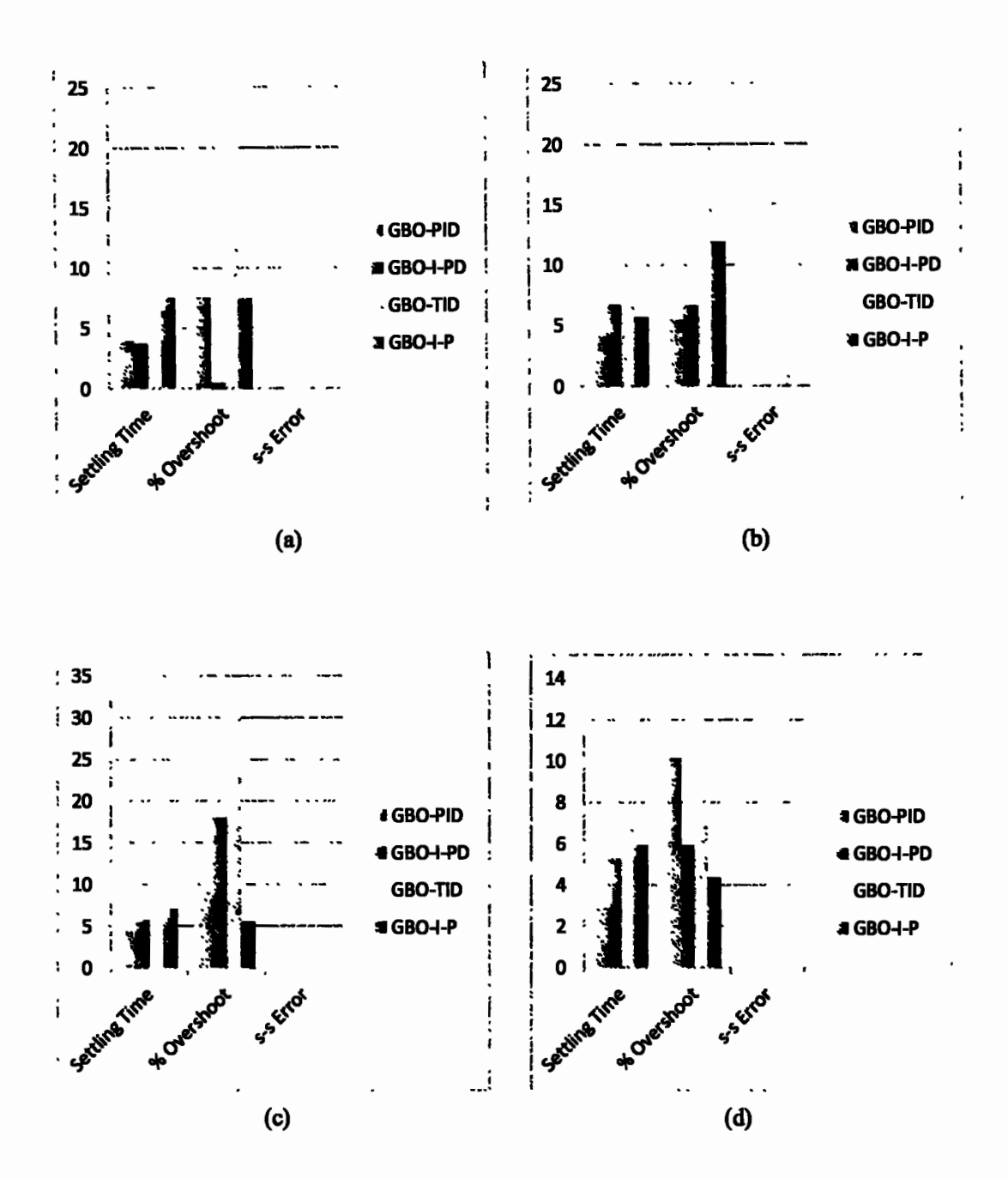


Figure 5.17: Graphical comparisons of performance specifications of terminal voltage responses using GBO based control strategies in a four-area multi-source IPS

(a) V_{11} (b) V_{12} (c) V_{13} (d) V_{14}

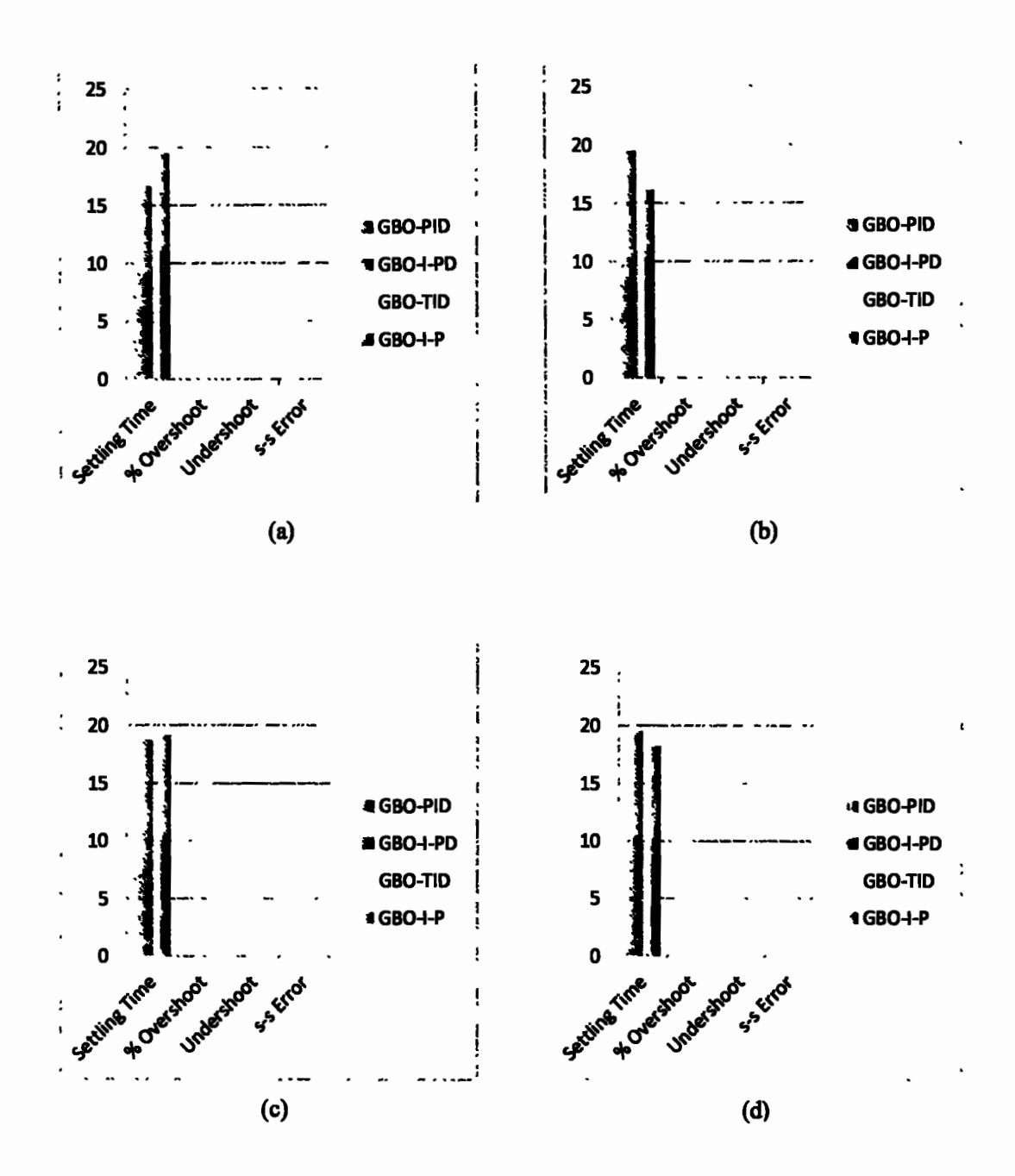


Figure 5.18: Graphical comparisons of performance specifications of tie-line power deviation responses using GBO based control strategies in a four-area multi-source IPS

(a) ΔP_{tie1} (b) ΔP_{tie2} (c) ΔP_{tie3} (d) ΔP_{tie4}

5.4.2 Sensitivity Analysis of a Four-area Multi-source IPS

In this section, we evaluated the robustness of the proposed GBO-PID control strategy in a four-area IPS by varying the system parameters. The speed regulation (R) and turbine time constant (T_{tr}) were changed to $\hat{A} \pm 25\%$ of their nominal values. In this study, optimal parameters of the GBO-PID controller were taken from the previous section. Figure 5.19, 5.20, 5.21, and 5.22 show the frequency deviation responses; Figure 5.24, 5.25, 5.26, and 5.27 show the terminal voltage responses; Figure 5.29, 5.30, 5.31, and 5.32 show the tie-line power deviation responses using GBO-PID control strategy with variations in T_{tr} and R.

Tables 5.5, 5.6, and 5.7 show the performance specifications of frequency deviation, terminal voltage, and tie-line power deviation respectively in this scenario. Despite ±25% variance in system parameters, it is clear from the results that all frequency deviation, terminal voltage, and tie-line power deviation responses are nearly identical to one another. The fact that values of all performance specification including settling time, % overshoot, undershoot, and % steady-state (s-s) error have barely changed with variation in system parameters is unmistakable proof that the suggested technique can function well under dynamic circumstances.

The graphical comparisons of frequency deviation, terminal voltage, and tie-line power deviation responses in this case are shown in Figures 5.23, 5.28, and 5.33 respectively. These results categorically demonstrate that the recommended GBO-PID controller is quite robust and does not require re-tuning for $\hat{A} \pm 25\%$ variations in T_{tr} and R.

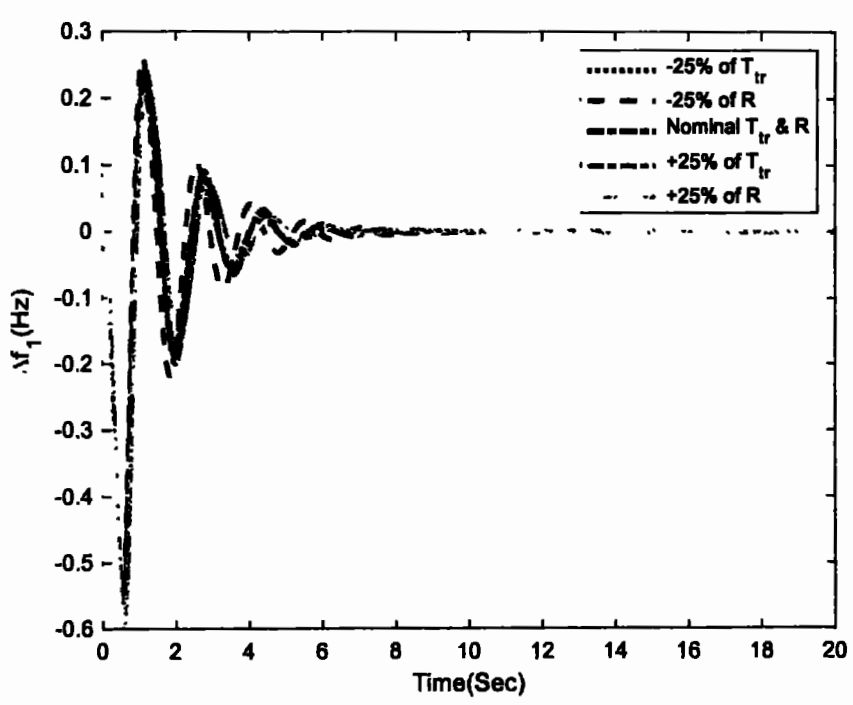


Figure 5.19: Response of Δf i with ±25% variations in system parameters using GBO based control strategy in a four-area multi-source IPS

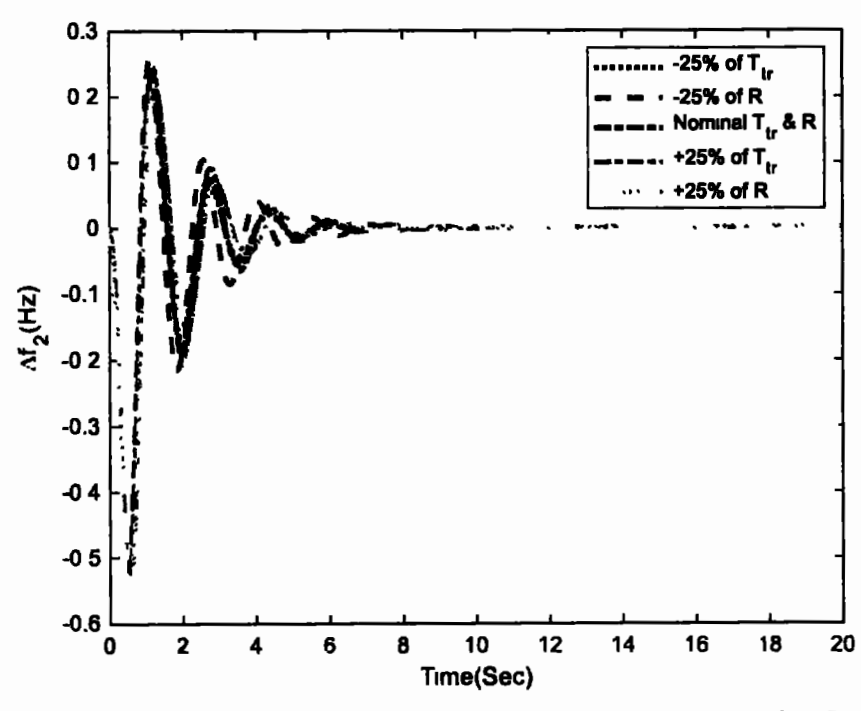


Figure 5.20: Response of Δf_2 with ±25% variations in system parameters using GBO based control strategy in a four-area multi-source IPS

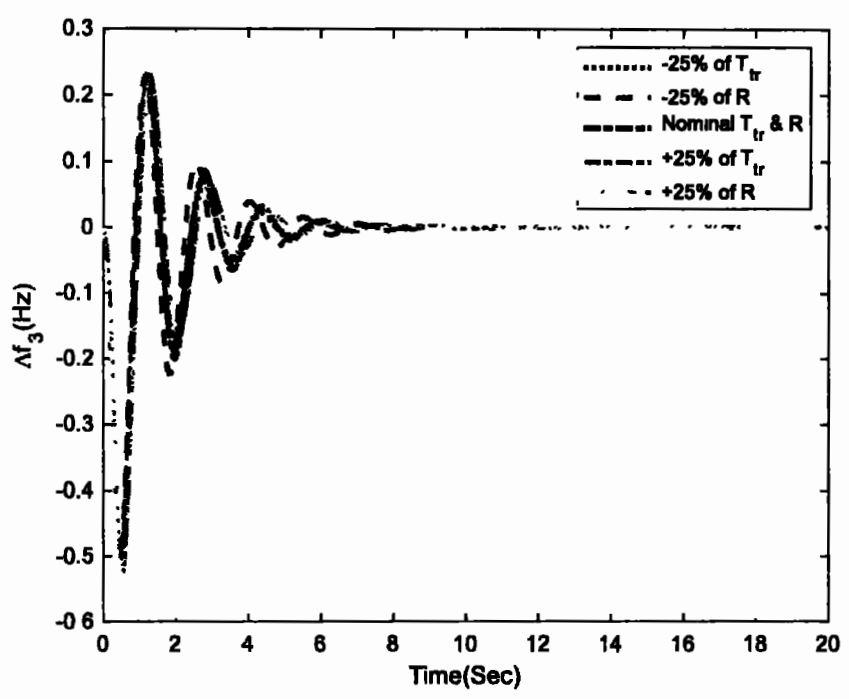


Figure 5.21: Response of Δf_3 with ±25% variations in system parameters using GBO based control strategy in a four-area multi-source IPS

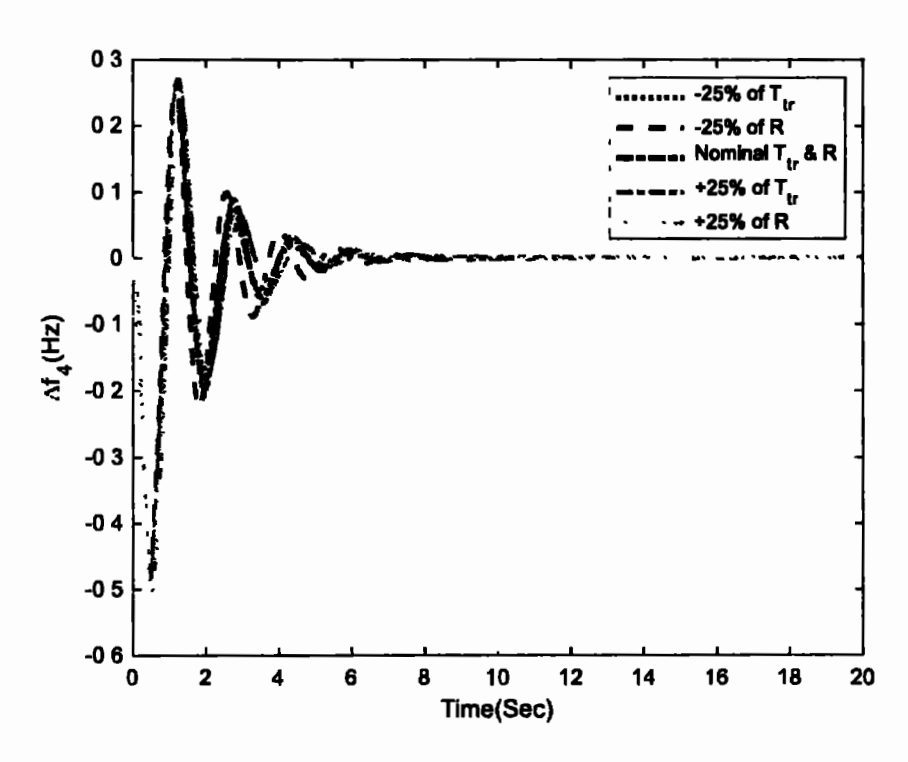


Figure 5.22: Response of Δf_4 with $\pm 25\%$ variations in system parameters using GBO based control strategy in a four-area multi-source IPS

Table 5.5: Performance specifications of frequency deviation responses with $\pm 25\%$ variations in system parameters using GBO-PID control strategy in a four-area multi-source IPS

Area	Case	Settling Time (s)	% Overshoot	Undershoot	% s-s Error
	-25% of T _{tri} , T _{tr2} , T _{tr3} , T _{tr4}	5.23	0.21	-0.57	0
	-25% of R _t , R _h , R _g , R _w	6.38	0.26	-0.55	0
Area-1	Nominal Values	5.37	0.23	-0.58	0
	+25% of T _{tr1} , T _{tr2} , T _{tr3} , T _{tr4}	5.44	0.24	-0.58	0
	+25% of R _t , R _h , R _g , R _w	4.89	0.21	-0.60	0
	-25% of T _{tr1} , T _{tr2} , T _{tr3} , T _{tr4}	5.26	0.21	-0.53	0
	-25% of R _t , R _b , R _g , R _w	6.39	0.24	-0.51	0
Area-2	Nominal Values	5.38	0.23	-0.54	0
	+25% of T _{tr1} , T _{tr2} , T _{tr3} , T _{tr4}	6.05	0.25	-0.55	0
	+25% of R _t , R _h , R _g , R _w	4.90	0.22	-0.56	0
	-25% of T _{trl} , T _{tr2} , T _{tr3} , T _{tr4}	5.27	0.21	-0.51	0
	-25% of R _t , R _h , R _g , R _w	6.39	0.21	-0.50	0
Area-3	Nominal Values	5.38	0.22	-0.52	0
	+25% of T _{tr1} , T _{tr2} , T _{tr3} , T _{tr4}	6.07	0.23	-0.52	0
	+25% of R _t , R _h , R _g , R _w	4.90	0.22	-0.53	0
	-25% of T _{tr1} , T _{tr2} , T _{tr3} , T _{tr4}	5.28	0.24	-0.49	0
	-25% of R _t , R _h , R _g , R _w	6.38	0.25	-0.47	0
Агеа-4	Nominal Values	5.98	0.26	-0.49	0
	+25% of T _{tr1} , T _{tr2} , T _{tr3} , T _{tr4}	6.17	0.27	-0.50	0
	+25% of R _t , R _h , R _g , R _w	4.92	0.25	-0.51	0

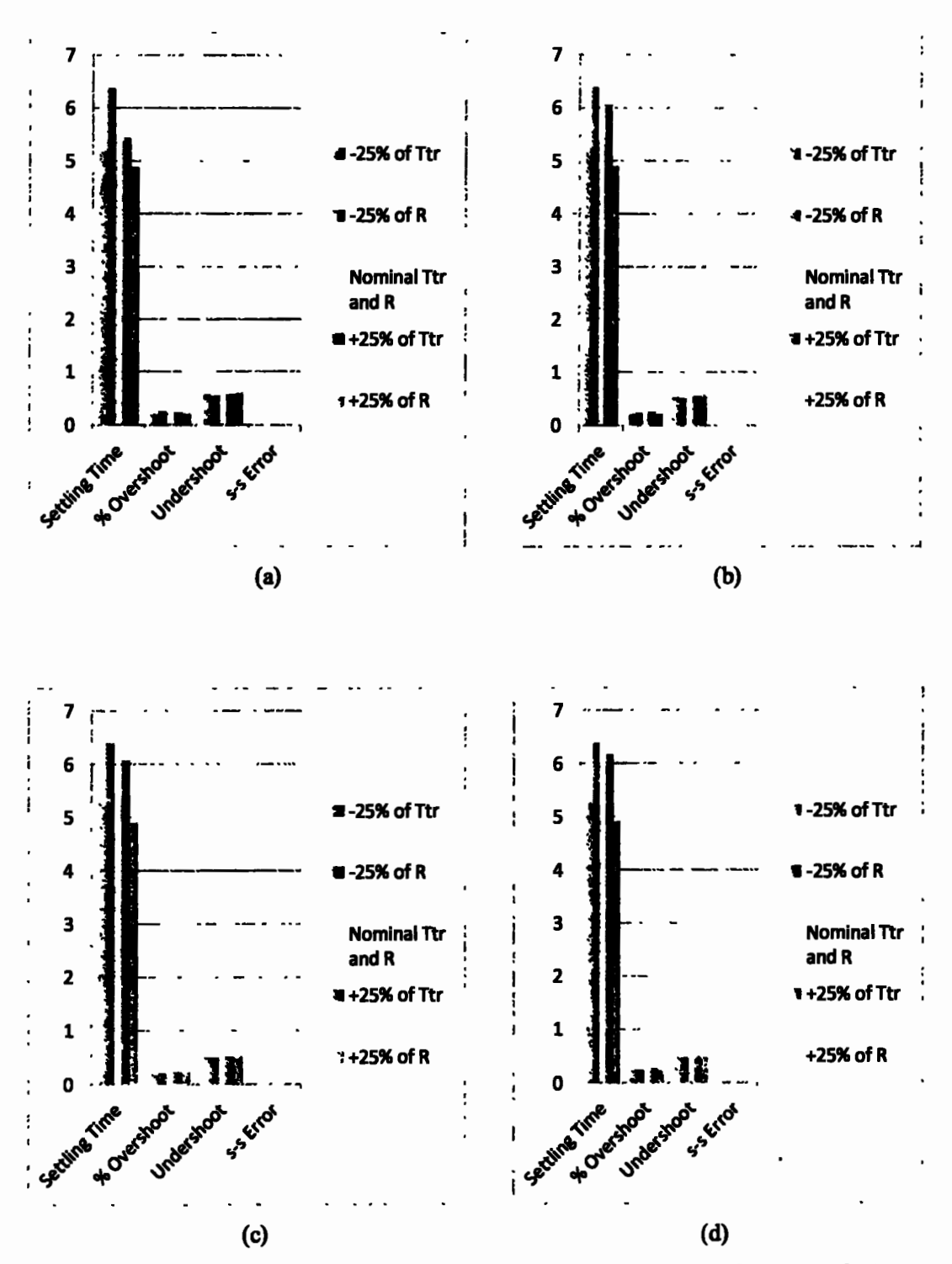


Figure 5.23: Graphical comparisons of performance specifications of frequency deviation responses with $\pm 25\%$ variations in system parameters using GBO-PID control strategy in a four-area multi-source IPS

(a) Δf_1 (b) Δf_2 (c) Δf_3 (d) Δf_4

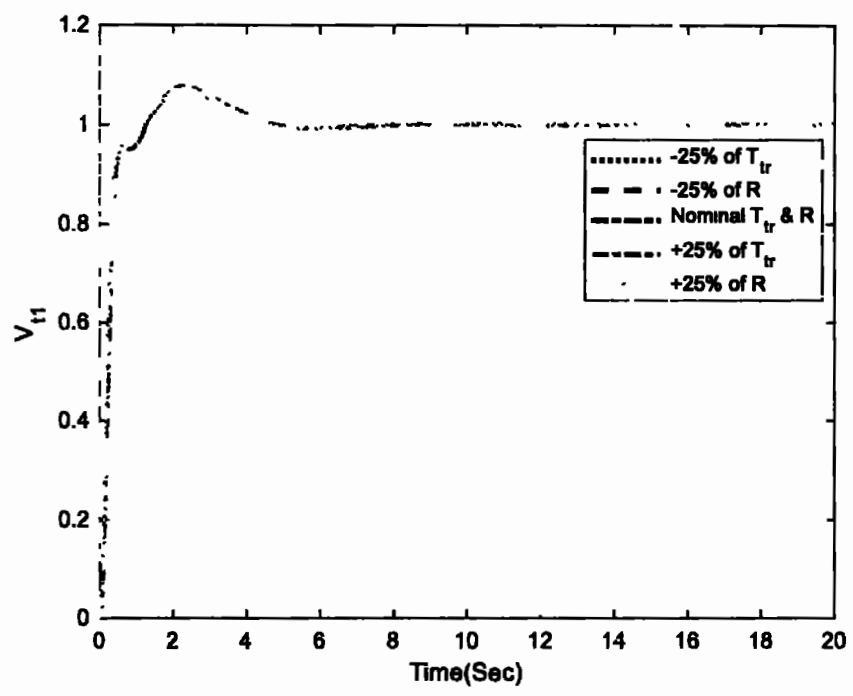


Figure 5.24: Response of V_{tl} with $\pm 25\%$ variations in system parameters using GBO based control strategy in a four-area multi-source IPS

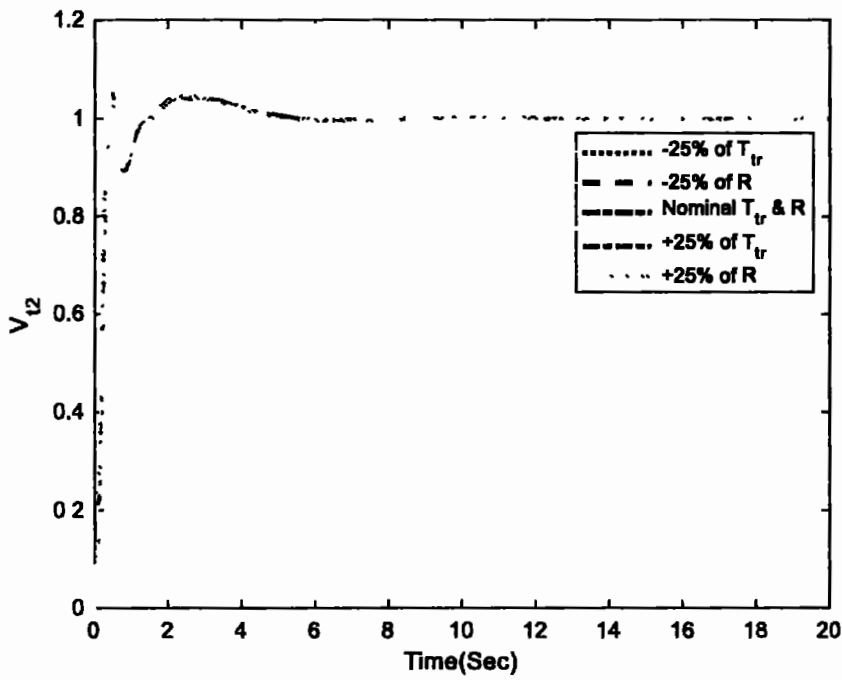


Figure 5.25: Response of V_2 with $\pm 25\%$ variations in system parameters using GBO based control strategy in a four-area multi-source IPS

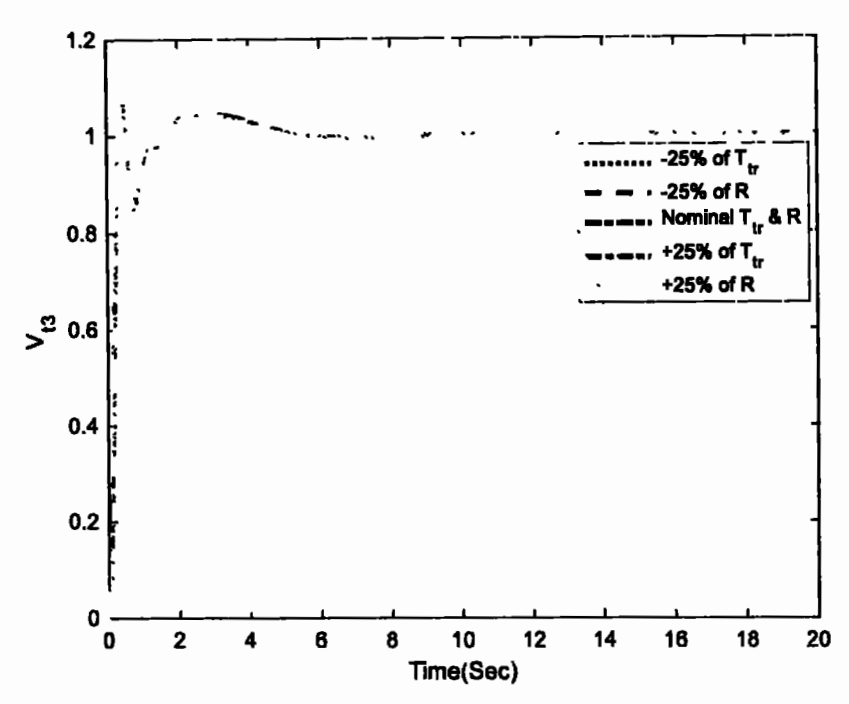


Figure 5.26: Response of $V_{\rm B}$ with $\pm 25\%$ variations in system parameters using GBO based control strategy in a four-area multi-source IPS

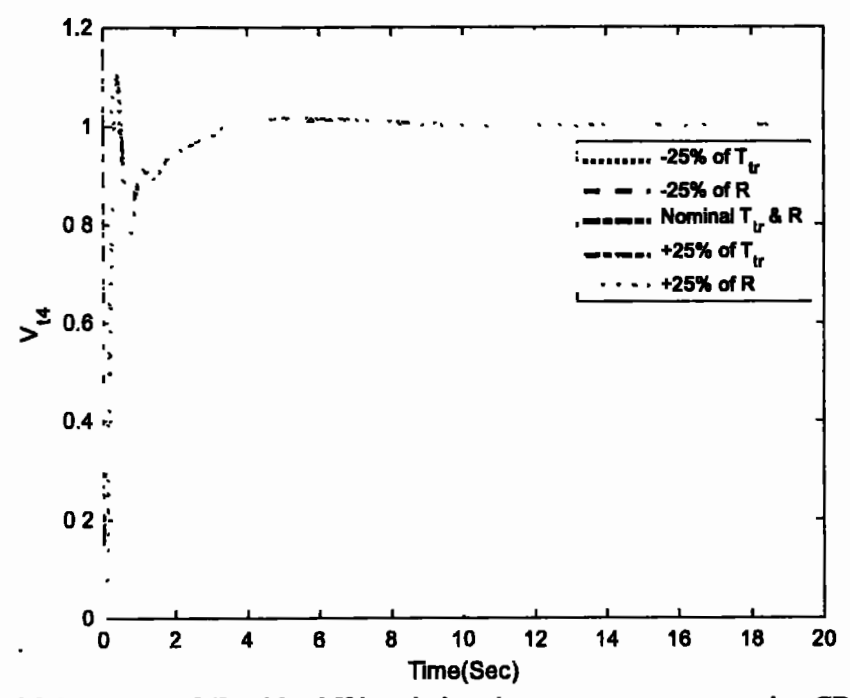


Figure 5.27: Response of V_{14} with $\pm 25\%$ variations in system parameters using GBO based control strategy in a four-area multi-source IPS

Table 5.6: Performance specifications of terminal voltage responses with ±25% variations in system parameters using GBO-PID control strategy in a four-area multi-source IPS

Area	Case	Settling Time (s)	% Overshoot	% s-s Error
	-25% of T _{tr1} , T _{tr2} , T _{tr3} , T _{tr4}	3.95	7.46	0
	-25% of R _t , R _h , R _g , R _w	396	7.57	0
Area-1	Nominal Values	3.96	7.52	0
	+25% of T _{tr1} , T _{tr2} , T _{tr3} , T _{tr4}	3.97	7.55	0
	+25% of R _t , R _b , R _g , R _w	3.92	7.40	0
	-25% of T _{trl} , T _{tr2} , T _{tr3} , T _{tr4}	4.08	5.44	0
	-25% of R _t , R _h , R _g , R _w	4.07	5.43	0
Area-2	Nominal Values	4.09	5.45	0
	+25% of T _{tr1} , T _{tr2} , T _{tr3} , T _{tr4}	4.1	5.46	0
	+25% of R _t , R _b , R _g , R _w	4.07	5.46	0
	-25% of T _{tr1} , T _{tr2} , T _{tr3} , T _{tr4}	4.36	9.0	0
	-25% of R _t , R _b , R _g , R _w	4.36	9.0	0
Area-3	Nominal Values	4.36	9.0	0
	+25% of T _{tr1} , T _{tr2} , T _{tr3} , T _{tr4}	4.36	9.0	0
	+25% of R _t , R _b , R _g , R _w	4.36	9.0	0
	-25% of T _{tr1} , T _{tr2} , T _{tr3} , T _{tr4}	2.91	10.13	0
	-25% of R _t , R _h , R _g , R _w	2.95	10.13	0
Area-4	Nominal Values	2.92	10.13	0
	+25% of T _{tr1} , T _{tr2} , T _{tr3} , T _{tr4}	2.93	10.14	0
	+25% of R _t , R _b , R _g , R _w	2.88	10.14	0

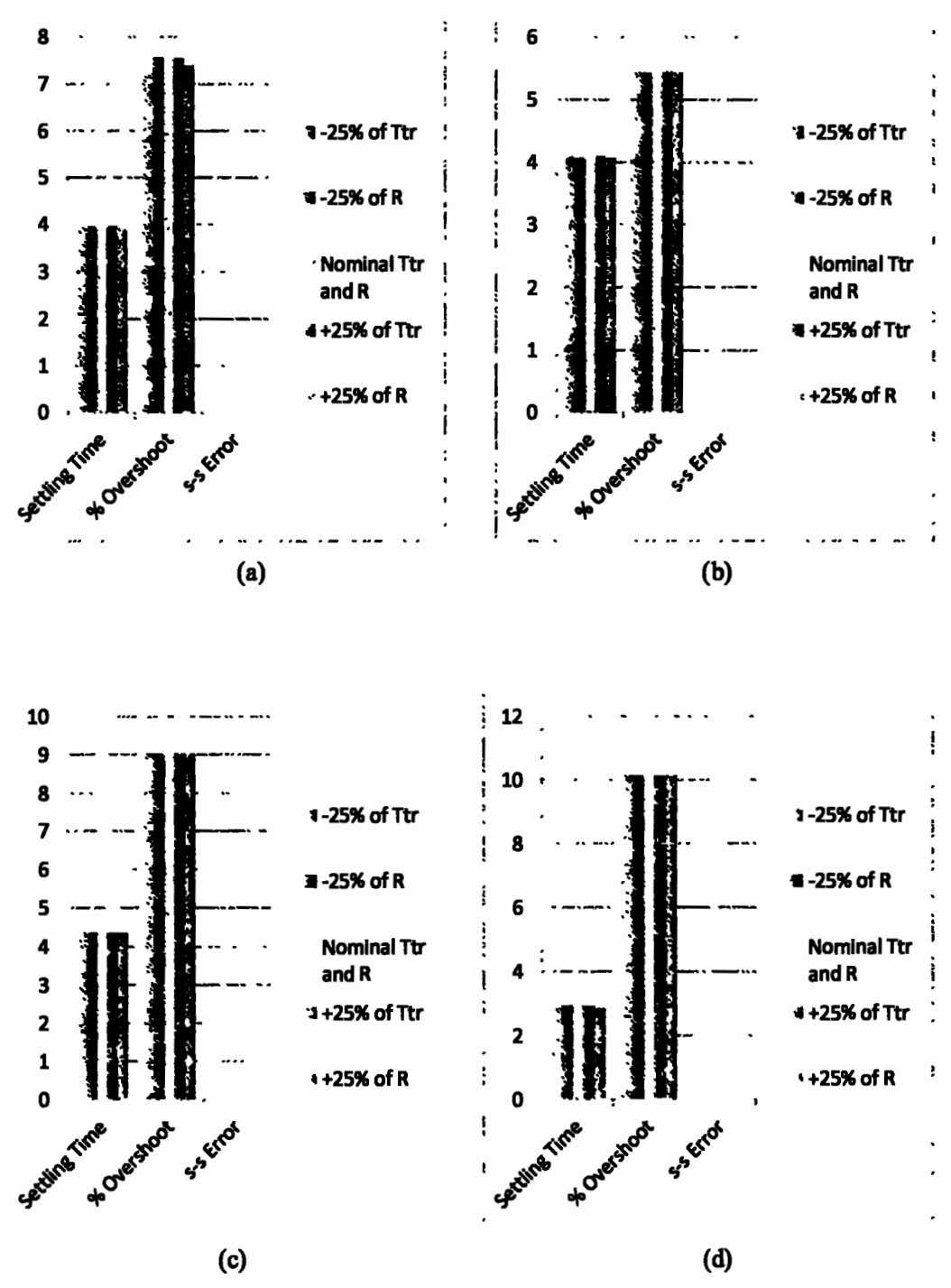


Figure 5.28: Graphical comparisons of performance specifications of terminal voltage responses with ±25% variations in system parameters using GBO-PID control strategy in a four-area multi-source IPS

(a) V_{t1} (b) V_{t2} (c) V_{t3} (d) V_{t4}

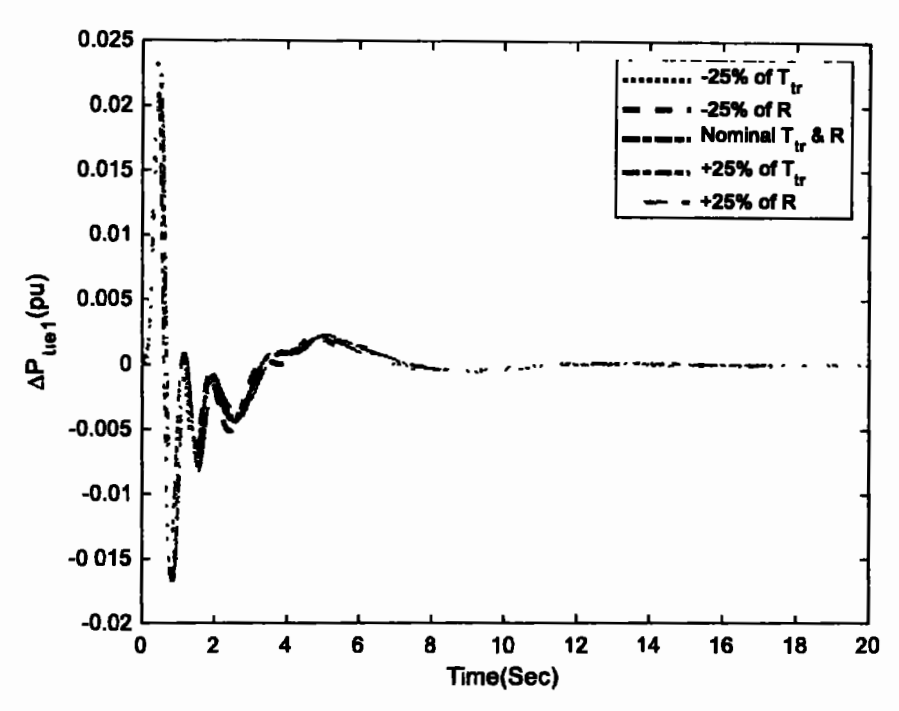


Figure 5.29: Response of ΔP_{tiel} with $\pm 25\%$ variations in system parameters using GBO based control strategy in a four-area multi-source IPS

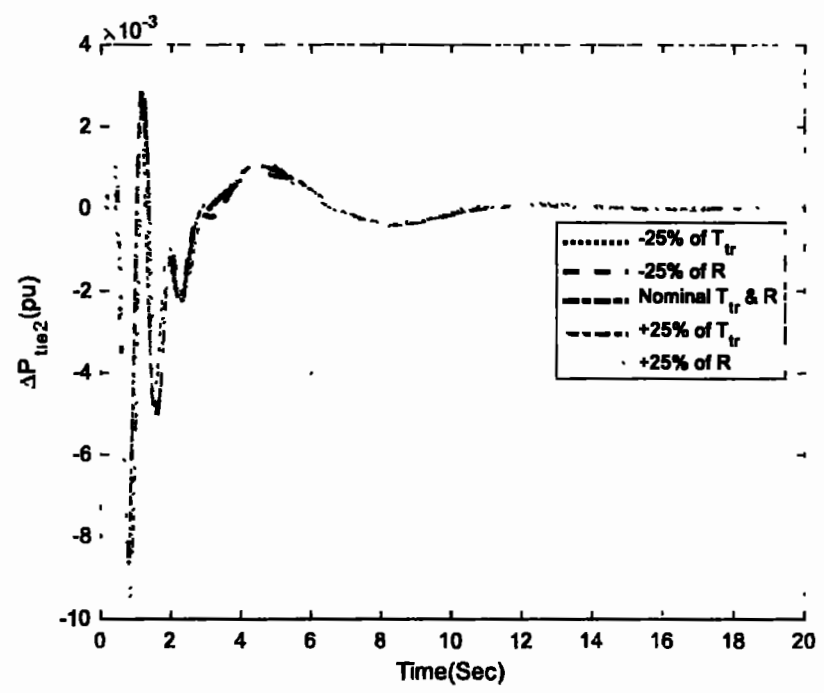


Figure 5.30: Response of ΔP_{tie2} with ±25% variations in system parameters using GBO based control strategy in a four-area multi-source IPS

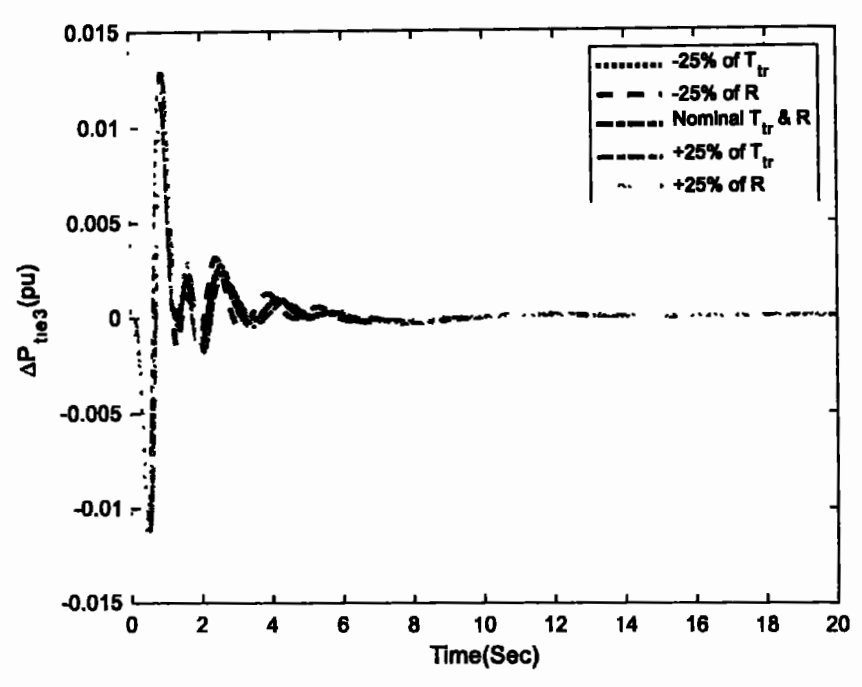


Figure 5.31: Response of ΔP_{tie3} with $\pm 25\%$ variations in system parameters using GBO based control strategy in a four-area multi-source IPS

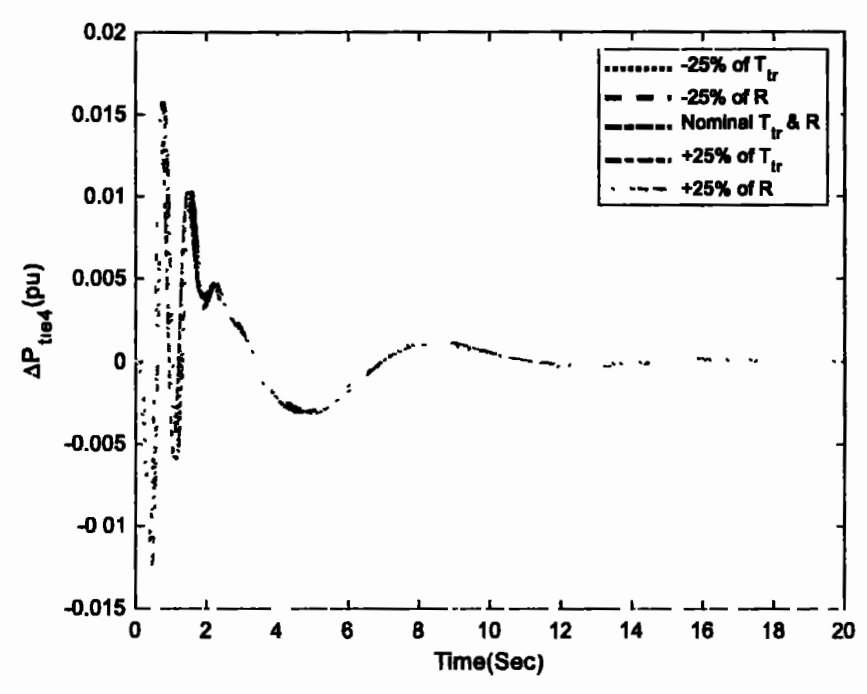


Figure 5.32: Response of ΔP_{tie4} with ±25% variations in system parameters using GBO based control strategy in a four-area multi-source IPS

Table 5.7: Performance specifications of tie-line power deviation responses with $\pm 25\%$ variations in system parameters using GBO-PID control strategy in a four-area multi-source IPS

Area	Case	Settling Time (s)	% Overshoot	Undershoot	% s-s Error
	-25% of T _{tr1} , T _{tr2} , T _{tr3} , T _{tr4}	9.39	0.022	-0.015	0
	-25% of R _t , R _h , R _g , R _w	9.26	0.023	-0.017	0
Area-1	Nominal Values	9.36	0.023	-0.016	0
	+25% of T _{tr1} , T _{tr2} , T _{tr3} , T _{tr4}	9.35	0.023	-0.017	0
	+25% of R _t , R _h , R _g , R _w	9.28	0.023	-0.016	0
	-25% of T _{tr1} , T _{tr2} , T _{tr3} , T _{tr4}	9.71	0.0022	-0.0091	0
	-25% of R _t , R _h , R _w	9.85	0.0029	-0.0089	0
Area-2	Nominal Values	9.69	0.0025	-0.0093	0
	+25% of T _{tr1} , T _{tr2} , T _{tr3} , T _{tr4}	9.67	0.0026	-0.0094	0
	+25% of R _t , R _h , R _g , R _w	9.61	0.0021	-0.0096	0
	-25% of T _{tr1} , T _{tr2} , T _{tr3} , T _{tr4}	8.48	0.012	-0.011	0
	-25% of R _t , R _b , R _w	8.13	0.013	-0.011	0
Area-3	Nominal Values	8.45	0.013	-0.012	0
	+25% of T _{tr1} , T _{tr2} , T _{tr3} , T _{tr4}	8.47	0.013	-0.012	0
	+25% of R _t , R _h , R _s , R _w	7.74	0.012	-0.012	0
	-25% of T _{tr1} , T _{tr2} , T _{tr3} , T _{tr4}	10.26	0.014	-0.012	0
	-25% of R _t , R _h , R _g , R _w	10.32	0.015	-0.012	0
Агеа-4	Nominal Values	10.23	0.015	-0.013	0
	+25% of T _{tr1} , T _{tr2} , T _{tr3} , T _{tr4}	10.21	0.016	-0.013	0
	+25% of R _t , R _h , R _g , R _w	10.18	0.015	-0.0013	0

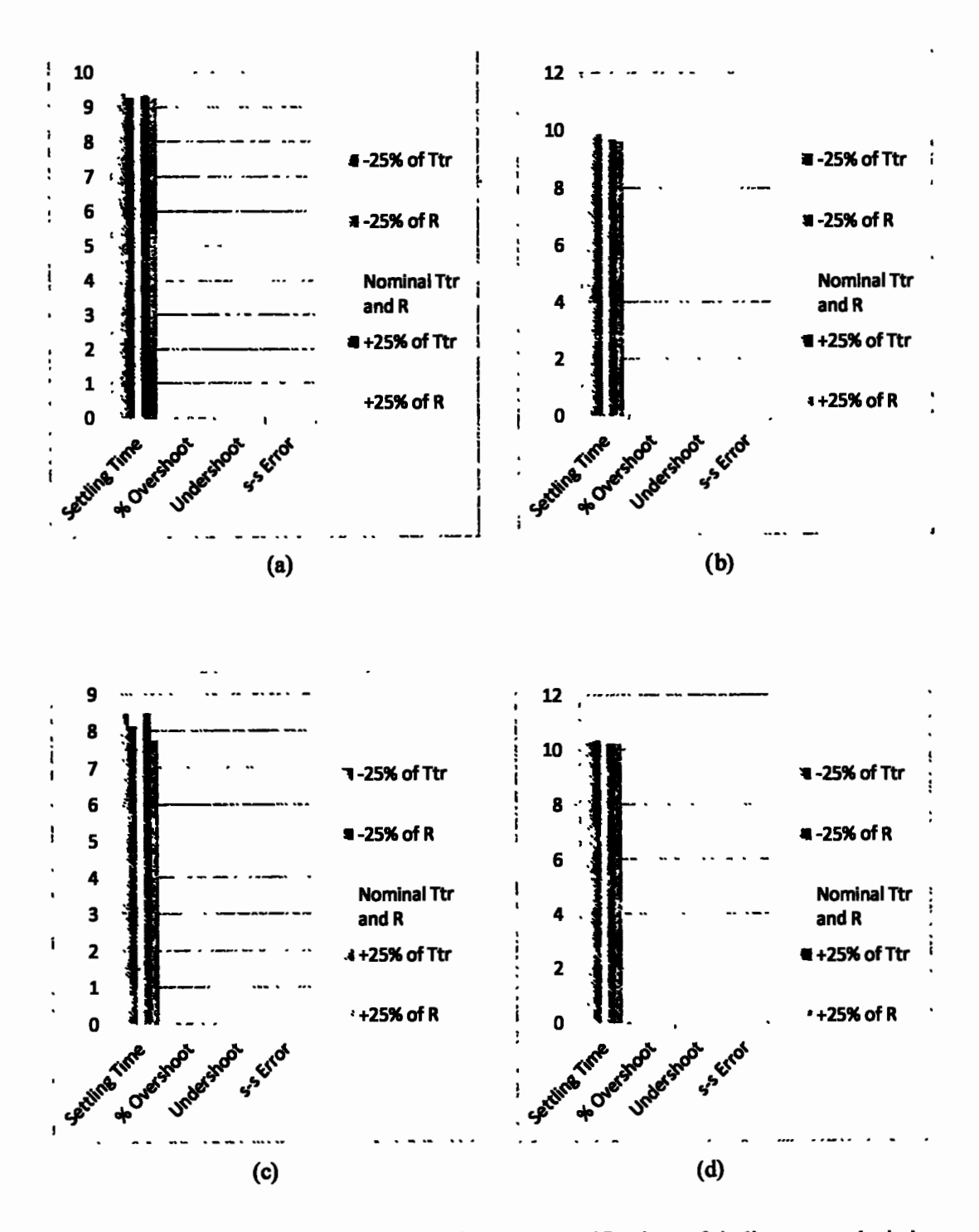


Figure 5.33: Graphical comparisons of performance specifications of tie-line power deviation responses with $\pm 25\%$ variations in system parameters using GBO-PID control strategy in a four-area multi-source IPS

(a) ΔP_{tiel} (b) ΔP_{tie2} (c) ΔP_{tie3} (d) ΔP_{tie4}

CHAPTER 6

Conclusions and Future Work

This chapter contains the summary of the analytical work presented and discussed in Chapter 3, 4 and 5. Based on the findings of this research work, final recommendations regarding different control methods have been made. The future work related to this study has also been highlighted in this chapter.

6.1 Conclusions

In this work, two-, three- and four-area multi-source interconnected power systems have been thoroughly investigated for the effective control of load frequency and terminal voltage. Some recently introduced nature inspired computation based control methods have been successfully explored to stabilize the terminal voltage and load with/without nonlinearities. The outcomes of different simulations have been summarized in this section.

6.1.1 Frequency and Voltage Stabilization in Multi-area Single-Source IPS

The multi-area IPS included numerous control areas, which are connected by the AC tie-line. The transient and steady-state behavior of a multi-area single-source IPS with 2% SLP for combined control of load frequency and terminal voltage was investigated in this study. Nature-inspired computation including MPSO, LPBO, and AOA based PI-PD control schemes have been proposed for the control of LFC and AVR loop in a multi-area IPS. The results of case study 1 suggest that all the proposed control schemes have relatively better LFC's undershoot performance compared to the NLTA-PID controller [14].

- ➤ AOA-PI-PD control scheme showed 60% and 56% better undershoots in the area-1 and area-2 LFC respectively compared to the NLTA-PID controller as shown in Table 3.3.
- > NLTA-PID provided 18% and 17% overshoot in area-1 and area-2 AVR respectively, but the proposed PI-PD control schemes completely eliminated the % overshoot with each tuning algorithm as shown in Table 3.4.
- > The results of case study 2 show that LPBO-PI-PD provided 14% and 31% fast settling times in area-1 LFC, while 3.3% and 11% fast settling times were obtained in the area-2 LFC compared to the MPSO-PI-PD and AOA-PI-PD control schemes respectively. MPSO-PI-PD provided relatively 25% and 16% lower settling times compared to LPBO-PI-PD and AOA-PI-PD control schemes respectively in area-3 LFC respectively. MPSO-PI-PD provided relatively 30% and 20% better undershoot performance compared to LPBO-PI-PD and AOA-PI-PD control schemes in area-1 LFC respectively; AOA-PI-PD provided 4.16% and 5.74% better undershoot performance in area-2 LFC while 22 % and

- 34 % better undershoot performance in area-3 LFC compared to MPSO-PI-PD and LPBO-PI-PD, control schemes respectively as shown in Table 3.6.
- ➤ In addition, AOA-PI-PD control scheme provided 26% and 2% faster rise times and 38% and 29% quicker settling times in area-1 AVR compared to the MPSO-PI-PD and LPBO-PI-PD control schemes respectively. MPSO-PI-PD provided 3% and 13% faster rise times in area-2 AVR compared to the LPBO-PI-PD and AOA-PI-PD control schemes respectively. LPBO-PI-PD provided 64% and 73% faster rise times compared to the MPSO-PI-PD and AOA-PI-PD control schemes respectively in area-3 AVR. AOA-PI-PD provided 21% and 19% quicker settling times in area-2 AVR and 0.3% and 5.45% lower settling times in area-3 AVR compared to the MPSO-PI-PD and AOA-PI-PD control schemes respectively as shown in Table 3.7.
- Finally, the resilience of the PI-PD control schemes was evaluated by varying the system parameters (Â ± 50%) and a comprehensive sensitivity analysis was performed to confirm its robustness. The results in Table 3.8 and 3.9 confirm the superiority of the proposed PI-PD control schemes when applied to a multi-area IPS for the combined control of terminal voltage and load frequency.

6.1.2 Frequency and Voltage Stabilization in Multi-area Multi-source IPS with/without Nonlinearities

The performance of a multi-area multi-source IPS with/without nonlinearities for combined control of terminal voltage and load frequency have been investigated using DO, AOA, LPBO, and MPSO based PI-PD control methodologies.

- ➤ For a two-area multi-source IPS with 10% SLP in area-1, DO, AOA, LPBO, and MPSO based PI-PD control methodologies yielded 53%, 47%, 39%, and 52% faster settling time response in area-1 LFC, while 32%, 26%, 12%, and 32% better settling time response in area-2 LFC respectively compared to HAEFA fuzzy PID controller [25] as shown in Table 4.3.
- Similarly, DO based PI-PD came up with 40% and 31% better settling time than HAEFA fuzzy PID in area-1 and area-2 AVR respectively. Moreover, DO, AOA, LPBO, and MPSO based PI-PD provides 86%, 99.9%, 10%, and 96% better % overshoot response in area-1 AVR and 86%, 99.7%, 99.8%, and 99.9% better % overshoot response in area-2 AVR respectively compared to HAEFA Fuzzy PID controller as presented in Table 4.4.
- In comparison to the HAEFA Fuzzy PID controller, it can be shown that DO, AOA, LPBO, and MPSO based PI-PD control methodologies provided 43%, 18%, 75%, and

- 12% faster tie-line settling time responses respectively as shown in Table 4.5.
- ➤ For two-area IPS with 5% SLP and three-area IPS with 2% SLP in the presence of nonlinearities, DO based PI-PD resulted in relatively better LFC's settling time response in both areas compared to AOA, LPBO, and MPSO based PI-PD control methodologies as shown in Table 4.7 and Table 4.11 respectively.
- ➤ Similarly, DO based PI-PD produced relatively better AVR settling time and % overshoot responses compared to AOA, LPBO, and MPSO based PI-PD control methodologies as shown in Table 4.8 and Table 4.12 respectively.
- Finally, DO based PI-PD provided relatively better tie-line power deviation's settling time response compared to the AOA, LPBO, and MPSO based PI-PD control methodologies as shown in Table 4.9 and Table 4.13 respectively. The results clearly show that the proposed DO based PI-PD control methodology is very effective to control terminal voltage and load frequency simultaneously in a multi-area multi-source IPS with nonlinearities.

6.1.3 Frequency and Voltage Stabilization in a Four-area Multi-source IPS

The transient response and steady-state performance of a four-area IPS for terminal voltage and load frequency control have been studied in detail. The classical PID controller has been successfully used for efficient control of IPS. Optimal tuning of the PID controller was performed using a gradient based optimizer (GBO). Moreover, the responses of various other controllers such as GBO-I- PD, GBO-TID, and GBO-I-P were compared with the proposed GBO-PID control strategy. With 5% SLP in each area, the frequency deviation, terminal voltage, and tie-line power deviation responses of IPS were evaluated.

- ➤ GBO-PID delivered relatively 67%, 44%, and 67% better settling time response in area-1 LFC; 72%, 43%, and 63% better settling time response in area-2 LFC; 51%, 44%, and 70% better settling time response in area-3 LFC; 65%, 38%, and 65% better settling time response in area-4 LFC respectively compared to GBO-I-PD, GBO-TID, and GBO-I-P control strategies as presented in Table 5.2.
- Moreover, GBO-PID offered 40% and 47% better settling time response for area-1 AVR than GBO-TID and GBO- I-P control strategies respectively. In comparison to GBO-I-PD, GBO-TID, and GBO-I-P control strategies, GBO-PID provided a relatively 39%, 47%, and 28% better settling time response in area-2 AVR; 24%, 17%, and 38% better settling time response in area-3 AVR; 45%, 57%, and 51% better settling time response in area-4 AVR respectively. In comparison to GBO-I-PD, GBO-TID, and GBO-I-P control

strategies, GBO-PID offered 18%, 72%, and 54% considerably better % overshoot response in area-2 AVR. Compared to GBO-I-PD and GBO-TID control strategies in area-3 AVR, GBO-PID gave 50% and 73% comparatively superior overshoot response as shown in Table 5.3.

- > Further, GBO-PID offered relatively 44%, 16%, and 52% better settling time response in area-1 tie-line power deviation; 50%, 12%, and 40% better settling time response in area-2 tie-line power deviation; 55%, 13%, and 56% better settling time response in area-3 tie-line power deviation compared to GBO-I-PD, GBO-TID, and GBO-I-P control strategies. Moreover, GBO-PID provided 47% and 44% better tie-line power deviation's settling time response as compared to GBO-I-PD and GBO-I-P control strategies in area-4 respectively. It can be concluded that GBO-PID performed relatively better compared to other control strategies as shown in Table 5.4.
- > Finally, the resilience of GBO-PID was evaluated by varying the system parameters (Â ± 25%) and the robustness of GBO-PID was confirmed by a comprehensive sensitivity analysis. The results in Tables 5.5, 5.6, and 5.7 clearly confirm the superiority of the proposed GBO-PID control strategy for terminal voltage and load frequency stabilization in a four-area IPS.

6.2 Future Work

In this thesis, nature computation based control methods have been implemented for AVR and LFC loops of interconnected power systems. The efficacy of proposed control methods has been validated under conventional environment and fixed loading conditions in two-, three- and four-area interconnected power systems. Interconnected power systems have not been examined under random loading conditions and deregulated environment. Moreover, four-area IPS has not been investigated in the presence of nonlinearities. These are the limitations of proposed control methods because proposed control methods cannot be applied in such type of power system directly.

- In future, two-, three- or four-area multi-source interconnected power systems can be investigated under deregulated environment and random loading conditions with minor modifications in proposed control methods.
- Moreover, it is suggested that recently introduced nature-inspired computing techniques such as artificial rabbits optimization and sea-horse optimization etc. or deterministic methodologies can be used to control terminal voltage and load frequency in a four-area IPS with nonlinearities such as GRC, GDB and BD etc.

- The terminal voltage and load frequency can be examined in the presence of different energy storage and FACTS devices to further improve the dynamic response of two-, three- or four-area multi-source interconnected power systems.
- Various renewable energy sources with conventional power plants such as diesel, nuclear, etc. can be added in multi-area multi-source interconnected power systems. Further, electric vehicles (EVs) and distributive generation (DG) can also be included to investigate and control the responses of a complex power system.
- Keeping in view the emerging trends in artificial intelligence based control techniques, it
 neuro-fuzzy, deep fuzzy, fuzzy deep neural networks and hybrid ANN based techniques
 can be explored to control the terminal voltage and load frequency in multi-area IPS.

REFERENCES

- [1] A. Daraz, S. A. Malik, H. Mokhlis, I. U. Haq, G. F. Laghari, and N. N. Mansor, "Fitness Dependent Optimizer-Based Automatic Generation Control of Multi-Source Interconnected Power System with Non-Linearities," *IEEE Access*, vol. 8, pp. 100989–101003, 2020, doi: 10.1109/ACCESS.2020.2998127.
- [2] A. Gupta, A. Chauhan, and R. Khanna, "Design of AVR and ALFC for single area power system including damping control," 2014 Recent Adv. Eng. Comput. Sci. RAECS 2014, pp. 6–8, 2014, doi: 10.1109/RAECS.2014.6799653.
- [3] S. K. Ramoji and L. C. Saikia, "Utilization of electric vehicles in combined voltage-frequency control of multi-area thermal- combined cycle gas turbine system using two degree of freedom tilt-integral-derivative controller," *Energy Storage*, vol. 3, no. 4, pp. 1-20, 2021, doi: 10.1002/est2.234.
- [4] K. R. M. Vijaya Chandrakala and S. Balamurugan, "Simulated annealing based optimal frequency and terminal voltage control of multi source multi area system," Int. J. Electr. Power Energy Syst., vol. 78, pp. 823-829, 2016, doi: 10.1016/j.ijepes.2015.12.026.
- [5] M. Gupta, S. Srivastava, and J. R. P. Gupta, "A Novel Controller for Model with Combined LFC and AVR Loops of Single Area Power System," J. Inst. Eng. Ser. B, vol. 97, no. 1, pp. 21-29, 2016, doi: 10.1007/s40031-014-0159-z.
- [6] D. Sharma, V. Kushwaha, K. Pandey, and N. Rani, "Intelligent avr control of a single thermal area combined with lfc loop," Adv. Intell. Syst. Comput., vol. 624, pp. 779-789, 2018, doi: 10.1007/978-981-10-5903-2_80.
- [7] R. Rajbongshi and L. C. Saikia, "Coordinated performance of interline power flow controller and superconducting magnetic energy storage in combined ALFC and AVR system under deregulated environment," J. Renew. Sustain. Energy, vol. 10, no. 4, 2018, doi: 10.1063/1.5025658.
- [8] D. K. Lal and A. K. Barisal, "Combined load frequency and terminal voltage control of power systems using moth flame optimization algorithm," J. Electr. Syst. Inf. Technol., vol. 6, no. 1, 2019, doi: 10.1186/s43067-019-0010-3.
- [9] A. K. Sahani, U. Raj, R. Shankar, and R. K. Mandal, "Firefly optimization based control strategies for combined load frequency control and automatic voltage regulation for two-area interconnected power system," *Int. J. Electr. Eng. Informatics*, vol. 11, no. 4, pp. 746-757, 2019, doi: 10.15676/ijeei.2019.11.4.8.
- [10] J. Morsali and Z. Esmaeili, "Proposing a new hybrid model for LFC and AVR loops to improve effectively frequency stability using coordinative CPSS," 2020 28th Iran. Conf. Electr. Eng. ICEE 2020, 2020, doi: 10.1109/ICEE50131.2020.9260695.
- [11] C. H. Naga Sai Kalyan and G. Sambasiva Rao, "Frequency and voltage stabilisation in

- combined load frequency control and automatic voltage regulation of multiarea system with hybrid generation utilities by AC/DC links," *Int. J. Sustain. Energy*, vol. 39, no. 10, pp. 1009–1029, 2020, doi: 10.1080/14786451.2020.1797740.
- [12] C. H. Naga Sai Kalyan and G. Sambasiva Rao, "Combined frequency and voltage stabilisation of multi-area multisource system by DE-AEFA optimised PID controller with coordinated performance of IPFC and RFBs," Int. J. Ambient Energy, no. 0, pp. 1-20, 2020, doi: 10.1080/01430750.2020.1860130.
- [13] A. Prakash and S. K. Parida, "Combined frequency and voltage stabilization of thermal-thermal system with UPFC and RFB," PIICON 2020 9th IEEE Power India Int. Conf., 2020, doi: 10.1109/PIICON49524.2020.9113034.
- [14] N. Nahas, M. Abouheaf, A. Sharaf, and W. Gueaieb, "A Self-Adjusting Adaptive AVR-LFC Scheme for Synchronous Generators," *IEEE Trans. Power Syst.*, vol. 34, no. 6, pp. 5073–5075, 2019, doi: 10.1109/TPWRS.2019.2920782.
- [15] C. N. S. Kalyan, "UPFC and SMES based Coordinated Control Strategy for Simultaneous Frequency and Voltage Stability of an Interconnected Power System," ICPEE 2021 - 2021 1st Int. Conf. Power Electron. Energy, 2021, doi: 10.1109/ICPEE50452.2021.9358576.
- [16] P. Anusha, S. Patra, A. Roy, and D. Saha, "Combined Frequency and Voltage Control of a Deregulated Hydro-Thermal Power System employing FA based Industrial Controller," 2021 Int. Conf. Comput. Perform. Eval. ComPE 2021, pp. 848-853, 2021, doi: 10.1109/ComPE53109.2021.9752331.
- [17] S. Oladipo, Y. Sun, and Z. Wang, "An effective hFPAPFA for a PIDA-based hybrid loop of Load Frequency and terminal voltage regulation system," 2021 IEEE PES/IAS PowerAfrica, PowerAfrica 2021, 2021, doi: 10.1109/PowerAfrica52236.2021.9543348.
- [18] S. K. Ramoji and L. C. Saikia, "Optimal Coordinated Frequency and Voltage Control of CCGT-Thermal Plants with TIDF Controller," *IETE J. Res.*, pp. 1–18, Aug. 2021, doi: 10.1080/03772063.2021.1959420.
- [19] S. Safiullah, A. Rahman, M. Asim Aftab, and S. M. S. Hussain, "Performance study of ADRC and PID for concurrent Frequency-Voltage Control of Electric Vehicle Incorporated Hybrid Power System," PESGRE 2022 IEEE Int. Conf. "Power Electron. Smart Grid, Renew. Energy," 2022, doi: 10.1109/PESGRE52268.2022.9715937.
- [20] S. K. Ramoji, L. C. Saikia, B. Dekaraja, M. K. Behera, and S. K. Bhagat, "Performance Comparison of Various Tilt Controllers in Coalesced Voltage and Frequency Regulation of Multi-Area Multi-Unit Power System," 2022 IEEE Delhi Sect. Conf. DELCON 2022, 2022, doi: 10.1109/DELCON54057.2022.9752811.
- [21] B. Dekaraja, L. C. Saikia, S. K. Ramoji, M. K. Behera, and S. K. Bhagat, "Impact of RFB and HVDC link on Combined ALFC-AVR Studies of a GTPP Integrated Hydro-Thermal Systems Using a Cascade Fuzzy PD-TID Controller," 4th Int. Conf. Energy, Power, Environ. ICEPE

- 2022, pp. 3-8, 2022, doi: 10.1109/ICEPE55035.2022.9798067.
- [22] B. Dekaraja, L. C. Saikia, and S. K. Ramoji, "Combined ALFC-AVR Control of Diverse Energy Source Based Interconnected Power System using Cascade Controller," pp. 1-6, 2022, doi: 10.1109/iciccsp53532.2022.9862433.
- [23] B. Dekaraja, L. C. Saikia, S. K. Ramoji, M. K. Behera, and S. K. Bhagat, "Performance Analysis of Diverse Energy Storage on Combined ALFC and AVR Control of Multiarea Multiunit System with AC/HVDC interconnection," *IFAC-PapersOnLine*, vol. 55, no. 1, pp. 479–485, 2022, doi: 10.1016/j.ifacol.2022.04.079.
- [24] H. H. Fayek and E. Rusu, "Novel Combined Load Frequency Control and Automatic Voltage Regulation of a 100% Sustainable Energy Interconnected Microgrids," Sustainability, vol. 14, no. 15, p. 9428, 2022, doi: 10.3390/su14159428.
- [25] C. H. Naga Sai Kalyan et al., "Comparative Performance Assessment of Different Energy Storage Devices in Combined LFC and AVR Analysis of Multi-Area Power System," Energies, vol. 15, no. 2, 2022, doi: 10.3390/en15020629.
- [26] A. Ghosh, A. Kumar, R. Nurujjaman, and M. Jamshidi, "Voltage and frequency control in conventional and PV integrated power systems by a particle swarm optimized Ziegler – Nichols based PID controller," SN Appl. Sci., 2021, doi: 10.1007/s42452-021-04327-8.
- [27] M. J. Chandrashekar and R. Jayapal, "AGC and AVR implementation in a deregulated power system using optimized controller with Renewable integrated DC link," Ist Int. Conf. Adv. Technol. Intell. Control. Environ. Comput. Commun. Eng. ICATIECE 2019, pp. 355-364, 2019, doi: 10.1109/ICATIECE45860.2019.9063775.
- [28] H. Grover, A. Verma, and T. S. Bhatti, "Load frequency control & automatic voltage regulation for a single area power system," PIICON 2020 9th IEEE Power India Int. Conf., pp. 1-5, 2020, doi: 10.1109/PIICON49524.2020.9112902.
- [29] G. A. Salman, A. S. Jafar, and A. I. Ismael, "Application of artificial intelligence techniques for LFC and AVR systems using PID controller," Int. J. Power Electron. Drive Syst., vol. 10, no. 3, pp. 1694-1704, 2019, doi: 10.11591/ijpeds.v10.i3.1694-1704.
- [30] N. E. Y. Kouba, M. Menaa, M. Hasni, and M. Boudour, "Optimal control of frequency and voltage variations using PID controller based on particle swarm optimization," 2015 4th Int. Conf. Syst. Control. ICSC 2015, pp. 424-429, 2015, doi: 10.1109/ICoSC.2015.7152777.
- [31] R. Rajbongshi, L. C. Saikia, W. Tasnin, A. Saha, and D. Saha, "Performance Analysis of Combined ALFC and AVR System Incorporating Power System Stabilizer," 2nd Int. Conf. Energy, Power Environ. Towar. Smart Technol. ICEPE 2018, pp. 0-5, 2019, doi: 10.1109/EPETSG.2018.8658874.
- [32] R. Mohammadikia, A. Nikoofard, and M. Tavakoli-Kakhki, "Application of MPC for an automatic voltage regulator and load frequency control of interconnected power system," 2020 28th Iran. Conf. Electr. Eng. ICEE 2020, 2020, doi: 10.1109/ICEE50131.2020.9260891.

- [33] R. Rajbongshi and L. C. Saikia, "ALFC and AVR system Performance of coordinated FACTS and energy storage devices in combined multiarea ALFC and AVR system," vol. 064101, 2017, doi: 10.1063/1.4986889.
- [34] "Combined LFC and AVR Regulation of Multi Area Interconnected Power System Using Energy Storage Devices".
- [35] V. Kumar, "Model Predictive Controller-Based Voltage and Frequency Regulation in Renewable Energy Integrated Power System Coordinated with Virtual Inertia and Redox Flow Battery," Iran. J. Sci. Technol. Trans. Electr. Eng., vol. 0123456789, 2022, doi: 10.1007/s40998-022-00561-x.
- [36] A. A. Hossam-eldin, E. Negm, M. Ragab, and K. M. Aboras, "A maiden robust FPIDD 2 regulator for frequency- voltage enhancement in a hybrid interconnected power system using Gradient-Based Optimizer," Alexandria Eng. J., 2022, doi: 10.1016/j.aej.2022.10.029.
- [37] S. Safiullah, A. Rahman, and S. A. Lone, "State-observer based IDD controller for concurrent frequency-voltage control of a hybrid power system with electric vehicle uncertainties," *Int. Trans. Electr. Energy Syst.*, vol. 31, no. 11, pp. 1–26, 2021, doi: 10.1002/2050-7038.13083.
- [38] M. Bhuyan, D. Chandra Das, and A. Kumar Barik, "Combined voltage and frequency response in a solar thermal system with thermostatically controlled loads in an isolated hybrid microgrid scheme," Int. J. Sustain. Energy, pp. 1–24, Sep. 2022, doi: 10.1080/14786451.2022.2126842.
- [39] S. Safiullah, A. Rahman, S. A. Lone, S. M. S. Hussain, and T. S. Ustun, "Robust frequency-voltage stabilization scheme for multi-area power systems incorporated with EVs and renewable generations using AI based modified disturbance rejection controller," *Energy Reports*, vol. 8, pp. 12186–12202, 2022, doi: 10.1016/j.egyr.2022.08.272.
- [40] V. Kumar, V. Sharma, and R. Naresh, "HHO-based Model Predictive Controller for Combined Voltage and Frequency Control Problem Including SMES," *IETE J. Res.*, pp. 1–15, Apr. 2021, doi: 10.1080/03772063.2021.1908180.
- [41] A. Soundarrajan, S. Sumathi, and C. Sundar, "Particle swarm optimization based LFC and AVR of autonomous power generating system," *IAENG Int. J. Comput. Sci.*, vol. 37, no. 1, 2010.
- [42] A. M. Hamza, M. S. Saad, H. M. Rashad, and A. Bahgat, "with PID Controller Tuning By BFO and Ziegler Methods," vol. 4, no. 5, pp. 12-17, 2013.
- [43] N. E. Y. Kouba, M. Menaa, M. Hasni, and M. Boudour, "Optimal control of frequency and voltage variations using PID controller based on particle swarm optimization," 2015 4th Int. Conf. Syst. Control. ICSC 2015, pp. 424-429, 2015, doi: 10.1109/ICoSC.2015.7152777.
- [44] M. Gupta and S. Srivastava, "A GMM-GFM based controller for LFC and AVR of a single area power system," Int. Conf. Emerg. Trends Eng. Technol. ICETET, pp. 216-219, 2012, doi: 10.1109/ICETET.2012.60.
- [45] N. E. Y. Kouba, M. Menaa, M. Hasni, and M. Boudour, "A novel robust automatic generation

- control in interconnected multi-area power system based on bat inspired algorithm," 3rd Int. Conf. Control. Eng. Inf. Technol. CEIT 2015, 2015, doi: 10.1109/CEIT.2015.7233025.
- [46] A. Soundarrajan, S. Sumathi, and G. Sivamurugan, "Voltage and frequency control in power generating system using hybrid evolutionary algorithms," *JVC/Journal Vib. Control*, vol. 18, no. 2, pp. 214–227, 2012, doi: 10.1177/1077546311404731.
- [47] S. M. Azizi and S. A. Khajehoddin, "Robust decentralized voltage and frequency control of generators in islanded microgrids using μ-synthesis," *ECCE 2016 IEEE Energy Convers. Congr. Expo. Proc.*, 2016, doi: 10.1109/ECCE.2016.7855406.
- [48] S. Prasad, S. Purwar, and N. Kishor, "Load frequency regulation using observer based non-linear sliding mode control," *Int. J. Electr. Power Energy Syst.*, vol. 104, no. July 2018, pp. 178–193, 2019, doi: 10.1016/j.ijepes.2018.06.035.
- [49] and S. R. M. Nabnit Panigrahi, Ayusman Nayak, Advances in Energy Technology. 2021. [Online]. Available: http://link.springer.com/10.1007/978-981-15-8700-9
- [50] J. Guo, "Application of a novel adaptive sliding mode control method to the load frequency control," Eur. J. Control, vol. 57, pp. 172-178, 2021, doi: 10.1016/j.ejcon.2020.03.007.
- [51] S. Tripathy, M. K. Debnath, and S. K. Kar, Optimal Design of Fractional Order 2DOF-PID Controller for Frequency Control in Interconnected System, vol. 151. Springer Singapore, 2021. doi: 10.1007/978-981-15-8218-9 2.
- [52] P. C. Sahu, R. C. Prusty, and B. K. Sahoo, "Modified sine cosine algorithm-based fuzzy-aided PID controller for automatic generation control of multiarea power systems," Soft Comput., vol. 24, no. 17, pp. 12919–12936, 2020, doi: 10.1007/s00500-020-04716-y.
- [53] S. Prasad, S. Purwar, and N. Kishor, "Non-linear sliding mode load frequency control in multiarea power system," *Control Eng. Pract.*, vol. 61, no. February, pp. 81–92, 2017, doi: 10.1016/j.conengprac.2017.02.001.
- [54] S. Ajithapriyadarsini, P. M. Mary, and M. W. Iruthayarajan, "Automatic generation control of a multi-area power system with renewable energy source under deregulated environment: adaptive fuzzy logic-based differential evolution (DE) algorithm," Soft Comput., vol. 23, no. 22, pp. 12087-12101, 2019, doi: 10.1007/s00500-019-03765-2.
- [55] E. Çelik, "Design of new fractional order PI-fractional order PD cascade controller through dragonfly search algorithm for advanced load frequency control of power systems," Soft Comput., vol. 25, no. 2, pp. 1193-1217, 2021, doi: 10.1007/s00500-020-05215-w.
- [56] V. Jeyalakshmi and P. Subburaj, "PSO-scaled fuzzy logic to load frequency control in hydrothermal power system," Soft Comput., vol. 20, no. 7, pp. 2577-2594, 2016, doi: 10.1007/s00500-015-1659-8.
- [57] M. Esmail. R. Tzoneva, and S. Krishnamurthy, "Review of Automatic Generation Control in Deregulated Environment," *IFAC-PapersOnLine*, vol. 50, no. 2, pp. 88–93, 2017, doi: 10.1016/j.ifacol.2017.12.016.

- [58] Y. Mi et al., "Sliding mode load frequency control for multi-area time-delay power system with wind power integration," *IET Gener. Transm. Distrib.*, vol. 11, no. 18, pp. 4644–4653, 2017, doi: 10.1049/iet-gtd.2017.0600.
- [59] B. Mohanty, "Hybrid flower pollination and pattern search algorithm optimized sliding mode controller for deregulated AGC system," J. Ambient Intell. Humaniz. Comput., vol. 11, no. 2, pp. 763-776, 2020, doi: 10.1007/s12652-019-01348-5.
- [60] N. C. Patel, "Controller Tuned by SCA," pp. 337-342, 2018.
- [61] B. Mohanty, "TLBO optimized sliding mode controller for multi-area multi-source nonlinear interconnected AGC system," Int. J. Electr. Power Energy Syst., vol. 73, pp. 872–881, 2015, doi: 10.1016/j.ijepes.2015.06.013.
- [62] Y. Sun, Y. Wang, Z. Wei, G. Sun, and X. Wu, "power system with time delay: A sliding mode control approach," pp. 1-8, 2017, doi: 10.1109/JAS.2017.7510649.Yonghui.
- [63] C. Pradhan and T. Gjengedal, "Adaptive Jaya Algorithm for Optimized PI-PD Cascade Controller of Load Frequency Control in Interconnected Two-Area Power System," Proc. 2020 Int. Conf. Smart Syst. Technol. SST 2020, pp. 181–186, 2020, doi: 10.1109/SST49455.2020.9263701.
- [64] P. Dahiya, V. Sharma, and R. Naresh, "Automatic generation control using disrupted oppositional based gravitational search algorithm optimised sliding mode controller under deregulated environment," *IET Gener. Transm. Distrib.*, vol. 10, no. 16, pp. 3995–4005, 2016, doi: 10.1049/iet-gtd.2016.0175.
- [65] Y. Arya, "Automatic generation control of two-area electrical power systems via optimal fuzzy classical controller," J. Franklin Inst., vol. 355, no. 5, pp. 2662-2688, 2018, doi: 10.1016/j.jfranklin.2018.02.004.
- [66] S. Biswas, P. K. Roy, and K. Chatterjee, "FACTS-based 3DOF-PID Controller for LFC of Renewable Power System Under Deregulation Using GOA," IETE J. Res., 2021, doi: 10.1080/03772063.2020.1870874.
- [67] A. Fathy, A. M. Kassem, and A. Y. Abdelaziz, "Optimal design of fuzzy PID controller for deregulated LFC of multi-area power system via mine blast algorithm," *Neural Comput. Appl.*, vol. 32, no. 9, pp. 4531–4551, 2020, doi: 10.1007/s00521-018-3720-x.
- [68] A. Daraz, S. Abdullah Malik, I. U. Haq, K. B. Khan, G. F. Laghari, and F. Zafar, Modified PID controller for automatic generation control of multi-source interconnected power system using fitness dependent optimizer algorithm, vol. 15, no. 11 November. 2020. doi: 10.1371/journal.pone.0242428.
- [69] A. Daraz et al., "Power System Using FOI-TD Controller," pp. 1-17, 2021.
- [70] A. Daraz, S. A. Malik, H. Mokhlis, I. U. Haq, F. Zafar, and N. N. Mansor, "Improved-Fitness Dependent Optimizer Based FOI-PD Controller for Automatic Generation Control of Multi-Source Interconnected Power System in Deregulated Environment," *IEEE Access*, vol. 8, pp.

- 197757-197775, 2020, doi: 10.1109/access.2020.3033983.
- [71] A. Daraz, S. A. Malik, A. T. Azar, S. Aslam, T. Alkhalifah, and F. Alturise, "Optimized Fractional Order Integral-Tilt Derivative Controller for Frequency Regulation of Interconnected Diverse Renewable Energy Resources," *IEEE Access*, vol. 10, pp. 43514–43527, 2022, doi: 10.1109/ACCESS.2022.3167811.
- [72] W. Tan, H. Zhang, and M. Yu, "Decentralized load frequency control in deregulated environments," *Int. J. Electr. Power Energy Syst.*, vol. 41, no. 1, pp. 16–26, 2012, doi: 10.1016/j.ijepes.2012.02.013.
- [73] F. Liu, Y. Li, Y. Cao, J. She, and M. Wu, "A Two-Layer Active Disturbance Rejection Controller Design for Load Frequency Control of Interconnected Power System," *IEEE Trans. Power Syst.*, vol. 31, no. 4, pp. 3320-3321, 2016, doi: 10.1109/TPWRS.2015.2480005.
- [74] M. H. Khooban, T. Niknam, M. Shasadeghi, T. Dragicevic, and F. Blaabjerg, "Load Frequency Control in Microgrids Based on a Stochastic Noninteger Controller," *IEEE Trans. Sustain. Energy*, vol. 9, no. 2, pp. 853–861, 2018, doi: 10.1109/TSTE.2017.2763607.
- [75] S. Trip, M. Cucuzzella, C. de Persis, A. van der Schaft, and A. Ferrara, "Passivity-Based Design of Sliding Modes for Optimal Load Frequency Control," *IEEE Trans. Control Syst. Technol.*, vol. 27, no. 5, pp. 1893–1906, 2019, doi: 10.1109/TCST.2018.2841844.
- [76] C. A. Macana, E. Mojica-Nava, and N. Quijano, "Time-delay effect on load frequency control for microgrids," 2013 10th IEEE Int. Conf. Networking, Sens. Control. ICNSC 2013, pp. 544– 549, 2013, doi: 10.1109/ICNSC.2013.6548797.
- [77] K. P. S. Parmar, S. Majhi, and D. P. Kothari, "Load frequency control of a realistic power system with multi-source power generation," *Int. J. Electr. Power Energy Syst.*, vol. 42, no. 1, pp. 426-433, 2012, doi: 10.1016/j.ijepes.2012.04.040.
- [78] S. K. Pandey, S. R. Mohanty, and N. Kishor, "A literature survey on load-frequency control for conventional and distribution generation power systems," *Renew. Sustain. Energy Rev.*, vol. 25, pp. 318–334, 2013, doi: 10.1016/j.rser.2013.04.029.
- [79] D. Guha, P. K. Roy, and S. Banerjee, "Equilibrium optimizer-tuned cascade fractional-order 3DOF-PID controller in load frequency control of power system having renewable energy resource integrated," *Int. Trans. Electr. Energy Syst.*, vol. 31, no. 1, pp. 1–25, 2021, doi: 10.1002/2050-7038.12702.
- [80] A. Sargolzaei, K. K. Yen, and M. N. Abdelghani, "Preventing Time-Delay Switch Attack on Load Frequency Control in Distributed Power Systems," *IEEE Trans. Smart Grid*, vol. 7, no. 2, pp. 1176-1185, 2016, doi: 10.1109/TSG.2015.2503429.
- [81] A. Oshnoei, M. Kheradmandi, and S. M. Muyeen, "Robust Control Scheme for Distributed Battery Energy Storage Systems in Load Frequency Control," *IEEE Trans. Power Syst.*, vol. 35, no. 6, pp. 4781–4791, 2020, doi: 10.1109/TPWRS.2020.2997950.
- [82] K. S. Ko and D. K. Sung, "The effect of EV aggregators with time-varying delays on the

- stability of a load frequency control system," *IEEE Trans. Power Syst.*, vol. 33, no. 1, pp. 669–680, 2018, doi: 10.1109/TPWRS.2017.2690915.
- [83] X. C. ShangGuan et al., "Switching system-based load frequency control for multi-area power system resilient to denial-of-service attacks," Control Eng. Pract., vol. 107, no. July 2020, p. 104678, 2021, doi: 10.1016/j.conengprac.2020.104678.
- [84] C. K. Zhang, L. Jiang, Q. H. Wu, Y. He, and M. Wu, "Delay-dependent robust load frequency control for time delay power systems," *IEEE Trans. Power Syst.*, vol. 28, no. 3, pp. 2192–2201, 2013, doi: 10.1109/TPWRS.2012.2228281.
- [85] Y. V. Hote and S. Jain, "PID controller design for load frequency control: Past, Present and future challenges," *IFAC-PapersOnLine*, vol. 51, no. 4, pp. 604–609, 2018, doi: 10.1016/j.ifacol.2018.06.162.
- [86] H. Javanmardi, M. Dehghani, M. Mohammadi, S. Siamak, and M. R. Hesamzadeh, "BMI-Based Load Frequency Control in Microgrids under False Data Injection Attacks," *IEEE Syst. J.*, vol. 16, no. 1, pp. 1021-1031, 2022, doi: 10.1109/JSYST.2021.3054947.
- [87] J. Yang, Z. Zeng, Y. Tang, J. Yan, H. He, and Y. Wu, "Load frequency control in isolated micro-grids with electrical vehicles based on multivariable generalized predictive theory," Energies, vol. 8, no. 3, pp. 2145-2164, 2015, doi: 10.3390/en8032145.
- [88] W. Tan, S. Chang, and R. Zhou, "Load frequency control of power systems with non-linearities," IET Gener. Transm. Distrib., vol. 11, no. 17, pp. 4307-4313, 2017, doi: 10.1049/iet-gtd.2017.0599.
- [89] X. C. Shangguan et al., "Robust Load Frequency Control for Power System Considering Transmission Delay and Sampling Period," *IEEE Trans. Ind. Informatics*, vol. 17, no. 8, pp. 5292-5303, 2021, doi: 10.1109/TII.2020.3026336.
- [90] M. A. Sobhy, A. Y. Abdelaziz, H. M. Hasanien, and M. Ezzat, "Marine predators algorithm for load frequency control of modern interconnected power systems including renewable energy sources and energy storage units," *Ain Shams Eng. J.*, vol. 12, no. 4, pp. 3843-3857, 2021, doi: 10.1016/j.asej.2021.04.031.
- [91] Z. Farooq, A. Rahman, and S. A. Lone, "Load frequency control of multi-source electrical power system integrated with solar-thermal and electric vehicle," *Int. Trans. Electr. Energy Syst.*, no. February, pp. 1–20, 2021, doi: 10.1002/2050-7038.12918.
- [92] Y. Arya, "Effect of electric vehicles on load frequency control in interconnected thermal and hydrothermal power systems utilising cf-foidf controller," *IET Gener. Transm. Distrib.*, vol. 14, no. 14, pp. 2666–2675, 2020, doi: 10.1049/iet-gtd.2019.1217.
- [93] S. Jiao, J. Xia, Z. Wang, X. Chen, J. Wang, and H. Shen, "An Improved Result on Stability Analysis of Delayed Load Frequency Control Power Systems," Int. J. Control. Autom. Syst., vol. 19, no. 4, pp. 1633–1639, 2021, doi: 10.1007/s12555-019-1063-8.
- [94] B. Mohanty, S. Panda, and P. K. Hota, "Controller parameters tuning of differential evolution

- algorithm and its application to load frequency control of multi-source power system," *Int. J. Electr. Power Energy Syst.*, vol. 54, pp. 77–85, 2014, doi: 10.1016/j.ijepes.2013.06.029.
- [95] Q. Zhong, J. Yang, K. Shi, S. Zhong, Z. Li, and M. A. Sotelo, "Event-Triggered H∞Load Frequency Control for Multi-Area Nonlinear Power Systems Based on Non-Fragile Proportional Integral Control Strategy," *IEEE Trans. Intell. Transp. Syst.*, vol. 23, no. 8, pp. 12191–12201, 2022, doi: 10.1109/TTTS.2021.3110759.
- [96] D. Guha, P. K. Roy, and S. Banerjee, "Disturbance observer aided optimised fractional-order three-degree-of-freedom tilt-integral-derivative controller for load frequency control of power systems," *IET Gener. Transm. Distrib.*, vol. 15, no. 4, pp. 716-736, 2021, doi: 10.1049/gtd2.12054.
- [97] S. Prakash and S. K. Sinha, "Simulation based neuro-fuzzy hybrid intelligent PI control approach in four-area load frequency control of interconnected power system," Appl. Soft Comput. J., vol. 23, pp. 152-164, 2014, doi: 10.1016/j.asoc.2014.05.020.
- [98] E. Çelik, N. Öztürk, Y. Arya, and C. Ocak, "(1 + PD)-PID cascade controller design for performance betterment of load frequency control in diverse electric power systems," *Neural Comput. Appl.*, vol. 33, no. 22, pp. 15433-15456, 2021, doi: 10.1007/s00521-021-06168-3.
- [99] N. Ram Babu, S. K. Bhagat, L. C. Saikia, T. Chiranjeevi, R. Devarapalli, and F. P. García Márquez, "A Comprehensive Review of Recent Strategies on Automatic Generation Control/Load Frequency Control in Power Systems," Arch. Comput. Methods Eng., 2022, doi: 10.1007/s11831-022-09810-y.
- [100] M. H. Khooban, T. Niknam, F. Blaabjerg, P. Davari, and T. Dragicevic, "A robust adaptive load frequency control for micro-grids," ISA Trans., vol. 65, pp. 220-229, 2016, doi: 10.1016/j.isatra.2016.07.002.
- [101] C. Mu, Y. Tang, and H. He, "Improved Sliding Mode Design for Load Frequency Control of Power System Integrated an Adaptive Learning Strategy," *IEEE Trans. Ind. Electron.*, vol. 64, no. 8, pp. 6742–6751, 2017, doi: 10.1109/TIE.2017.2694396.
- [102] M.-H. Khooban, "Secondary Load Frequency Control of," IEEE Trans. Ind. Electron., vol. 65, no. 9, pp. 7416-7422, 2018.
- [103] X. C. Shangguan et al., "Control Performance Standards-Oriented Event-Triggered Load Frequency Control for Power Systems Under Limited Communication Bandwidth," IEEE Trans. Control Syst. Technol., vol. 30, no. 2, pp. 860-868, 2022, doi: 10.1109/TCST.2021.3070861.
- [104] R. Umrao, S. Kumar, M. Mohan, and D. K. Chaturvedi, "Load Frequency Control methodologies for power system," ICPCES 2012 2012 2nd Int. Conf. Power, Control Embed. Syst., 2012, doi: 10.1109/ICPCES.2012.6508133.
- [105] C. Peng and J. Zhang, "Delay-Distribution-Dependent Load Frequency Control of Power Systems with Probabilistic Interval Delays," *IEEE Trans. Power Syst.*, vol. 31, no. 4, pp.

- 3309-3317, 2016, doi: 10.1109/TPWRS.2015.2485272.
- [106] S. Kayalvizhi and D. M. Vinod Kumar, "Load frequency control of an isolated micro grid using fuzzy adaptive model predictive control," *IEEE Access*, vol. 5, pp. 16241-16251, 2017, doi: 10.1109/ACCESS.2017.2735545.
- [107] A. H. Chowdhury and M. Asaduz-Zaman, "Load frequency control of multi-microgrid using energy storage system," 8th Int. Conf. Electr. Comput. Eng. Adv. Technol. a Better Tomorrow, ICECE 2014, pp. 548-551, 2015, doi: 10.1109/ICECE.2014.7026975.
- [108] M. Gheisarnejad, "An effective hybrid harmony search and cuckoo optimization algorithm based fuzzy PID controller for load frequency control," *Appl. Soft Comput. J.*, vol. 65, pp. 121-138, 2018, doi: 10.1016/j.asoc.2018.01.007.
- [109] A. Pappachen and A. Peer Fathima, "Critical research areas on load frequency control issues in a deregulated power system: A state-of-the-art-of-review," *Renew. Sustain. Energy Rev.*, vol. 72, no. January, pp. 163-177, 2017, doi: 10.1016/j.rser.2017.01.053.
- [110] M. R. Toulabi, M. Shiroei, and A. M. Ranjbar, "Robust analysis and design of power system load frequency control using the Kharitonov's theorem," *Int. J. Electr. Power Energy Syst.*, vol. 55, pp. 51-58, 2014, doi: 10.1016/j.ijepes.2013.08.014.
- [111] R. K. Sahu, T. S. Gorripotu, and S. Panda, "A hybrid DE-PS algorithm for load frequency control under deregulated power system with UPFC and RFB," Ain Shams Eng. J., vol. 6, no. 3, pp. 893-911, 2015, doi: 10.1016/j.asej.2015.03.011.
- [112] V. Gholamrezaie, M. G. Dozein, H. Monsef, and B. Wu, "An Optimal Frequency Control Method Through a Dynamic Load Frequency Control (LFC) Model Incorporating Wind Farm," *IEEE Syst. J.*, vol. 12, no. 1, pp. 392-401, 2018, doi: 10.1109/JSYST.2016.2563979.
- [113] S. Trip and C. De Persis, "Distributed optimal load frequency control with non-passive dynamics," *IEEE Trans. Control Netw. Syst.*, vol. 5, no. 3, pp. 1232–1244, 2018, doi: 10.1109/TCNS.2017.2698259.
- [114] S. Panda, B. K. Sahu, and P. K. Mohanty, "Design and performance analysis of PID controller for an automatic voltage regulator system using simplified particle swarm optimization," J. Franklin Inst., vol. 349, no. 8, pp. 2609-2625, 2012, doi: 10.1016/j.jfranklin.2012.06.008.
- [115] M. S. Ayas and E. Sahin, "FOPID controller with fractional filter for an automatic voltage regulator," *Comput. Electr. Eng.*, vol. 90, no. xxxx, 2021, doi: 10.1016/j.compeleceng.2020.106895.
- [116] B. Hekimoğlu and S. Ekinci, "Grasshopper optimization algorithm for automatic voltage regulator system," 2018 5th Int. Conf. Electr. Electron. Eng. ICEEE 2018, pp. 152-156, 2018, doi: 10.1109/ICEEE2.2018.8391320.
- [117] S. Kansit and W. Assawinchaichote, "Optimization of PID Controller Based on PSOGSA for an Automatic Voltage Regulator System," *Procedia Comput. Sci.*, vol. 86, no. March, pp. 87– 90, 2016, doi: 10.1016/j.procs.2016.05.022.

- [118] M. H. Suid and M. A. Ahmad, "Optimal tuning of sigmoid PID controller using Nonlinear Sine Cosine Algorithm for the Automatic Voltage Regulator system," ISA Trans., vol. 128, pp. 265–286, 2022.
- [119] S. M. A. Altbawi, A. S. Bin Mokhtar, T. A. Jumani, I. Khan, N. N. Hamadneh, and A. Khan, "Optimal design of Fractional order PID controller based Automatic voltage regulator system using gradient-based optimization algorithm," J. King Saud Univ. Eng. Sci., no. xxxx, 2021, doi: 10.1016/j.jksues.2021.07.009.
- [120] E. Çelik and R. Durgut, "Performance enhancement of automatic voltage regulator by modified cost function and symbiotic organisms search algorithm," Eng. Sci. Technol. an Int. J., vol. 21, no. 5, pp. 1104-1111, 2018, doi: 10.1016/j.jestch.2018.08.006.
- [121] B. Hekimoğlu, "Sine-cosine algorithm-based optimization for automatic voltage regulator system," *Trans. Inst. Meas. Control*, vol. 41, no. 6, pp. 1761–1771, 2019, doi: 10.1177/0142331218811453.
- [122] A. K. Vamsi Krishna and T. Tyagi, "Improved whale optimization algorithm for numerical optimization," Adv. Intell. Syst. Comput., vol. 1086, pp. 59-71, 2021, doi: 10.1007/978-981-15-1275-9 6.
- [123] T. A. Jumani *et al.*, "Jaya optimization algorithm for transient response and stability enhancement of a fractional-order PID based automatic voltage regulator system," *Alexandria Eng. J.*, vol. 59, no. 4, pp. 2429–2440, 2020, doi: 10.1016/j.aej.2020.03.005.
- [124] S. Ekinci, D. Izci, E. Eker, and L. Abualigah, An effective control design approach based on novel enhanced aquila optimizer for automatic voltage regulator, no. 0123456789. Springer Netherlands, 2022. doi: 10.1007/s10462-022-10216-2.
- [125] H. Shayeghi, A. Younesi, and Y. Hashemi, "Optimal design of a robust discrete parallel FP + FI + FD controller for the Automatic Voltage Regulator system," *Int. J. Electr. Power Energy Syst.*, vol. 67, pp. 66-75, 2015, doi: 10.1016/j.ijepes.2014.11.013.
- [126] D. Mokeddem and S. Mirjalili, "Improved Whale Optimization Algorithm applied to design PID plus second-order derivative controller for automatic voltage regulator system," *J. Chinese Inst. Eng. Trans. Chinese Inst. Eng. A*, vol. 00, no. 00, pp. 541–552, 2020, doi: 10.1080/02533839.2020.1771205.
- [127] S. Chatterjee and V. Mukherjee, "PID controller for automatic voltage regulator using teaching-learning based optimization technique," *Int. J. Electr. Power Energy Syst.*, vol. 77, pp. 418–429, 2016, doi: 10.1016/j.ijepes.2015.11.010.
- [128] E. Çelik and N. Öztürk, "A hybrid symbiotic organisms search and simulated annealing technique applied to efficient design of PID controller for automatic voltage regulator," *Soft Comput.*, vol. 22, no. 23, pp. 8011–8024, 2018, doi: 10.1007/s00500-018-3432-2.
- [129] M. C. Rais, F. Z. Dekhandji, A. Recioui, M. S. Rechid, and L. Djedi, "Comparative Study of Optimization Techniques Based PID Tuning for Automatic Voltage Regulator System," p. 21,

- 2022, doi: 10.3390/engproc2022014021.
- [130] E. Çelik, "Incorporation of stochastic fractal search algorithm into efficient design of PID controller for an automatic voltage regulator system," Neural Comput. Appl., vol. 30, no. 6, pp. 1991–2002, 2018, doi: 10.1007/s00521-017-3335-7.
- [131] I. Eke, M. Saka, H. Gozde, Y. Arya, and M. C. Taplamacioglu, "Engineering Science and Technology, an International Journal Heuristic optimization based dynamic weighted state feedback approach for 2DOF PI-controller in automatic voltage regulator q," Eng. Sci. Technol. an Int. J., vol. 24, no. 4, pp. 899-910, 2021, doi: 10.1016/j.jestch.2020.12.023.
- [132] M. Elsisi and M. Soliman, "Optimal design of robust resilient automatic voltage regulators," ISA Trans., no. xxxx, 2020, doi: 10.1016/j.isatra.2020.09.003.
- [133] I. A. Khan, A. S. Alghamdi, T. A. Jumani, A. Alamgir, A. B. Awan, and A. Khidrani, "Salp Swarm Optimization Algorithm-Based Fractional Order PID Controller for Dynamic Response and Stability Enhancement of an Automatic Voltage Regulator System," *Electronics*, vol. 8, no. 12, p. 1472, 2019, doi: 10.3390/electronics8121472.
- [134] N. Paliwal, L. Srivastava, and M. Pandit, "Equilibrium optimizer tuned novel FOPID-DN controller for automatic voltage regulator system," *Int. Trans. Electr. Energy Syst.*, vol. 31, no. 8, pp. 1–28, 2021, doi: 10.1002/2050-7038.12930.
- [135] A. J. H. Al Gizi, "A particle swarm optimization, fuzzy PID controller with generator automatic voltage regulator," Soft Comput., vol. 23, no. 18, pp. 8839–8853, 2019, doi: 10.1007/s00500-018-3483-4.
- [136] M. Elsisi, "Design of neural network predictive controller based on imperialist competitive algorithm for automatic voltage regulator," *Neural Comput. Appl.*, vol. 31, no. 9, pp. 5017– 5027, 2019, doi: 10.1007/s00521-018-03995-9.
- [137] A. Sikander and P. Thakur, "A new control design strategy for automatic voltage regulator in power system," ISA Trans., vol. 100, no. xxxx, pp. 235-243, 2020, doi: 10.1016/j.isatra.2019.11.031.
- [138] Y. Batmani and H. Golpîra, "Automatic voltage regulator design using a modified adaptive optimal approach," *Int. J. Electr. Power Energy Syst.*, vol. 104, no. February 2018, pp. 349–357, 2019, doi: 10.1016/j.ijepes.2018.07.001.
- [139] S. Duman, N. Yörükeren, and I. H. Altaş, "Gravitational search algorithm for determining controller parameters in an automatic voltage regulator system," *Turkish J. Electr. Eng. Comput. Sci.*, vol. 24, no. 4, pp. 2387–2400, 2016, doi: 10.3906/elk-1404-14.
- [140] X. Li, Y. Wang, N. Li, M. Han, Y. Tang, and F. Liu, "Optimal fractional order PID controller design for automatic voltage regulator system based on reference model using particle swarm optimization," *Int. J. Mach. Learn. Cybern.*, vol. 8, no. 5, pp. 1595–1605, 2017, doi: 10.1007/s13042-016-0530-2.
- [141] HongboZou and H. Li, "Tuning of PI-PD controller using extended non-minimal state space

- model predictive control for the stabilized gasoline vapor pressure in a stabilized tower," *Chemom. Intell. Lab. Syst.*, vol. 142, pp. 1–8, 2015, doi: 10.1016/j.chemolab.2014.12.012.
- [142] G. Lloyds Raja and A. Ali, "New PI-PD Controller Design Strategy for Industrial Unstable and Integrating Processes with Dead Time and Inverse Response," J. Control. Autom. Electr. Syst., vol. 32, no. 2, pp. 266-280, 2021, doi: 10.1007/s40313-020-00679-5.
- [143] I. Kaya, "Optimal PI-PD Controller Design for Pure Integrating Processes with Time Delay," J. Control. Autom. Electr. Syst., vol. 32, no. 3, pp. 563-572, 2021, doi: 10.1007/s40313-021-00692-2.
- [144] M. Irshad and A. Ali, "Robust PI-PD controller design for integrating and unstable processes," IFAC-PapersOnLine, vol. 53, no. 1, pp. 135-140, 2020, doi: 10.1016/j.ifacol.2020.06.023.
- [145] M. Peram, S. Mishra, M. Vemulapaty, B. Verma, and P. K. Padhy, "Optimal PI-PD and I-PD Controller Design Using Cuckoo Search Algorithm," 2018 5th Int. Conf. Signal Process. Integr. Networks, SPIN 2018, pp. 643-646, 2018, doi: 10.1109/SPIN.2018.8474214.
- [146] F. N. Deniz, A. Yüce, and N. Tan, "Tuning of PI-PD controller based on standard forms for fractional order systems," J. Appl. Nonlinear Dyn., vol. 8, no. 1, pp. 5-23, 2019, doi: 10.5890/JAND.2019.03.002.
- [147] M. Zheng, T. Huang, and G. Zhang, "A New Design Method for PI-PD Control of Unstable Fractional-Order System with Time Delay," Complexity, vol. 2019, 2019, doi: 10.1155/2019/3253497.
- [148] T. Ali, M. Adeel, S. A. Malik, and M. Amir, "Stability Control of Ball and Beam System Using Heuristic Computation Based PI-D and PI-PD Controller," Tech. Journal, Univ. Eng. Technol., vol. 24, no. 1, pp. 21-29, 2019.
- [149] T. Ali, S. A. Malik, M. Adeel, and M. Amir, "Set Point Tracking of Ball and Beam System using Genetic Algorithm based PI-PD Controller," no. 1, 2018.
- [150] T. Ali, M. Adeel, S. Abdullah, M. Amir, N. Ahmad, and W. U. K. Tareen, "Nature Inspired Computation Based Fractional Order I-TD and TID Controllers for Magnetic Levitation System," vol. 24, no. 3, pp. 24-32, 2019.
- [151] L. Wang, Q. Cao, Z. Zhang, S. Mirjalili, and W. Zhao, "Artificial rabbits optimization: A new bio-inspired meta-heuristic algorithm for solving engineering optimization problems," Eng. Appl. Artif. Intell., vol. 114, no. March, p. 105082, 2022, doi: 10.1016/j.engappai.2022.105082.
- [152] S. Zhao, T. Zhang, S. Ma, and M. Chen, "Dandelion Optimizer: A nature-inspired metaheuristic algorithm for engineering applications," Eng. Appl. Artif. Intell., vol. 114, p. 105075, 2022, doi: https://doi.org/10.1016/j.engappai.2022.105075.
- [153] S. Zhao, T. Zhang, S. Ma, and M. Wang, "Sea-horse optimizer: a novel nature-inspired meta-heuristic for global optimization problems," *Appl. Intell.*, 2022, doi: 10.1007/s10489-022-03994-3.

- [154] F. A. Hashim, K. Hussain, E. H. Houssein, M. S. Mabrouk, and W. Al-Atabany, "Archimedes optimization algorithm: a new metaheuristic algorithm for solving optimization problems," Appl. Intell., vol. 51, no. 3, pp. 1531-1551, 2021, doi: 10.1007/s10489-020-01893-z.
- [155] M. H. Qais, H. M. Hasanien, and S. Alghuwainem, "Transient search optimization: a new meta-heuristic optimization algorithm," *Appl. Intell.*, vol. 50, no. 11, pp. 3926–3941, 2020, doi: 10.1007/s10489-020-01727-y.
- [156] C. M. Rahman and T. A. Rashid, "A new evolutionary algorithm: Learner performance based behavior algorithm," *Egypt. Informatics J.*, vol. 22, no. 2, pp. 213–223, 2021, doi: 10.1016/j.eij.2020.08.003.
- [157] A. Fathy, A. G. Alharbi, S. Alshammari, and H. M. Hasanien, "Archimedes optimization algorithm based maximum power point tracker for wind energy generation system," Ain Shams Eng. J., vol. 13, no. 2, p. 101548, 2022, doi: 10.1016/j.asej.2021.06.032.
- [158] X. Sun, G. Wang, L. Xu, H. Yuan, and N. Yousefi, "Optimal estimation of the PEM fuel cells applying deep belief network optimized by improved archimedes optimization algorithm," *Energy*, vol. 237, 2021, doi: 10.1016/j.energy.2021.121532.
- [159] D. Yousri, Y. Shaker, S. Mirjalili, and D. Allam, "An efficient photovoltaic modeling using an Adaptive Fractional-order Archimedes Optimization Algorithm: Validation with partial shading conditions," Sol. Energy, vol. 236, no. January 2021, pp. 26-50, 2022, doi: 10.1016/j.solener.2021.12.063.
- [160] J. Wang, C. Zhan, S. Li, Q. Zhao, J. Liu, and Z. Xie, "Adaptive variational mode decomposition based on Archimedes optimization algorithm and its application to bearing fault diagnosis," *Meas. J. Int. Meas. Confed.*, vol. 191, no. November 2021, p. 110798, 2022, doi: 10.1016/j.measurement.2022.110798.
- [161] L. Zhang, J. Wang, X. Niu, and Z. Liu, "Ensemble wind speed forecasting with multi-objective Archimedes optimization algorithm and sub-model selection," *Appl. Energy*, vol. 301, no. June, p. 117449, 2021, doi: 10.1016/j.apenergy.2021.117449.
- [162] J. Kennedy and R. Eberhart, "Particle swarm optimization," in *Proceedings of ICNN'95-international conference on neural networks*, 1995, vol. 4, pp. 1942–1948.
- [163] D. Tian and Z. Shi, "MPSO: Modified particle swarm optimization and its applications," Swarm Evol. Comput., vol. 41, pp. 49-68, 2018, doi: 10.1016/j.swevo.2018.01.011.
- [164] D. Guha, P. K. Roy, and S. Banerjee, "Application of backtracking search algorithm in load frequency control of multi-area interconnected power system," Ain Shams Eng. J., vol. 9, no. 2, pp. 257-276, 2018, doi: 10.1016/j.asej.2016.01.004.
- [165] D. Guha, P. K. Roy, and S. Banerjee, "Symbiotic organism search algorithm applied to load frequency control of multi-area power system," *Energy Syst.*, vol. 9, no. 2, pp. 439–468, 2018, doi: 10.1007/s12667-017-0232-1.
- [166] S. C. Tripathy, R. Balasubramanian, and P. S. C. Nair, "Effect of Superconducting Magnetic

- Energy Storage on Automatic Generation Control Considering Governor Deadband and Boiler Dynamics," *IEEE Trans. Power Syst.*, vol. 7, no. 3, pp. 1266–1273, 1992, doi: 10.1109/59.207343.
- [167] S. Zhao, T. Zhang, S. Ma, and M. Chen, "Dandelion Optimizer: A nature-inspired metaheuristic algorithm for engineering applications," Eng. Appl. Artif. Intell., vol. 114, no. May, p. 105075, 2022, doi: 10.1016/j.engappai.2022.105075.
- [168] M. Khamies, G. Magdy, M. Ebeed, and S. Kamel, "A robust PID controller based on linear quadratic gaussian approach for improving frequency stability of power systems considering renewables," ISA Trans., vol. 117, pp. 118-138, 2021, doi: 10.1016/j.isatra.2021.01.052.
- [169] R. Alayi, F. Zishan, S. R. Seyednouri, R. Kumar, M. H. Ahmadi, and M. Sharifpur, "Optimal load frequency control of island microgrids via a pid controller in the presence of wind turbine and pv," Sustain., vol. 13, no. 19, 2021, doi: 10.3390/su131910728.
- [170] R. Ramachandran, B. Madasamy, V. Veerasamy, and L. Saravanan, "Load frequency control of a dynamic interconnected power system using generalised Hopfield neural network based self-adaptive PID controller," *IET Gener. Transm. Distrib.*, vol. 12, no. 21, pp. 5713-5722, 2018, doi: 10.1049/iet-gtd.2018.5622.
- [171] X. Jin, K. Chen, Y. Zhao, J. Ji, and P. Jing, "Simulation of hydraulic transplanting robot control system based on fuzzy PID controller," Meas. J. Int. Meas. Confed., vol. 164, p. 108023, 2020, doi: 10.1016/j.measurement.2020.108023.
- [172] K. Eltag, M. S. Aslamx, and R. Ullah, "Dynamic Stability Enhancement Using Fuzzy PID Control Technology for Power System," Int. J. Control. Autom. Syst., vol. 17, no. 1, pp. 234–242, 2019, doi: 10.1007/s12555-018-0109-7.
- [173] A. H. A. Elkasem, M. Khamies, G. Magdy, I. B. M. Taha, and S. Kamel, "Frequency stability of ac/dc interconnected power systems with wind energy using arithmetic optimization algorithm-based fuzzy-pid controller," Sustain., vol. 13, no. 21, 2021, doi: 10.3390/su132112095.
- [174] B. P. Sahoo and S. Panda, "Improved grey wolf optimization technique for fuzzy aided PID controller design for power system frequency control," Sustain. Energy, Grids Networks, vol. 16, pp. 278–299, 2018, doi: 10.1016/j.segan.2018.09.006.
- [175] H. Feng, W. Ma, C. Yin, and D. Cao, "Trajectory control of electro-hydraulic position servo system using improved PSO-PID controller," *Autom. Constr.*, vol. 127, no. April, p. 103722, 2021, doi: 10.1016/j.autcon.2021.103722.
- [176] M. A. El-Dabah, S. Kamel, M. Khamies, H. Shahinzadeh, and G. B. Gharehpetian, "Artificial Gorilla Troops Optimizer for Optimum Tuning of TlD Based Power System Stabilizer," 2022 9th Iran. Jt. Congr. Fuzzy Intell. Syst. CFIS 2022, no. 2, 2022, doi: 10.1109/CFIS54774.2022.9756463.
- [177] S. P. Behera, A. Biswal, B. Swain, and S. S. Samantray, "Hybrid power systems Frequency

- regulation using TID based robust controller design and differential evolution (DE) algorithm," Int. Conf. Technol. Smart City Energy Secur. Power Smart Solut. Smart Cities, ICSESP 2018 Proc., vol. 2018-Janua, pp. 1-6, 2018, doi: 10.1109/ICSESP.2018.8376728.
- [178] S. P. Behera and A. Biswal, "TID Controller in Two Area Multi Unit Power Systems with SMES and HVDC Link," 2019 Glob. Conf. Adv. Technol. GCAT 2019, pp. 1-5, 2019, doi: 10.1109/GCAT47503.2019.8978470.
- [179] H. Shukla, S. Nikolovski, M. Raju, A. S. Rana, and P. Kumar, "A Particle Swarm Optimization Technique Tuned TID Controller for Frequency and Voltage Regulation with," 2022.
- [180] M. M. Elsaied, W. H. Abdel Hameed, and H. M. Hasanien, "Frequency stabilization of a hybrid three-area power system equipped with energy storage units and renewable energy sources," *IET Renew. Power Gener.*, no. August, pp. 3267–3286, 2022, doi: 10.1049/rpg2.12577.
- [181] S. A. Bhatti, S. A. Malik, and A. Daraz, "Comparison of P-I and I-P controller by using Ziegler-Nichols tuning method for speed control of DC motor," 2016 Int. Conf. Intell. Syst. Eng. ICISE 2016, pp. 330-334, 2016, doi: 10.1109/INTELSE.2016.7475144.
- [182] A. Daraz, E. S. A. Malik, and A. Waseem, "Genetic Algorithm based I-P Controller for Superheated Steam Temperature Control System," 3rd Int. Conf. Electr. Commun. Comput. Eng. ICECCE 2021, no. June, pp. 12-13, 2021, doi: 10.1109/ICECCE52056.2021.9514213.
- [183] I. Ahmadianfar, O. Bozorg-Haddad, and X. Chu, "Gradient-based optimizer: A new metaheuristic optimization algorithm," *Inf. Sci. (Ny).*, vol. 540, pp. 131–159, 2020, doi: 10.1016/j.ins.2020.06.037.
- [184] M. H. Hassan, S. Kamel, M. A. El-Dabah, and H. Rezk, "A novel solution methodology based on a modified gradient-based optimizer for parameter estimation of photovoltaic models," *Electron.*, vol. 10, no. 4, pp. 1–23, 2021, doi: 10.3390/electronics10040472.
- [185] A. A. K. Ismaeel, E. H. Houssein, D. Oliva, and M. Said, "Gradient-based optimizer for parameter extraction in photovoltaic models," *IEEE Access*, vol. 9, pp. 13403–13416, 2021, doi: 10.1109/ACCESS.2021.3052153.
- [186] S. Deb, D. S. Abdelminaam, M. Said, and E. H. Houssein, "Recent Methodology-Based Gradient-Based Optimizer for Economic Load Dispatch Problem," *IEEE Access*, vol. 9, pp. 44322-44338, 2021, doi: 10.1109/ACCESS.2021.3066329.
- [187] S. Yu, Z. Chen, A. A. Heidari, W. Zhou, H. Chen, and L. Xiao, "Parameter identification of photovoltaic models using a sine cosine differential gradient based optimizer," *IET Renew. Power Gener.*, vol. 16, no. 8, pp. 1535–1561, 2022, doi: 10.1049/rpg2.12451.

APPENDIX A

Parameter	Value	Parameter	Value	Parameter	Value
B ₁ , B ₂ , B ₃	1	G4	1.4	T _{G3}	0.12
Rı	2.4	G ₅	0.5	K ₃	1
K _{G1}	1	R ₂	1.20	To	0.15
T _{G1}	0.08	K _{G2}	1	K _{p3}	100
Ktl	1	T _{G2}	0.12	T _{p3}	10
Ttl	0.3	K ₂	1	K _{a3}	10
K _{pl}	120	T ₂	0.15	T _{a3}	0.1
T _{pl}	20	K _{p2}	100	Ke3	1.8
Kal	10	T _{p2}	10	Te3	0.8
Tat	0.1	K _{e2}	10	Kg3	1.8
Kel	1	T _{a2}	0.1	T _{g3}	1.8
Tel	0.4	K _{e2}	1.5	Ka	1
K _{gl}	1	T _{e2}	0.6	Ts3	0.01
T _{gl}	1	K _{g2}	1.5	T ₁₂	0.545
Kal	1	T _{g2}	1.5	T ₁₃	0.545
T _{sl}	0.01	K ₄₂	1	T ₂₁	0.545
Gı	1.5	T _{s2}	0.01	T ₂₃	0.545
G ₂	0.3	R ₃	1.20	T ₃₁	0.545
G ₃	0.1	K _{G3}	1	T ₃₂	0.545

APPENDIX B

Parameter	Value	Parameter	Value
B ₁ , B ₂ , B ₃	0.045	Н	5
f	60	K _{ps} = 1/D	68.97
Rt	2.4	$T_{ps} = 2^{+}H/f^{+}D$	11.49
Rh	2.4	Kı	0.2
Rg	2.4	K ₂	0.1
Tgr	0.08	K ₃	0.5
Tre	10	K4	1.4
Kre	0.3	P _s	1.5
Ttr	0.3	K _a	10
Th	0.3	Ta	0.1
T _{rs}	5	K _e	1
T _{rh}	28.75	Te	0.4
Tw	0.025	Kg	0.8
х	0.6	Tg	1.4
Y	1	K _a	1
a	1	Ts	0.05
b	0.05	T ₁₂	0.545
С	1	T ₁₃	0.545
T _{cr}	0.01	T ₂₁	0.545
T_{f}	0.23	T ₂₂	0.545
T _{cd}	0.2	T ₃₁	0.545
D	0.0145	T ₃₂	0.545

APPENDIX C

Parameter	Value	Parameter	Value
B ₁ , B ₂ , B ₃ , B ₄	0.045	K4	1.4
Rt	2.4	P _s	1.5
R _h	2.4	Ka	10
$R_{\mathbf{g}}$	2.4	T _a	0.1
R _w	2.4	K _e	1
Tgr	0.08	Te	0.4
Tre	10	Kg	0.8
K _{re}	0.3	Tg	1.4
Ttr	0.3	Ks	1
Th	0.3	Ts	0.05
Trs	5	T _{w1}	0.6
T _{th}	28.75	T _{w2}	0.041
T _w	0.025	Kwi	1.25
х	0.6	K _{w2}	1.4
Y	1	T_{pv}	1.8
a	1	K _{pv}	1
ь	0.05	T ₁₂	0.545
С	1	T ₁₃	0.545
TCR	0.01	T ₁₄	0.545
T _f	0.23	T ₂₁	0.545
T _{CD}	0.2	T ₂₃	0.545
D	0.0145	T ₂₄	0.545
Н	5	T ₃₁	0.545
f	60	T ₃₂	0.545
$K_{ps} = 1/D$	68.97	T ₃₄	0.545
$T_{ps} = 2*H/f*D$	11.49	T41	0.545
K ₁	0.2	T ₄₂	0.545
K ₂	0.1	T43	0.545
K ₃	0.5		(har \ 1

ione:

ENTRAL DEPARTURE STAMARIO